MICROMACHINED THREE-DIMENSIONAL ELECTRODE ARRAYS FOR *IN-VITRO* AND *IN-VIVO* ELECTROGENIC CELLULAR NETWORKS

A Dissertation Presented to
The Academic Faculty

by

Swaminathan Rajaraman

In Partial Fulfillment
of the Requirements for the Degree
Doctor of Philosophy in the
School of Electrical and Computer Engineering

Georgia Institute of Technology
May 2009

MICROMACHINED THREE-DIMENSIONAL ELECTRODE ARRAYS FOR *IN-VITRO* AND *IN-VIVO* ELECTROGENIC CELLULAR NETWORKS

Approved by:

Dr. Mark G. Allen, Advisor
School of Electrical & Computer Engineering
Georgia Institute of Technology

Dr. Ionnis (John) Papapolymerou
School of Electrical & Computer Engineering
Georgia Institute of Technology

Dr. Oliver Brand
School of Electrical & Computer Engineering
Georgia Institute of Technology

Dr. Elliot L. Chaikof
Wallace H. Coulter Department of Biomedical Engineering
Georgia Institute of Technology/Emory University

Dr. Maysam Ghovanloo
School of Electrical & Computer Engineering
Georgia Institute of Technology

Date Approved: March 5th, 2009

Dedicated
To my parents and my sister

ACKNOWLEDGEMENTS

First and foremost I would like to thank my advisor Prof. Mark G. Allen. It has been an absolute dream come true to work for one of the pre-eminent names in the field of MEMS, something I would not have imagined when I started out in this field 10 years ago. His brilliance, ideas, patience, creativity, guidance, dedication and scholarly leadership are absolutely outstanding. He also introduced me to CardioMEMS (where I was fortunate to work for a year) and allowed me to pursue semi-entrepreneurial activities with Axion Biosystems and Teneo MicroInstruments for which I'm eternally grateful.

I would further like to thank my thesis committee members: Profs. Brand, Ghovanloo, Papapolymerou and Chaikof, for participating in my dissertation defense committee, and for their valuable suggestions to improve this document.

I would like to thank MSMA group members both past and present for their advice on fabrication techniques, cleanroom/laser training, testing methodologies, memorable group get-togethers and conference trips. Specifically, I express my gratitude toward Drs. Yoonsu Choi and Seong-O Choi, who have been instrumental in guiding me through the initial work in the MSMA group and shaping some of the work in this dissertation. I would further like to thank Mr. Richard Shafer and Ms. Purnima Sharma for the amazing technical and administrative duties they perform to keep the MSMA group running.

Mr. Gary Spinner and the staff of the MiRC cleanroom deserve tremendous kudos for keeping what I think is the "best academic cleanroom in the country" running

efficiently. I would like to mention the facilities in the Laboratory of Neuroengineering which served to support testing of the devices built as part of this work. The funding for this research work came through the aegis of the National Institute of Health (NIH) for which I'm really thankful (NIH BRP grants EB 00786-01 and EB 006369-01A1).

An inter-disciplinary thesis like this would not be possible without the input and collaboration with several co-workers. The key amongst these excellent scholars was Dr. James Ross, who helped shape several ideas and tirelessly tested devices with me in spite of having a multitude of responsibilities. I would also like to acknowledge the contributions of Mr. Edgar Brown toward the impedance theory in this work. Biological testing on the devices I built was performed by Ms. Maxine McClain, Mr. Varadraj Vernekar, Dr. D. Kacy Cullen and Dr. J. Alex Bragg for which I'm eternally grateful. I would also like to thank Mr. Brock Wester for working tirelessly with me on many of the illustrations presented in this work.

I would like to acknowledge the friendship of several people (too many to name here) in both Atlanta and Boston, who made my life in graduate school very memorable. Finally I would like to recognize my parents Chandra and Arunachalam Rajaraman and my sister Vidya Rajaraman. Their support, love, sacrifice, patience and constant encouragement even in bad times cannot be replaced by anything else in this world. I'm forever indebted to them and not sure if I can ever repay them for their efforts.

TABLE OF CONTENTS

LIST OF TABLES

LIST OF FIGURES

SUMMARY

This dissertation presents development of three-dimensional microelectrode arrays (3-D MEAs) for a variety of applications in the *in-vitro* and *in-vivo* arenas. MEAs are important tools for scientific discovery and medical advancement. Since MEAs can actively manipulate and monitor cellular activity at both the single cell and tissue levels, they provide extraordinary insight into complex electrogenic cellular interactions. MEAs are utilized for a wide range of applications: basic neural research, biosensors for chemical, biological and environmental detection of compounds, pharmacological screening, toxicology, prosthetic devices, cardiac pacing, epilepsy research and bioelectrodes. Planar or 2-D MEAs have been in existence for over 30 years but in order to study complex cellular network morphologies and tissue cultures (with 3-D network of electrogenic cells), 3-D MEAs are required. Current 3-D MEAs are based on silicon micromachining and/or complex assembly processes resulting in expensive manufacturing, questionable biocompatibility, and limited accessibility to end users. The 3-D MEAs developed in this work are polymer-based, thereby potentially enabling low cost mass manufacturing, biocompatibility and familiarity for end users of this technology – biologists, chemists, doctors and pharmacologists.

This research begins with the development of laser micromachining based 3-D MEAs. Lasers are ideal for 3-D fabrication as they can machine material with substantial topographies in a non-contact manner. In order to develop 3-D MEAs, high aspect ratio micro-towers were fabricated using a double-side exposure technology of a negative tone epoxy-composite called SU-8. These tower arrays were then coated with a metal layer

and a conformal polymer that was micromachined selectively with a laser in both 2-D and 3-D to create a mold. Metal was electrodeposited on this mold to create the MEAs. These MEAs were packaged and then evaluated electrically utilizing impedance spectroscopy and baseline noise measurements. 3-D cortical co-cultures of neurons and astrocytes were grown on these MEAs and excellent biocompatibility was demonstrated for up to 21 days *in-vitro*.

For a true extension to a manufacturing process, a metal transfer micromolding based technique was developed to fabricate 3-D MEAs. The MEA master structures were fabricated using advanced mold fabrication technologies including inclined rotational exposure of SU-8 and micromolding. Two separate techniques were developed for selective metallization of micromolds – a shadow mask approach and an intentionally formed non-planar mold approach. Both these techniques enable self-aligned metal patterning in highly non-planar topographies without the need for complex, expensive and non-repeatable 3-D lithography processes. 3-D MEAs were micromolded from these metalized molds multiple times. Simple packaging technologies were developed to accommodate the MEA in a footprint compatible with commercial test setups. 2-D cortical cultures of neurons were grown on the MEAs for up to 5 days *in-vitro* to demonstrate biocompatibility of the materials used in MEA fabrication. Acute tissue slice electrophysiology was performed to demonstrate biological functionality. Analytical models were developed for the electrode impedance, baseline noise and shape prediction of molds. Process changes were developed to improve the yield of microelectrodes on the MEAs.

The application of these MEAs was demonstrated in an *in-vitro* arena for nerve tracking. The design, fabrication and packaging processes were modified to fit the desired application. Characterization of master structure sharpening techniques was performed to produce 3-D MEAs that can pierce the epithelial layers of human skin. EMG and nerve conduction measurements were demonstrated with these MEAs. A potential application of MEA patches to nerve tracking was explored.

CHAPTER 1

INTRODUCTION

1.1 Motivation and Goals of this Dissertation

Cellular function and response has been a significant subject of human fascination since time immemorial and a major field of study that has improved understanding of the mechanics of the human body. Specifically the functioning of electrogenic or electrically active cells is of particular interest in this dissertation as these cells control several important physiological functions. Advances in both engineering (including microelectronics) and biology (including electrophysiology) have contributed toward this field by introducing instrumentation capable of interfacing with cells and tissue. This dissertation addresses the development of one such tool − three-dimensional microelectrode arrays (3-D MEAs), also called multielectrode arrays or micromachined probes, fabricated from polymeric substrates. These electrode arrays will be utilized in stimulating and recording *in-vitro* (outside the body) and *in-vivo* (within the body) from neural tissue, neuro-muscular tissue and cultured networks of cells.

Most physiological functions controlled by the brain involve a coordinated activity of networks of cells making it imperative that network activity be studied in addition to single cell activity (even though single cell action potentials are important in certain experiments for eg. studying isolated ion channels). MEAs, which are tiny electrodes arranged in a geometrically repeatable fashion, can be utilized to study such network functionality. Theoretically, MEAs can be used to stimulate and record from any network of excitable cells (such as neural, cardiac and muscular). Such cells are also known as

electrogenic cells. Specifically, MEAs have been used to record from neural networks to improve our understanding of the operation of the brain [Potter 2005]; as biosensors to sense chemical, biological and environmental toxins [Kovacs 2003]; detection of biohazard/bioterrorism agents [DeBusschere 2001]; screening for pharmacologically active compounds [Meyer 2004]; neural prosthetic applications [Wise 2005]; and as bioelectrodes for various electrical measurements *in-vivo* [Griss 2001] (eg. electromyography, electrocardiography etc).

The goals of this dissertation are to design and develop technologies for microfabrication and packaging of 3-D MEAs. An analogous goal is the characterization of these MEAs in both *in-vitro* and *in-vivo* environments.

1.2 MEAs as a Electrogenic Cellular Network Interfacing Platform

There are two paradigms of studying networks of excitable cells – *in-vitro* and *in-vivo*. The *in-vivo* paradigm has been in existence for several centuries due to human accessibility to live animals and the ability to monitor them real-time. The *in-vitro* paradigm developed later and has some distinct advantages. It makes cultures easier to control as they are in a dish now rather than inside an animal which makes external stimuli, environmental conditions, injury to cells and observation through microscopy much easier. Additionally, variables such as immune response, inflammation and infection that are present in an *in-vivo* setting are eliminated in an *in-vitro* environment [Potter 2005]. Both the paradigms are however important in furthering our knowledge of

excitable cells; occasionally, design considerations for instrumentation in one area can be applied to another and vice-versa.

The earliest tools for establishing an electrical connection to cells were wires, pipettes and patch clamps [Frank 1964]. These tools have the capability of studying single cells or a small network of cells (and are still used today) but their construction is considered more "art" than science and imposes inherent limitations on the precision and reproducibility of shapes, sizes and characteristics of the resulting electrodes. The size of excitable cells ranges from 4μm to several 100μm making macro-scale tools incompatible and microfabrication an attractive option to produce instrumentation used to study them. With the development of Integrated Circuit (IC) and Micro Electro Mechanical Systems (MEMS) technologies, the idea of closely controlling these electrode characteristics in the micro-scale became feasible. This led to the development of MEAs, first reported in the late 1960s [Wise 1969]. Several of these early MEAs [Wise 1969; Thomas 1972; Wise 1975; May 1979] were planar, though the ones developed by Wise et al. [Wise 1969; Wise 1975] were in the form of a micromachined probe for *in-vivo* measurements. With application of MEMS techniques, the possibility of realizing three-dimensional MEA technology for both paradigms became a reality. The ability to stimulate/record in the third dimension is important due to a number of reasons -

- Recent developments in *in-vitro* 3-D cultures of excitable cells [Grinnell 2003; Cullen 2005] have shown that cells cultured in a 3-D environment better depict the cell-cell and cell-matrix interactions of *in-vivo* experiments.

- Fundamental differences in morphology, growth/proliferation, viability, gene/protein expression, response to mechanical/electrical stimuli exist between 2-D and 3-D cultures.
- In the case of *in-vitro* tissue slice cultures establishing a tight seal between cell membrane and electrode surface, which is related to the signal to noise performance of these cultures and implies finding a pathway for electrodes to get past dead cell layers from dissection.
- For *in-vivo* applications, the MEA has to overcome the skin impedance problem, predominantly determined by the resistance of the *Stratum Corneum*, the outer-most layer of skin.

MEMS-based approaches are ideal for creation of 3-D MEAs as they offer advanced 3-D fabrication techniques and batch fabrication which results in reduction in cost and high throughput. Furthermore, if these MEMS approaches can be polymer-based, an improved cost performance (due to large area processing and cheaper tools/facilities) compared to traditional silicon-based approaches can be envisioned.

In the human body, the brain is the largest source of complex electrogenic cellular network activity [Mountcastle 1997]. Hence most of the research in the area (and a heavy portion of characterization experiments in this dissertation) of excitable cells is obviously focused on the understanding the cellular networks (neurons) of this complex organ. The *in-vivo* portion of this dissertation has focused on a more easily accessible excitable cellular network – muscle cells. The neuromuscular network can be accessed in a minimally invasive fashion as opposed to the neural network which requires substantial

invasive procedures. In both these networks, due to their size and density, MEAs and accompanying electronics provide the means to stimulate/record highly parallel events occurring in such a complex sub-millimeter scale. They can also be utilized to stimulate one region and record the response from another.

The wide ranges of applications of MEAs discussed in this chapter are summarized in Figure 1.1.

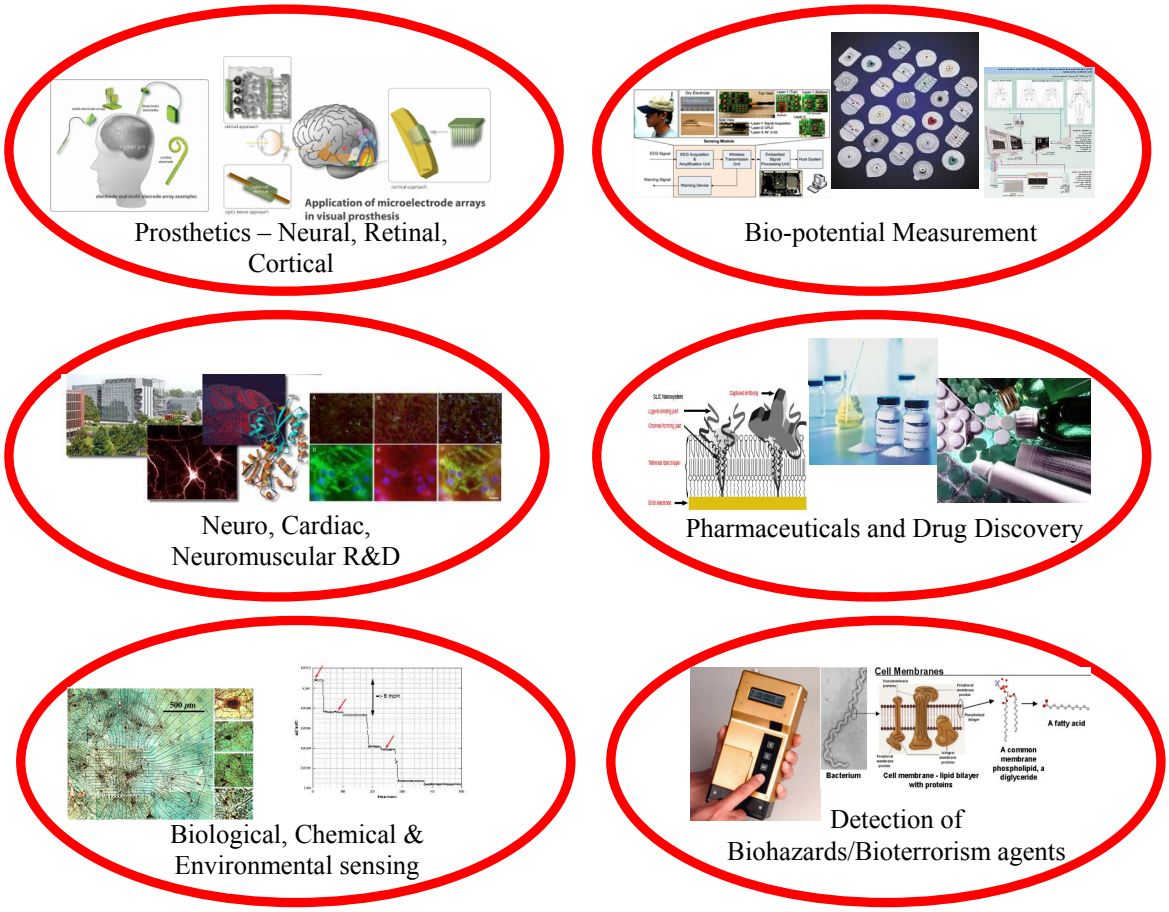

Figure 1.1: Schematic depicting various applications of MEAs in the real world.

It is estimated that brain/muscle/cardiac related illnesses affect one in three humans' world-wide [NeuroTech Industry 2008]. The demand for instrumentation and electronics for this area is ever growing with an estimated world-wide market of US$120 billion in 2006 [NeuroTech Industry 2008]. This includes all aspects of research, technology development in the areas depicted above and more. Thus there is tremendous need for bioinstrumentation (such as MEAs) and technologies that interface with excitable cells. A vital contribution to the improvement in the quality of human life can be achieved with improvement in existing techniques and development of newer technologies in this area.

1.3 Dissertation Overview

This chapter serves as a motivation for the need for MEAs with the following Chapters providing a background, design, development and characterization of various MEAs and finally conclusions for this research.

Chapter 2 introduces background work in the area of MEAs. A brief summary of 2-D MEA technologies that have been developed by various researchers is described, followed by an introduction to 3-D MEAs developed around the world. Microelectrode theory is explored along with a background for electrogenic cellular networks. Two specific cellular networks related to this dissertation have been introduced – neural and neuro-muscular.

Chapter 3 presents design, microfabrication, packaging and characterization of laser micromachined *in-vitro* 3-D MEAs. This includes microfabrication technologies to produce high-aspect ratio micro-towers using a negative-tone, UV sensitive epoxy,

characterization of laser micromachining of thin polymer on thin film metal and scribing microelectrodes on the constructed micro-towers. The characterization apparatus for impedance spectrum and baseline noise are described along with the measurements. Protocols for *in-vitro* 3-D cortical cultures of neurons are described along with *in-vitro* culture experiments and results.

Chapter 4 presents design, microfabrication, packaging and characterization of metal transfer micromolded 3-D MEAs. These MEAs are designed to be versatile for both *in-vitro* and *in-vivo* applications. Advanced micro-mold fabrication techniques are introduced along with shape-prediction algorithms for these complex micro-molds. Two techniques for selective metallization on 3-D surfaces are explored. Metal transfer micromolding is utilized to microfabricate MEAs which are then packaged. Process improvements to increase the yield of the microelectrodes in the MEA are studied. Analytical models of impedance and baseline noise are developed and compared to experimental data. Protocols for *in-vitro* electrophysiological spike recording from hippocampal slices and biocompatibility are described along with the experiments and results.

Chapter 5 presents the design, microfabrication, packaging and characterization of metal transfer micromolded 3-D MEAs for *in-vivo* biopotential measurement. Two separate techniques for master structure fabrication (both based on chapters 3 and 4) and microneedle sharpening (to penetrate the outer layer of skin for *in-vivo* application) techniques are developed. Metal transfer micromolding is utilized to fabricate MEAs multiple times using these master structures. Experimental apparatus for i*n-vivo* measurements including impedance through the skin, electromyography and nerve

conduction are described along with the results. A potential nerve tracking application that would present a multi-fold improvement over the current state of the art is described.

Chapter 6 presents conclusions to this dissertation and prospects for future research in this interesting area.

CHAPTER 2

BACKGROUND

2.1 Microfabrication Background

Since the development of integrated circuits in the early 60s, silicon microfabrication has been applied to biomedical devices. Some of the earliest work is reported in the late 60s and early 70s in the development of images sensors for the blind, implantable sensors for blood flow, pressure sensors and microelectrode arrays (MEAs) [Meindl 1969; Wise 1969; Gill 1975]. For the first couple of decades (and in several applications even today) silicon technologies are the predominant driver of microfabrication. Some of the early reported work in non-traditional microfabrication for MEAs was on glass and ceramics [Thomas 1972; May 1979]. In the 90s however researchers started exploring microfabrication on non-silicon materials especially for biomedical applications. The reasons for this were manifold: usage of bio-friendly materials, questions on the biocompatibility of silicon, access of silicon technologies to chemists and biologists, expensive silicon manufacturing equipment/processes, and planar lithography being largely ineffective in generating 3-D structures. Some of the earliest reported techniques include LIGA [Ehrfeld 1988], polyimide micromachining [Brodie 1990; Frazier 1993], SU-8 micromachining [LaBianca 1995; Lorenz 1997] and soft lithography [Jackman 1998]. This section explores both traditional MEMS (silicon) and non-traditional MEMS (glass, ceramics and polymers) approaches developed by various researchers to achieve two-dimensional and three-dimensional MEAs.

2.1.1 Two-Dimensional Microelectrode Arrays (2-D MEAs)

The first reported approach in the use of integrated circuit technologies to fabricate microelectrode arrays was reported at Stanford University (Palo Alto, CA) from the laboratory of Prof. James Angell [Wise 1969; Wise 1975] in the late 60s-early 70s. Silicon etching was being used at that time by Bell Telephone Laboratories for beam-lead ICs, and it seemed reasonable to see if similar structures could be used for electrode arrays capable of sampling neural activity throughout a volume of tissue. The resulting neural probes were the first examples of microelectrode arrays and one of the first micromachined sensors of any kind. These approaches were targeted toward *in-vivo* applications. These electrodes were constructed on thin silicon beams using gold as the electrode material. Silicon dioxide was used as the insulation material. Figure 2.1 depicts these early MEAs with recorded neural activity from cat cortex.

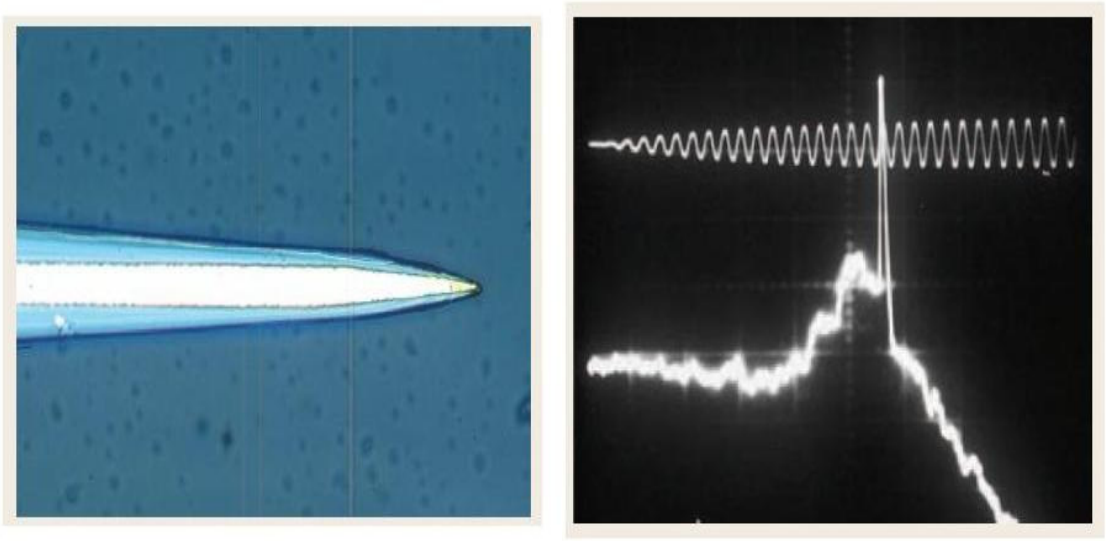

Figure 2.1: Optical image of an early 2-D MEA (left); Screen capture of neural activity of cat cortex (right) [From Wise 1969].

Around the same time Thomas et al. [Thomas 1972] at Harvard University (Cambridge, MA) constructed miniature microelectrodes with culture chambers by etching thin metal layers on glass cover slips. These MEAs were designed to interface with heart cells externally making this the first reported approach for *in-vitro* MEAs.

At the time of this pioneering research by Wise et al. and Thomas et al., the conventional approaches for studying electrogenic cells was metal wires or glass micropipettes with an electrolyte to conduct electrical activity of cells [Frank 1964]. These traditional approaches result in a great deal of knowledge about the activity of single cells and hence are applicable even today [Safranov 2007; Koppl 2007], but these approaches offer little in terms of the functional organization of electrogenic cells and networks. The fabrication of these devices is more "art" than science and imposes inherent limitations in reproducibility, precision and impedance of these devices. Examples of a wire electrode is depicted in Figure 2.2.

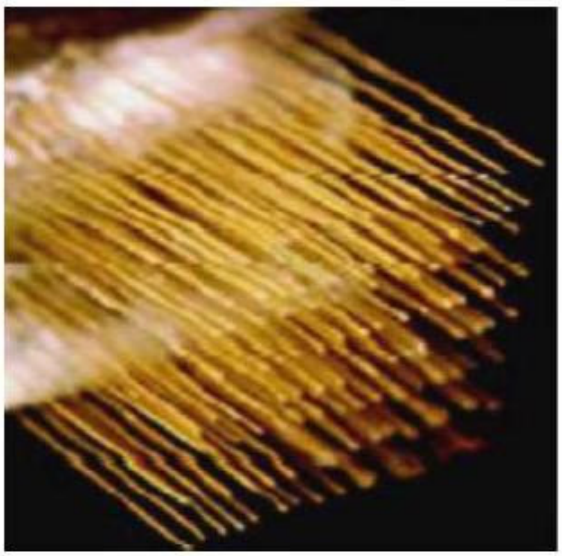

Figure 2.2: Example of an array of wire electrodes for *in-vivo* applications [From Polikov 2005].

Another early approach toward development of MEAs was on non-conventional substrates and is reported by May et al. [May 1979]. They demonstrated the fabrication of a 2-D MEA on a sapphire substrate with tantalum metal traces and platinum electrodes. They used tantalum due to the excellent properties of a self passivating layer of tantalum pentoxide (native oxide of tantalum) that preserves the quality of the metal electrodes and traces for long-term *in-vivo* stimulation and recording (not demonstrated). Sapphire also provides the excellent mechanical ruggedness required for an *in-vivo* MEA.

Prof. Guenther Gross, now at University of North Texas (Denton, TX) reported the fabrication of MEAs and *in-vitro* cultures as early as 1977 [Gross 1977; Gross 1979]. These MEAs combine photolithography and laser-etch techniques to achieve a high density array and *in-vitro* recordings of electrical activity of more than 30 neurons that were dissociated from snail ganglia.

Prof. Jerome Pine at California Institute of Technology (Pasadena, CA) has been working with MEAs since the 1980s [Pine 1980]. In collaboration with Prof. Yu-Chong Tai (also at Cal Tech) the Pine group report integrated fabrication approaches for an all silicon structure consisting of etched wells whose size is slightly smaller than hippocampal neuronal cell (around 16μm) integrated with platinum electrodes and silicon nitride insulation [Tatic-Lucic 1994; Maher 1999]. The idea was to trap the body of a single neuron in a well and an array of such well electrodes to culture networks of neurons *in-vitro*. Figure 2.3 portrays an SEM of such a device.

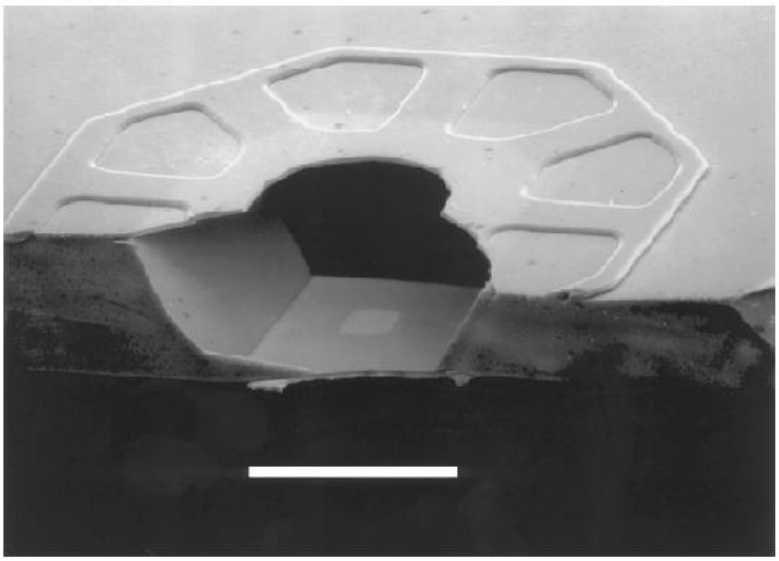

Figure 2.3: Single well approach to capturing a neuron on a planar MEA. The scale bar in the image is 20μm [From Maher 1999].

Prof. Bruce Wheeler at the University of Illinois (Urbana-Champaign, IL) is another pioneer of the MEA technology and reports on 2-D MEA fabrication techniques from his group start as early as 1986 [Novak 1986]. These MEAs were rigid structures fabricated on glass substrates with gold electrodes that had deposits of platinum black. This is probably the first reported use of platinum-black (to help lower the impedance of electrodes) in MEA fabrication. They also report recoding spike activity in abdominal ganglion of marine mollusk. Boppart et al. [Boppart 1992] report one of the first attempts to fabricate flexible (potential advantages include conforming to shapes of various tissue, cultures and injury studies) and perforated (ensures better circulation of nutrients, longer culture times *in-vitro*) 2-D MEAs using polyimide as the substrate. They have used gold as the electrode material and polyimide as the insulation. These perforated structures

have been reported to have improved the longevity of slice cultures by around 4 times as opposed to non-perforated devices.

Naturwissenschaftliches und Medizinisches Institut an der Universitat Tubingen (Reutlingen, Germany) has been a major player in the MEA development since early 1990s [Nisch 1994; Janders 1996; Stett 2003]. Nisch et al., report fabrication of MEAs on glass substrates with either TiN or iridium as the electrode material using standard lift-off processes. The metal traces on the glass substrates are defined using another lift-off process with gold. These electrode materials have been selected to achieve a high specific capacitance of the electrodes enabled by a higher surface area. This process has been commercialized by Multi Channel Systems (MCS, Reutlingen, Germany) along with interfacing circuits and systems. The MCS interfacing systems have been used in this dissertation for biological characterization of the MEAs. Figure 2.4 depicts optical and SEM images of these MEAs.

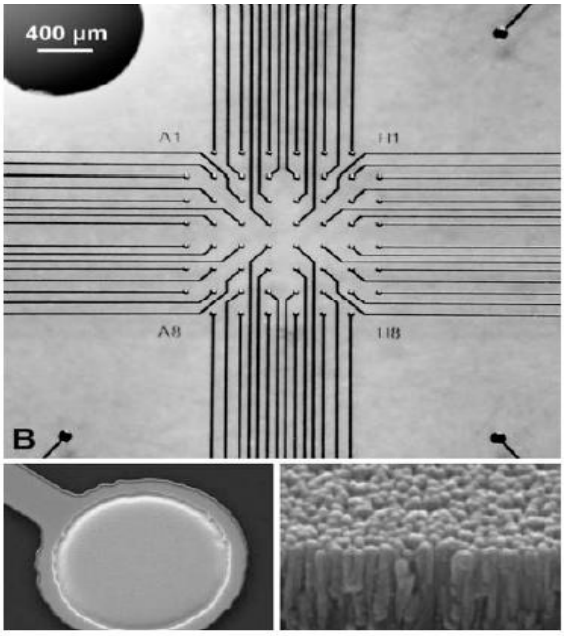

Figure 2.4: Optical (top) and SEM images (bottom) of 2-D MEAs from NMI [From Stett 2003]

In all of the approaches reported so far in this section, the electronics to interface with the MEAs (signal conditioning, stimulation, multiplexing, amplification, data collection etc) is performed with off-chip components. This leads to potential issues with MEA-CMOS interconnection, packaging, loss of weak electric signals generated and also poses limits on the array size. As the 2-D MEA technology matured in the 1990s and with the dramatic progress in silicon CMOS, it is only natural that researchers began to investigate the integration of MEAs onto CMOS chips. Prof. Gregory Kovacs' group at Stanford University (Palo Alto, CA) and Prof. Andreas Hierlemann's group at ETH Zurich (Zurich, Switzerland) are at the forefront of this CMOS-MEA technology [Borkholder 1998; DeBusschere 2001; Franks 2003; Heer 2006; Frey 2007] These groups along with the Fromherz group [Eversmann 2003] at Max Planck Institute (Martinsried, Germany) and the de Rooij group at University of Neuchatel (Neuchatel, Switzerland) [Berdondini 2002] have reported various high density 2-D arrays that use post-processing techniques to fabricate the microelectrodes after the CMOS electronics has been structured using commercially available processes. Some of these approaches report stimulation and recording functionalities while certain others report just recording and imaging. Figure 2.5 represents an optical image of such an integrated MEA. Many of these reported CMOS-MEAs are used as sensors for detection of chemical and biological toxins. They have also been utilized for screening of pharmacological compounds.

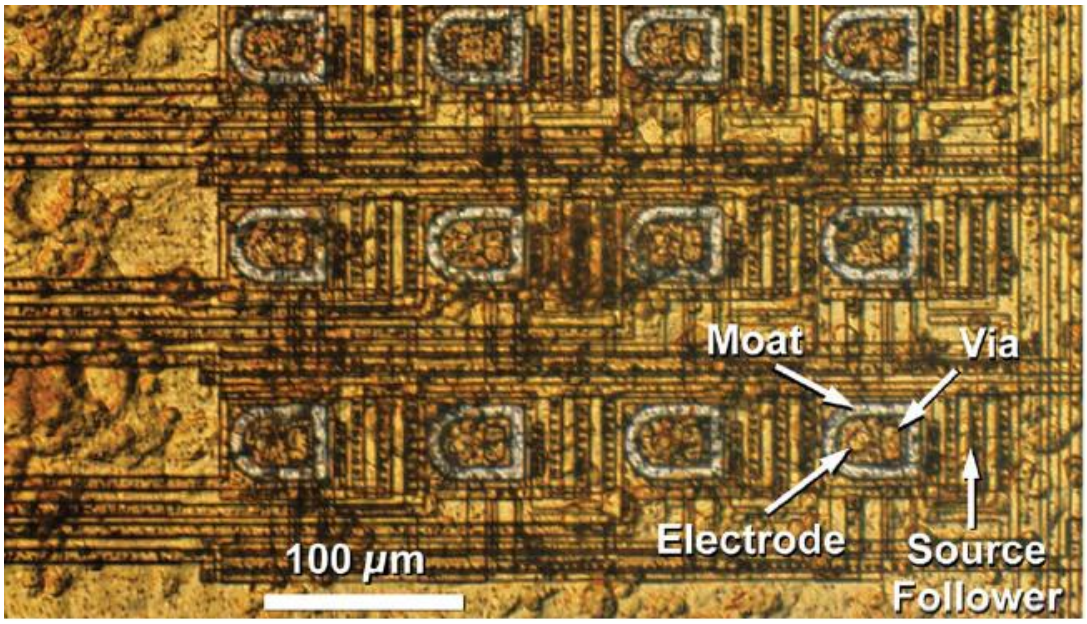

Figure 2.5 CMOS MEAs with HL1 myocardial cells growing on the MEA. The optical image clearly depicts electrode and CMOS areas [From DeBusschere 2001].

Another novel application for MEAs is the study of traumatic brain injury (TBI), which is a major area of study for neurophysiologists [Cullen 2005]. In order to mimic TBI *in-vitro* to obtain models that are comparable to *in-vivo* studies, stretchable MEAs are required so that electrophysiological events can be recorded before, during and after an injury. This requirement is resulting in a recent trend toward fabrication of MEAs using elastomeric polymers. Fabrication of MEAs using polymers also has advantages of cost-effectiveness and potential for large volume manufacturing. Lacour et al. report MEAs fabricated on a PDMS substrate toward such a goal [Lacour 2005] with gold leads and PDMS insulation. Since PDMS is not compatible with rigid insulation materials and susceptible to organic solvents dry film resists and water-based solvents are used in this novel process.

Flexible MEAs for *in-vivo* applications like retinal prosthesis, cochlear implants and insertion devices have been demonstrated by various researchers. Bell et al. [Bell 1997] report the first use of implantable rigid MEAs for cochlear applications. These electrodes are defined using a layer of titanium-iridium on a silicon wafer and released using the dissolved wafer process [Bell 1998]. The devices were tested by implanting them in guinea pig cochlea and stimulating the cochlea and recording responses to this stimulation in the brain. Rodger et al. [Rodger 2007] recently reported the use of flexible MEAs for retinal prosthesis and spinal cord stimulation. The MEAs were fabricated using alternating layers of parylene and metal (Ti/Au) with vias to interconnect these layers defined using RIE etching of parylene. These are currently being tested for retinal stimulation in canine models. Figure 2.6 shows an image of such a flexible MEA which can conform to the shape of the organ it is being implanted in.

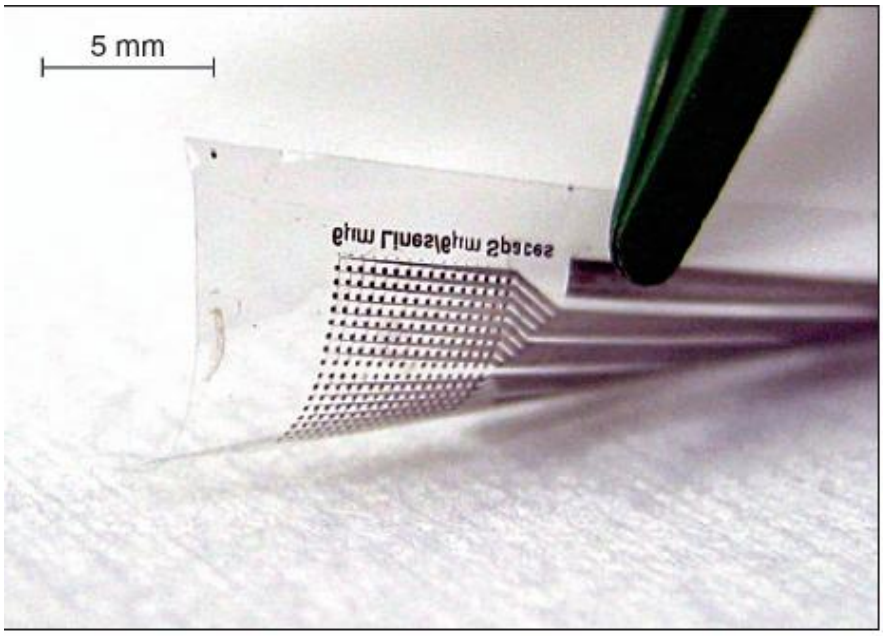

Figure 2.6: Parylene MEAs with 256 recording sites used for *in-vivo* implants [From Rodger 2007]

The MSMA group at Georgia Tech has been working in the area of MEAs since 1993. Rigid and flexible MEAs for use as insertion devices have been demonstrated by our group. Frazier et al. [Frazier 1993] report construction of metallic shank electrodes by electroplating nickel (or other suitable biocompatible metal) using a polyimide mold on an etched silicon diaphragm and using silicon nitride as the insulation material for chronic implants. These structures have shown repeated insertion in olfactory bulb of lab rats with very little damage to the electrode structure due to the high yield strength of nickel.

O'Brien et al. [O'Brien 2001] have reported the fabrication of flexible MEAs with embedded rigid structures that have been demonstrated for insertion into neural tissue. The structural material used for the flex MEAs is polyimide with a layer of metal embedded between two compliant polymer layers as portrayed in Figure 2.7. The rigid metallic structure that provides the structural rigidity needed to handle the MEAs is electrodeposited in the final step of the process.

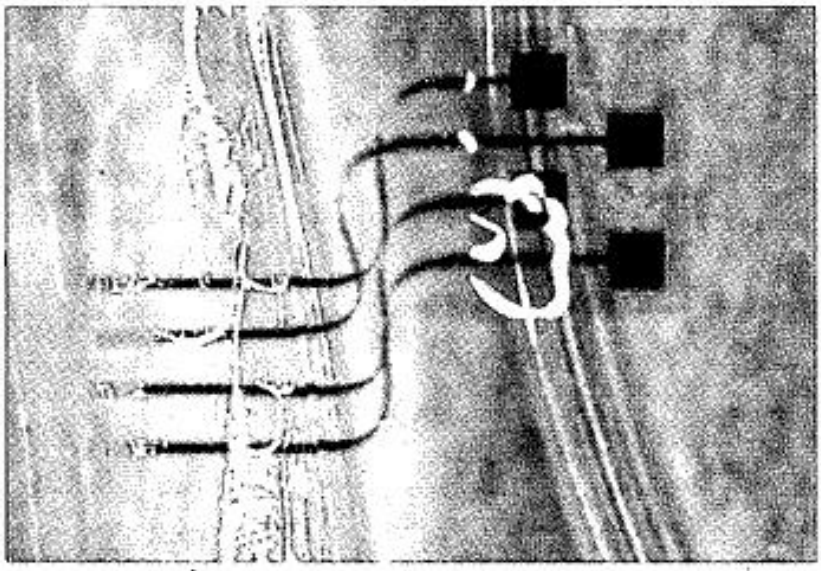

Figure 2.7: Polyimide based flex MEAs inserted in gelatin [From O'Brien 2001].

These MEAs were inserted into the distal tendon of a cat gastrocnemius muscle whose activation using the corresponding nerve was picked up by the MEAs. More recently McClain et al. [McClain 2008] have demonstrated embedded gold electrodes created using lift-off on multiple layers of PDMS to create flexible MEAs as shown in Figure 2.8.

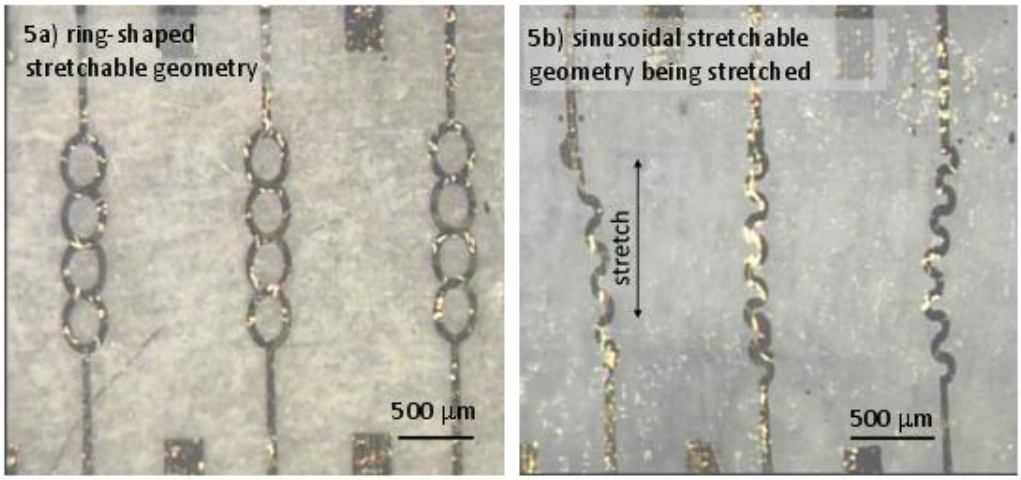

Figure 2.8: Flexible PDMS MEAs with different geometries for different applications [From McClain 2008].

These MEAs are designed to address the needs of implantable devices to study mechanical injury to the brain. PDMS has 2 major advantages over silicon *in-vivo* MEAs – biocompatibility and softer material with low stiffness (2.4MPa) which is only approximately two orders of magnitude greater than brain tissue as opposed to silicon (stiffness of 200GPa) which is 6-8 orders of magnitude greater.

Some of the MEA work reported in this chapter has been commercialized. The prominent 2-D MEAs manufacturers are:

1. Ayanda Biosystems based out of Lausanne, Switzerland [Ayanda Biosystems, 2007].

2. Alpha Med Sciences, a division of Panasonic based out of Osaka, Japan [Alpha Med Sciences 2007].

3. Multichannel Systems [Multichannel Systems 2007] based out of Reutlingen, Germany which has been discussed before.

4. Axion Biosystems [Axion Biosystems 2008] is a start-up based out of Georgia Tech is currently trying to commercialize novel MEA technologies and interfacing circuits.

2-D MEA technology is well characterized and is still a standard in most electrogenic cell measurements, but has enormous limitations. First and foremost, most of these approaches are still based on glass or silicon making their manufacturing expensive and inaccessible to majority of the end users who usually tend to be biologists or chemists. For *in-vivo* applications, acquiring data from probes requires lead cables and wires coming out of an implanted MEA which is cumbersome and extremely invasive. Wireless neurosystems is a solution that has been proposed by the University of Michigan (Ann Arbor, MI) with a silicon shank system of probes with supporting electronics at the periphery of the probe [Wise 2005]. However there are limitations on the length of the shank, biocompatibility, versatility (this technology would be applicable only in an invasive *in-vivo* setting) and material set involved (has to be an all silicon process for CMOS-MEMS integration). The demonstration of this technology is still in its nascent stage. The most important limitation of 2-D MEAs is the fact that as cultures of electrogenic cells mature in an *in-vitro* setting, they tend to have a 3-D structure.

Tissue slices are inherently 3-D in nature. Establishing a tight seal between the culture and electrode surface becomes a difficult proposition due to dead cell layers leading to loss of synaptic arrangement, poor signal to noise, loss in amount of data, possibility of aberrant recordings, and contamination.

Heuschkel et al. simulated 2-D and 3-D microelectrodes for *in-vitro* applications and found 3-D electrodes to be much superior to their 2-D counterparts [Heuschkel 2002] as they provide the spatial environment that resembles the *in-vivo* setting. They analyzed the data obtained from 2-D MEAs and compared it to data from glass pipettes and found that the data from the 2-D MEA structures were an order of magnitude lower than the traditional, non-repeatable pipettes approach. Taking into account the lack of tight seal due to the dead cellular layer, it is evident that electrode is not close to the point of origination of the signal. Their simulations were for electrodes that were elevated just a 100µm above the planar surface. If this height can be increased to 300-500µm, the problems with signal attenuation, dead cell layers etc. can be alleviated and many potential neural network properties can be unraveled.

Thus, there is an enormous need for 3-D MEAs in basic neural research, biosensing, pharmacological, prosthetics and neuro-muscular applications. Section 2.1.2 presents a summary of the developed 3-D MEA approaches by researchers around the world with their advantages and limitations. Table 2.1 summarizes all the approaches for 2-D MEAs that are described in this section.

Table 2.1: Summary of approaches described for two-dimensional MEAs.

Source	Material	Fabrication Approach	Application	Features
Wise 1969; 1975	Silicon	Thin film; silicon etch	*in-vivo* neural in cats	First reported MEAs
Thomas 1972	Glass	Thin film; glass etch	*in-vitro* cardiac cells	First reported *in-vitro*
May 1979	Sapphire	Thin film		
Gross 1977; 1979	Glass	Laser etch; lithography	*in-vitro* neural snail ganglia	
Novak 1986	Glass	Thin film	*in-vitro* marine mollusk	First Pt-black deposition
Boppart 1992	Polyimide	Thin film on PI; lift-off	*in-vitro* rat hippocampal	Perforated MEAs
Frazier 1993	Nickel	Electroplating on PI mold	*in-vivo* insertion cats	MSMA Group
Tatic-Lucic 1994; Maher 1999	Silicon	Etched Si wells for single neurons	*in-vitro*	
Nisch 1994; Stett 2003	Glass	Thin film; lift-off	*in-vitro* cardiac, neural	Commercialized
DeBusschere 2001; Frey 2007	Silicon	CMOS MEAs	*in-vitro*	Circuits & MEA on same chip
O'Brien 2001	Polyimide	Lithography; electroplating	*in-vivo* muscular, insertion	MSMA Group
Lacour 2005	PDMS	PDMS coat; lift-off	*in-vitro* TBI	
Rodger 2007	Parylene	Multi-layer parylene & metal	*in-vivo* retinal, spinal	
McClain 2008	PDMS	PDMS coat; lift-off	*in-vivo* TBI	MSMA Group

2.1.2 Three-Dimensional Microelectrode Arrays (3-D MEAs)

Prof. Kensall Wise's group at the University of Michigan (Ann Arbor, MI) and Prof. Richard Normann's group at the University of Utah (Salt Lake City, UT) have been at the forefront of 3-D MEAs for *in-vivo*, implantable applications. Overviews of these probes with their tailored applications are given in review articles by Wise [Wise 2005] and Normann [Normann 2007]. They are briefly discussed in this section.

The Michigan probes are electrode structures embedded in a platform that supports on-chip electronics and signal processing for wireless communication to the outside world. Recording sites are placed along the length of a silicon shank and several hundred can be placed on a single 2-D probe. The basic structure of these probes is similar to the one described in the 2-D MEA section [Bell 1997]. It has a silicon shank of a certain length that contains gold or iridium recording sites. Figure 2.9(a) illustrates a schematic of a single probe and Figure 2.9(b) depicts images of fabricated Michigan probes.

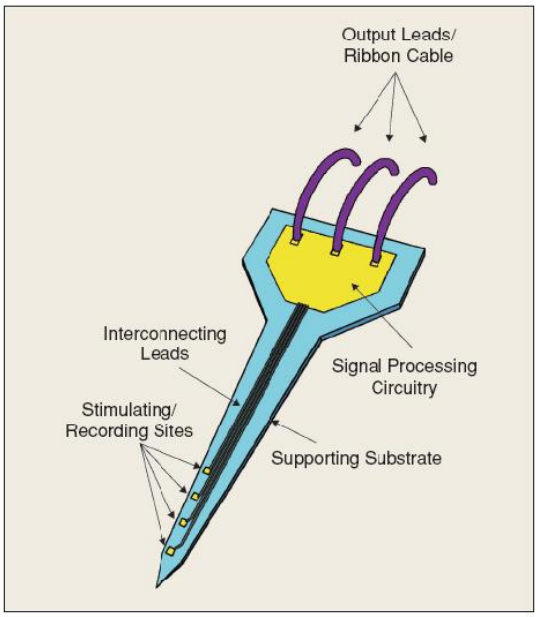

Figure 2.9 (a): Schematic of the integrated Michigan probes [From Wise 2005].

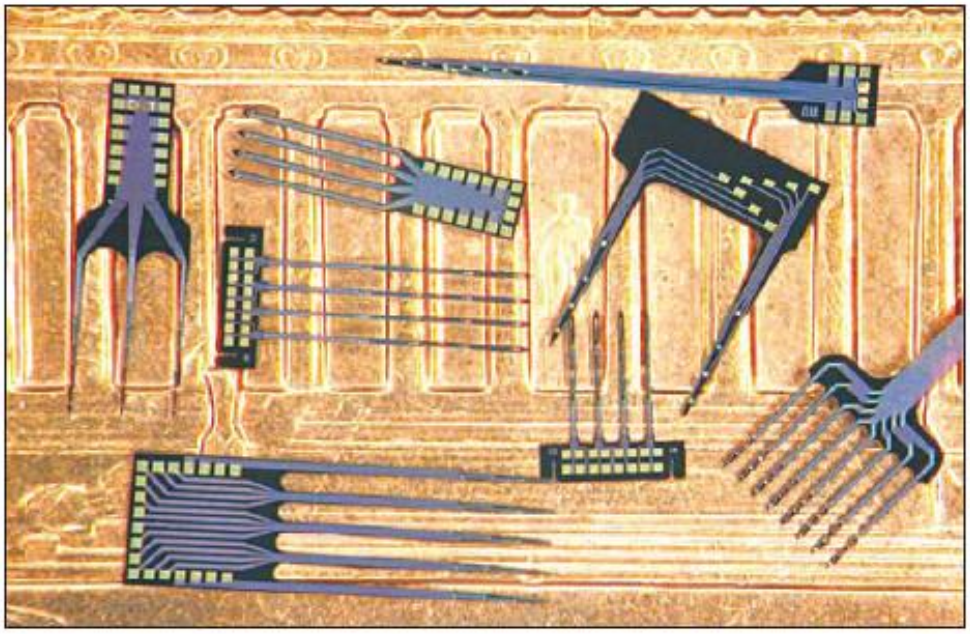

Figure 2.9 (b): A variety of silicon probes on the back of a US penny [From Wise 2005].

Doped etch stops are defined at the beginning of the process [Najafi 1985]. Conductors of polysilicon or metals extend from the recording sites up to the probe shanks at the rear end of the substrate and are insulated above and below using silicon dioxide and silicon nitride layers. Once the definition of the metal and insulation layers has been accomplished, the 2-D shanks are released in basic etchants such as ethylenediamine pyrocatechol (EDP). This fabrication technique is versatile to produce arbitrary 2-D probe shapes and site configurations with dimensions controlled to an accuracy of ± 1μm. Active probes (with circuitry) are fabricated along similar lines with additional CMOS processing and combining steps (eg. boron etch stop diffusion and p-well diffusion performed at the same time) where possible.

In order to develop a truly 3-D MEA, Qing et al. [Qing 2000] and Ghovanloo et al. [Ghovanloo 2005] report assembly processes that take these individual 2-D probes and arrange them together on a silicon substrate or with glass spacers with pads defined to connect the metal pads on the probes to the pads on the substrate. Assembled 3-D MEAs are shown in Figure 2.10.

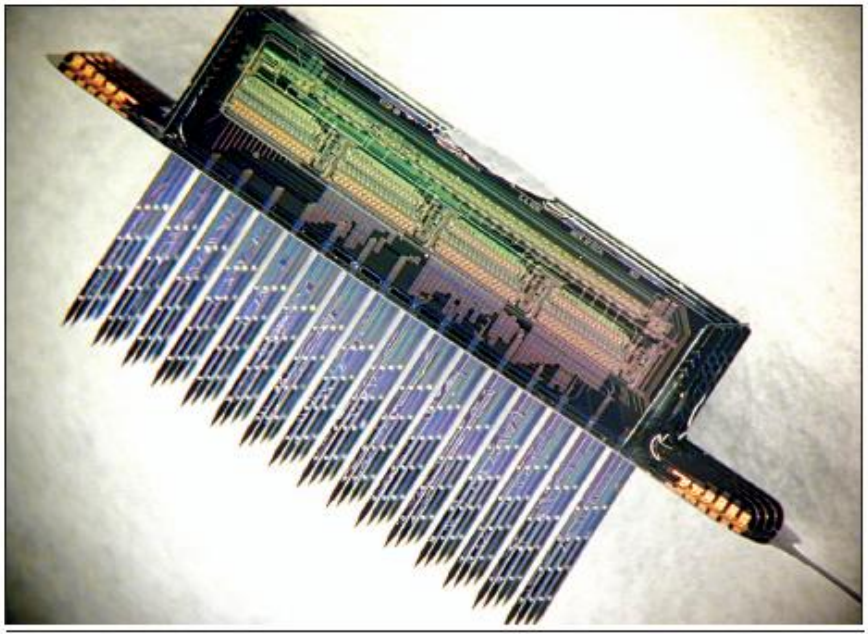

Figure 2.10: An assembled 3-D MEA with 64 site stimulating probes [From Wise 2005].

The assembly process involves the use of vacuum, micromanipulators and ultrasonic bonding for interconnects. Papageorgiou et al. [Papageorgiou 2001] report the integration of microfluidic ports by the addition of one single mask to the basic 2-D probe fabrication approach for drug delivery applications. The Michigan probe arrays are well characterized for *in-vivo* applications including retinal prosthesis, cochlear implants, and fundamental neural interfacing studies. However, the probes are silicon-based thus requiring additional processing (like parylene encapsulation) to ensure biocompatibility

for chronic use. The process of fabricating the probes is a complex multi-mask process and in order to produce truly 3-D MEAs, manual assembly processes are required.

The Utah Electrode Array (UAE) consists of one hundred 1.5mm long microneedles that were designed to be inserted into the cerebral cortex at a depth of 1.5mm, the level of normal neural input to the cerebral cortex [Rousche 1998]. The electrodes of the UEA and Utah Slanted Electrode Array (USEA) are built on a square grid with 400μm spacing. The fabrication process is described by Jones et al. [Jones 1992] and Campbell et al. [Campbell 1991]. It consists of steps for fabrication of microneedles on a monolithic piece of silicon using thermomigration to create p-silicon islands in n-silicon followed by microsawing and acid etching to form a sharp, individually isolated 10 x 10 array of needle type structures. The silicon needles were converted to electrodes by depositing multiple metal stacks and a 2-3μm polyimide layer was used as insulation. Both these steps used a metal foil as a shadow mask to define individual metal traces or polyimide etching in areas between the microneedles. Figure 2.11 shows a representative array each of UAE and USAE.

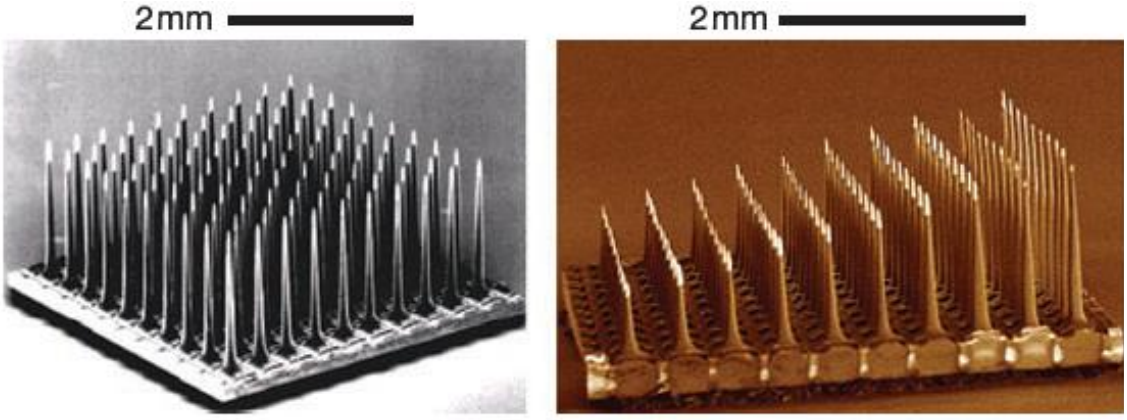

Figure 2.11: Optical images of Utah electrode arrays and Utah slanted electrode arrays [From Normann 2007].

A multiple metal stack bond pad was deposited on the backside of each electrode and wires were hand-soldered for external access to circuits. Recently Bhandari et al. [Bhandari 2007] describe fabrication of convoluted shaped Utah Array electrodes for similar applications. The process utilizes microsawing and acid etching to create the microneedles followed by metal foil masked metallization and utilization of parylene to insulate the microneedles. The tips are de-insulated by coating a thick layer of photoresist and plasma etching the parylene. These arrays have been successfully inserted in several cortical studies for neural, retinal and motion-based prosthetic applications. Cyberkinectics Inc. [Cyberkinectics 2007] based out of Foxborough, MA (with production at Salt Lake City, UT) has been able to successfully commercialize this rather complicated process and also provides electronics to interface with these arrays. The disadvantages of the Utah array in spite of the tremendous progress made over the years are cumbersome fabrication that involves microsawing and thermomigration based processes. The packaging of these devices is not trivial either.

Fofonoff et al. [Fofonoff 2004] report a very interesting Electrical Discharge Machining (EDM) based fabrication technique for 3-D MEAs for *in-vivo* recordings from cortex of a mouse. Using EDM micromachining of individual electrodes in a 10 x 10 array fashion (and other designs) is accomplished. The microelectrodes are 1mm in length, 80μm wide and have an inter-electrode distance of 400μm. These can be machined out of several biocompatible metals like stainless steel and titanium. EDM is expensive, limited to metals and size of holes that can be machined is limited to 50μm [Kobsa 1996]. Also packaging and isolation of electrodes are challenging. Some initial

demonstration of polyimide packages and parylene deposition (followed by laser removal) as insulation has been reported.

There have been other reported assembly-based approaches toward 3-D MEAs. At Georgia Tech, Rowe et al., [Rowe 2005] report a microscaffold system consisting of an 8 x 8 array of SU-8 probes packaged in a silicon orifice plate. Fabrication of the SU-8 probes with fluidic and electrical functionalities in a planar fashion with multiple SU-8 coating steps interspersed with metallization on a silicon substrate is reported. The probes are then released by undercutting a sacrificial chrome layer that is deposited at the beginning of the process. The planar probes are assembled manually in a DRIE etched silicon substrate to form a 3-D MEA as represented in Figure 2.12.

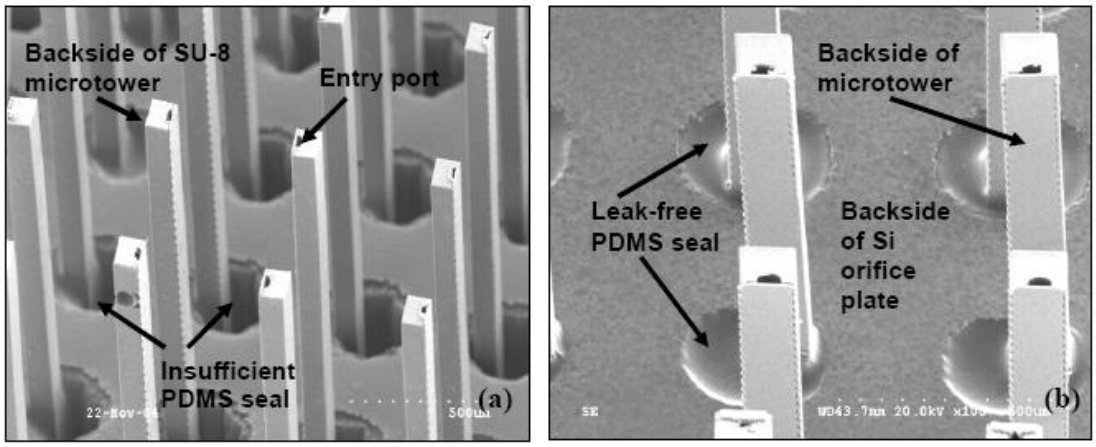

Figure 2.12: SEM of assembled 3-D MEAs fabricated by planar 2-D arrays with electrical and fluidic functionalities and packaging these arrays with hand in a silicon orifice [From Rowe 2005].

The probe assembly process is not trivial as is the actual electrical connectivity to the outside world. Preliminary electrical characterization of these probe arrays and survival of 3-D neuronal cultures on these arrays for 21 days *in-vitro* has been reported [Rowe

2007]. This approach is very novel in its scope and is a step toward polymer-based 3-D MEAs, but the tedious assembly process makes it manufacturing-unfriendly. Also the extent of biocompatibility of thick SU-8 is an ongoing debate in the neurological community.

NeuroProbes is a recent European Commission project with the aim of manufacturing integrated neurosystems for *in-vivo* applications like management of epilepsy. Kisban et al. [Kisban 2007] have demonstrated a preliminary probe fabrication process consisting of standard silicon etching and lift-off metallization. These probes are shown in Figure 2.13.

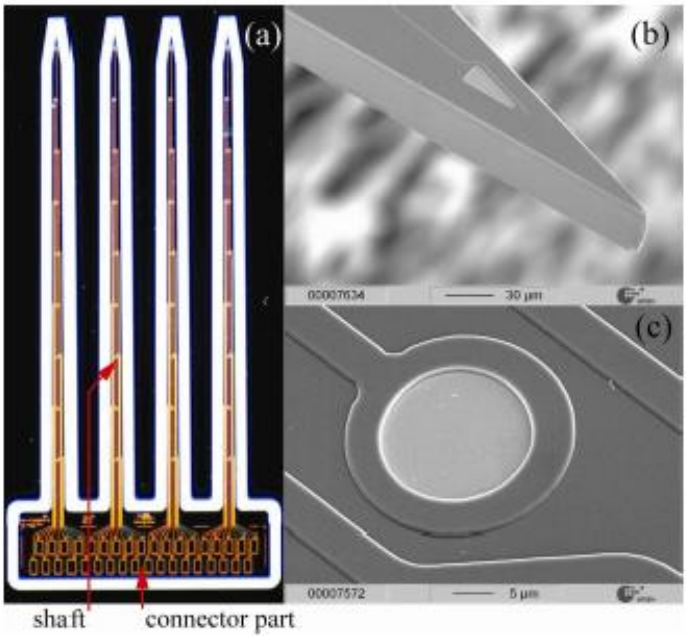

Figure 2.13: Optical and SEM images of silicon probes from the NeuroProbes project [From Kisban 2007].

A silicon dioxide/silicon nitride stack is used as the insulating material in this process. Multiple packaging approaches are necessary in this process – one to connect the leads of

the probes to a ribbon cable which then serves as an interface to a PCB where the electronics is embedded (proposed, not demonstrated yet). This technology is still in its infancy with questions about packaging and assembly of probes still not completely answered.

Integrated fabrication approaches for *in-vitro* MEAs are however very rare. This is in part due to difficulties in 3-D lithography and packaging challenges. Thiebaud et al., report one of the first approaches in this area. Two versions of 3-D MEAs are reported – one that is "3-D-like" (electrodes that are actually 2-D but are constructed on a tall perforated substrate making them 3-D like) and 3-D tip electrodes (47μm in height) using similar approaches [Thiebaud 1997 and 1999]. 2-D electrodes on a silicon wafer were created by standard techniques of metal lift-off (Ta/Pt has been used as the electrode) and a composite SiO_2/ Si_3N_4 insulation. Trenches that are 380μm deep have been created using the standard BOSCH etching process and platinum has been deposited near the top of these trenches using cyclic voltammetry giving the MEA "3-D-like" properties. They have further demonstrated the use of the MEA as a biosensor by recording the response of a toxin (picrotoxin) from hippocampal slices of rats.

Metz et al. [Metz 2001] and Heuschkel et al. [Heuschkel 2002] of the Prof. Philippe Renaud group at EPFL, Switzerland (Lausanne, Switzerland) report fabrication of 30-70μm tall tip shaped electrodes in polyimide and glass respectively as shown in Figure 2.14. In the case of the polyimide devices, the electrodes are made of platinum and are constructed using anisotropic etching of silicon to create V-shaped sharp grooves and finally released by sacrificially etching the silicon away.

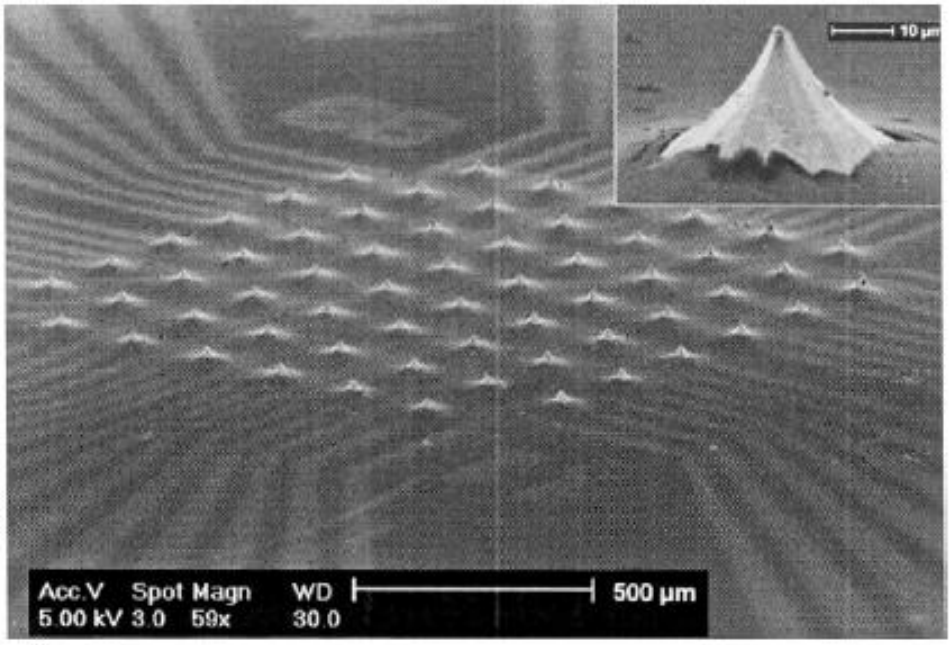

Figure 2.14: Tip shaped electrodes fabricated by etching glass. Height of the electrodes is around 60 µm [From Heuschkel 2002].

The glass based devices are fabricated by undercutting a mask of photoresist/chrome in HF and then depositing an electrode (Ti/Pt) and a layer of SU-8 as insulation. These devices have been tested by several *in-vitro* neuronal cultures and are currently being commercialized by Ayanda Biosystems (Lausanne, Switzerland). These devices have a very interesting approach with potential for high-density arrays but there are limitations on how tall these can be fabricated (typically lower than 100µm). As stated in section 2.1.1, better performance metrics (signal to noise, elimination of aberrant recordings and minimizing the effect of dead cell layers) are obtained with *in-vitro* MEAs approaching the height of *in-vivo* ones (usually 1-1.5mm long).

Recently integrated microfabrication approaches for 3-D MEAs have been reported by Chu et al. [Chu 2005], Koo et al. [Koo 2006] and Takei et al. [Takei 2007]. The

features common to these fabrication approaches are: 1. The MEAs are all silicon-based devices. So the biocompatibility and cost-effectiveness are debatable; 2. These involve a combination of ICP, KOH or XeF_2 etching processes to create 3-D electrodes in silicon. In the case of Takei et al., an exotic yet unproven technique to grow silicon tubes on a wafer by vapor liquid-solid (VLS) technique is reported; 3. All these technologies provide electrodes that are less than 100μm tall; 4: Packaging of these electrodes is still rudimentary and not completely characterized. Figure 2.15 shows an SEM image of a probe with CMOS circuitry using the VLS approach.

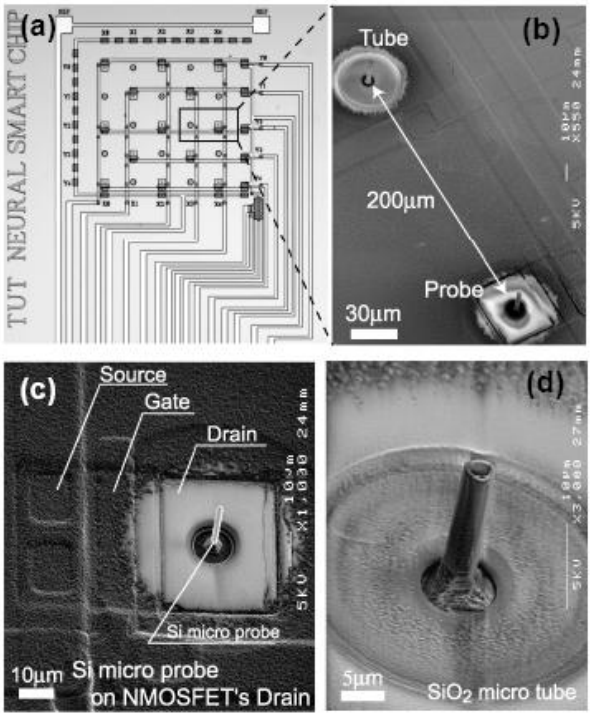

Figure 2.15: Silicon probes fabricated using VLS technique with CMOS circuits on same chip [From Takei 2007].

In conclusions there is a growing need for integrated MEMS fabrication and packaging approaches that are versatile (*in-vitro* and *in-vivo* applications), polymer-based

(addresses biocompatibility problems) and manufacturing-friendly. These approaches will answer the ever-growing needs of the neurophysiological, pharmacological, prosthetic and clinical diagnostic communities. This dissertation tries to address this need by developing technology platforms that overcome some of the limitations discussed above. A summary of 3-D MEA technologies is provided in Table 2.2.

Table 2.2: Summary of approaches described for 3-D MEAs.

Source	**Material**	**Fabrication Approach**	**Application**	**Features**
Najafi 1985; Qing 2001; Wise 2005	Silicon	Silicon planar shanks; Assembly	*in-vivo* neural, retinal, cochlear	Michigan probes; Wireless data
Campbell 1991; Normann 2007	Silicon	Microsawing; thermomigration	*in-vivo* brain stimulators	Utah Probes; Commercialized
Thiebaud 1997; 1999	Silicon	Bosch etching; cyclic voltametry	*in-vitro* biosensing	Electrode height 47μm
Metz 2001; Heuschkel 2002	Polyimide; Glass	Glass undercut; PI on silicon	*in-vitro* neural	Commercialized by Ayanda
Fofonoff 2004	Ti; Stainless Steel	Electron Discharge Machining	*in-vivo*	
Rowe 2005; 2007	SU-8	Planar fabrication; Assembly	*in-vitro* neural	Georgia Tech 3-D MEAs
Chu 2005; Koo 2006	Silicon	Etching using ICP, KOH or XeF2		Electrode height <100μm
Takei 2007	Silicon	Vapor Liquid Solid; CMOS	*in-vitro* neural	CMOS integrated; probe height< 10μm
Kisban 2007	Silicon	Planar fabrication; Assembly	*in-vivo*	Complex assembly

2.2 Electrical Background

When a metal microelectrode is immersed in a conducting medium an electrochemical equilibrium is established. This system can be modeled with passive circuit elements. The components of this lumped circuit model are discussed in this section.

2.2.1 Microelectrode Theory

When a metal is placed into an electrolyte which is a conducting solution carrying ions an electrified interface is immediately formed. Chemical reactions occur whereby electrons are transferred between the metal and the electrolyte resulting in the establishment of an electric field which influences further reactions. This electric field obviously has an influence on the electrolyte. Water dipoles orient themselves close to the metallic surface forming a hydration sheath. Beyond the water dipoles are solvated ions forming what is called the Helmholtz plane. The area beyond that is where the influence of the electric field is the strong at the interface with the Helmholtz plane but diminishes away from it in the bulk electrolyte and is called the space charge region.

Initial theories developed by Helmholtz assumed that the charge of the solvated ions was confined to the Helmholtz plane and was equal and opposite to the charge on the metal. With the water dipoles acting as a dielectric, this formed a simple capacitor [Helmholtz 1879] given by:

$$C_H = \frac{\varepsilon_0 \varepsilon_r A}{d} \qquad (2.1)$$

Here A is the area of the interface, d is the distance of the Helmholtz plane from the metal surface and $\varepsilon_0\varepsilon_r$ is the permittivity of the electrolyte. An estimated calculation for this capacitance is 0.14pF/μm^2 given by Kovacs [Kovacs 1994]. Helmholtz model is constructed on the assumption that the sheath of solvated ions is rigid. This however is not true. Gouy and Chapman introduced a sheath of mobile ions to accommodate for their movement [Gouy 1910; Chapman 1913]. This allowed for the capacitance to change with applied potential, something that was observed experimentally. The Gouy-Chapman capacitance is given by:

$$C_G = \left(\frac{\varepsilon_0\varepsilon_r}{L_D}\right)\cosh\left(\frac{zV_0}{2V_t}\right) \tag{2.2}$$

Here L_D is the Debye length that characterizes the spatial decay of potential, V_0 is the potential at zero distance from the electrode and V_t is the thermal voltage.

Stern in 1924 combined the two models above since he observed that the capacitance varied too strongly with the applied voltage [Stern 1924] with a layer of bound ions at the Helmholtz plane and a diffuse ion cloud beyond it leading to the representation of interfacial capacitance as a series combination of C_H and C_G given as follows:

$$\frac{1}{C_I} = \left(\frac{1}{C_H}\right) + \left(\frac{1}{C_G}\right) \tag{2.3}$$

Situations can be imagined where one of the components dominate this series combination leading to the value of C_I being closer to 0.14pF/μm^2, but for most

physiological systems with zero applied bias both C_H and C_G are equal to 0.14pF/μm^2 leading to a total interfacial capacitance of 0.07pF/μm^2.

The interfacial capacitance at the electrode/electrolyte interface does not describe the entire electrical picture of this interface. If a DC potential is applied across this interface, a current will flow. So it is important to add a resistor in parallel with the interfacial capacitor. The chemical reactions (oxidation and reduction) that occur when a metal is placed in an electrolyte are in equilibrium resulting in a net current of zero without the application of a potential. But there are two distinct equal and opposite currents and the absolute value of this current per unit area is called exchange current density (J_0). This is dependent on the material properties of the electrode, electrolyte and the resulting reactions. Najafi et al. calculated the value of J_0 experimentally to be equal to 2.00 x 10^{-9} A/cm^2 [Najafi 1986] for gold in buffered saline. With this current density the net current flow can be calculated in the case of the applied potential and hence the charge transfer resistance that is in parallel with the interfacial capacitance is given by:

$$R_T = \frac{V_t}{zJ_0} \qquad (2.4)$$

Here V_t is the thermal voltage at T = 37˚C and z is the valence of the ion involved in the charge transfer.

These two equations (2.3 and 2.4) describe the basic metal electrode placed in an electrolyte where the applied potential is vanishingly small. However, the spreading effects of the current from this localized electrode to a distant counter electrode (for eg. a ground placed in the electrolyte solution) also need to be included in the electrode-

electrolyte model. This resistance is called the spreading resistance (R_S) that is in series with the C_I, R_T combination and is given by:

$$R_S = \frac{\rho L}{A} \tag{2.5}$$

Here ρ is the resistivity of the electrolyte in Ω.cm, L is the effective length and A is the effective cross-sectional area of the solution through which the current passes. Various researchers have developed approximations for R_S based on the shape and configuration of the electrode. Of particular interest is a circular electrode, which is the geometric shape of the electrodes developed in this dissertation. Newman in 1966 calculated the spreading resistance to have an inverse relationship with the radius (r) of a circular electrode [Newman 1966] as given by:

$$R_S = \frac{\rho}{4r} = \frac{\left(\rho\sqrt{\pi}\right)}{\left(4\sqrt{A}\right)} \tag{2.6}$$

So we have the full lumped circuit model for this complex electrode-electrolyte interaction given by the circuit representation in Figure 2.16:

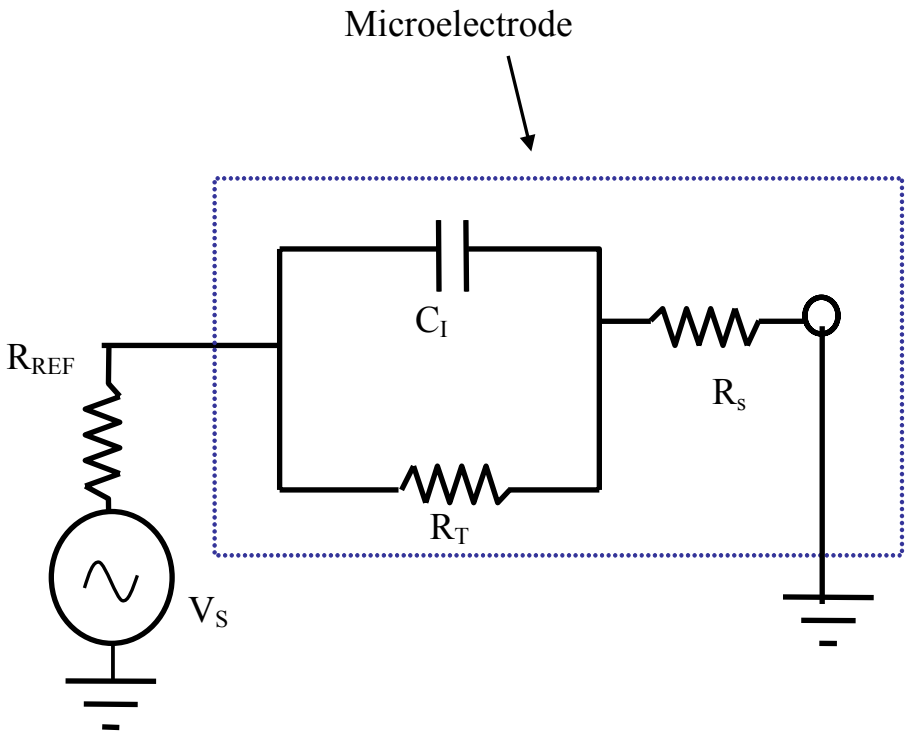

Figure 2.16: Equivalent circuit with all components for an electrode-electrolyte interface.

This model works for electrolytes that do not contain proteins or other biological material. Also the geometric area of the electrode becomes very important and it is discussed further in Chapter 4.

2.3 Biological Background

The application of the microelectrodes created using microfabrication approaches are in the biological arena specifically monitoring electrically active cells and networks. This section summarizes the prospects for MEAs with an introduction to electrically active cells.

2.3.1 Electrogenic Cellular Networks

Electrical activity of cells is responsible for much of the complex behavior of organisms. Sensory processing, cardiac and muscle functions are controlled partially by this activity of different cell types in the body. The brain and the spinal cord are at the center of much of this activity, and neurons form the functional unit of the human nervous system. In vertebrate systems, while a single neuron is not as interesting function-wise, it is the combination of many neurons working together in concert that result in triggering many of the bodily functions. Only a brief introduction to this electrical activity of cells is provided here. More detailed information in this area is provided by excellent books such as Foundations of Cellular Neurophysiology [Johnston 1995].

While there are several types of electrically active or electrogenic cells, the fundamental mechanisms of electrical activity are very similar. Structurally these cells are composed of a lipid bilayer membrane enclosing an intracellular ionic solution. This membrane contains many proteins, receptors, ion channels and pumps that are responsible for controlling the concentration of various ions with respect to the extracellular environment. Ion channels are the electrically excitable sections of a cell membrane. These allow the passage of different ionic species (Na^+, K^+, Ca^{2+}, Cl^- etc) between the intracellular and extracellular environments. The activity of an ion channel can be "gated" like that of a CMOS transistor by controlling factors like the charge, temperature, pH, mechanical force etc.

The structure of a neuron is composed of soma (the cell body), dendrites and an axon. The size of a neuron can vary from a few microns to several 100μm. Figure 2.17 schematically depicts different parts of a neuron.

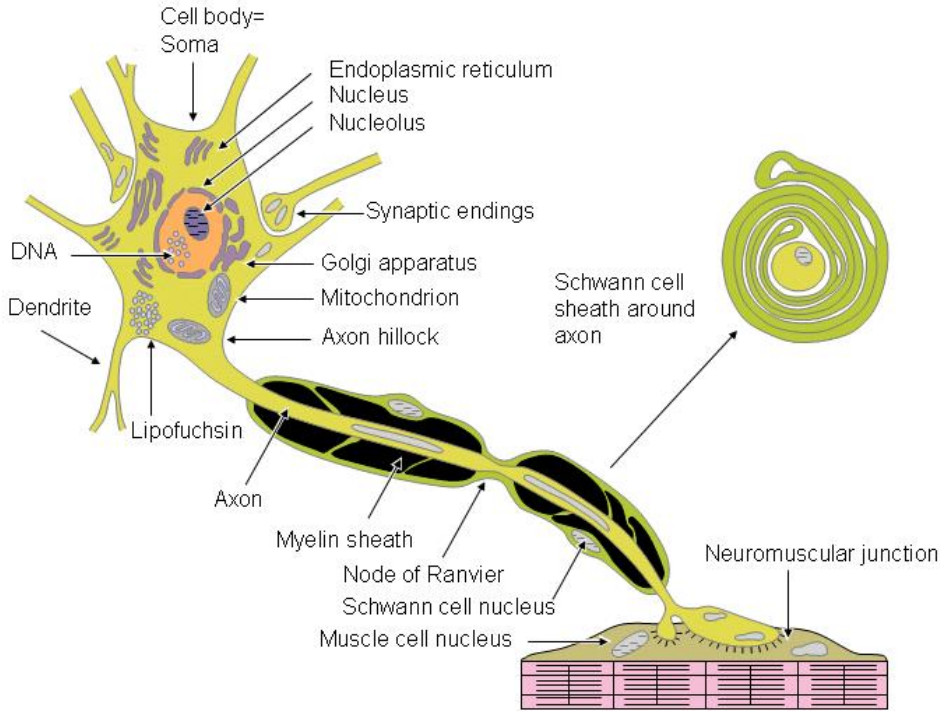

Figure 2.17: Schematic of a neuron depicting various parts of the body of a neuron and connection to a neuro-muscular junction

The cell body is similar to other cellular structures and is composed of the nucleus, mitrochondria, robosomes etc. The dendrites receive impulses from other cells and transfer then to the cell body. The axon is a long nerve fiber that transfers signals from one cell to another (neuron or muscle cell). The junction between an axon and the next cell it communicates with is called a synapse. This is the mechanism through which neurons "talk" to one another.

Muscle cells which are the other major electrogenic cellular networks that are studied as part of this dissertation. These cells are composed of among other things myofibrils which are cylindrical organells that are important in muscular contraction which in turn controls the excitability of the cell. There are three types of muscle cells: skeletal, smooth and cardiac as shown in Figure 2.18.

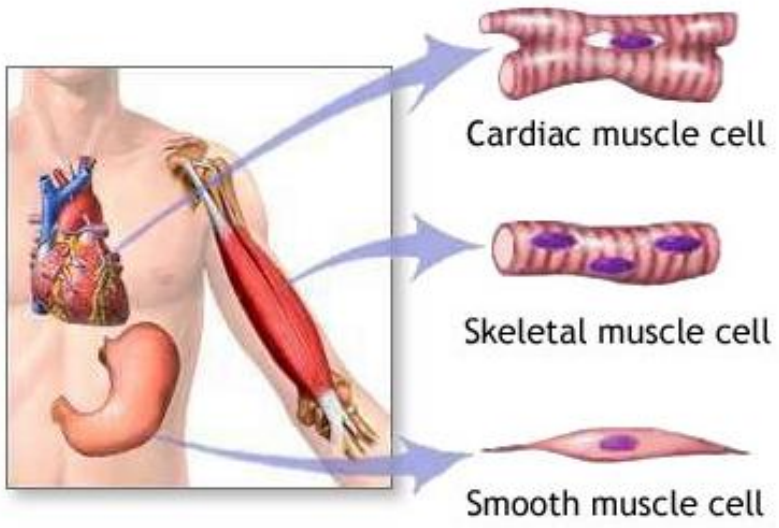

Figure 2.18: Schematic depicting various types of muscle cells and their construction in the human body.

Only a brief overview of these three types is provided here. For a detailed review of muscular activity the reader is referred to books such as Physiology of Sport and Exercise [Wilmore 2004]. The three types of muscle cells have significant differences. However, all three use the movement of actin against myosin to create contraction. In skeletal muscle, contraction is stimulated by electrical impulses transmitted by the nerves, the

motor nerves and motoneurons in particular. Cardiac and smooth muscle contractions are stimulated by internal pacemaker cells which regularly contract, and propagate contractions to other muscle cells they are in contact with. All skeletal muscle and many smooth muscle contractions are facilitated by the neurotransmitter acetylcholine.

2.3.2 *In-vitro* and *in-vivo* Prospects

Electrically interfacing with cells offers enormous opportunities for scientific discovery and medical advancement. Knowledge of the functional organization of this electrical activity and its role in disease management, therapeutic manipulations and prosthetic applications are of great importance to biology, medicine and pharmacology. MEAs offer opportunities to advance the knowledge of and develop applications for all of these fields.

Traditional neural research to unearth the properties of large networks of neurons was performed with wire electrodes and micropipettes but such approaches do not adequately capture the activity of a spatio-temporal distribution of networks of neurons. MEAs on the other hand offer opportunities to manipulate and monitor cellular activity both at a single cell level as well as at a tissue level providing extraordinary insight into the complex nature of neural interactions.

An increased number of diseases have been shown to be related to ion channel dysfunction or affected regulatory pathways [Lehmann-Horn 1999] leading to a growing interest among the pharmacology community toward instrumentation and systems targeted at studying this phenomenon. High throughput screening compatible formats are

particularly of interest in this application meaning the development of large area processes (eg. micromolding, lamination) for MEAs.

Cell based biosensing has been of considerable interest for detection of chemical, biological and environmental toxins [Kovacs 2003]. Unlike sensors based on specific molecular detection (eg. binding of antibodies) cellular responses are physiological and allow for the detection of unanticipated threat agents (as opposed to a reaction taking place) making MEA-based microsensors far more sensitive than any reaction-based sensors.

Establishing man-machine interfaces to the central or peripheral nervous systems opens up a wide variety of prosthetic applications for MEAs. In these applications high density electrode arrays are necessary to serve as the functional piece to record nerve signals and to stimulate neurons and muscles for control of limbs and organs or to elicit sensations of feeling, hearing or seeing [Wise 2005; Stieglitz 2005].

Biopotential measurements offer another avenue for MEAs to improve the current state of the art (planar electrodes). Classical minimally invasive interfaces for this application are used in a clinical setting almost of a daily basis for electrocardiography (ECG), electromyography (EMG), electroencephalography (EEG) etc. But these suffer from considerable limitations including high noise levels, low spatial resolution and unpredictable electrode placement due to anatomical variation between patients. MEAs can be utilized in this application to decrease the electrode area by an order of magnitude while maintaining signal resolution and also to minimize the invasiveness of this process (compared to needle EMG and nerve conduction studies that are painful to patients).

2.4 Chapter Discussions and Conclusions

This chapter provides the background for this dissertation. Microfabrication technologies for both **planar (2-D) and three-dimensional (3-D) electrode arrays** have been developed by various researchers around the globe. These are summarized in this chapter. Work in this fascinating area started in the late 1960s and continues today with an ever-growing list of applications developed for both *in-vitro* and *in-vivo* arenas. Both **silicon-based** and **non-silicon based** technologies are summarized. The limitations of 2-D MEAs are listed motivating the need for 3-D MEAs, which is relatively still a nascent field.

An **introduction to electrode-electrolyte** interface from a circuit perspective is presented with a lumped circuit equivalent of this interface. A model for the electrodes is developed later in this dissertation based on this equivalent circuit. Electrogenic cellular networks are also introduced with the two major types of cells that have been studied in this dissertation neurons and muscle cells described. A variety of applications for MEAs can be developed in clinical, biological, medical, pharmacological and neurological settings. The prospects for these applications are listed.

CHAPTER 3

MICROMACHINED *IN-VITRO* MEAs: LASER MICROMACHINING APPROACH

3.1 Laser Micromachining based 3-D MEAs

3.1.1 Introduction

Laser micromachining has been utilized for MEMS applications since the introduction of well focused, high intensity lasers in the 1990s [Kobsa 1996]. An excimer laser system operating at 248nm is ideally suited for micromachining polymers [Kim 2003]. In this work an excimer laser has been used to accurately micromachine a conformally evaporated polymer on metal seed layers to define electrodes on previously fabricated SU-8 tower arrays. The negative-tone photodefinable epoxy, SU-8 is a popular material in the MEMS field with single and multi-layer fabrication technologies reported by various researchers to achieve complex MEMS structures [Lorenz 1997; Cros 1998; Mata 2006; Rowe 2007]. This technology has been utilized to fabricate high aspect ratio towers that serve as excellent sites for growth and adherence of neuronal cultures. To address biocompatibility issues, a bio-friendly polymer layer has been utilized as the insulation material. These tower arrays have been packaged and evaluated electrically and biologically as described in the sections below.

3.1.2 Concept and Design

A schematic of the proposed 3-D MEA is shown in Figure 3.1. Towers are provided at a certain height above a substrate with metal traces defined on them. This structure is designed to have fluidic and electrical functionalities combined in a single device.

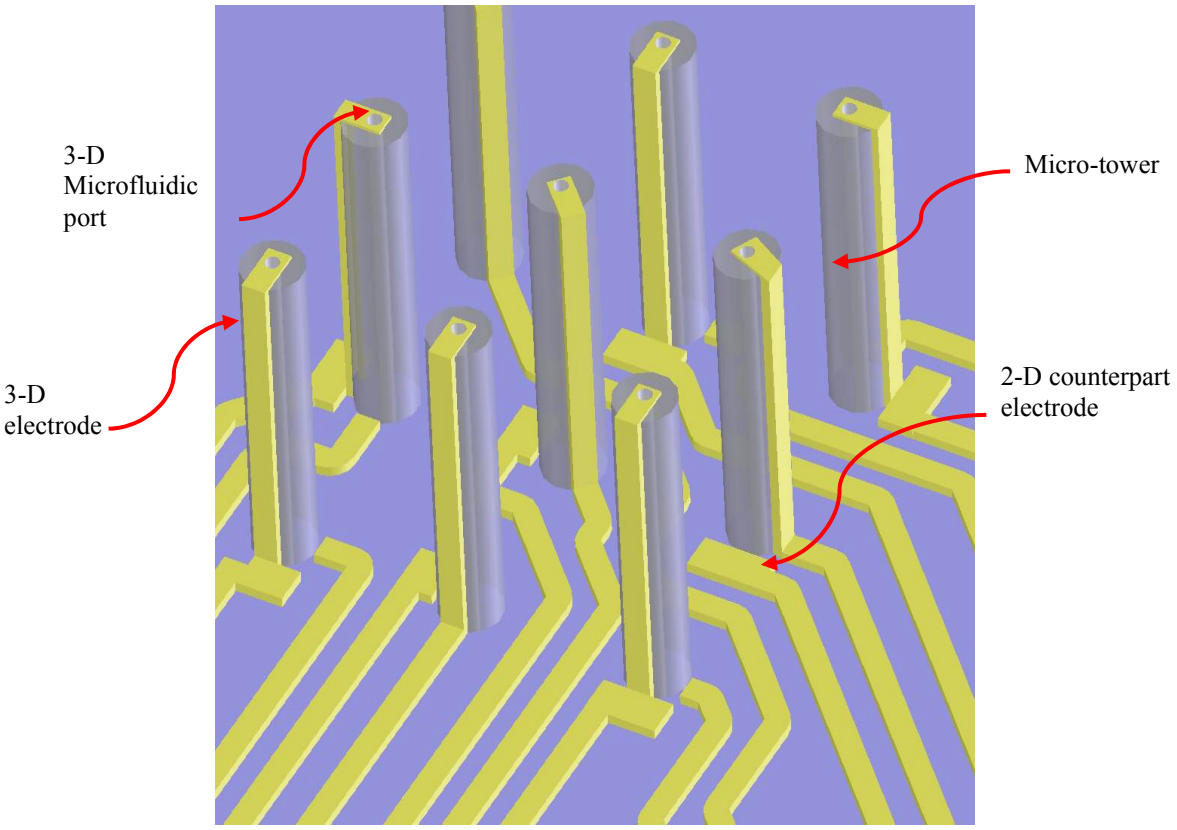

Figure3.1: Schematic illustration of the proposed 3-D MEA with metal traces to define the electrodes and a central fluidic port with neuronal culture all around the MEA.

In order to accomplish fluidic functionality, ports are provided in the center of the tower. Neuronal cultures can be grown as a network all around the towers. It is proposed that recording and stimulation of these cells is performed using the electrodes and

nutrients are introduced through the fluidic ports to keep the cells alive for longer periods of time. The concept of keeping 3-D neuronal cultures alive for longer periods of time through microfluidic nutrient perfusion (Appendix A describes some techniques to achieve 2-D and 3-D microfluidic ports) has been reported by Cullen et al. [Cullen 2007].

The design of these structures consists of a 2.75mm diameter circular substrate that will eventually house all the towers and cell networks. It was conceived for various evaluation experiments that both solid (electrical functionality only) and hollow (both electrical and fluidic functionalities) towers are built on these substrates. The mask design for both these arrays is shown in Figure 3.2. A 12 tower array design placed in the center of the circular substrate was selected for the hollow tower array.

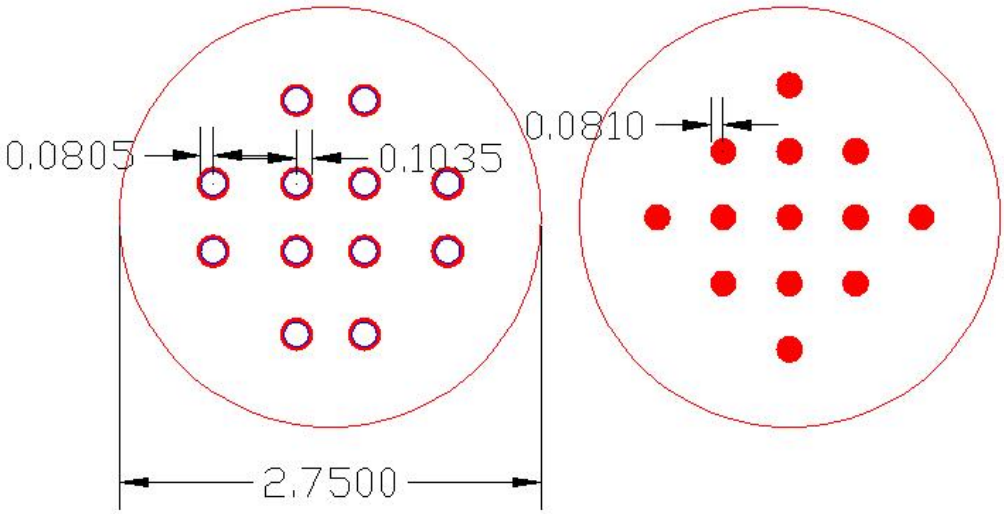

Figure 3.2: Mask design for hollow (left) and solid (right) MEA micro-tower structures. All units in the image are in mm.

These towers were designed to have an inner diameter of 160μm and outer diameter of 200μm, so that the wall thickness was designed to be 40μm. The tower arrays were targeted to be 500μm tall to get an aspect ratio of 3.125:1. Although higher aspect ratio structures have been built, this ratio was chosen to be a moderate compromise between ease of fabrication and biological application (consistent 3-D neuronal cultures to a height of 500μm). The solid structures were also built on a similar sized substrate with the same diameter as the inner diameter of the hollow towers. The number of towers however was 13. A single 4" substrate yields several hundreds of both solid and hollow micro-tower array structures resulting in batch fabrication. The two designs described above were selected for all the biological studies that were performed (described in Section 3.2.3).

3.1.3 Microfabrication: Double-side Exposure Technology

Complex 3-D fabrication technologies for MEMS devices have been developed by many researchers as stated in section 3.1.1 using the negative-tone epoxy SU-8 (Microchem Inc., Newton, MA). SU-8 was first introduced by IBM (Rueschlikon, Switzerland) and the Swiss Federal Institute of Technology (Lausanne, Switzerland) [La Bianca 1995; Lorenz 1997; Lorenz 1998A]. SU-8 can be structured to greater than 2mm in thickness with vertical sidewall definition. High aspect ratios of up to 18:1 have also been demonstrated using this material [Lorenz 1998B]. The properties of SU-8 that make it attractive for MEMS fabrication are: chemical resistance, thermal stability and photo definition. SU-8 is the ideal material for structurally defining micro-towers proposed in section 3.1.2. SU-8 has been utilized for many MEMS applications including

microfluidics [Bohl 2005], mechanical structures like microgears [Lorenz 1998B], rigid molds for micromolding [Juncker 2001], RF MEMS devices [Yoon 2005; Pan 2005] etc. The MSMA group at Georgia Tech has been active in SU-8 based research since its introduction to the MEMS community [Cros 1998] and has pioneered several technologies based on the use of SU-8 for a variety of MEMS applications.

As stated in the design section, structures for both MEAs (solid micro-towers) and MEAs with fluidic ports (hollow micro-towers) have been fabricated. The solid tower arrays with electrodes can be used to study the morphological organization and electrophysiological activity in short-term neural cultures whereas the dual functionality tower arrays are targeted for relatively long term perfused neural cultures. The fabrication process for solid and hollow (microfluidic) tower arrays is detailed in Figure 3.3. The substrate consists of a 4" chrome mask that serves a dual function: it not only acts as a temporary substrate for tower array fabrication, but is also used in the double-side exposure which will be described later in this section. The process begins with definition of the micro-tower structure locations onto the substrate (Step 1). This is performed by transferring the location patterns from a transparency mask. The transparency mask is designed using AutoCAD (Autodesk, San Rafael, CA) and printed using high resolution printers of commercial vendors like J.D Photo Tools (Oldham, England), Fineline Imaging (Colorado Springs, CO) etc. The mask is then brought in contact with a 4" chrome plate that is coated with positive resist and exposed using 100mJ of energy. The mask is removed and the exposed regions of the resist are developed away in a 5:1 solution of AZ 400K developer (Futurrex Inc, Franklin, NJ) in DI water (5 parts DI to 1

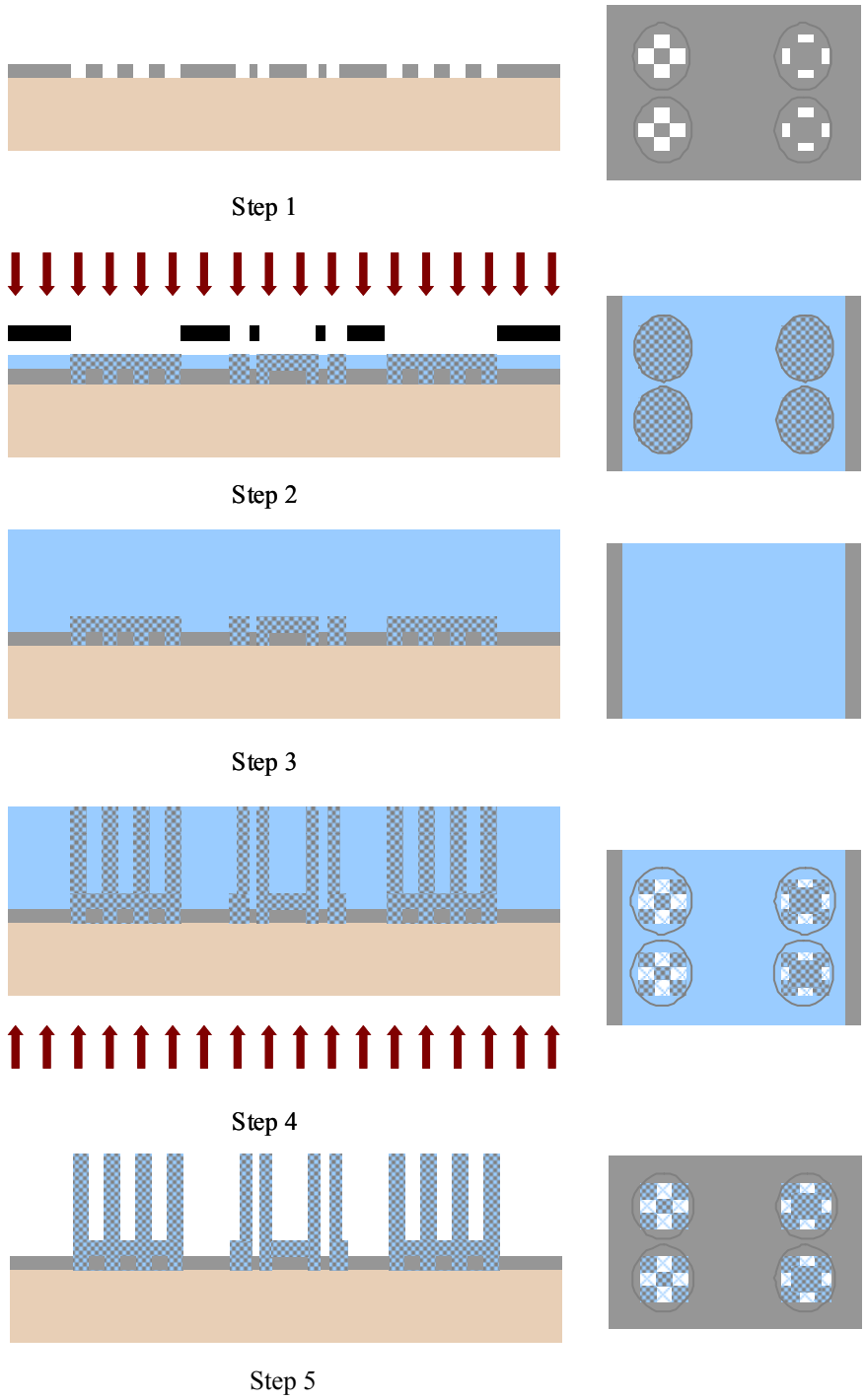

Figure 3.3: Fabrication process flow for solid and hollow micro-tower arrays. Side view of the process is depicted on the left hand side (solid & hollow) and top view on the right.

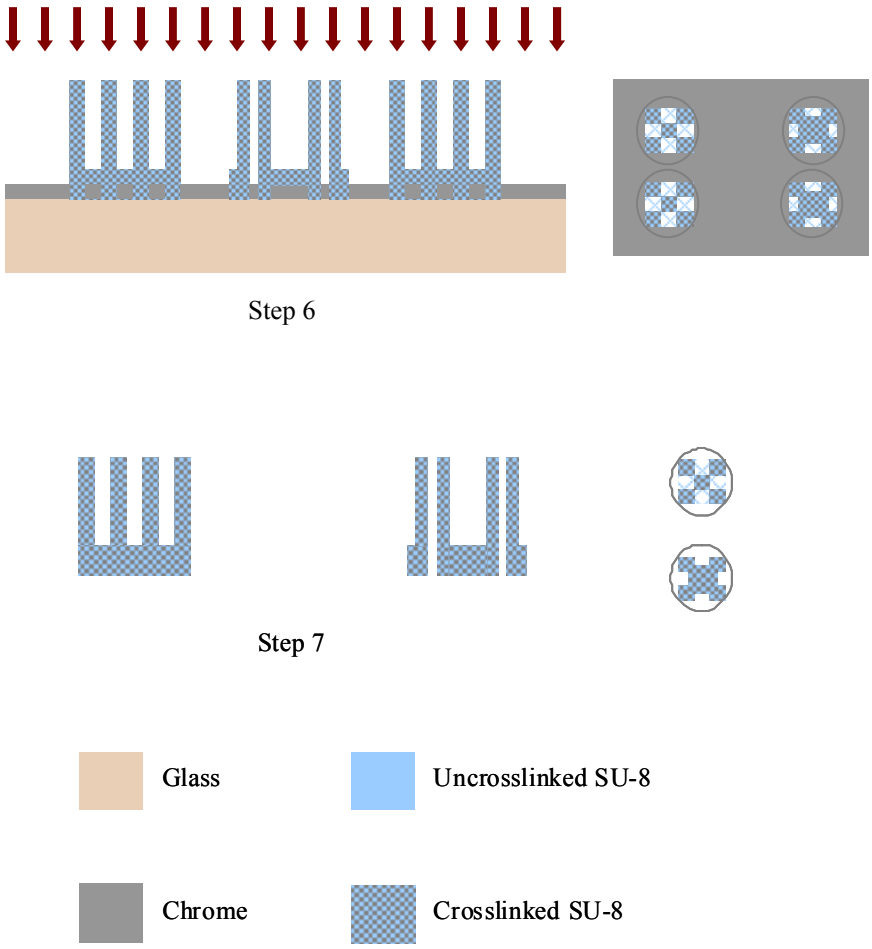

Figure 3.3: Continued.

part AZ 400K) followed by a quick DI water rinse. The unprotected chrome region is then etched in a bath of Cr-7S (Cyantek Corp, Fremont, CA) to fabricate a chrome mask. The photoresist is then removed in an acetone bath followed by a DI water rinse (1 minute) and a 10 minute bake at 100°C in an oven to remove all water particles.

A 100μm thick SU-8 layer (SU-8 2025) is then coated onto the substrate and soft-baked for 30 minutes at 95°C. A second mask is then used to expose circular SU-8 regions (which will ultimately become the device substrate) from the top using standard photolithography (Step 2), followed by post-exposure baking (30 minutes at 95°C). The

energy used for this exposure step is 500mJ. A second layer of SU-8 is coated (by weight) without developing the first layer (Step 3). The density of SU-8 2025 (1.219 g/mL [Microchem Inc 2008]) and it contains 68.55% solids. Using this information Equation 3.1 can be used to calculate the weight of SU-8 for any thickness desired as:

$$\text{Weight of SU8} = \frac{\rho t 10^{-2}}{C_S} \text{ (in g/cm}^2\text{)} \tag{3.1}$$

Here ρ is the density of SU-8, t the thickness required and C_s, percentage of solids in the type of SU-8 being used. This SU-8 is evenly spread along the 4" substrate and soft-baked for 10 hours at 95°C (Step 3). The substrate is carefully monitored for the first hour or so and bubbles from solvent evaporation are removed carefully. A temperature ramp from 65°C to 95°C over a period of 30 minutes is performed to lower the effect of thermal stress on SU-8. The sample is then exposed from the backside (Step 4) using a larger energy dose (5000mJ) to accommodate the thicker SU-8. An I line 365nm UV source (Karl Suss MA-6, Suss MicroTek, Garching, Germany or OAI, Optical Associates, San Jose, CA) is used for all the exposures in this process flow. The mask for this step is already defined on the chrome plate (Step 1). It makes this process a "double-side exposure" technique. The 4" chrome plate is then developed in propylene glycol methyl ether acetate (PGMEA) (Microchem Inc., Newton, MA) with stirring for 1.5 hours (Step 5) after post-exposure baking (1 hour at 95°C). A "shaker system" from Becton Dickinson (BD Medical Products, Franklin Lakes, NJ) is used to aid the process of removal of uncrosslinked SU-8. After the development process, the 4" chrome plate is blanket exposed (2000mJ) from the topside (Step 6) to fully cross-link the structures and

baked (1.5 hours at 95°C) to aid the separation of the tower arrays from the plate. The tower arrays are then mechanically released from the substrate (Step 7).

The two designs (12 tower hollow array with dimensions: average inner diameter ~ 140µm; average height ~ 460µm; and 13 tower solid array with dimensions: average diameter ~ 130µm, average height ~ 450µm) that were selected for fabrication of 3-D microelectrodes are shown in Figures 3.4 and 3.5. Figure 3.4 portrays optical micrographs of both the solid and hollow micro-towers. Figure 3.5 illustrates SEM images of the separated tower arrays.

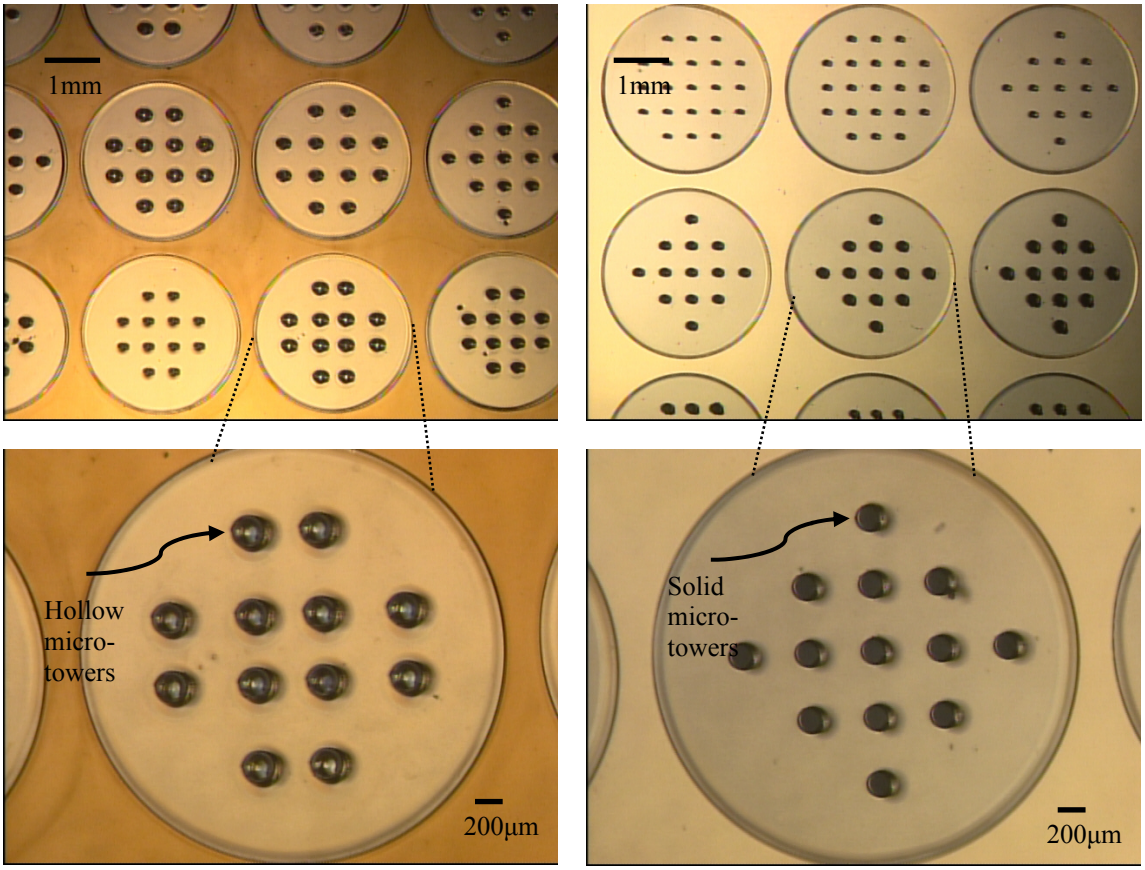

Figure 3.4: Optical micrographs of solid and hollow micro-tower arrays.

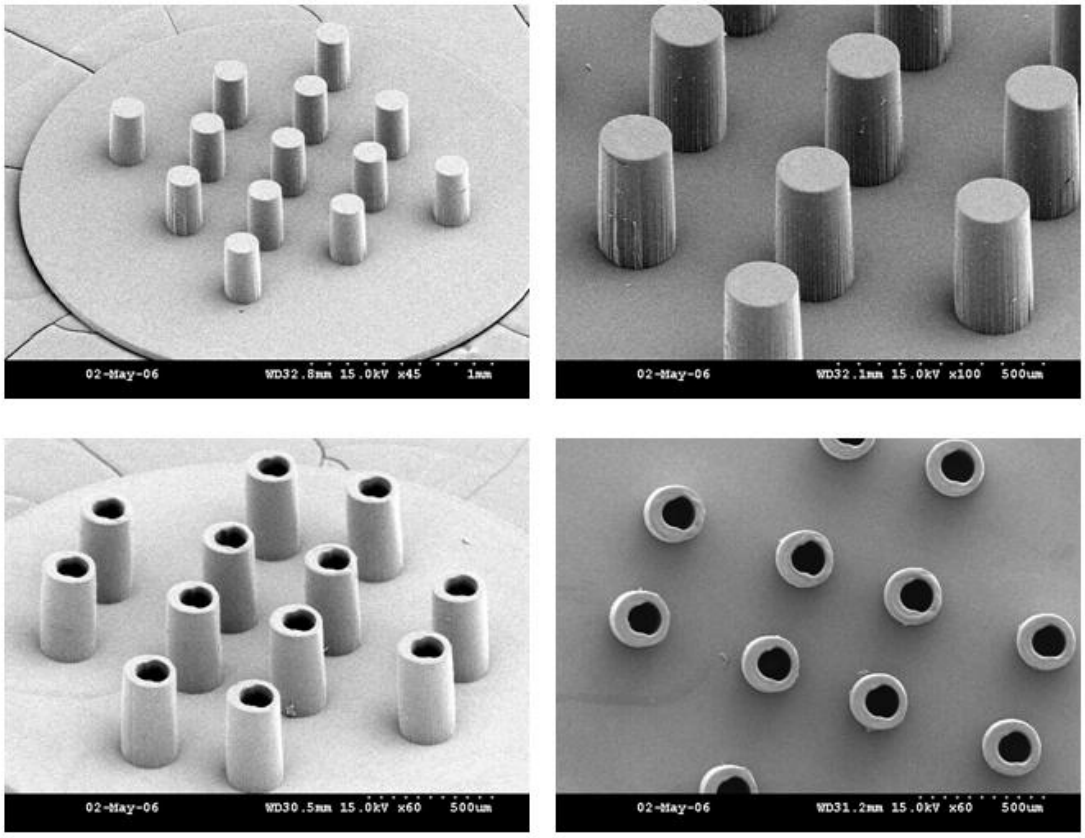

Figure 3.5: SEM images of solid micro-tower arrays (top) and hollow micro-tower arrays (bottom).

3.1.4 Microfabrication: Laser Micromachining Characterization

Laser micromachining is the removal or ablation of materials using a laser. Laser-material interactions during ablation are complex and depend both on the laser (wavelength, pulse duration and intensity) and material (absorption spectra, ease of evaporation). Material is removed above a certain threshold that is a dependent on the properties of that particular material. Lasers have been used in 3-D micromachining since 1996 [Kobsa 1996; Holmes 1997]. As the popularity of non-silicon MEMS grows, lasers

are becoming increasingly useful in producing several micromachined structures, especially arbitrary 3-D and high aspect ratio devices that are usually difficult to produce using traditional microfabrication processes in several materials. Processes that have been developed include direct laser machining [Davis 2003], laser-assisted etching [Tucker 1983], laser-assisted deposition [Lumpp 1996], laser-LIGA [Ghantasala 2001] and laser manipulation/assembly of microparts [Ota 2007]. Table 3.1 summarizes some of the typical lasers used in MEMS.

Table 3.1: Summary of some of the common types of lasers used in the MEMS area

Type	**Wavelength**	**Pulse Width**	**Pulse Energy**	**Target Materials**
Excimer (ArF, KrF, XeCl)	193, 248, 308 nm	~20ns	.01-1J	Polymers
Nd YAG	1.064μm	~10ns	10mJ	
CO_2	10.6μm			High throughput applications
Fluorine vapor	157nm			
Nd YAG	355nm, 266nm	~10ns	<1mJ	PTFE, PMMA, Polyimide
IR	10μm			Metals, ceramics
Copper vapor	255, 271, 289nm			
Diode Lasers	808-980nm			

In this work we have utilized the 248nm Excimer laser system for micromachining a conformally deposited polymer in X, Y and Z directions. Excimer laser micromachining relies on the interaction between UV pulsed laser radiation and the material to be machined. The short wavelength implies that the radiation is efficiently absorbed in the surface layers of many materials. This combination of UV radiation and

short pulse results in the removal of layers by many mechanisms: vaporization in the case of ceramics and metals; molecular disintegration or photoablative decomposition in the case of many polymers.

The excimer laser used in this work is distributed by Resonetics Inc (Resonetics Inc, Nashua, NH). It consists of a lasing section where the gases interact to produce a high energy beam and an optics section where the beam is manipulated and attenuated by advanced optical tools. The lasing section of the machine is manufactured by Lambda Physik (Lambda Physik, Ft. Lauderdale, FL) and the optics is manufactured by Optec SA (Optec SA, Honru, Belgium). Figure 3.6 is a photograph of the entire assembled system.

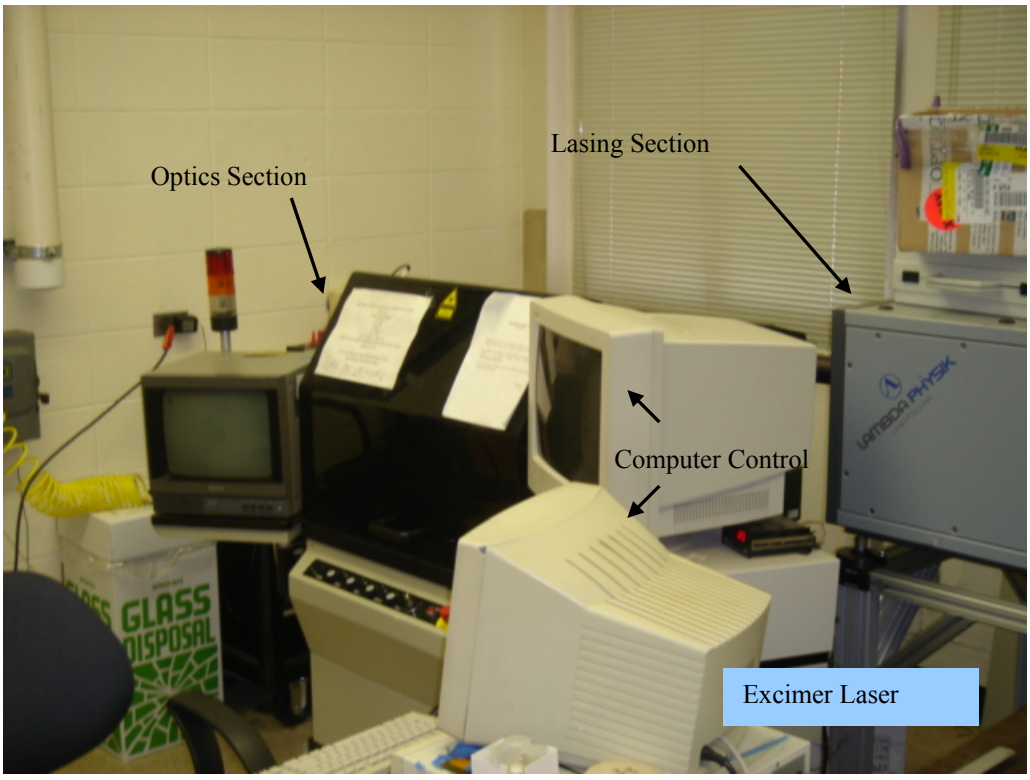

Figure 3.6: Optical image on excimer laser setup depicting the lasing section where a high intensity beam is produced, the optics section where the beam is manipulated and focused on the object of interest and computer control of the entire unit.

An excellent review of the operation of various lasers is given by von Allmen and Blatter [von Allmen 1995]. Briefly, when an inert gas (Kr) is combined with a halide (F) at high energies (lasing system) it forms an unstable compound KrF. When the source of energy is stopped the unstable compound decomposes releasing strongly synchronized radiation. This radiation is then focused and attenuated by the optical section of the system. A suitable mask is used to shape the beam before it makes contact with the material to be ablated (sitting on a work piece). By controlling the mask different shapes can be etched on the material. The motion of the work piece can also be controlled using the X-Y motion stage. The mask can be standard circular or square masks or a chrome mask (fabricated using the same techniques as in Section 3.1.3).

Parylene is used as the conformally deposited polymer in this work. Excimer laser ablation of parylene deposited on thin metal seed layers has been extensively studied. Parylene or poly-p-xylylene is an insulating thermoplastic polymer that has some very interesting characteristics that are exploited in this dissertation. It is chemically inert, biocompatible and can be conformally deposited on varied topographies at room temperature [SCS Inc, 2007]. A system for this deposition was initially developed at Union Carbide and is commercially available from Specialty Coating Systems (SCS, Indianapolis, IN). This coating process is shown in Figure 3.7.

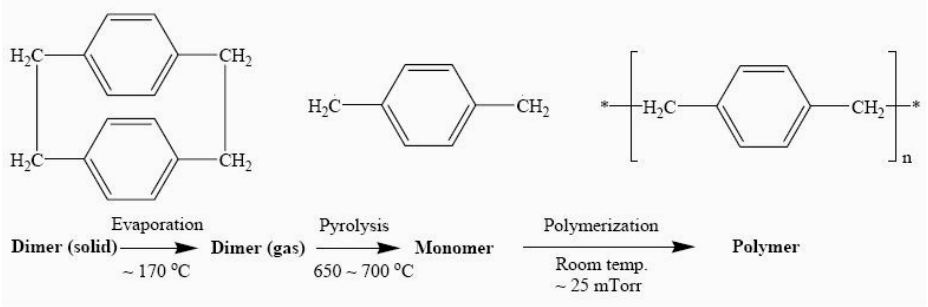

Figure 3.7: Coating process for parylene from dimer to polymer.

Parylene dimer is a stable compound and can be purchased as a solid. This dimer is evaporated into vapor phase at approximately 170˚C. The dimer is then pyrolized into a monomer at elevated temperatures 650˚C - 700˚C. This happens in a furnace that is isolated from the deposition chamber. The monomer is thermally stable but kinetically very reactive to molecules of its kind and forms a stable polymer at room temperature. By placing the sample in the deposition chamber conformal deposition to a sub-micron scale can be achieved using this system. Depending on the functional group that is attached to ring position of the dimer, different types of parylene are commercially available. The type used in this research is Parylene-C which has a chlorine functional group attached in the ring position. In order to characterize the parylene ablation process, several glass substrates were cleaned using a piranha solution (2:1 solution of H_2SO_4 and H_2O_2) for 10 minutes and a layer of Cr/Cu (30nm/600nm) was deposited on the substrates using a unifilm sputtering system. The thin film layer thickness is the same as the seed layer used for electroplating (described later). Different thicknesses of parylene (1-32μm) were deposited on these substrates. Figure 3.8 illustrates a schematic of the ablation process on non-planar topographies (left) and examples of optical microscopic images of various ablated/non-ablated patterns (right). A microscope in high magnification is one way to determine the extent of ablation of various patterns (Figure 3.8). These results have been confirmed as explained later in this section with profilometry and electroplating. A typical protocol for ablation evaluation is a series of circular patterns of a particular size (controlled by the size of the mask and demagnification used) with increasing pulses in the X direction and increasing energy (controlled by attenuation) in the Y direction. Table 3.2 gives a typical protocol used for the parylene ablation process.

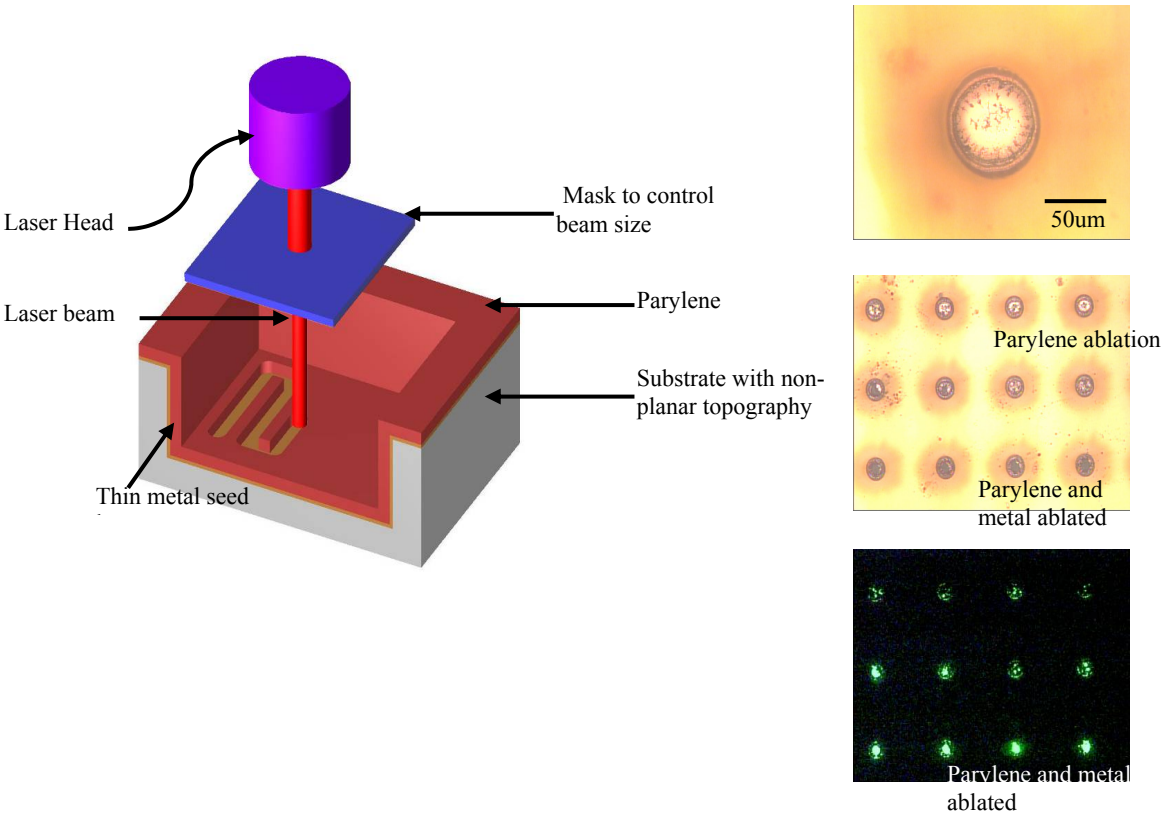

Figure 3.8: Schematic of parylene ablation on non-planar topographies particularly on thin metal seed layers (left); ablated samples (right).

Table 3.2: Typical protocol for parylene ablation with various parameters.

Parameter	**Nominal Value**	**Comments**
Energy	200mJ	Constant
Pulses	30	Start with 20 and increase
		by 2 in X direction (20-38)
Power Attenuation	10%	Start with 6% and increase
		by 2 in Y direction (6-24)
Velocity	120µm/s	Constant
Frequency	90Hz	Constant

Figure 3.9 portrays the data for ablation of parylene at various fluences (energy/unit area). From this graph one can conclude that the threshold for parylene ablation is low. Parylene starts ablating at a threshold of 3mJ/cm^2 with less than 50 pulses. The amount of energy required to ablate various thicknesses of parylene is summarized in Table 3.3. It shows that the average energy required for removing 1µm of parylene increases as the thickness increases. This is due to the requirement of removal of parylene residue as the thickness is increasing. The threshold for ablation of thin metal seed layers was also measured and this turns out to be approximately 15mJ/cm^2 for Cr/Cu (30nm/600nm). Ablation of parylene below this threshold results in minimal effect on the metal layer even with increased numbers of pulses. Whereas above this threshold (Figure 3.9, graph for 26.7mJ/cm^2), removal of this seed layer is observed. So the optimum operation point for parylene ablation is below the threshold of the underlying seed layer.

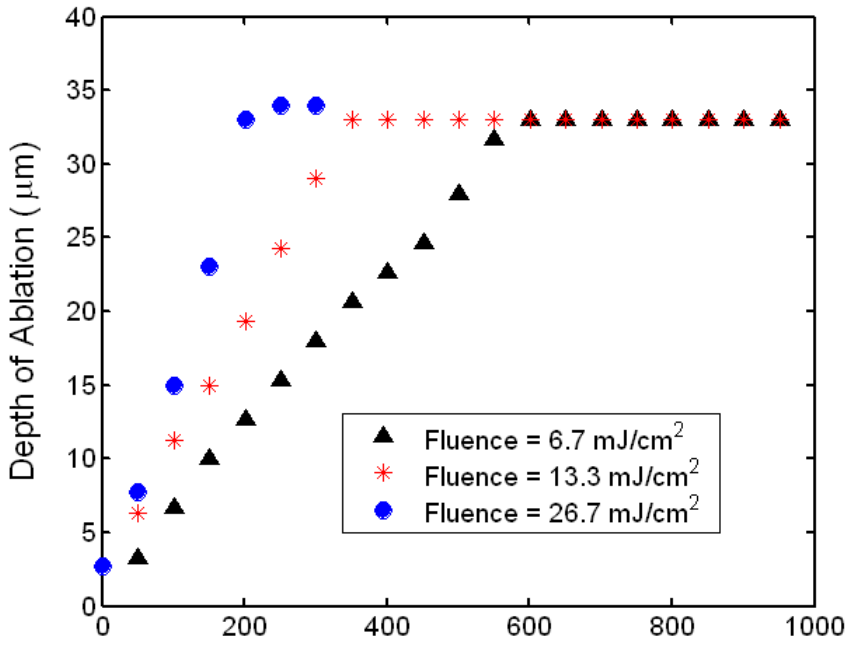

Figure 3.9: Ablation paramaters for parylene at different fluences.

Table 3.3: Optimum value of energy required to remove a variety of thicknesses of parylene.

Parylene Thickness (µm)	Fluence (mJ/cm^2)	Number of Pulses	Energy/um ablated (mJ/µm)
2	3	20	90
5	8	20	96
10	10	60	240
25	25	200	600
32	27	250	625

The ablation has also been confirmed with profilometry (KLA Tencor P-15, KLA - Tencor, San Jose, CA) and electroplating copper or nickel. Figure 3.10 illustrates the scanned region of 10µm parylene ablation and Figure 3.11 shows a series of 65µm size spots where nickel has been electrodeposited (process parameters given in section 3.1.6). This image clearly demonstrates areas where nickel has been deposited and areas where it is not.

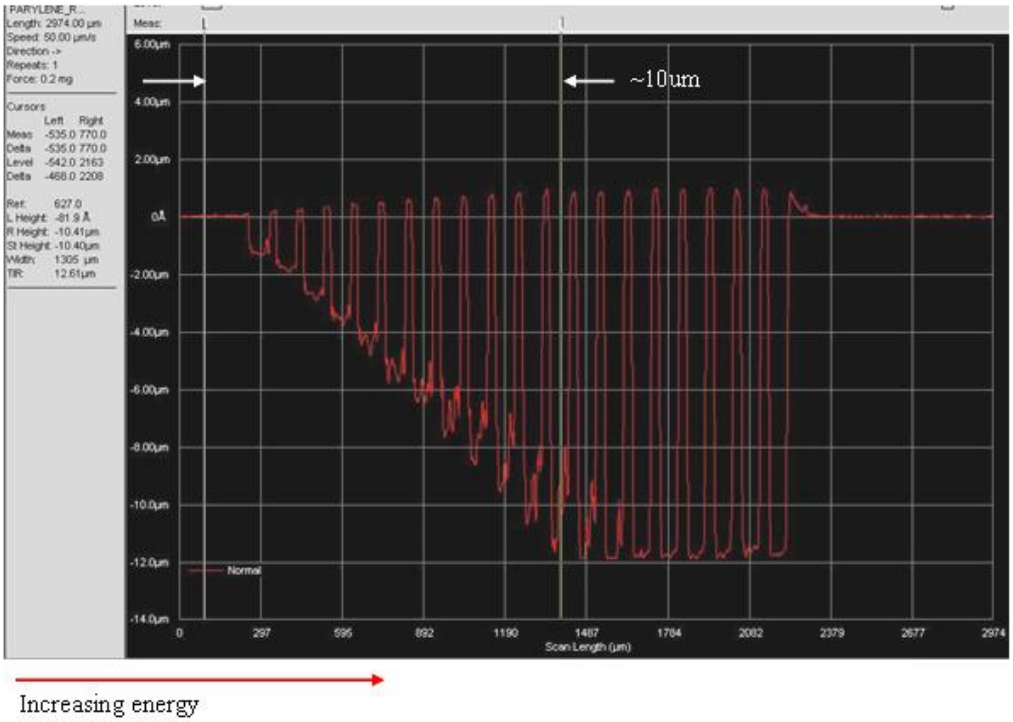

Figure 3.10: Profilometric scan of progressive ablation of 10 µm thick parylene.

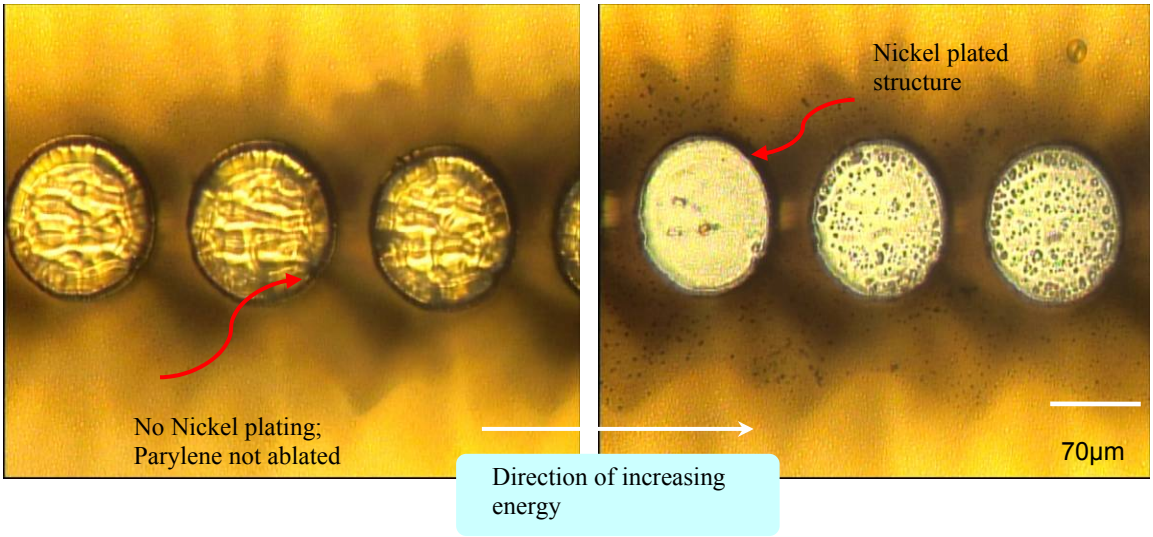

Figure 3.11: A series of 65µm laser ablated parylene regions where the ablation has been confirmed using electrodeposition. Regions on the left are not completely ablated (no nickel deposition) whereas the regions on the right are electrodeposited structures.

3.1.5 Theoretical Calculation: Parylene Dissociation

Laser ablation of parylene was evaluated in the previous section experimentally by microfabricating samples that were micromachined with an excimer laser. In this section a theoretical calculation is performed to estimate the amount of energy needed to dissociate parylene to compare it with the experimental values. This calculation assumes that the two steps in the dissociation of parylene (represented in Figure 3.7) are – breakage of two C-C single bonds followed by vaporization of the volatile aromatic repeat unit. The enthalpies of these processes are 348 KJ/mol and 30.9 KJ/mol respectively [Dept. of Chemistry, Michigan State, 2009]. Using these numbers the energy needed to break one single unit of parylene is calculated as 1.21×10^{-18} J. Parylene is a polymer with an estimated degree of polymerization of 2000-4000 [Pokhodnya 2004]. So

the amount of energy required to break up an entire polymer chain can be calculated by multiplying the energy required to break a single unit with the degree of polymerization. This is calculated to be 4.83×10^{-15} J (assuming a degree of polymerization of 4000).

Experimentally it was observed that parylene starts ablating at a fluence of $3 mJ/cm^2$ with less than 50 pulses. One specific data point in Figure 3.9 is the ablation of 2µm of parylene using a 65µm spot size at 6.7 mJ/cm^2 and 50 pulses. Figure 3.12 is a schematic representing this specific volume of parylene.

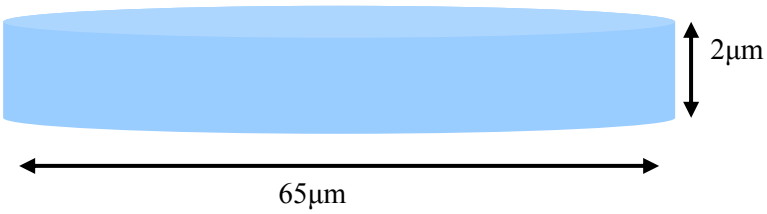

Figure 3.12: Volume estimate of the 65µm spot size ablating 2µm thick parylene.

The volume of parylene and the corresponding mass of this volume are estimated using equations 3.2 and 3.3.

$$\text{Volume of Parylene} = \pi r^2 h \qquad (3.2)$$

$$\text{Mass of Parylene} = \text{Density} \times \text{Volume} \qquad (3.3)$$

where r is the radius of the spot size is 32.5µm and h is the height of the parylene (2µm). The density of parylene is obtained from its material data sheet as supplied by the manufacturer and is equal to 1.309 g/cm^3 [SCS Inc 2007]. From Equations 3.2 and 3.3,

the mass of the volume of parylene represented in Figure 3.12 is calculated to be equal to 8.69×10^{-9}gms. The mass corresponds to 1.26×10^{10} chains of parylene monomer calculated using Equation 3.4.

$$\#\ \text{of Parylene Chains} \equiv \frac{\text{Mass} \times \text{Avagadro Number}}{\text{Degree of Polymerization} \times \text{Parylene Repeat unit (gm)}} \qquad (3.4)$$

Where Avagadro number is 6.023×10^{23} and the molecular weight of 1 mole of parylene repeat unit is 104gms. Multiplying the result of this calculation with the amount of energy needed to dissociate a chain, we can get the theoretical estimate for the amount of energy required to dissociate parylene as 0.06mJ. The experimental energy is calculated from the data point of the amount of energy required to ablate 2μm of parylene (fluence of 6.7mJ/cm^2 at 50 pulses) and the area of a 65μm circular spot. This value is approximately equal to 0.01mJ which is in the same order of magnitude as the theoretical estimate. This validates our experimental observation.

3.1.6 Microfabrication: Laser Scribed 3-D MEAs

For several MEMS applications, pattern transfer onto silicon wafers and other substrates with extensive topography requires a uniform photoresist layer over nonplanar surfaces. This is not an easy problem to tackle as uniform coating of resists becomes challenging over topographies greater than a few tens of microns and exposure becomes inconsistent as the substrate is in contact with the mask in some areas and in non-contact proximity to the mask in others. Four different coating techniques are common in the

MEMS area: (a) spin coating [Nga Phuong 2004] which is the most common technique but is suited primarily for flat substrates; (b) electrodeposited resists [Linder 1996] have been utilized for 3-D stacks of chips and anisotropic etched grooves but requires a conductive seed layer and high current densities; (c) spray coating [Ji 2008; Pham 2003], which can yield uniform films but often requires custom optimization for each substrate; (d) dip coating, which is generally applicable for coating layers on 3-D structures post fabrication [Jun 2007]. Commercially SUSS MicroTec has recently released AltaSpray^{TM}, a spray coater which can be used to uniformly coat resists in topographies of up to 600μm in height [Suss MictoTec 2007]. Several new approaches have been developed as part of this thesis to solve this problem. One of the approaches developed is 3-D metal transfer micromolding which is discussed in Chapter 4. This is a relatively newer approach that has been studied extensively for various applications in the MSMA group [Rajaraman 2008]. In this section, laser micromachining which was discussed in section 3.1.4 has been used to address this rather complex problem. Lasers are attractive tools for 3-D microfabrication because it is possible to directly machine material with substantial topography in a non-contact manner. Excimer laser has been utilized to ***scribe*** features in parylene coated on thin metal that is deposited on the SU-8 towers described in Section 3.1.4. This is followed by using the scribed parylene as an electroplating mold, as reported in the paragraphs below. The process described here is different from a conventional electroplating process [Allen 1993] where a photoresist layer is defined on a metalized substrate to act as a barrier for electrodeposition of structures that are subsequently released by dissolving the resist in the final step.

Figure 3.13 details the process flow of laser scribing of microelectrodes on SU-8 tower arrays (from Section 3.1.3). Prior to laser scribing, the tower array sample is mounted on a glass slide with dimensions 10mm x 20mm using Shipley S1813 photoresist (Rohm and Haas, Marlborough, MA) and cured at 100°C for 10 minutes. The tower array is then coated with a seed layer of Ti/Cu (30nm/600nm) using a unifilm sputterer (Step 1). A parylene layer (1μm thick) is then conformally coated onto the substrates (Step 2). Parylene is then patterned using the excimer laser with the parameters that are determined from the test samples as described in Section 3.1.4 (Step 3). This patterning is carried out in the X-Y direction to define the pad connections (for wirebonding described in Section 3.1.7) that are 65μm in width and metal traces to the bottom of the towers (2-D counterpart electrodes and 3-D electrode connections). The metal traces are 20μm in width. This process can be performed by executing an AutoCAD file (depicted in Figure 3.14). However for electrodes those are to be defined (***scribed***) on the sidewall of the towers all the way to the top, the micro-tower array was mounted on a custom-machined substrate with a 45˚ angle of inclination and traces were scribed in a serial manner. An important point to note here is that these parameters can drift based on the condition of the laser: gas pressures, changes in power level and wear in the attenuators. Characterization of parylene ablation, immediately followed by the ablation on the 3-D MEA sample is the protocol that was therefore followed for this process. The sample is then electroplated using a current density of 3mA/cm^2 (Step 4).

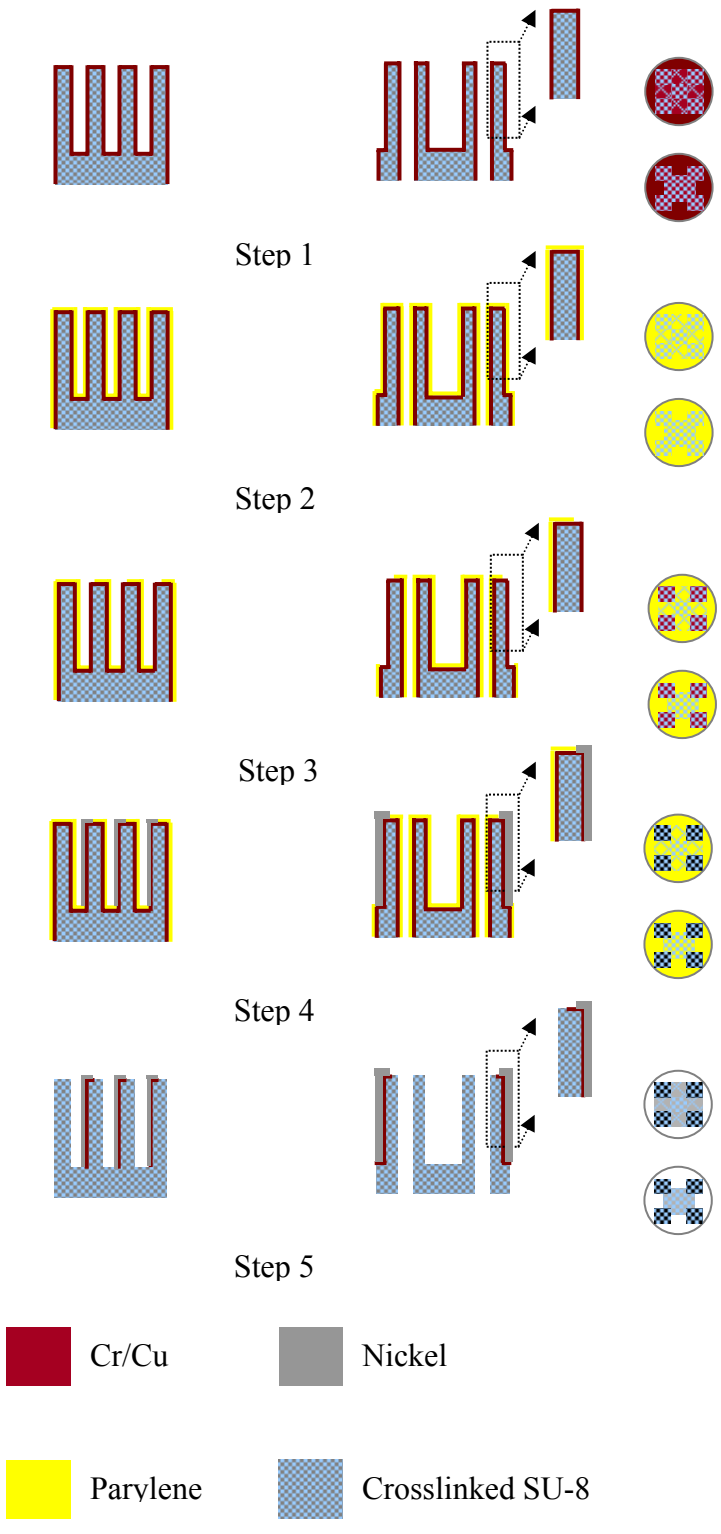

Figure 3.13: Fabrication process flow for laser ***scribing*** microelectrodes on micro-tower arrays fabricated in section 3.1.1. Side view of the process (solid & hollow respectively) is depicted on the left and top view on the right side of the schematic.

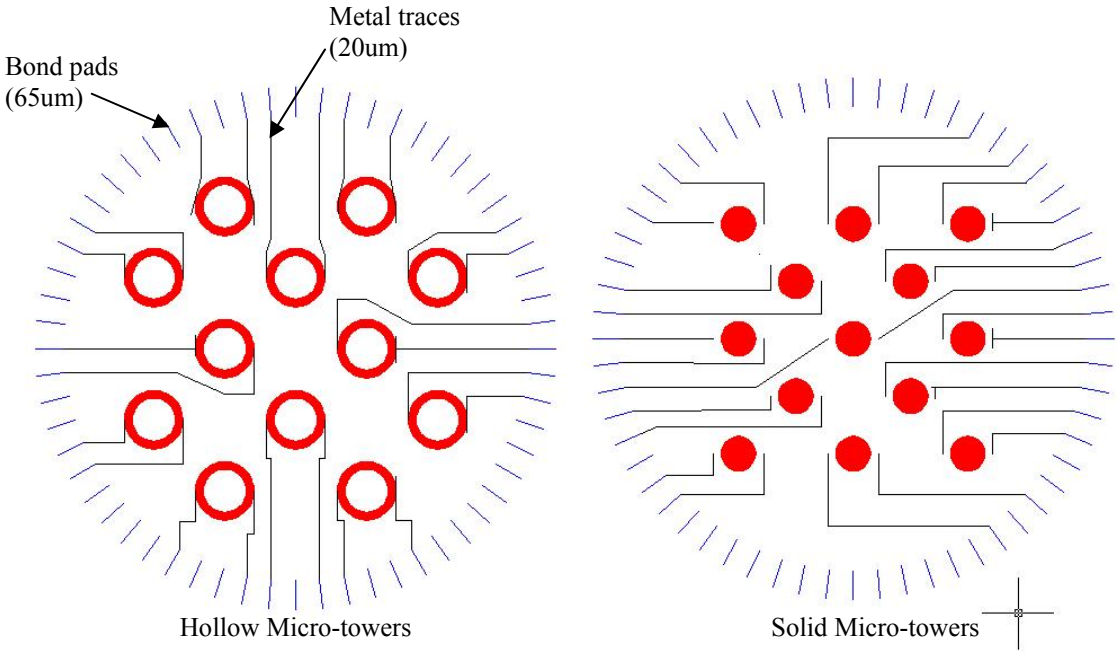

Figure 3.14: AutoCAD file (schematic) used to automate the laser scribing of bond pads and metal traces

A thin square nickel foil is used as the anode in this electroplating step and nickel sulfamate (Enthone, West Haven, CT) is used as the plating solution. Prior to electroplating the sample is dipped in a solution of 15% hydrochloric acid (J.T. Baker Inc, Phillipsburg, NJ) in DI water, followed by a solution of 25% nitric acid (J.T. Baker Inc, Phillipsburg, NJ) in DI water. These treatment steps are followed by a quick DI water rinse and nitrogen blow-drying. This is performed in order to remove the native layer of copper oxide. Table 3.4 lists the parameters used in this electroplating process.

Table 3.4: Parameters for Nickel Electroplating

Parameter	Value
Current Density	3mA/cm^2
Total Area	5cm^2
Total Current	15mA
Temperature	Room Temperature
Stirring	300rpm
Electroplating rate	~12μm/hour

The parylene is subsequently blanket etched using CHF_3/ O_2 plasma (Plasma Therm RIE, Plasma Therm Inc., St. Petersburg, FL). The parameters for this process are given in Table 3.5.

Table 3.5: Process parameters for etching parylene in RIE.

Parameter	Value
O_2 Flow Rate	45 sccm
CHF_3 Flow Rate	5 sccm
Pressure	200 mTorr
Power	150 Watts
Time	7 mins
Etch Rate	1μm*

* Varies with conditions of machine

The device is observed optically and under the SEM (before seed layers are removed). Figure 3.15 presents optical images of the device and Figure 3.16 presents SEM images of the device. This is followed by seed layer (Ti/Cu) removal (Step 5). Copper is removed by submerging the sample in blue etch solution (acqueos NH_4OH saturated with cupric sulfate) and titanium is removed by dipping the sample in buffered oxide etch solution (J.T. Baker Inc, Phillipsburg, NJ). The tower array is then dipped in

acetone for 5 minutes for release from the glass substrate. Figure 3.17 shows an optical micrograph of the released device depicting electrodeposited electrodes and microfluidic ports.

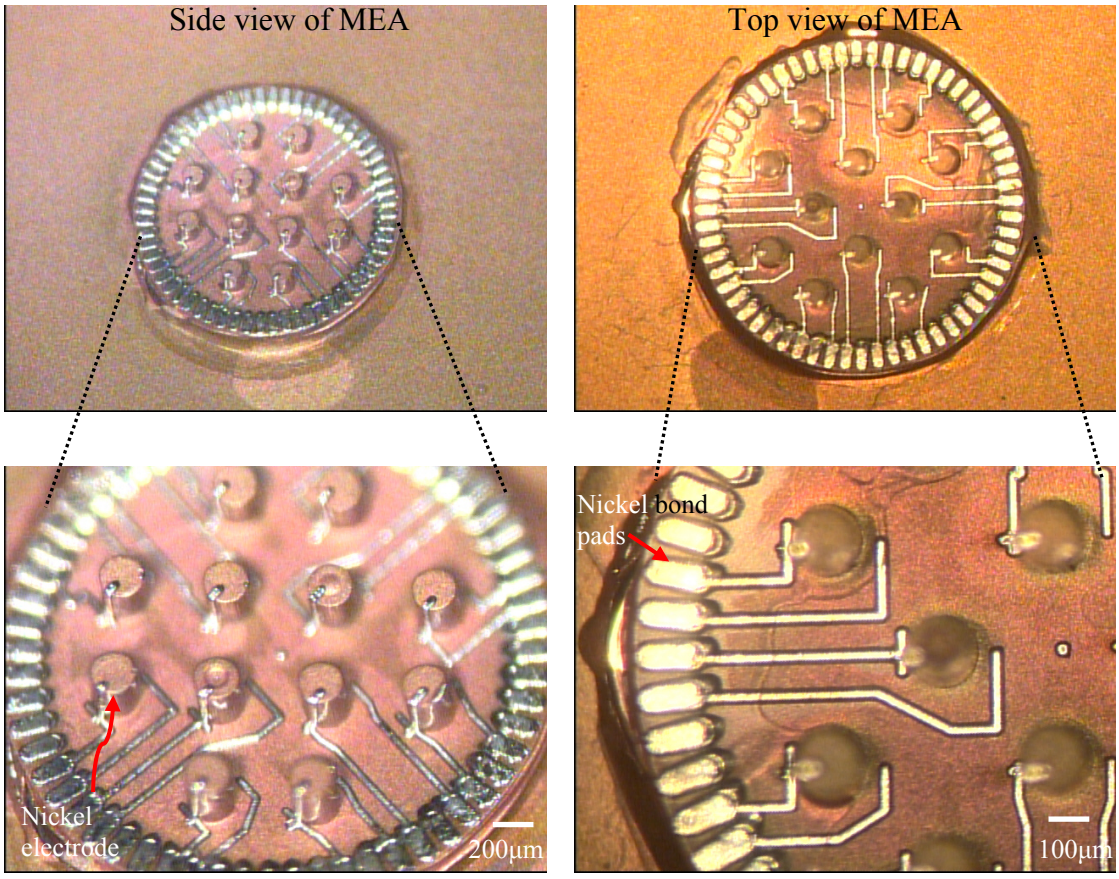

Figure 3.15: Optical micrographs of the side (left) and top (right) views of nickel plated 3-D MEAs. These images are taken prior to seed layer etching.

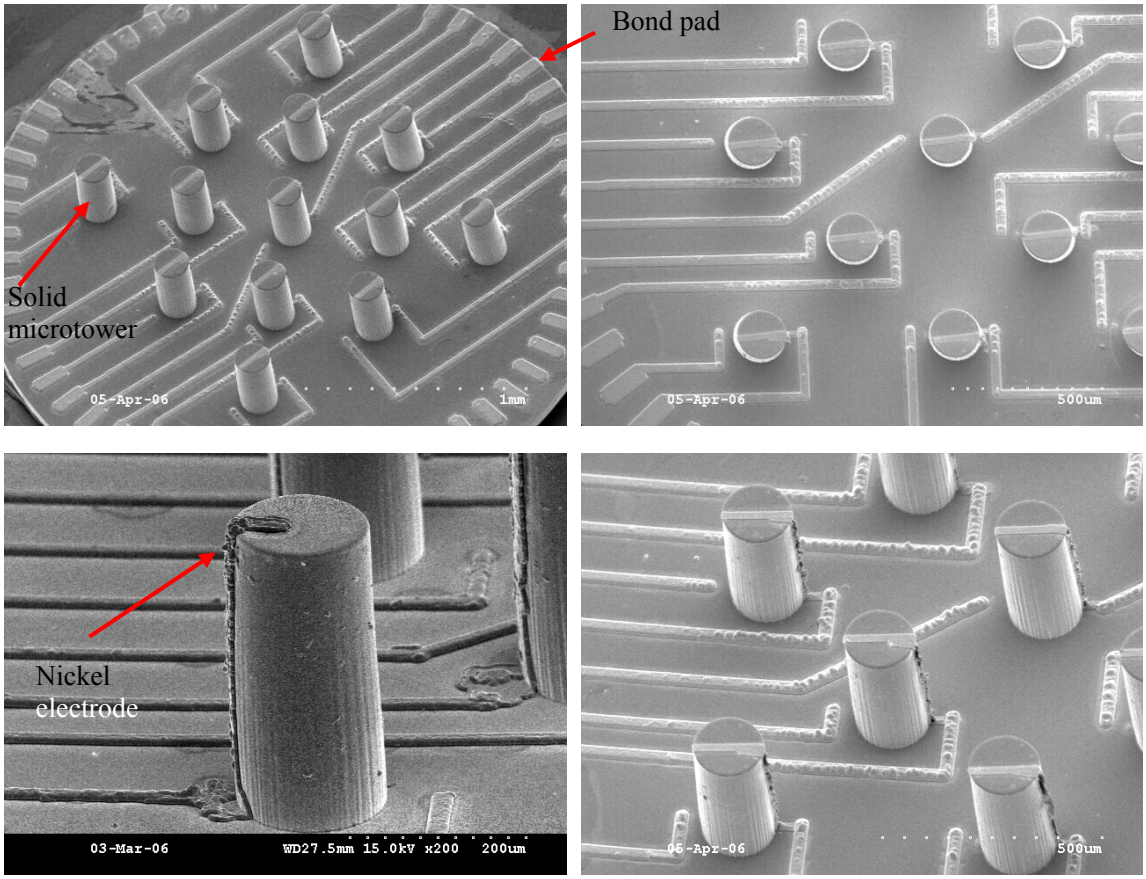

Figure 3.16: SEM images of the top, side views and single nickel microelectrode.

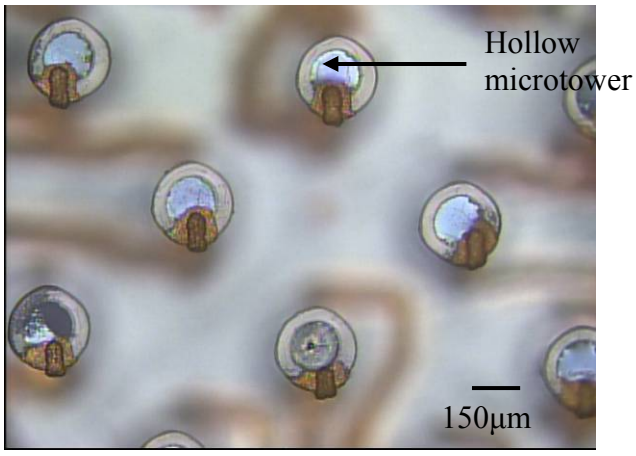

Figure 3.17: Optical micrograph of 3-D MEA after removal of seed layers.

The fabricated 3-D MEAs are packaged in order to complete the device. This is performed as explained in Section 3.1.7.

3.1.7 Packaging of Laser-scribed 3-D MEAs

The fabricated tower arrays must be packaged to form a complete device. For packaging, fused-silica substrates are used. Other conventional packaging substrates such as alumina ceramic, FR-4 epoxy-glass composite PWB, or liquid crystal polymer (LCP) can also be used for this purpose but fused-silica was preferred due to the fact that it is biocompatible and also laser micromachinable [Resonetics Inc 2007] for fluidic ports (fluidic inlet for a coupled microfluidic, microelectrode MEA). Fused silica wafers (500μm thick, 4" diameter; Mark Optics Inc., Santa Ana, CA) were diced into 49mm x 49mm chips (size of commercial 2-D MEA). The fabrication process for the packaging chips is shown in Figure 3.18. It is a standard lift-off process and is described briefly below.

The 49mm x 49mm chips are first cleaned in a piranha solution (2:1 solution of H_2SO_4 and H_2O_2 at 120˚C). A thin layer of negative resist (NR-9 8000, Futurrex Inc, Franklin, NJ) is then coated on these substrates (Step 1). A mask defining the metal traces is drawn in AutoCAD (Figure. 3.19) and printed using a commercial high resolution printer. This transparency mask is converted into a chrome mask as described in Section 3.1.3. This mask is used to define the metal traces in the photoresist (Step 2). Before metal deposition, a short descum is performed using the Plasma Therm RIE. Metal (Ti/Au, 10nm/400nm) is deposited (Step 3) using an e-beam evaporator (CVC Products,

Rochester, NY). Metal is then lifted-off to define the traces for the packaging chip in an acetone bath (Step 4).

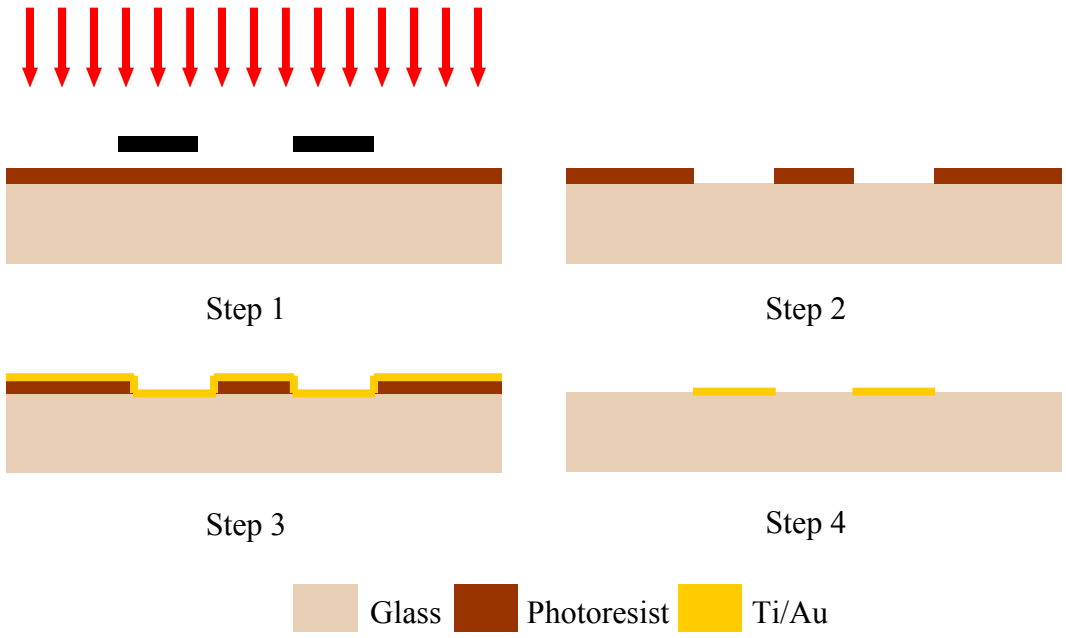

Figure 3.18: Fabrication process flow for fabrication of packaging chips.

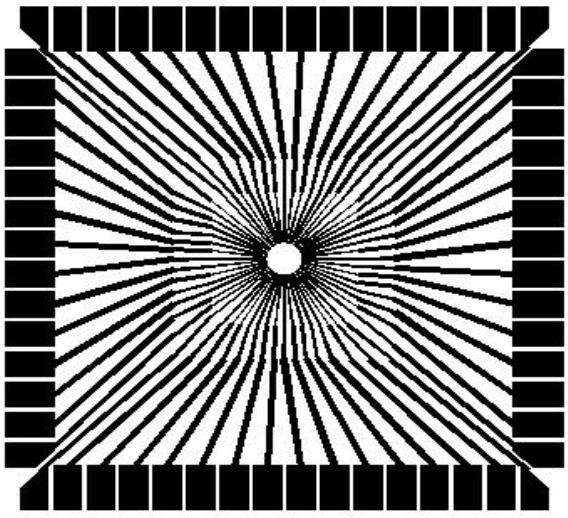

Figure 3.19: AutoCAD layout for lift-off metal mask used in the fabrication of packaging chips on fused silica substrates.

For solid microtower arrays, the fabricated fused silica substrate is used to house the MEA. For incorporation of fluidics, external fluid access ports were drilled using a CO_2 laser (LS500 Laser Engraving System, *New Hermes-Gravograph Inc.*, Duluth, GA). After the drilling of the fluidic ports with the laser, the chips are treated with O_2 plasma at 200mT pressure and 200W energy for 10 minutes to remove surface contamination. Once the chips are fabricated, the laser scribed 3-D MEAs (from Section 3.1.6) are mounted onto the chips with a thin layer of polydimethylsiloxane (PDMS). The tower array is then wire-bonded to complete the packaging. Wire bonding to a thin SU-8 substrate with non-similar metals (gold to nickel) presents a challenge as SU-8 with a PDMS under-layer is complaint and not as rigid a surface as silicon or glass. So a combination of wire bonding (to the gold pads on the glass substrate) and conductive epoxy bonding (to nickel pads on SU-8) was adopted to overcome this problem. Figure 3.20 depicts a wirebonded, packaged 3-D MEA.

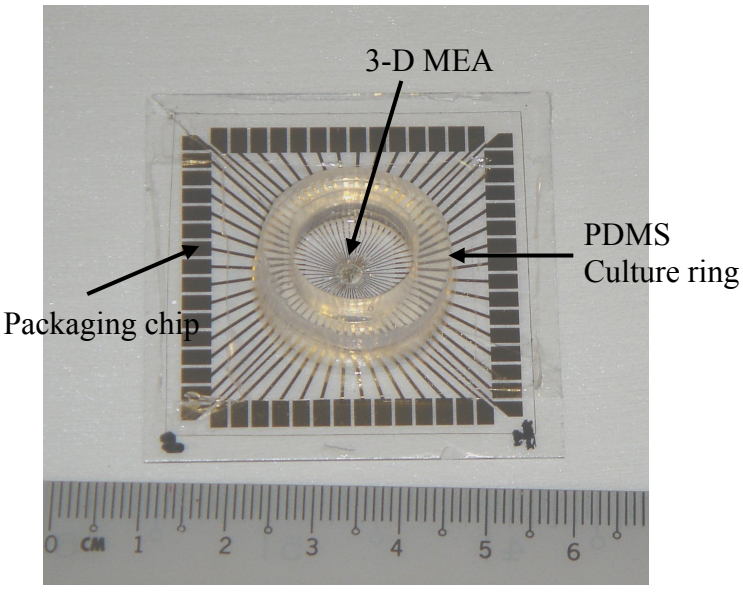

Figure 3.20: Fabricated, packaged, wirebonded laser-scribed 3-D MEA. A PDMS culture ring is attached to serve as a containment chamber for biologicalculture/electrical test solution.

Commercial 2-D MEAs typically have a 5μm layer of biocompatible insulation deposited [Ayanda Biosystems 2007] and active sites opened for electrical stimulation and recording by planar lithography. An additional requirement for the insulation layer of 3-D MEAs is that it should be laser micromachinable so that the definition of recording sites can be carried out in a similar way as the electrodes. Parylene has been selected as the insulation material in this work. It is highly biocompatible [Rodger 2007], can be deposited uniformly on varied topographies and laser micromachinable as has been demonstrated in Section 3.1.4. There is conflicting evidence about the toxicity of SU-8 [Berdodini 2006; Vernekar 2008]. Copper and nickel also have biocompatibility issues [Hultberg 1997; Sunderman 1993]. However, all these materials are commonly used for MEMS processing. In order to accommodate the use of these materials, a thick insulation layer of parylene (25μm) was used according to the guidelines established by Vernekar et al. [Vernekar 2008]. Excimer laser ablation of this thicker parylene layer was evaluated as described in Section 3.1.4 on test substrates. The spot size used for this ablation was 50μm. Recording sites were ablated at both 2-D and 3-D electrode sites. A 5mm tall PDMS culture ring (ID: 15mm; OD: 25mm) was attached to the chip using a thin layer of PDMS. PDMS is known to be biocompatible [Sia 2003], thereby having no negative effect on the MEA assembly. It serves two purposes: it acts as containment ring for both the static cell culture (described in Section 3.2.3 and 3.2.4) and for the platinum-black electroplating solution (described below).

Electroplating platinum-black increases the surface area of the electrodes and also serves to reduce the impedance of the electrodes [Ross 2008]. If some measure of control can be achieved over this plating process, uniform impedances can be achieved across all

the electrodes in the MEA chip. Ross [Ross 2008] describes the design and implementation of a platinum electroplating setup in more detail. Briefly a mechanical clamp connects up to 16 electrodes with control circuitry, which in turn is connected to a laptop. MATLAB is used to setup programs to pulse-plate platinum at a desired current density. The electrolyte for the plating process is a solution of 1% chloroplatinic acid with 0.0025% HCl and 0.01% lead (trace quantity of lead) acetate all diluted in DI water. Platinum-black is electroplated onto the recording sites of the 3-D MEA using a current density of 4.9μA/cm^2 at room temperature. Figures 3.21 (a) and (b) a illustrate schematic of the electroplating setup and mechanical assembly used to interface the electronics for the plating setup with the packaged MEA respectively. Optical micrographs of electroplated recording sites are portrayed in Figure 3.22.

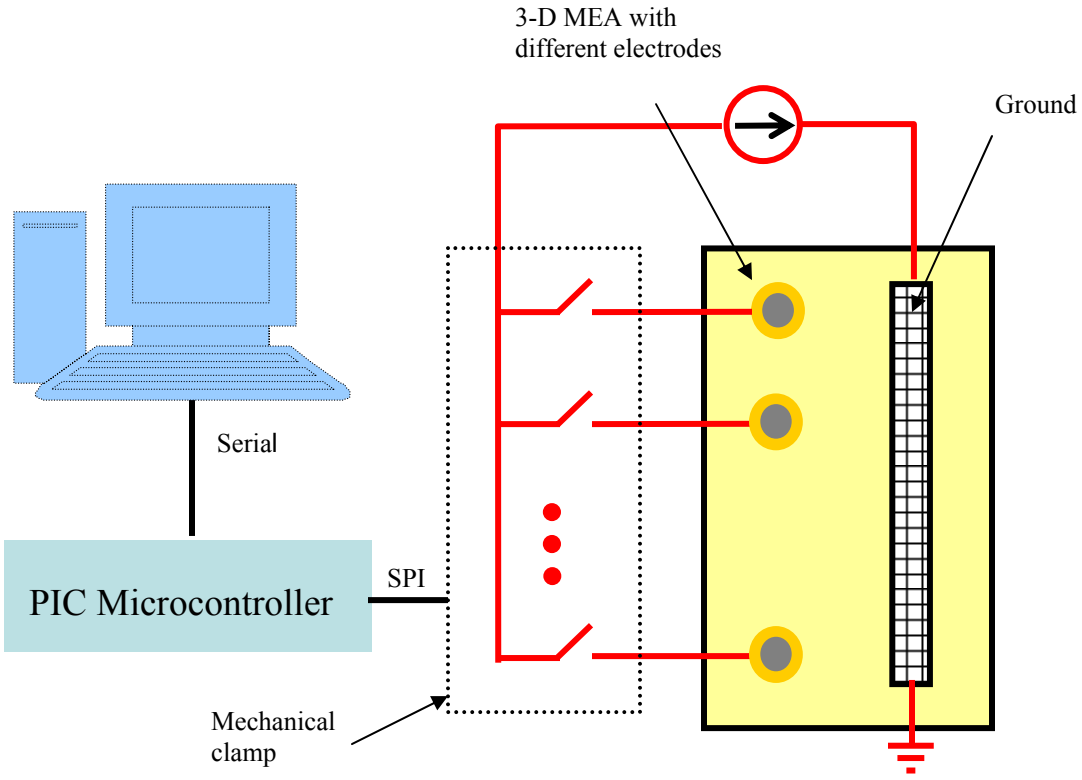

Figure. 3.21 (a): Schematic of Pt-black electroplating setup with mechanical interface to the MEA, control circuitry and MATLAB routines

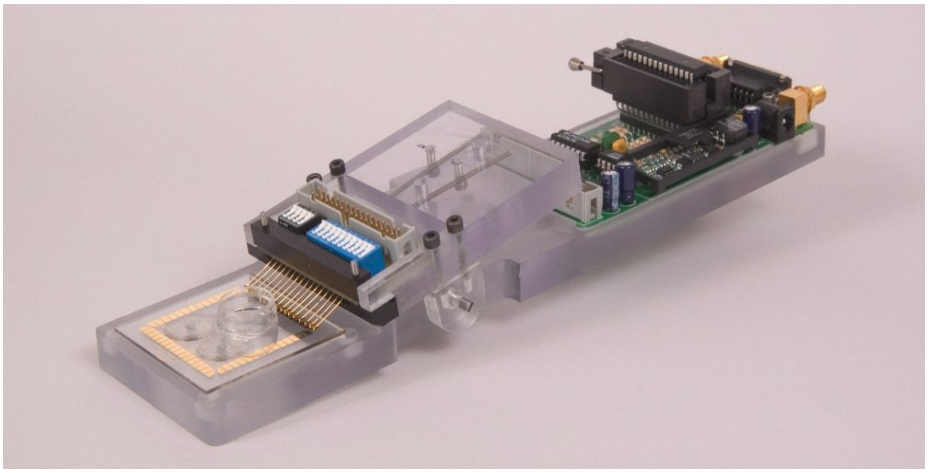

Figure 3.21(b): Optical image of the mechanical clamp developed to interface with the MEA along with the control circuitry [Ross 2008].

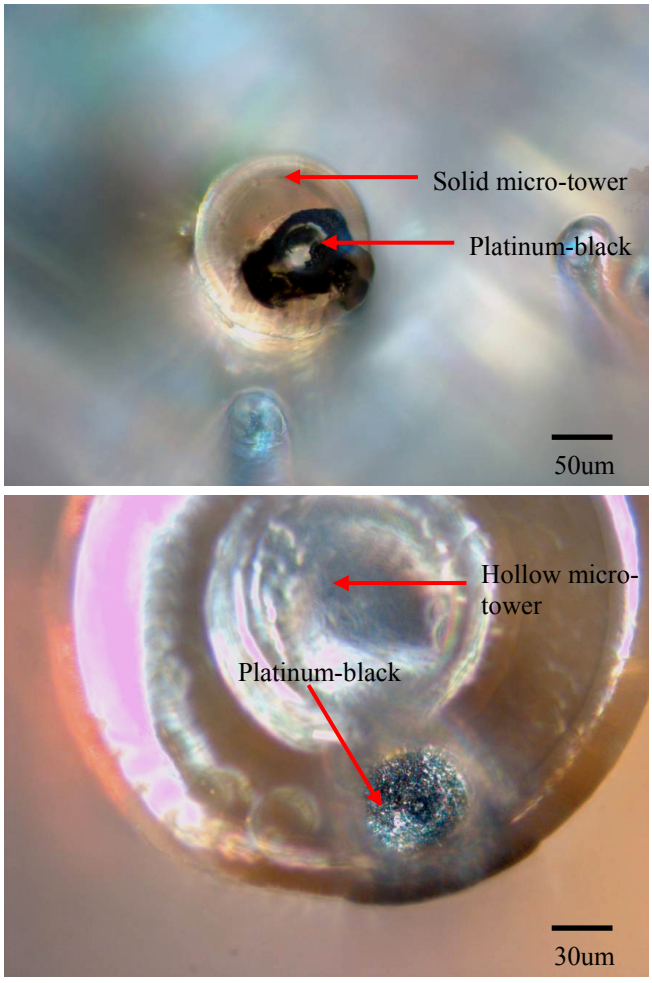

Figure 3.22: Optical micrographs of electrodeposited Pt-black on hollow and solid micro-tower MEAs.

3.2 Laser Scribed 3-D MEAs: Characterization

The fabricated and packaged MEAs are characterized through both electrical and biological tests. For electrical characterization, the impedance spectrum of the device has been measured in the frequency range of interest. Passive thermal noise recording has also been performed. The noise recording ensures that the Signal to Noise Ratio (SNR) of the 3-D MEA is adequate for electrophysiological spike recordings from biological cultures. For biological characterization, 3-D co-cultures of neurons have been successfully grown on the MEAs and the viability of these cultures has been measured. These tests along with the results are discussed in a detailed fashion in the sections below.

3.2.1 Electrical Impedance Spectroscopy

Impedance of a microelectrode is the signature electrical characteristic of the electrode. The classical impedance theory behind these microelectrodes has been given in detail in Chapter 2 and analytical models will be evaluated in Chapter 4. These models serve not only to verify experimental data but also are techniques to ascertain the quality of the electrodes. In this section the system used to measure this impedance is described along with impedance results of laser scribed 3-D MEAs.

An impedance spectroscopy tool was developed by members of Prof. Steve DeWeerth's group (Dr. James Ross and Mr. Scott Buschemi). This tool enabled virtually any conformation of electrode selection, through 206 digitally controlled switching and multiplexing elements (MAX335, MAX306). A desktop computer, via a custom

MATLAB interface, coordinated all communication between a dynamic signal analyzer (Stanford Research SR725, through GPIB) and the custom switching board (PIC 18F442, through RS-232). For full-spectrum impedance measurements, the signal analyzer was configured to source a small (<= 100 mV), sweeping sinusoidal voltage. The automated switching and measuring system was configured using a MATLAB code to apply the voltage source across an individual electrode, reference resistor, and a distant platinum wire ground. Specifically, the spectrum analyzer measured the voltage across the electrode and a 100 KΩ reference resistor (as depicted in Figure 3.23) using two instrumentation amplifiers (INA129P), and MATLAB software calculated the impedance magnitude according to Equation 3.5.

$$Z_{ELECTRODE} = R_{REF} \frac{V_{ELECTRODE}}{V_{REF}} \tag{3.5}$$

where R_{REF} is the reference resistor and $V_{ELECTRODE}$ and V_{REF} are voltages across the electrode and reference resistor respectively.

As a result of this implementation, the full-spectrum impedance magnitude of 60 individual microelectrodes could be measured within a few minutes. Figure 3.24 depicts a schematic of this measurement system and Figure 3.25 provides a photograph of the system.

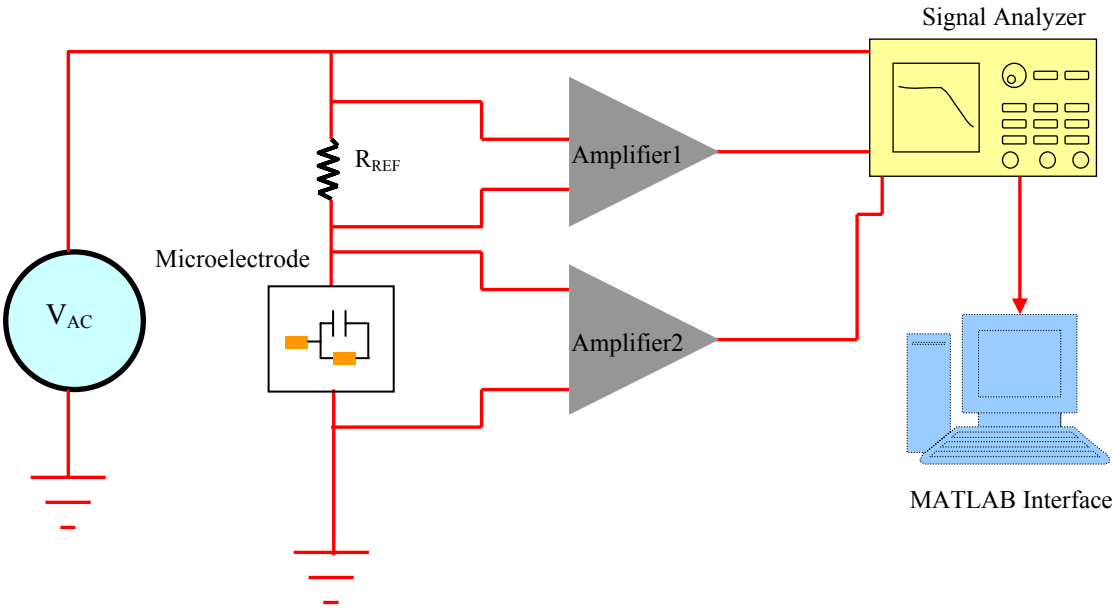

Figure 3.23: Circuit representing calculation of the impedance of the microelectrodes.

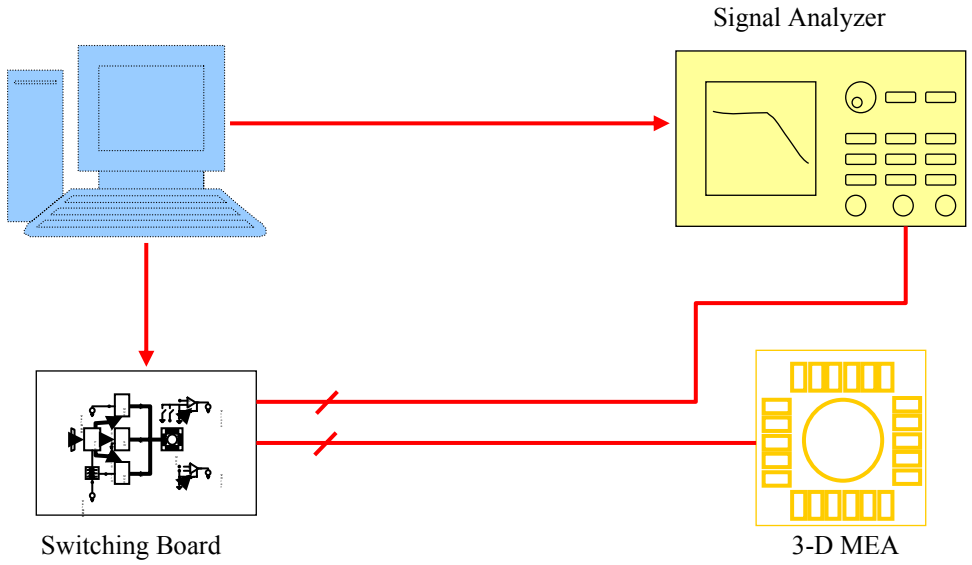

Figure 3.24: Schematic illustrating the impedance spectroscopy setup with MATLAB computer interface, custom swiching board, and dynamic signal analyzer interfaced with the 3-D MEA.

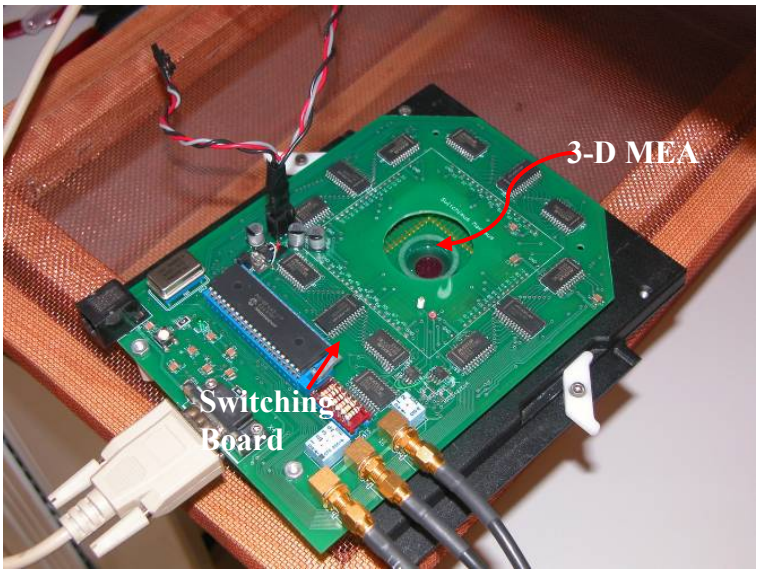

Figure 3.25: Optical image of a 3-D MEA interfaced with the switching board during impedance measurement.

Impedance measurements were performed between the microelectrode, the ground and the cellular conducting media (Hank's Balanced Salt Solution, Invitrogen Corporation, Carlsbad, CA). These testing procedures ensure that the microelectrodes perform as expected, and allow biologists to calibrate stimulation protocols. These tests also identify any problems with the fabrication process (eg. insulation peeling, parylene residue etc). The fabricated and packaged 3-D MEAs were interfaced with the system shown in Figure 3.25 and the impedance of each electrode was measured across a scanned frequency range of 1Hz-100 kHz. Viable electrodes are the fabricated electrodes that show significant deviation from an open circuit (straight line sloping upwards). Figure 3.26 shows the clear distinction between viable and non-viable electrodes among the 24 possible ones. Figure 3.27 depicts a 2-D color map (corresponding to the electrode configuration in the switching system shown on the right hand side of the same figure) at

1 kHz (most relevant electrophysiological frequency [Borkholder 1998] for the same result, which can be used to identify the location of the viable electrodes. The viable electrodes are in the range 10^5 – 10^6 Ohms measured at 1 kHz (shown using a red line in Figure 3.26). Even though 100% viability has not been achieved, these devices are very useful for biological experiments (described in Section 3.2.3).

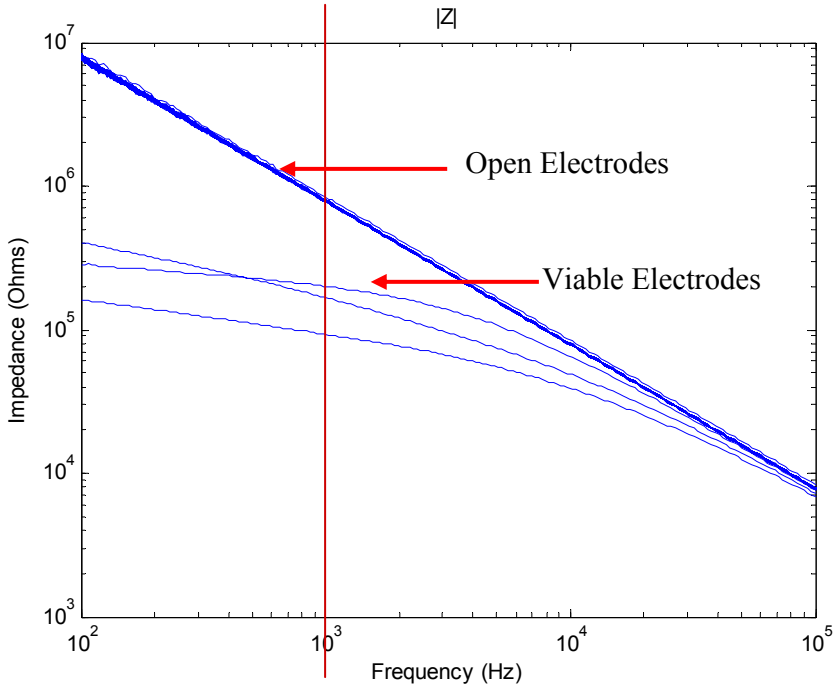

Figure 3.26: Impedance spectroscopy measurements for laser scribed 3-D MEAs.

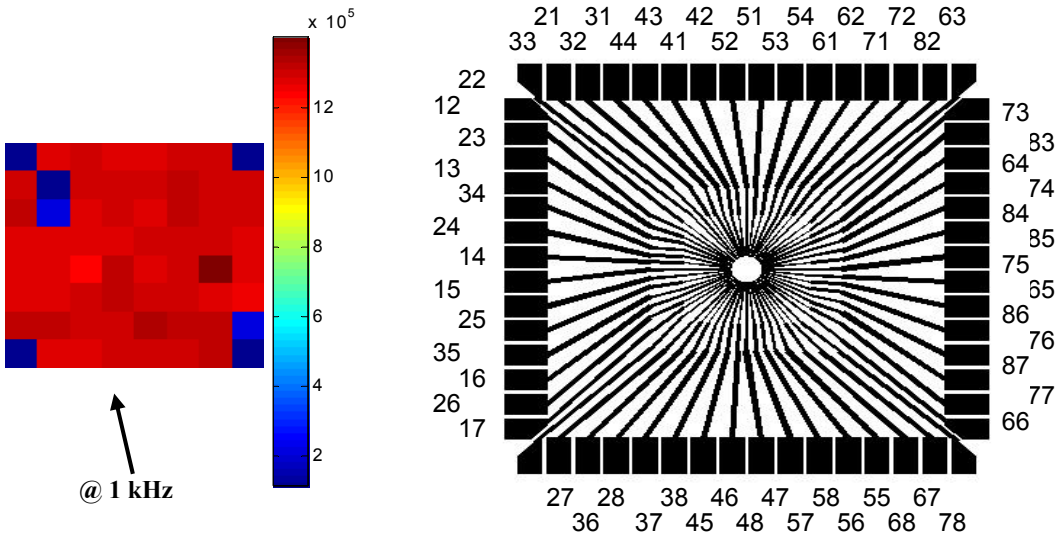

Figure 3.27: Color map of the impedance spectrum (left) at 1kHz showing the clear distinction between viable (blue) and open (red) microelectrodes. This map is useful in determining the location of the microelectrodes on the packaged MEA (location corresponding to the packaging die shown on the right hand side).

3.2.2 Baseline Noise Measurement

Measurement of ambient thermal passive noise of a microelectrode system is very important for neurophysiological experiments since action potentials in cells/networks are in the μV range and a microelectrode should have adequately high SNR in order to detect such a small amplitude signal. A simple baseline noise model has been investigated in Chapter 4. In this section the apparatus used to measure baseline noise is described along with the measured results for laser scribed 3-D MEAs.

The baseline noise of an electrode needs to be low (less than 40 μV [Borkholder 1998]) in order to record electrophysiological activity from a neuronal culture. This measurement was performed using a Multichannel Systems (MCS) measurement setup (MEA-60 System). The MEA-60 system is composed of CMOS electronics, mechanical

interfaces, firmware and software (MC-Rack) integrated into a single unit to characterize microelectrode arrays electrically and biologically. The MEA-1060 amplifier provides data collection and amplification capability from the microelectrodes. The amplifier setup is shown in Figure. 3.28. It also has an integrated heater (below the amplifier) to maintain the temperature of a neuronal culture at a particular value. The system is also equipped with a data acquisition card and software that helps visualize and record the data. MCS is the premium manufacturer of MEAs and interfacing electronics for MEAs. They are based out of Reutlingen, Germany.

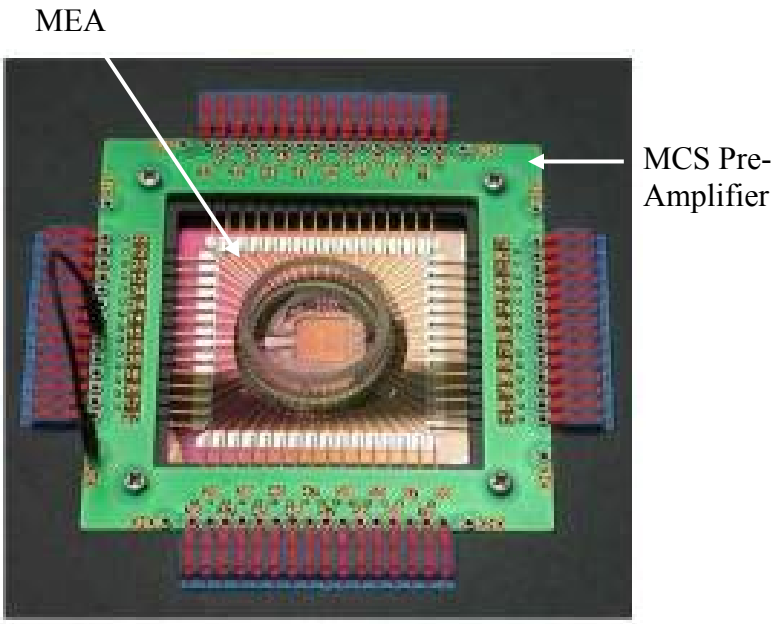

Figure 3.28: Optical photograph of the MCS pre-amplifier setup interfaced with an MEA.

The packaged 3-D MEA was interfaced with the MCS set-up and the measurements were made in a laminar flow hood (minimum particulate matter) under minimum surrounding noise (no ambient lighting or blowers in hoods) between the

microelectrodes, ground and the cellular conducting medium (Hank's Balanced Salt Solution). It was observed that several channels had RMS baseline noise levels of 10-15μV. A snap shot of the data recorded from all the channels and one of the channels with low noise is shown in Figure 3.29. Typical electrophysiological signals from a extracellular measurement of a network of neurons is in the order of a few tens of microvolts [Borkholder 1998]. This shows that these devices have the capability of measuring the action potentials from viable neuronal cultures.

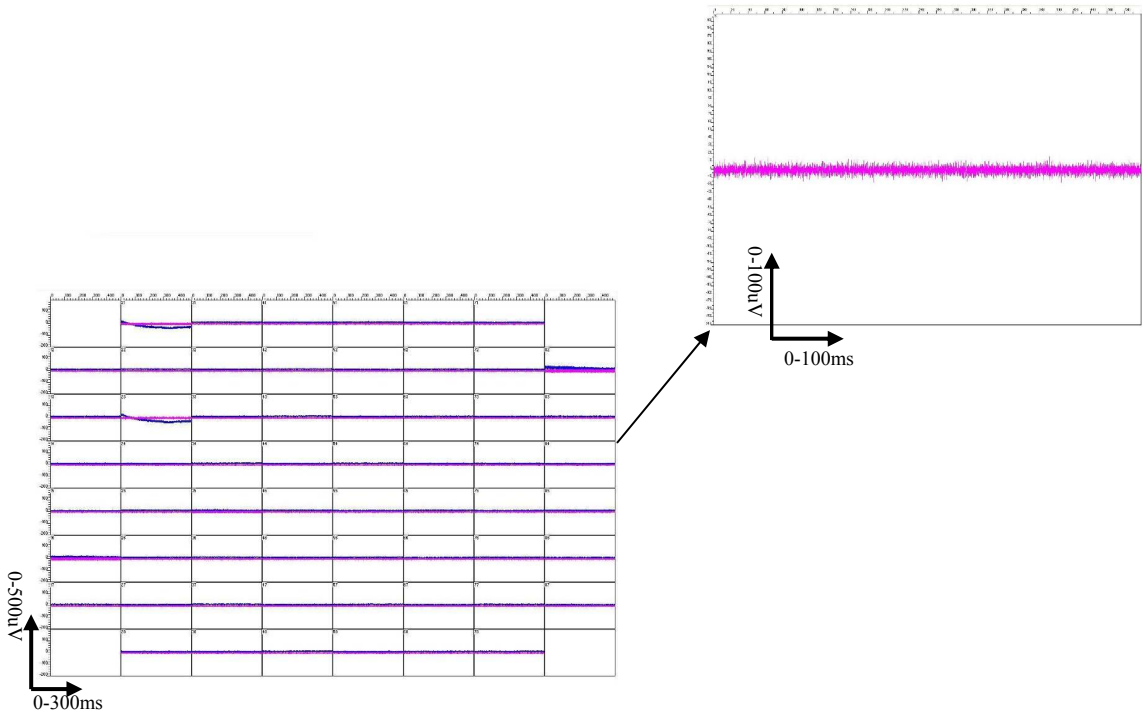

Figure 3.29: Snap shot of the baseline noise of all the electrodes (left) in a 3-D MEA with an example of low noise electrode on the right.

With the important electrical properties of the MEA evaluated, we turn our attention to biological results.

3.2.3 Growth and Survival of 3-D Neuronal Cultures

Since their introduction, MEAs have found applicability in academic and research environments in any area where a cluster of electrically active cells needs to be studied. This includes areas like pharmacology [Stett 2003; Meyer 2004], biosensing [Gholmieh 2003], basic neural research [Wagenaar 2004], traumatic brain injury [Cullen 2005] etc. *In-vivo* animal models are the obvious technique to study a cluster of neurons but these are invasive, need complicated MEMS/RF chips for real time monitoring, and are not very friendly with microscopic imaging [Qing 2000]. The other paradigm that has become popular in the last 20 years or so with electrophysiologists is the *in-vitro* paradigm where clusters of neurons are cultured **outside** the body in a dish [Droge 1986]. The *in-vitro* approach offers obvious advantages including microscopic imaging accessibility, easy pharmacological manipulation, and potential for separation of MEMS and data acquisition electronics. Most of the early work in this paradigm was with 2-D planar networks of cells. However, recently 3-D *in-vitro* cultures of neurons and other electrogenic cells have been demonstrated as a tool to study the functional organization of bodily organs outside the human body [Fawcett 1995, Grinnell 2003]. These cultures more accurately represent the complex nature of cell-cell interactions (especially in a complicated organ such as the brain) and have been shown to have comparable performance to *in-vivo* studies [Potter 2005].

Prof. Michelle LaPlaca's group at Georgia Tech has developed viable 3-D neuronal cultures and co-cultures [Cullen 2005, Vernerkar 2008]. The neural cell culture models developed by the LaPlaca group have been developed using Matrigel (Becton Dickinson, Bedford, MA) matrix, a reconstituted basement membrane that is biologically active for

neural cell growth. It was found by Cullen et al. [Cullen 2005] that cellular models consisting of neurons and astrocytes (which are a type of glial cells that primarily support neuronal outgrowth) distributed throughout a 3-D matrix more closely approximate the heterogeneous composition and architecture of native tissue and thus may exhibit more *in vivo*-like behavior than previous *in-vitro* models consisting of 2-D monotypic populations. The experiments for growth and study of neuronal cultures were performed in collaboration with the LaPlaca group (Dr. D. Kacy Cullen and Mr. Varadraj Vernekar). Details of culture characterization are outside the scope of this dissertation and the reader is referred to the dissertation of Dr. D. Kacy Cullen [Cullen 2005] for the further review. The necessary protocols are described below.

All procedures involving animals were approved by the Institutional Animal Care and Use Committee (IACUC) of the Georgia Institute of Technology. For the harvesting of neurons, timed-pregnant (day 17) Sasco Sprague-Dawley rats (Charles River, Wilmington, MA) were anesthetized using halothane (Halocarbon, River Edge, NJ) and decapitated. The uterus was removed by caesarian section and placed in Hanks Balanced Salt Solution (HBSS). Each fetus was removed from the amniotic sac, rapidly decapitated, and the brains removed. The cortex was isolated and the hippocampal formation removed. To dissociate the tissue, pre-warmed trypsin (0.25%) + 1 mM EDTA (Invitrogen, Carlsbad, CA) was added for 10 min at 37ºC. The trypsin-EDTA was then removed and deoxyribonuclease I (0.15 mg/mL, DNase, Sigma, St. Louis, MO) in HBSS was added. The tissue was then triturated with a flame-narrowed pastuer pipet and then centrifuged at 1000 rpm for 3 minutes after which the supernatant was aspirated and the cells were resuspended in neuronal media (Neurobasal medium + 2% B-27 + 500 μM L-

glutamine). For harvesting astrocytes, postnatal (day 0-1) Sasco Sprague-Dawley rats were anesthetized using halothane and rapidly decapitated. The brain was removed and the cortical region isolated as described above. Upon isolation of the cortical regions, the tissue was minced and pre-warmed trypsin (0.25%) with EDTA (1mM) was added and placed in at 37ºC for 5 minutes. DNase was added and the tissue was triturated using a flame-narrowed pasteur pipet. Neurobasal medium was added and the cells were centrifuged (1000 rpm, 3 minutes) after which the supernatant was aspirated, the cells were resuspended in neurobasal medium and transferred to T-75 tissue culture flasks.

3-D cultures were plated on control polystyrene culture wells, commercial 2-D MEAs (from Ayanda Biosystems, Lausanne, Switzerland) and laser-scribed 3-D MEAs (with both 10μm and 25μm parylene insulation). Before plating, the devices were pre-treated with 0.05mg/mL poly-L-lysine (Sigma Aldrich, St. Louis, MO) followed by 0.5mL of Materigel. The neurons and astrocytes were mixed in a 2:1 ratio at 2500 cells/mm^3. The cultures were plated within the Matrigel which provides dispersion of dissociated cells throughout the matrix material.

The 3-D co-culture was observed under confocal microscopy (LSM 510, Carl Zeiss, Oberkochen, Germany) for 23 DIV (days *in-vitro*). Cells contacting the towers were measured at 1, 6, 13, 19 and 23 DIV. The number of cells contacting the towers is displayed in Figure 3.30. This is important because the higher the density of cells around the towers, the greater the chance of recording the activity of networks of cells as they grow and spread out. It was also observed that the cells were attracted toward the rigid micro-tower structures, preferring to adhere to the walls rather than the bulk of the MEA. This is especially true on days 13 and 19 when close to 40% of the cells plated were

adhering to the micro-tower structures enabling a higher chance of spike recordings. This measurement of course does not account for the growth and proliferation of the neurons.

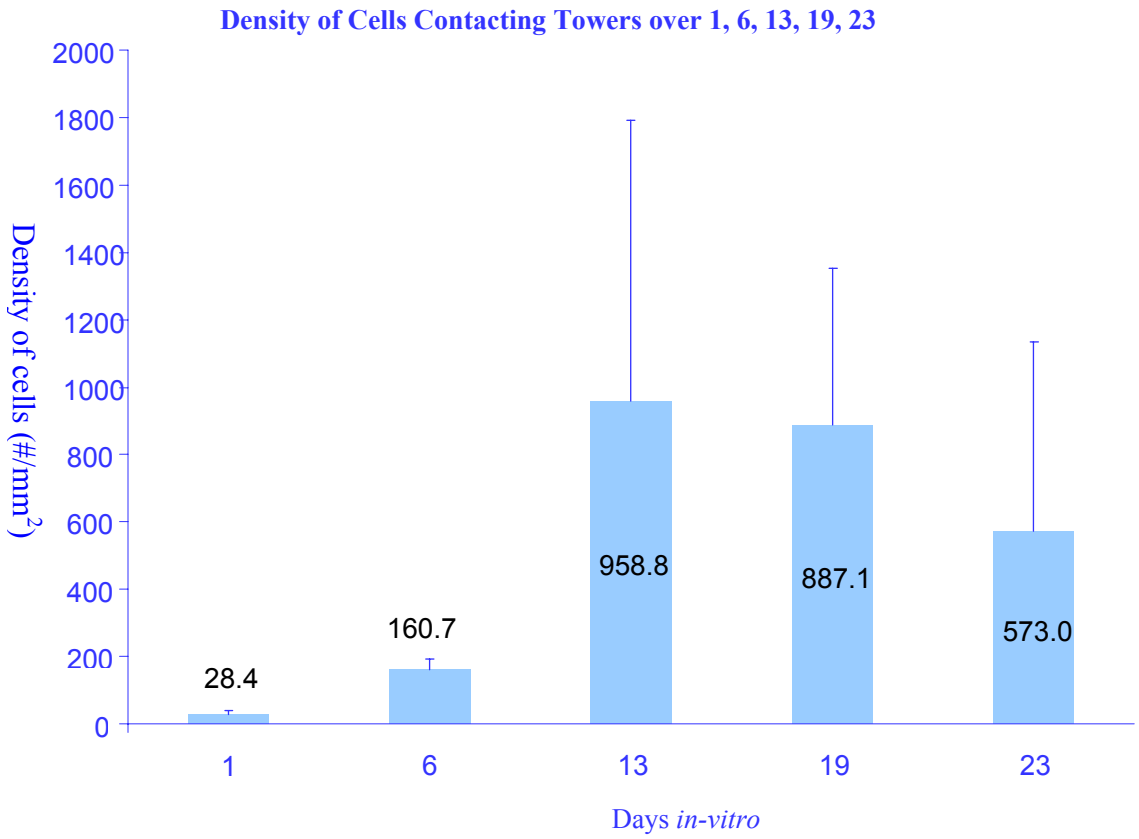

Figure 3.30: Density of cells contacting the towers upto 23 days in-vitro.

Cell viability was evaluated at 21 DIV using fluorescent probes to distinguish between live and dead cells in the following way: the cultures were incubated with 4 µM ethidium homodimer-1 (EthD-1) and 2 µM calcein AM (both from Molecular Probes, Eugene, OR) at 37 °C for 30 min and then rinsed with 0.1 M Dulbecco's phosphate-buffered saline (DPBS, Invitrogen, Carlsbad, CA). The percentage of viable cells was calculated by counting the number of live cells (fluorescing green by calcein) and the

number of cells with compromised membranes (nuclei fluorescing red by EthD-1). Equation 3.6 explains the formula used to evaluate viability.

$$\text{Viability}\,(\%) = \frac{\text{Total \# cells fluorescing green}}{\text{Total \# cells fluorescing green \& red}} \qquad (3.6)$$

Figure 3.31 (top) depicts live and dead cells around a tower separately. Figure 3.30 (bottom) shows the images of live dead cells merged together and the 3-D nature of the culture.

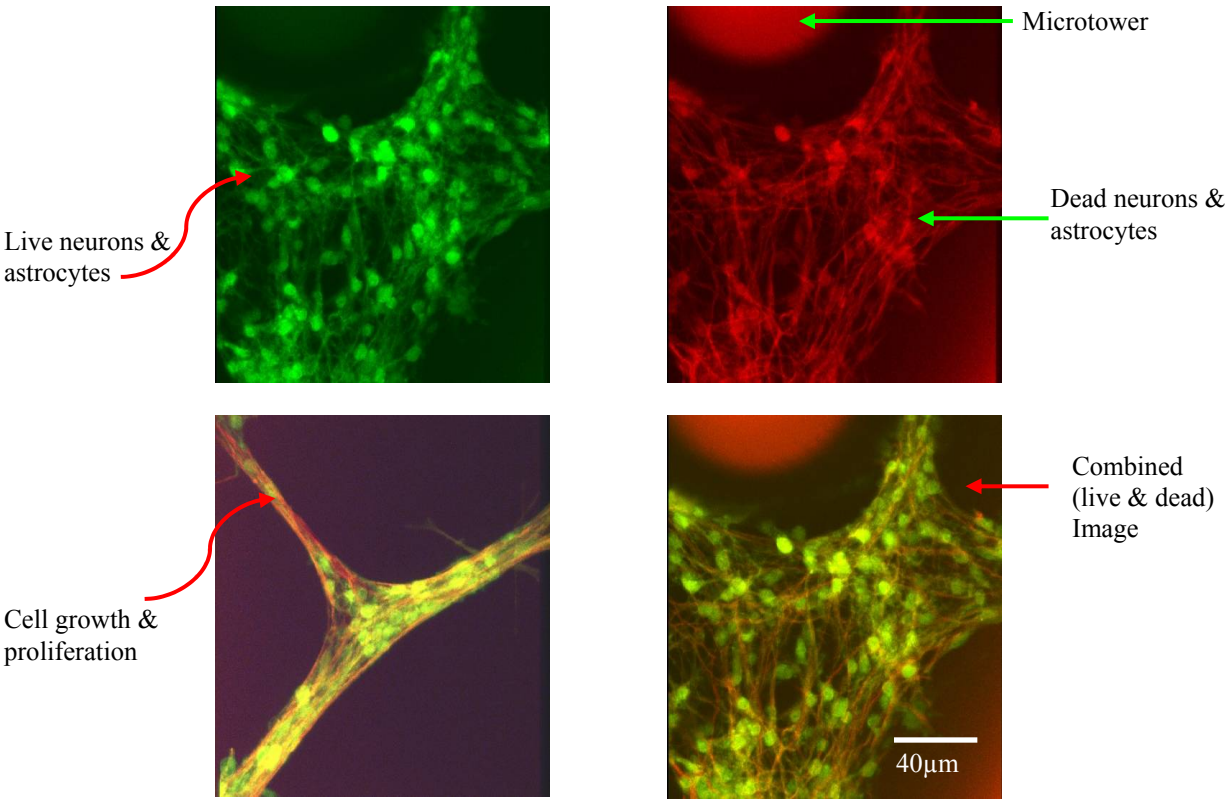

Figure 3.31: Confocal microscopy images of live neurons and astrocytes (above, left) fluorescing green by calcein, dead cells (above right) fluorescing red due to EthD-1. The images in the bottom are the combined images of dead and live cells that demonstrates the growth and proliferation of cells on the MEAs.

The percentage viability of cells is measured and plotted at 21 DIV as shown in Figure 3.32. This graph demonstrates that the laser scribed 3-D MEAs perform very comparably (average reading of 87-90% cell viability) with PS controls. The 3-D MEAs have also shown to out-perform commercial 2-D MEAs in these experiments (> 35% cell viability). This is a significant boost to parylene as an encapsulation, biocompatible polymer that successfully shields neuronal cells from the cytotoxic effects of MEMS fabrication materials. A further significant result is the comparable performance of 10µm insulation with 25µm parylene. This implies that the thickness of the insulation can be reduced offering advantages to the laser micromachining process (to define the recording sites).

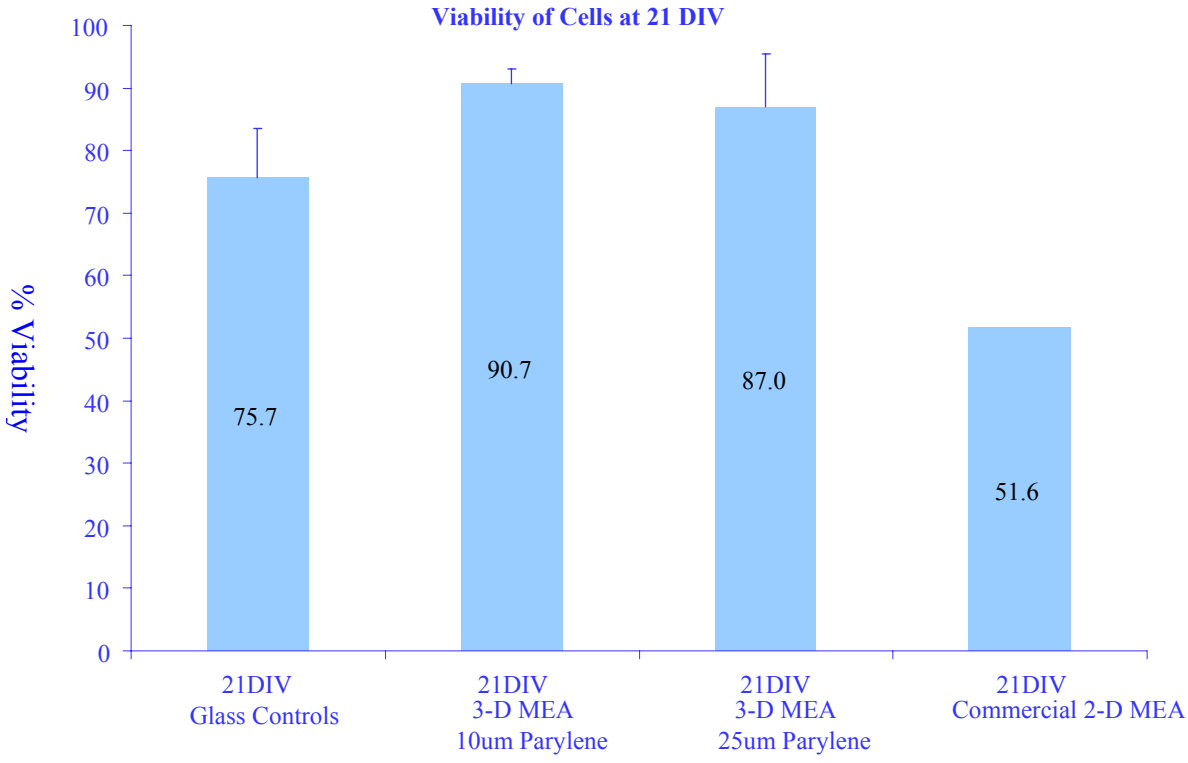

Figure 3.32: Percentage viability of cells on the various devices on which 3-D co-cultures were plated at 21 DIV.

Electrophysiological recordings were performed on these MEAs but did not yield any good results (spike recordings). This can be explained by as follows:

- Number of viable electrodes in the MEA was low (3 out of 24 potential ones) to record any substantial activity. But a high-yield (90% of the potential 64 electrodes on an Ayanda array) commercial 2-D MEA did not register any electrophysiological activity either.
- This leads to the belief that the 3-D co-culture of neurons and astrocytes needs further qualification before it is subject to any recordings.
- It was also observed that the recorded signals showed enormous drift. So the activity could have been lost in the drift

3.3 Chapter Discussions and Conclusions

In this chapter we have demonstrated laser micromachining as a technology for fabricating 3-D MEAs. We have developed a **double-side exposure of thick negative-tone resist** (SU-8) to fabricate solid and hollow micro-tower arrays. A conformally evaporated polymer has been coated on metallized micro-towers and ***scribed*** using excimer laser micromachining. Ablation parameters for micromachining this polymer have been extensively studied along with a theoretical calculation of ablation energy which is in the same order of magnitude as the experimentally observed value. The ***scribed*** **polymer has been utilized as a mold to electroplate electrodes on micro-tower arrays thereby constructing a 3-D MEA**. The MEA has been packaged and parylene insulation has been deposited on the arrays. Recording sites have been defined with laser micromachining. Electrical impedance spectroscopy and baseline noise

measurements have been performed to electrically characterize the 3-D MEAs. 3-D co-cultures of neurons and astrocytes have been **successfully grown for 23 DIV on the MEAs**. Cell viability experiments were performed on the arrays as well as commercial 2-D MEAs and controls. The **3-D MEAs out-performed commercial MEAs in percentage viability at 21 DIV** and showed comparable performance to control polystyrene wells. Electrophysiological measurements on these MEAs were unsuccessful and this is due to either the absence of a large number of viable electrodes on the MEAs or the properties of the co-cultures.

Laser micromachining is a novel technique but due to its serial nature and difficulty in controlling process parameters becomes a manufacturing-unfriendly and a low yield process for 3-D MEAs. Manufacturing-friendliness is an important characteristic for 3-D MEAs as a large number of simultaneous experiments are necessary for statistically significant biological results. So this is explored further in Chapter 4 where we have developed a micromolding-based approach to fabricate 3-D MEAs.

CHAPTER 4

MICROMACHINED *IN-VITRO* MEAs: METAL TRANSFER MICROMOLDING APPROACH

4.1 Metal Transfer Micromolded 3-D MEAs

4.1.1 Introduction

One of the largest challenges in the microfabrication of 3-D MEAs is three-dimensional lithography, which is not easily accomplished as explained in Chapter 3. Laser micromachining was utilized as a technique in Chapter 3 to address this problem, but the process was found to be too serial for any extension to a micro-manufacturing process. Micromolding or soft lithography is a technique that was pioneered by Prof. George M. Whitesides at Harvard University (Cambridge, MA) in the late 90s [Brittain 1998; Jackman 1998; Sia 2003]. It involves the use of elastomeric stamps fabricated from Poly dimethyl siloxane (PDMS), and micromolding structures from these templates for a variety of micro and nano-scale applications. Micromolding presents excellent flexibility in the kind of materials that can be utilized to fabricate micro and nano-scale devices. For biological applications, integration of biocompatible polymers becomes a possibility with micromolding.

There has also been considerable interest in 2-D pattern transfer using elastomeric stamps and self-assembled monolayer inks. Loo et al. [Loo 2002] describe a nano-transfer printing (nTP) approach where they report transferring metal patterns from an elevated elastomeric stamp into various oxidized surfaces. The reported feature sizes are

in the nanometer scale using this type of technique. This section explores a micron-scale 3-D extension of nTP utilizing PDMS molds. Apart from micromolding and transferring functional metal patterns, advanced 3-D mold structure fabrication techniques are required to achieve 3-D MEA templates. The considerable knowledge-base of the MSMA group in this arena utilizing SU-8 has been exploited in this effort [Cros 1998; Cros 2000; Choi, 2002; Yoon 2006; Park 2007]. The combination of all these technologies that contribute to this new technique is aptly titled "Metal Transfer Micromolding", since functional metal patterns will be transferred from one substrate to another during a micromolding step. This technique is described in this chapter along with packaging technologies for 3-D MEAs. The packaged MEAs are then characterized electrically and biologically.

4.1.2 Concept and Design

A schematic of the proposed metal transfer micromolded 3-D MEA is shown in Figure 4.1. It portrays a 5x5 array of metallized micro-towers in the center of a chip and metal traces connecting the towers to bond pads at the periphery of the chip. Traces can also be observed at the bottom of each tower. The traces at the bottom of each micro-tower will serve as the 2-D electrodes and the metallized micro-towers themselves serve as 3-D microelectrodes. All the 50 electrodes can be individually addressed electrically at the periphery of the chip. The bond pads at the periphery serve this purpose. The bond pads, metal traces and the towers have been designed to be elevated above the rest of the chip in order to accommodate the metal transfer process as explained in Section 4.1.3. The overall chip dimensions are designed to be 10mm x 10mm.

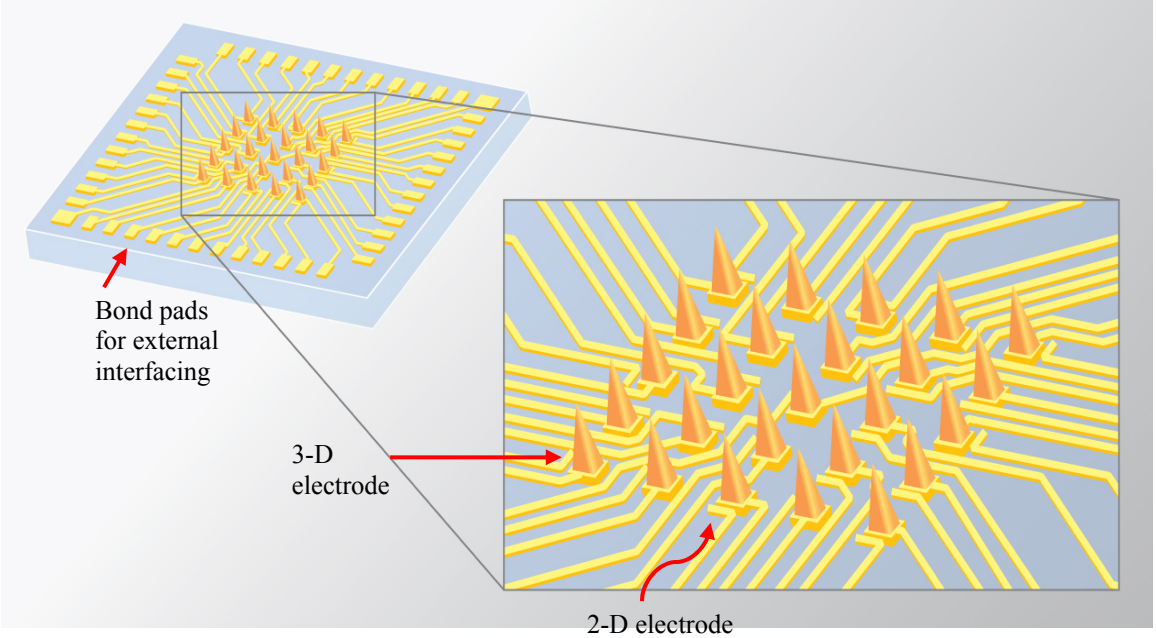

Figure 4.1: Schematic of the proposed metal transfer micromolding-based 3-D MEA. The schematic illustrates the 50 2-D and 3-D electrodes along with the bond pads at the periphery.

The towers themselves are typically either conical or cylindrical with a peripheral dimension of 280µm (side of a square or diameter of a circle) and a pitch of 800µm. The height of the towers is fixed at 500µm. The height however can be controlled to suit the application as explained in the microfabrication section. These dimensions were defined as a compromise between ease of fabrication and application in the biological arena. Figure 4.2 depicts the AutoCAD design of the mask for a pyramidal micro-tower structure with metal traces and bond pads. The shape of the towers is controlled by the type of mask used as described by Choi [Choi 2007]. It is proposed that neuronal cultures similar to those described in Chapter 3 are grown with these towers as the supporting structures. Also recording and stimulation of electrically active neuronal cells is performed using the created electrical pathways.

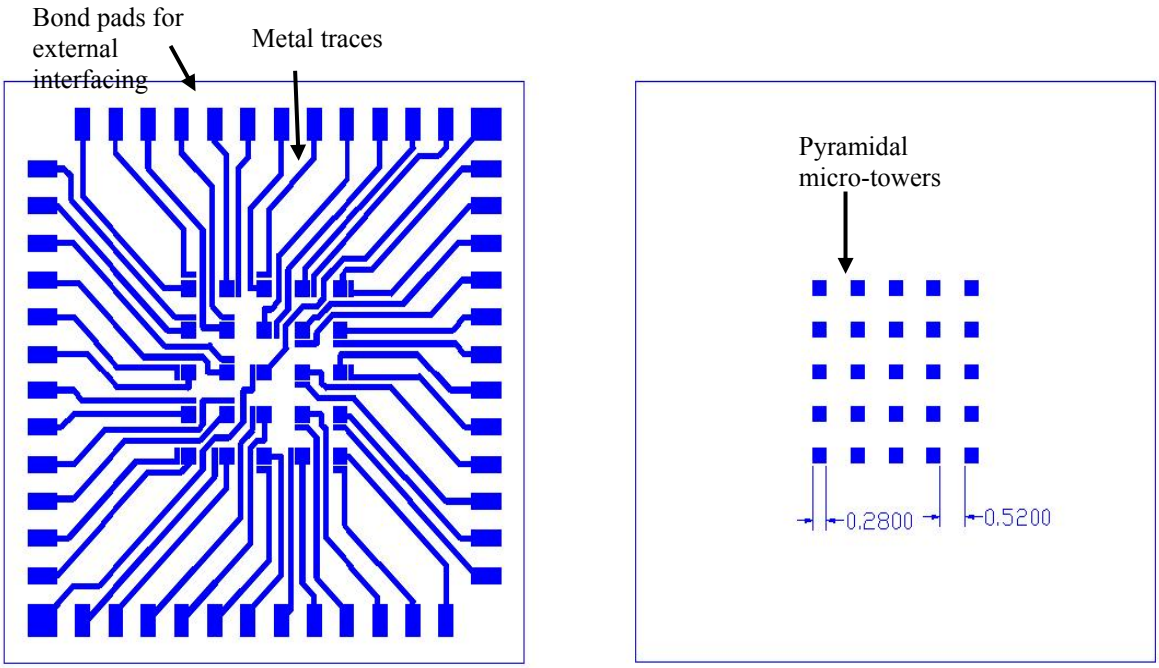

Figure 4.2: AutoCAD mask design for the proposed 3-D MEAs. On the left is the metal traces mask and on the right is the mask for the pyramidal micro-tower structures.

These structures and can also used to stimulate and record from neural tissue slices and other types of neuromuscular tissue. The structures have been designed to be versatile to fit *in-vivo* paradigms (like deep brain stimulators) of recording and stimulating from electrogenic cells in addition to all the above mentioned *in-vitro* applications.

4.1.3 Microfabrication: Inclined UV Exposure to Fabricate Rigid and Flexible Molds

Fabrication of complex 3-D structures is of considerable interest in the MEMS community. Lithographie Galvanoformung Abformung, or LIGA, is one of the first direct high aspect ratio micromachining technologies that was developed at the Karlsruhe

Nuclear Research Center (Karlsruhe, Germany) and at Sandia National Labs (Livermore, CA) [Ehrfeld 1988]. Complex 3-D MEMS structures can be fabricated using LIGA but it comes with a cost – expensive x-ray sources are utilized to expose the thick resist. Ultraviolet (UV) lithography is the most common technique for exposing resist in MEMS as the equipment used is relatively inexpensive as compared to these x-ray sources or deep UV or even laser systems [Ehrfeld 1988; Mohr 2000; Behrmann 1997]. However UV lithography relies on intimate contact between substrate and mask thereby is compatible mainly with planar lithography or 3-D patterning where the structure was extruded normally from the substrate with a height of less than 100μm. But with the introduction of SU-8 to the MEMS community in the mid-late 90s [LaBianca 1995; Lorenz 1997], it became possible to structure high aspect ratio structures normal to the surface with 90˚ sidewalls with top-side exposure. By utilizing bottom side UV exposure of SU-8 with a UV transparent substrate such as glass, high aspect ratio structures and tapered structures can be fabricated [Rajaraman 2007; Rajaraman 2008]. The top and bottom side exposure of SU-8 is schematically illustrated in Figure 4.3 together with the resultant SU-8 structures. Applications that have been reported for this technology include dispensers [Koltay 2004], microneedles [Kim 2004], optical components [Fan-Gang 2003; Kuo-Yung 2003], and mixers and filters [Balslev 2006; Sato 2003]. If we take this a step further, the exposure inclination can be varied resulting in some very interesting shapes. If this variation can be performed in a controlled, continuous fashion, trenches can be defined in a thick SU-8 layer. This process is called “Inclined rotational UV exposure of SU-8” [Yoon 2006]. Figure 4.4 depicts a cleanroom compatible setup for this process that has been developed by our group.

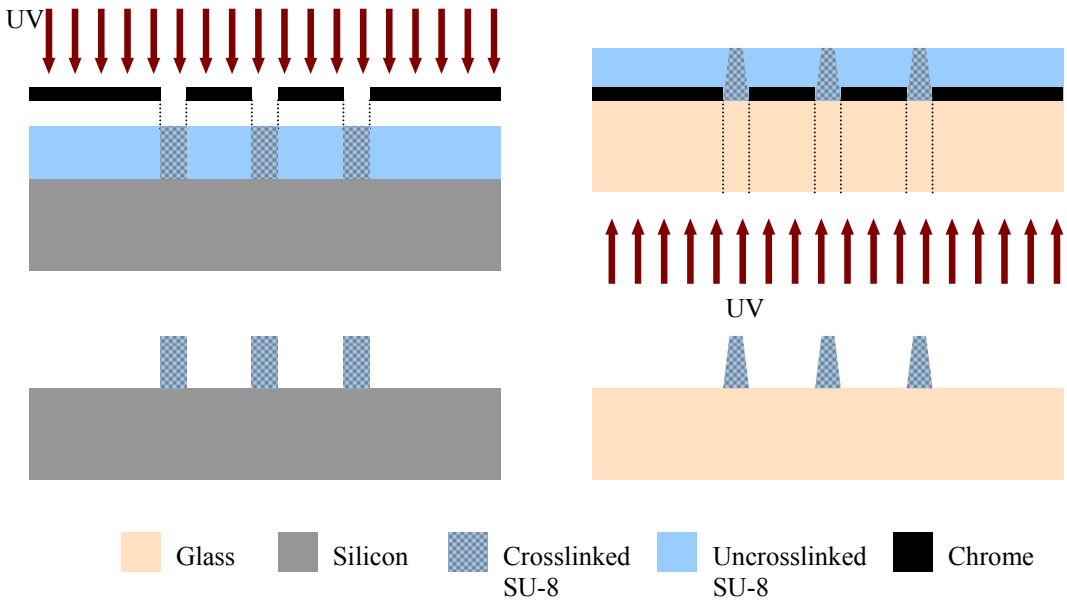

Figure 4.3: Schematic depicting topside (left) and controlled bottom side (right) exposure of SU-8 with the expected structures.

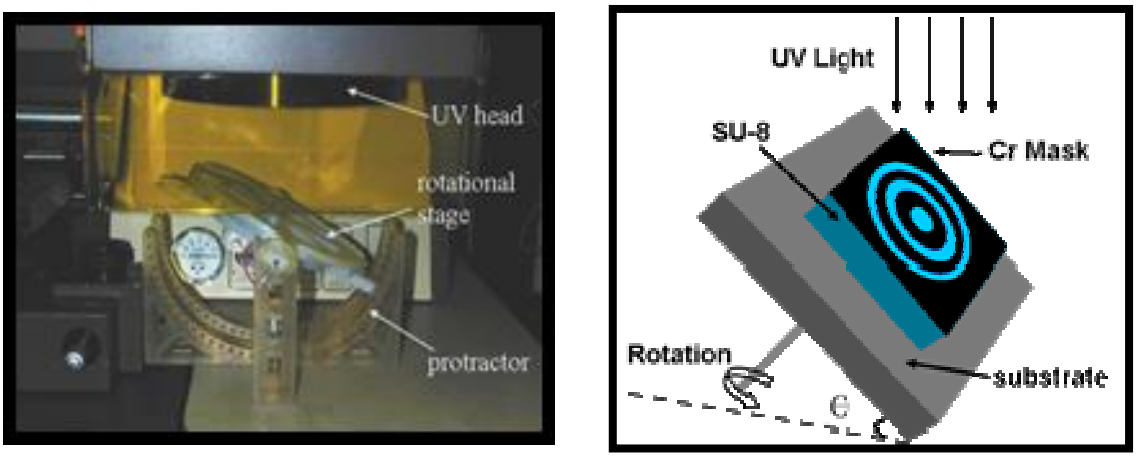

Figure 4.4: Photograph of a tool for controlled inclined exposure of SU-8 (left) and schematic of an inclined exposure process (right).

The inclined rotational UV exposure of SU-8 has been adopted in this chapter to achieve cylindrical and conical micro-towers for the 3-D MEA. The dimension of the feature and angle of inclination determine the shape and depth of the cavity. Rigid SU-8, flexible PDMS molds, and intermediate master structures can be fabricated using this technique combined with micromolding. Figure 4.5 depicts a typical process used for this fabrication. It starts with the dicing of a 4" silicon wafer into smaller 15mm x15mm substrates. These diced substrates are then cleaned in a piranha solution (2:1 H_2SO_4 and H_2O_2 at room temperature) for 10 minutes followed by a 5 minute DI water rinse. A thick layer of SU-8 2025 is then cast by weight to define an 800µm layer and soft baked at 95˚C for 20 hours. It is relatively harder to achieve thick coatings by spin casting of SU-8 due to the requirement of multiple coating and baking steps. This results in enormous thermal stress on the bottom-most coated layer of SU-8 leading to bowing of the material. Weight casting is a far more elegant way for achieving SU-8 layers of up to 1.2mm. The weight of SU-8 can be calculated based on the density of SU-8 (1.219 g/mL for 2025) [Microchem Inc 2008] and the volume of the SU-8 layer required by the application (described in Chapter 3). This SU-8 is exposed using the inclined rotational system (Step 1) using 9000mJ of UV (365nm I line exposure system, OAI, San Jose, CA). The angle of exposure is set to be 23˚ which will result in a recessed trench depth of around 500µm according to Choi [Choi 2007]. This can be varied to change the depth of exposure. The crosslinked SU-8 is then developed after a post-exposure bake for 1 hr at 95˚C in PGMEA (Step 2). Intermediate master structures are then fabricated from these molds. In order to fabricate the master structure a separation layer (Cr/Au, 15nm/100nm) is deposited on the rigid SU-8 mold using a sputtering system (Step 3).

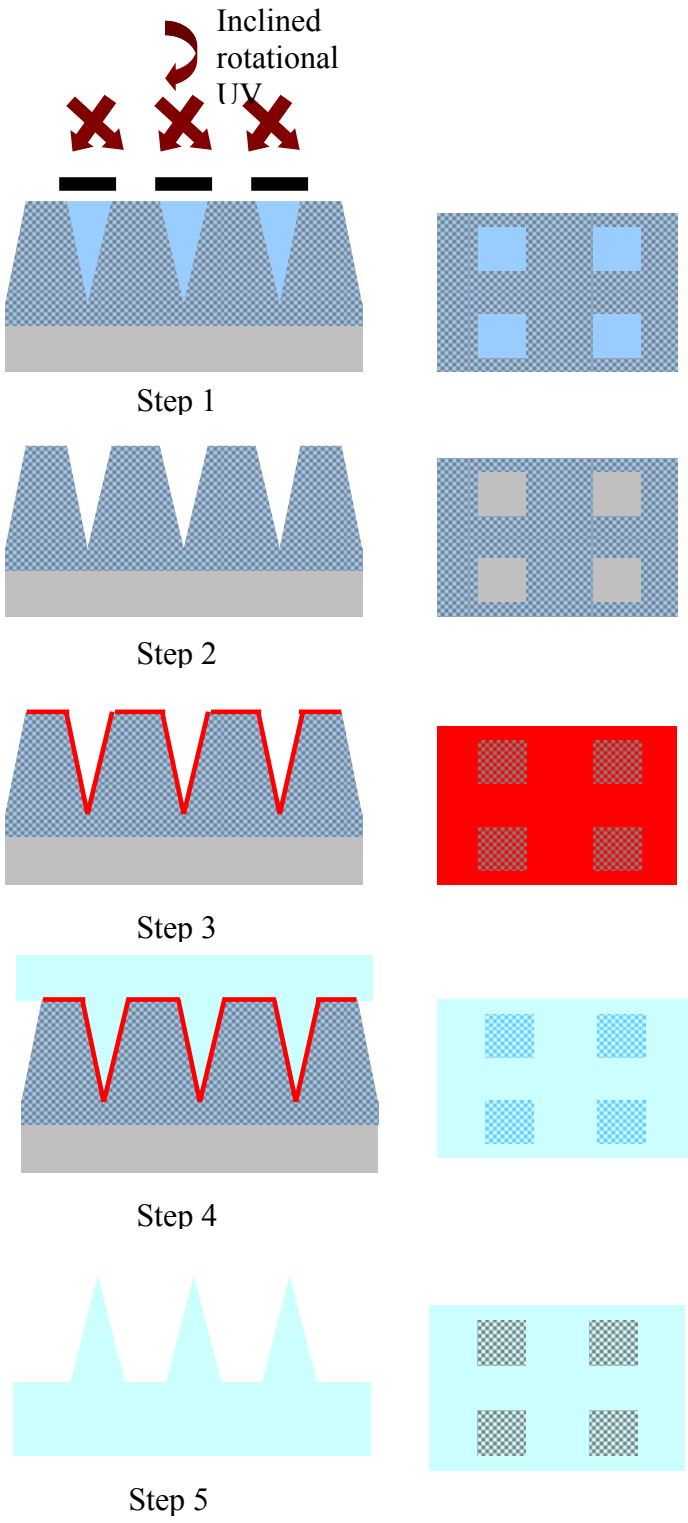

Figure 4.5: Schematic of the process flow for microfabrication of rigid and flexible molds using inclined UV exposure. Side views are depicted on the left and top views of the various steps are depicted on the right.

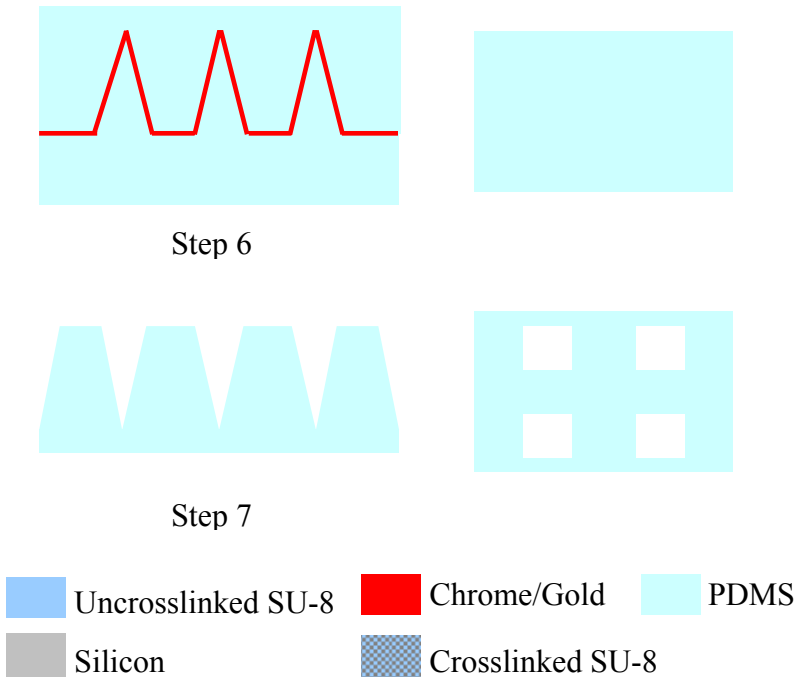

Figure 4.5: Continued.

Since the SU-8 mold is a rigid structure, a flexible material (eg. PDMS) is used for the master structure for ease of demolding. PDMS is preferred in replica molding processes due to its high dimensional fidelity, chemical inertness and ease of processing. However the high hydrophobicity of the material often necessitates the need for a wetting layer in PDMS processing. The separation layer of Cr/Au serves this purpose. A layer of PDMS 184 (Sylgard 184) is pre-mixed (10:1 ratio of base and curing agent) and cast onto and into the rigid mold features. PDMS is supplied by Dow Corning Chemicals (Midland, MI) and can be cured relatively quickly at higher temperatures (15 minutes at 150˚C). It achieves its full mechanical properties in 7 days [Dow Corning Silicones

2008]. An intermediate optimum temperature of 50˚C is selected for the curing. In order to accommodate the requirement necessitated by the mechanical properties of the material keeping in mind the time constraints, the PDMS layer is cured at this temperature for 24 hours in an oven (Step 4). The master structure is then carefully demolded from the rigid SU-8 mold (Step 5). Flexible mold structures that have the same features as the rigid mold in Step 3 are fabricated using another micromolding step. This time PDMS is pre-mixed and cast (Step 6) on the PDMS master (which is coated with a separation/wetting layer of Cr/Au). The PDMS layer is cured using the same conditions as in Step 5 and then demolded to release a flexible PDMS mold (Step 7). One disadvantage of using a Cr/Au separation layer is degradation of the master surface (due to the thermal stress on PDMS during metal sputtering) leading to replication of the degraded surface features in the flexible mold. Literature review suggests usage of plasma treatments or corona discharges to accomplish the alteration of PDMS surface from hydrophobic to hydrophillic [Fritz 1995; Hillborg 1998] but these usually result in strong adhesion of the master structure to the mold. Also the potential contamination of the master structure in the Plasma Therm RIE system due to the lack of control of the materials used in the tool lead us away from these techniques.

Figure 4.6 depicts SEM images of conical and pyramidal rigid molds. Figure 4.7 illustrates SEM images of the PDMS master. Figure 4.8 depicts SEM images of the flexible PDMS mold.

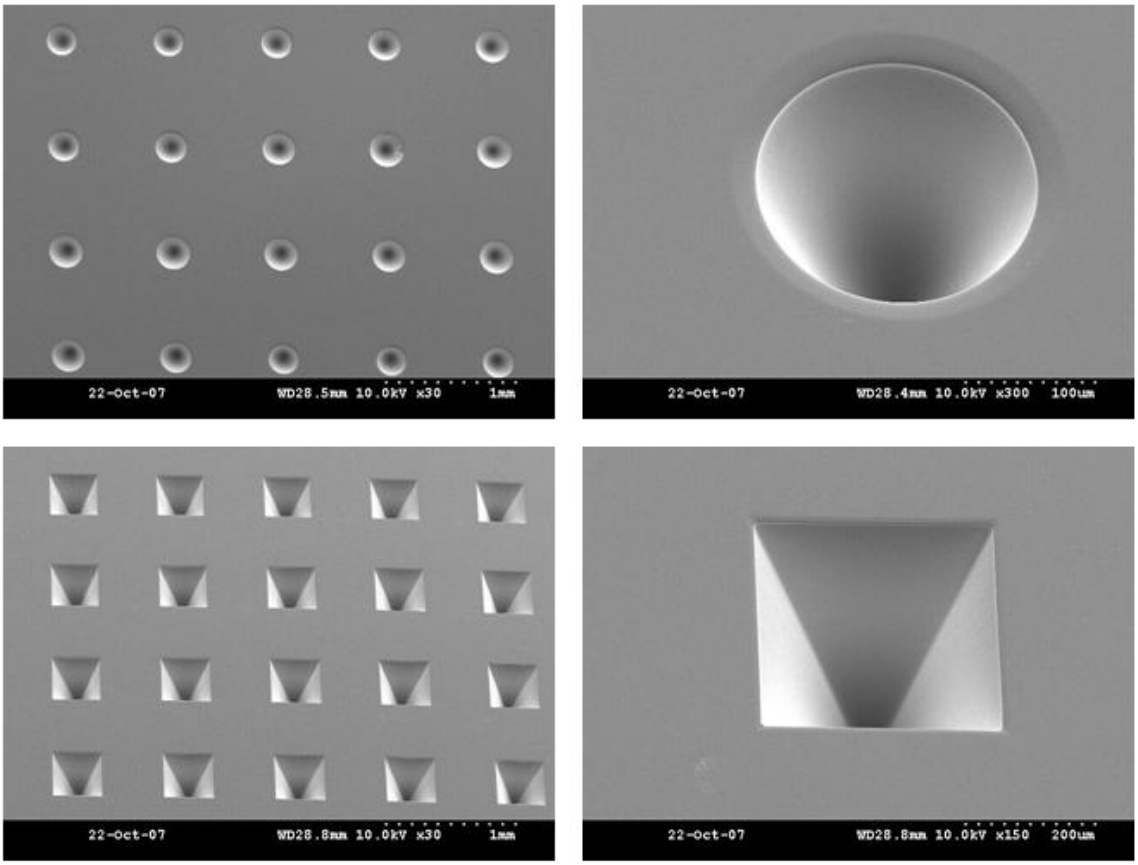

Figure 4.6: SEM images of conical (top) and pyramidal (bottom) rigid SU-8 mold structures.

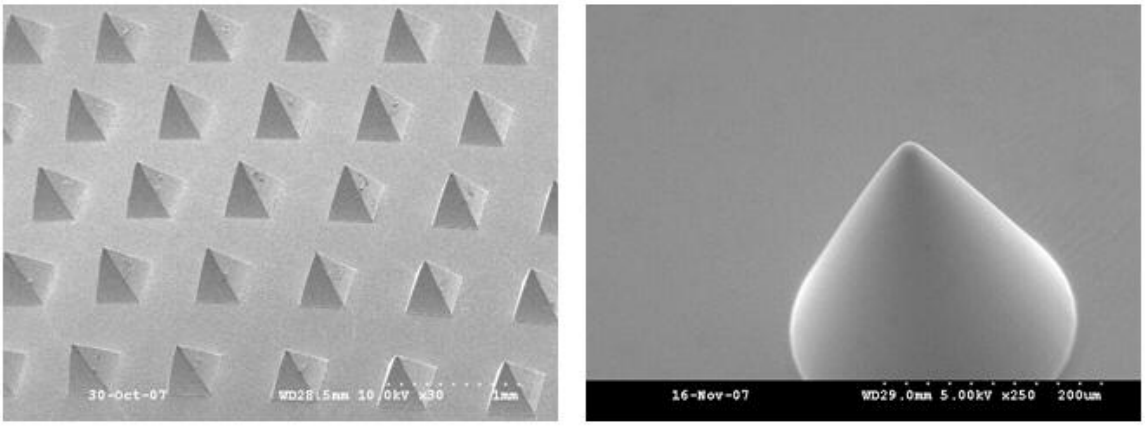

Figure 4.7: SEM images of PDMS master structures for pyramidal micro-towers (left) and conical micro-tower (right).

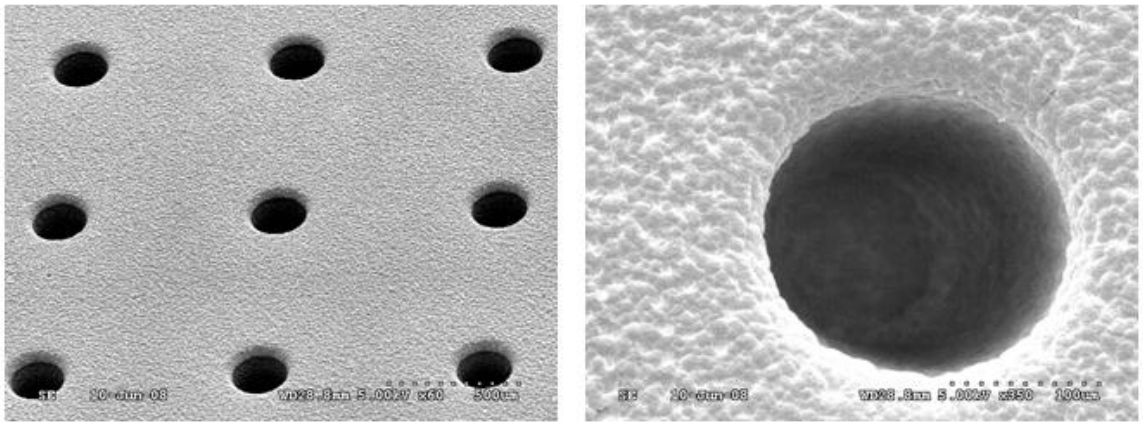

Figure 4.8: SEM images of conical micro-tower molds fabricated from PDMS.

This flexible mold structure is selectively metallized utilizing techniques that are described in Sections 4.1.5 and 4.1.6. Polymer microstructures (from a variety of polymers) of various heights can be fabricated from this flexible mold with functional metal patterns transferred during micromolding. One of the key advantages of this process is that since it is a micromolding based approach, it lends itself to scaling and mass manufacturability.

4.1.4 Shape Prediction of 3-D MEA Molds

The geometry of the final 3-D structure that is fabricated using inclined UV lithography can be predicted using the footprint of the mask used in 2-D. As the complexity of the 2-D mask increases, so does the shape obtained in 3-D. In this section, the mathematical theory behind the extrusion of a square in 2-D is explored. Ray tracing techniques can be utilized to predict the shapes of 3-D structures obtained from 2-D

footprints [Choi 2007]. Computer aided design (CAD) tools such as AutoCAD (Autodesk, San Rafael, CA) can be utilized for demonstrating the ray tracing extrusions.

Figure 4.9 depicts an arbitrary parametric curve C(t), which happens to be a square in this case and its extrusion ($C_e(t)$) at a certain height, h. The extrusion is performed at an angle θ as shown.

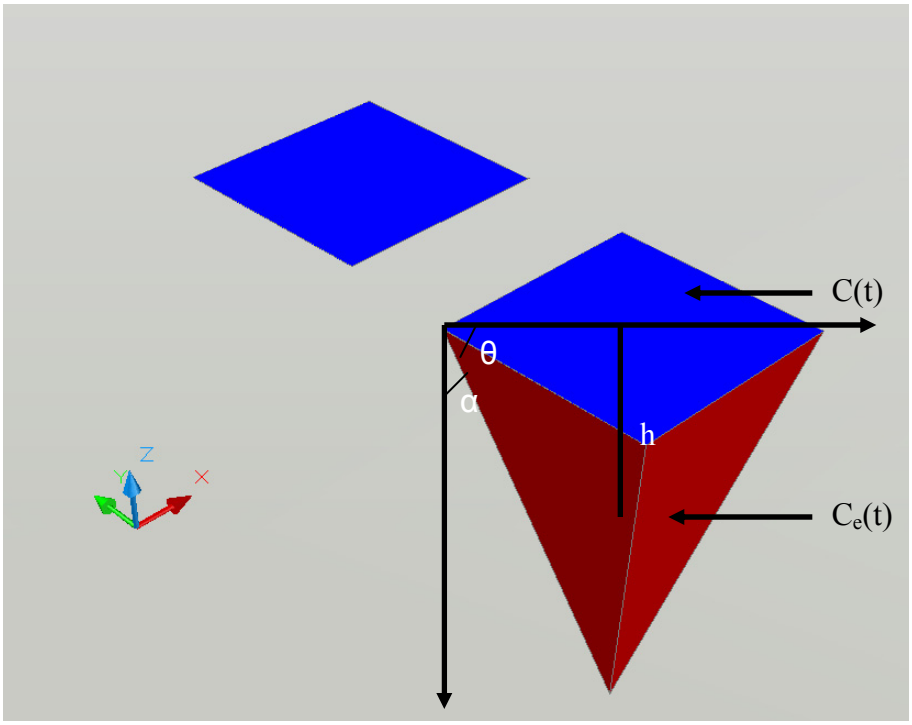

Figure 4.9: AutoCAD representation of a square in 2-D extruded in 3-D at a certain negative height.

C(t) and $C_e(t)$ can be defined by Equations 4.1- 4.4 for a set of points [x(t), y(t)] in space.

$$C(t) = [x(t), y(t)] \tag{4.1}$$

$$C_e(t) = C(t) - eN(t) \tag{4.2}$$

$$N(t) = \left[\frac{y'(t)}{\sqrt{x'(t)^2 + y'(t)^2}}, \frac{x'(t)}{\sqrt{x'(t)^2 + y'(t)^2}}\right] \tag{4.3}$$

$$e = h\tan\alpha \tag{4.4}$$

In polar coordinates, any point in space can be represented by a radius R and an angle θ. So if C(t) is represented using this notation, new representations for C(t) and $C_e(t)$ can be calculated using simple mathematical manipulations.

$$C(t) = [R\mathrm{Cos}\theta, R\mathrm{Sin}\theta] \tag{4.5}$$

$$N(t) = [\mathrm{Cos}\theta, \mathrm{Sin}\theta] \tag{4.6}$$

$$C_e(t) = [(R - e)\mathrm{Cos}\theta, (R - e)\mathrm{Sin}\theta] \tag{4.7}$$

From Equation 4.7 it is apparent that as h increases, i.e., an increase in the height of extrusion, R-e (when α varies from 0-90˚) decreases until it converges to a point. This essentially means that the extrusion of a square in 2-D is a pyramid in 3-D. Figure 4.10 depicts the extrusion of a 5x5 array of squares in 2-D. Pyramids are the result of the ray tracing process for squares in two dimensions.

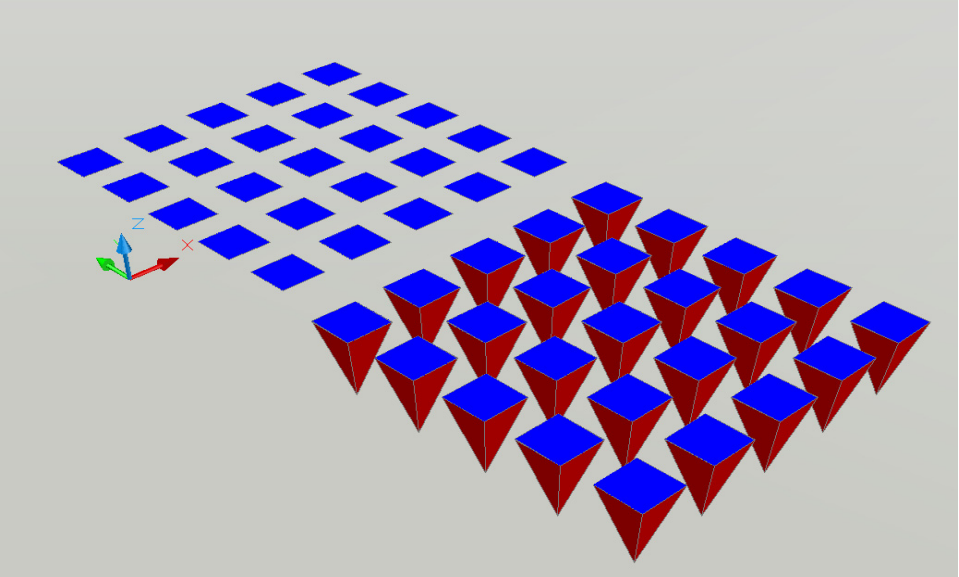

Figure 4.10: Extrusion of an array of 5x5 square shapes in 2-D using AutoCAD.

4.1.5 Microfabrication: Shadow Mask Metallization and Metal Transfer Micromolding

An important step toward the realization of manufacturing-friendly approaches for producing 3-D MEAs is self-aligned metallization and metal patterning. 3-D fabrication to pattern metal in trenches or towers is a complex problem in MEMS and requires difficult approaches described in Chapter 3. A serial approach (laser micromachining) to tackle this problem was developed in Chapter 3. In order to simplify fabrication, in this chapter we introduce a metal transfer micromolding based approach which can be thought of as an extension of 2-D metal transfer processes like those used in nanoimprinting [Ko 2007]. Two separate approaches have been demonstrated to accomplish the selective metallization: (a) Selective metal deposition onto and into the mold features using a shadow mask; (b) Selective metal removal using an intentionally

formed non-planar mold using 2-D metal transfer which is described in detail in the next section. The shadow mask process is detailed in Figure 4.11.

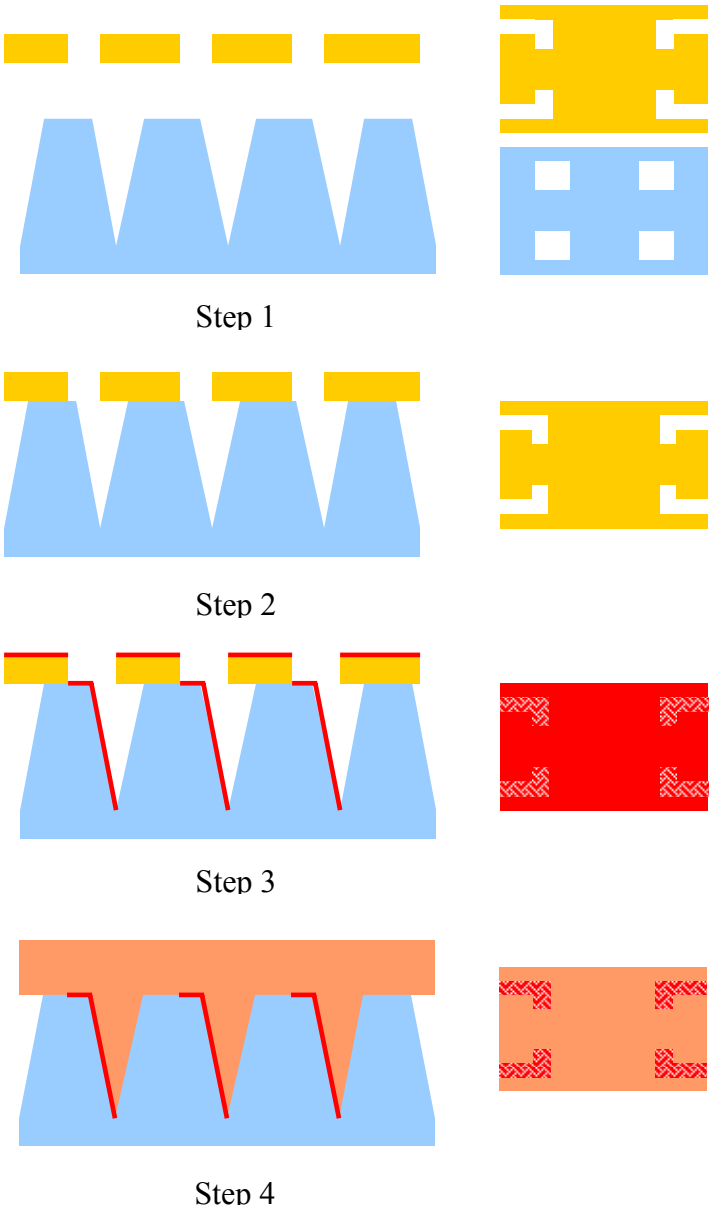

Figure 4.11: Schematic process flow for shadow mask metallization process used in selective metallization and metal transfer micromolding 3-D MEAs. Side view of the process steps is shown on the left and top views on the right.

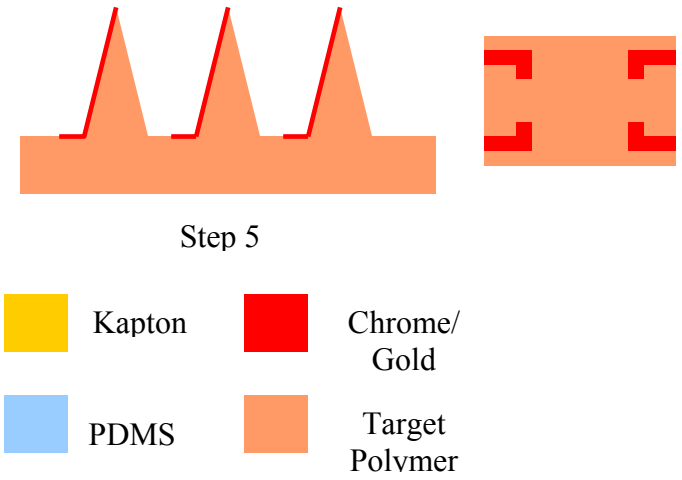

Figure 4.11: Continued.

The fabrication process begins with the creation of a shadow mask (Step 1). The shadow mask is fabricated using an excimer laser ablation process of thin Kapton (125-150µm) sheets [DuPont Inc, 2008]. The ablation parameters are given in Table 4.1. Since the critical function of this process is removal of Kapton all the way through the sheet, the process is not as sensitive as the removal of thin parylene on thin metal that was described in Chapter 3. Thus detailed process characterization was not performed.

Table 4.1: Excimer laser micromachining parameters for Kapton shadow mask

Parameter	Nominal Value	Comments
Energy	250mJ	
Power Attenuation	20%*	Process window ±5%
Pulses	100*	Process window ± 25
Velocity	60µm/s	Constant
Frequency	90Hz	Constant
Ablation rate	50-60µm/cut	

* varies with condition of the system

It is essential to determine a process window (mainly laser power), so that the shadow mask features are within 10% of the intended size. The process window is also provided in Table 4.1. This mask is then aligned with a PDMS mold (fabricated as described in Section 4.1.3) and held in place with pins (Step 2). Alignment marks are micromachined on the shadow mask to aid the alignment process that is performed under a stereoscope. A layer of Au/Cr (500nm/10nm) is evaporated (Step 3) onto this mold using a filament evaporator (Kurt J. Leskar Company, Clairton, PA) or e-beam evaporator (CVC Products, Rochester, NY).

Several target polymers were evaluated to fabricate the final 3-D MEAs. The determining factors for a polymer to be used in this metal transfer process are twofold - a higher surface energy than PDMS and ease of processing. PDMS has a surface energy of 19.8mJ/m^2 [Hur 2004]. Thus, metal does not adhere well to PDMS. If this metal layer is exposed to another polymer with a larger surface energy theoretically the metal layer should bond itself to the polymer (with higher surface energy) and be transferred from the PDMS layer. Metal transfer is described theoretically by Equation 4.8 which denotes the differences in work of adhesion between a metal surface and a polymer surface:

$$W_{Polymer-metal} - W_{PDMS-metal} = (\gamma_{Polymer} - \gamma_{PDMS}) - (\gamma_{Polymer-metal} - \gamma_{PDMS-metal}) \quad (4.8)$$

In this equation γ_{PDMS}, $\gamma_{Polymer}$ represent the surface energies of PDMS and the target polymer while $\gamma_{PDMS\text{-}metal}$, $\gamma_{Polymer\text{-}metal}$ denote interfacial energies between PDMS-metal and target polymer-metal respectively.

The three target polymers that were evaluated include SU-8, Poly-Methyl Methacrylate (PMMA) and Poly-urethane (PU). The surface energies of these polymers along with their method of processing are listed in Table 4.2.

Table 4.2: Surface energies of the various polymers used in the MTM process

Polymer	Surface Energy	Processing
SU-8	46mJ/m^2	weight casting; UV exposure
PMMA	41mJ/m^2	solvent casting; heat
PU	43mJ/m^2	solvent casting
PDMS	19.8mJ/m^2	

ref: Hur 2004, Suh, 2004

Returning attention to the metalized PDMS mold, the shadow mask is then removed and the target polymer (PMMA, SU-8 or PU) is cast onto the metalized mold (Step 4). The polymer is post processed and demolded from the PDMS mold (Step 5). Metal is transferred during this process from the PDMS mold to the target polymer. In the case of SU-8, the material (SU-8 2075) is cast into the metal patterned mold and soft baked at 95˚C for 20 hours. It is then exposed using 9000mJ of UV energy to crosslink the 3-D MEA structure. The 3-D MEA is then carefully separated from the mold. The success rate of SU-8 demolding is low (less than 50%) due to adhesion between SU-8 and the unmetallized PDMS. PU and PMMA have a much higher success rate of demolding (greater than 90%). This is due to the fact that neither of these polymers binds well with PDMS. PMMA is available in the form of a solid (Scientific Polymer Products Inc., Ontario, NY) that is dissolved in ethyl L-lactate (Acros Organics, Geel, Belgium) at the rate of 20-25% solid in solution. The solution is then cast onto and into the metal

patterned mold and the solvent is evaporated. Room temperature gave the best results for solvent evaporation. Bubbles were usually observed at higher temperatures. The curing time for PMMA is approximately 48 hours and the solution is replenished multiple times during this step. Poly-urethane is available as a two component polymer (base and curing agent) from Smooth-On Polymers, (Smooth-On, Easton, PA). The components are mixed in a 1:1 ratio, cast on the metallized mold and cured at room temperature for 24 hours. Figure 4.12 depicts optical micrographs of a Kapton shadow mask and the PDMS mold aligned to the shadow mask. Figure 4.13 portrays optical images of the PDMS mold with metal deposited using the shadow mask. Figures 4.14 and 4.15 illustrate optical images of demolded SU-8 3-D MEAs fabricated using this technique.

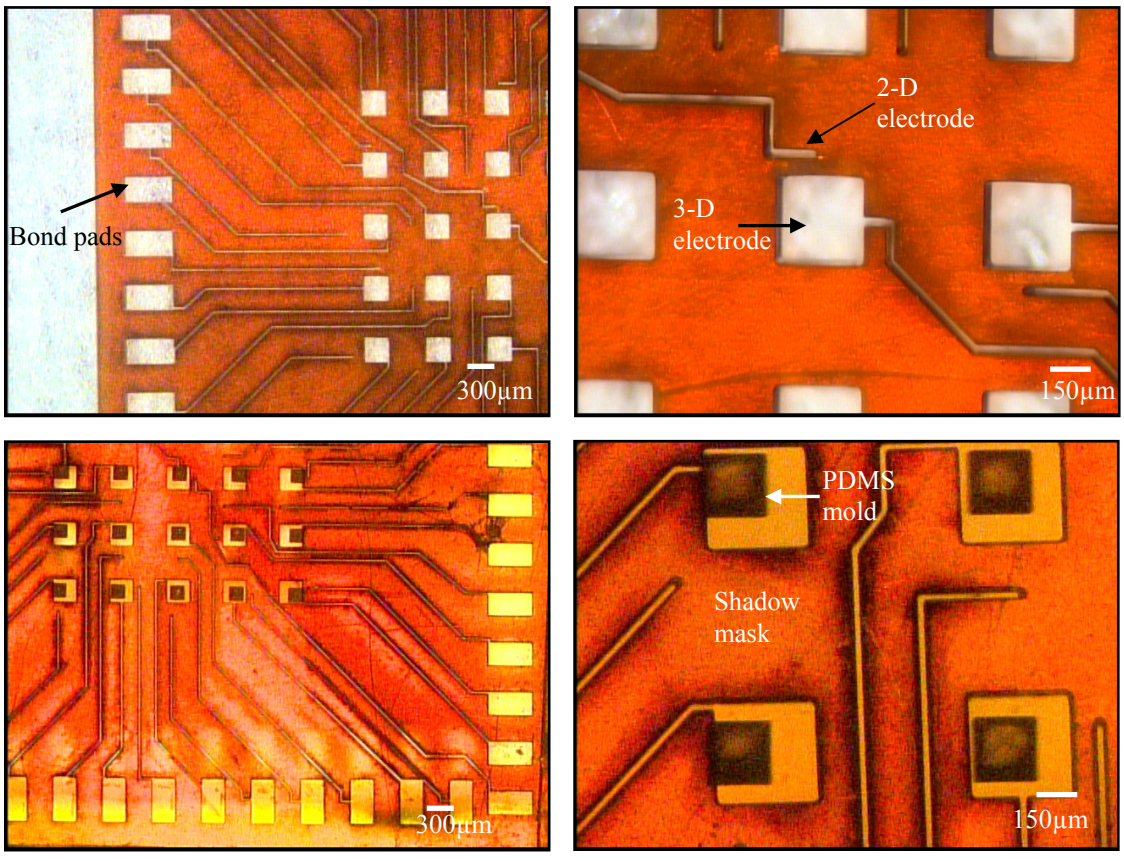

Figure 4.12: Optical micrographs of laser micromachined kapton shadow mask (top) and shadow mask aligned to the PDMS mold (bottom).

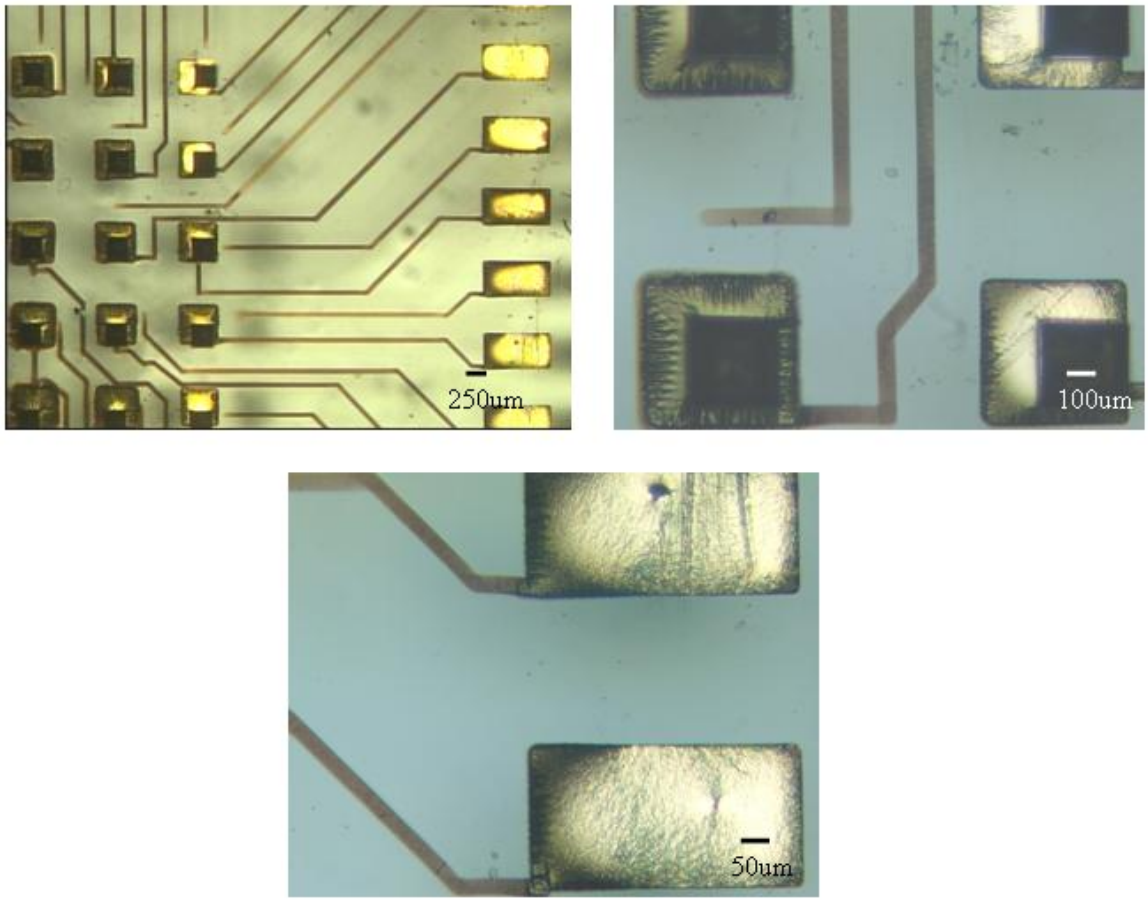

Figure 4.13: Optical micrographs of a metallized PDMS mold using a shadow mask.

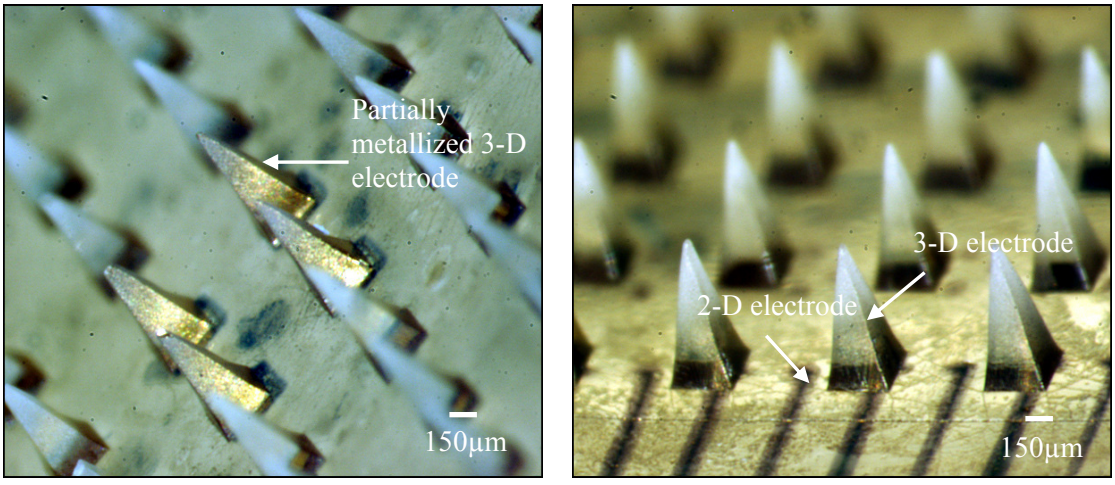

Figure 4.14: Optical micrographs of the side view of MTM 3-D MEAs. The figures depict electrodes at various heights along the length of the micro-towers.

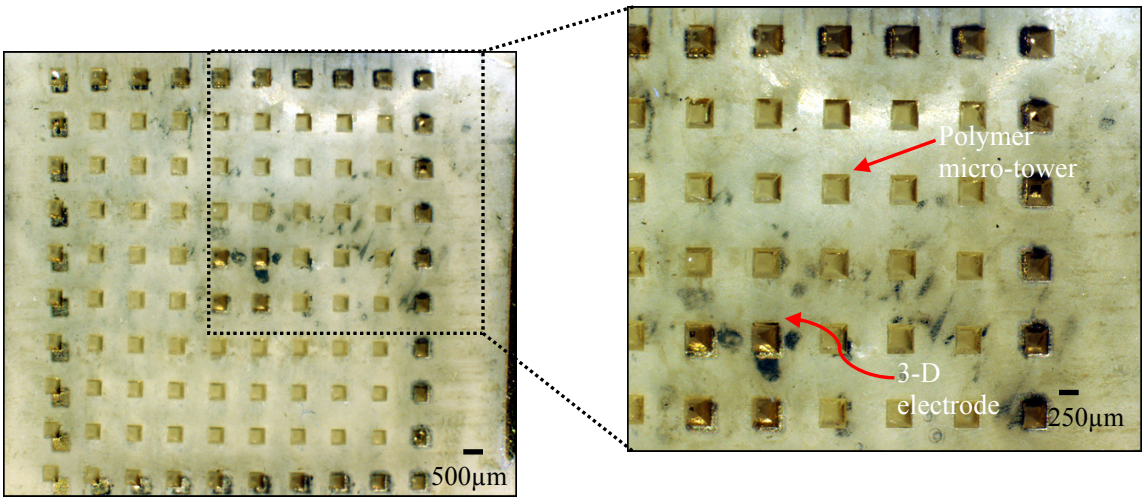

Figure 4.15: Optical micrograhs of the top view of MTM 3-D MEAs with 3-D electrodes and polymer unmetallized micro-towers clearly indicated.

This method however suffers from a few disadvantages: (a) The process of making a shadow mask is time consuming and serial; (b) Alignment of the shadow mask to the mold is non-trivial; (c) Due to coefficient of thermal expansion (CTE) mismatch between mold (PDMS, 310ppm/°C [Dow Corning Silicones 2008]) and the shadow mask (Kapton 20ppm/°C [DuPont Inc 2008]), the resulting metal trace width is larger than the intended value which could lead to potential shorting in high density arrays. Hence a non-planar mold approach, which allows for self-alignment that removes the need for a shadow mask, concerns for high density arrays, and eliminates serial processing, was investigated. This technique is described in detail in the following section.

4.1.6 Microfabrication: Non-planar Mold Metallization

The microfabrication process using a self-aligned, non-planar mold for a 3-D MEA is schematically depicted in Figure 4.16. It begins with the exposure of pyramidal pits on

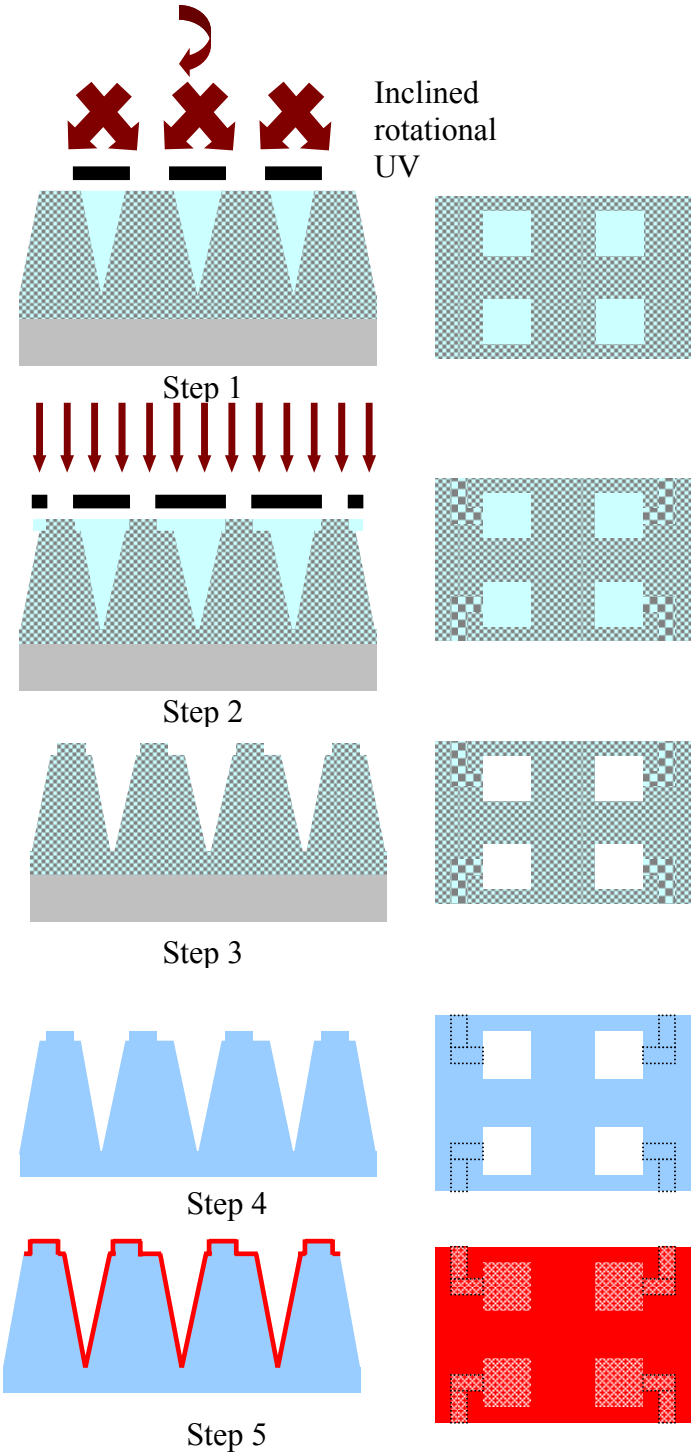

Figure 4.16: Schematic of the process flow for non-planar mold approach for metallization of MTM 3-D MEAs. On the left is the side view of the process steps and on the right, the top view of the process steps.

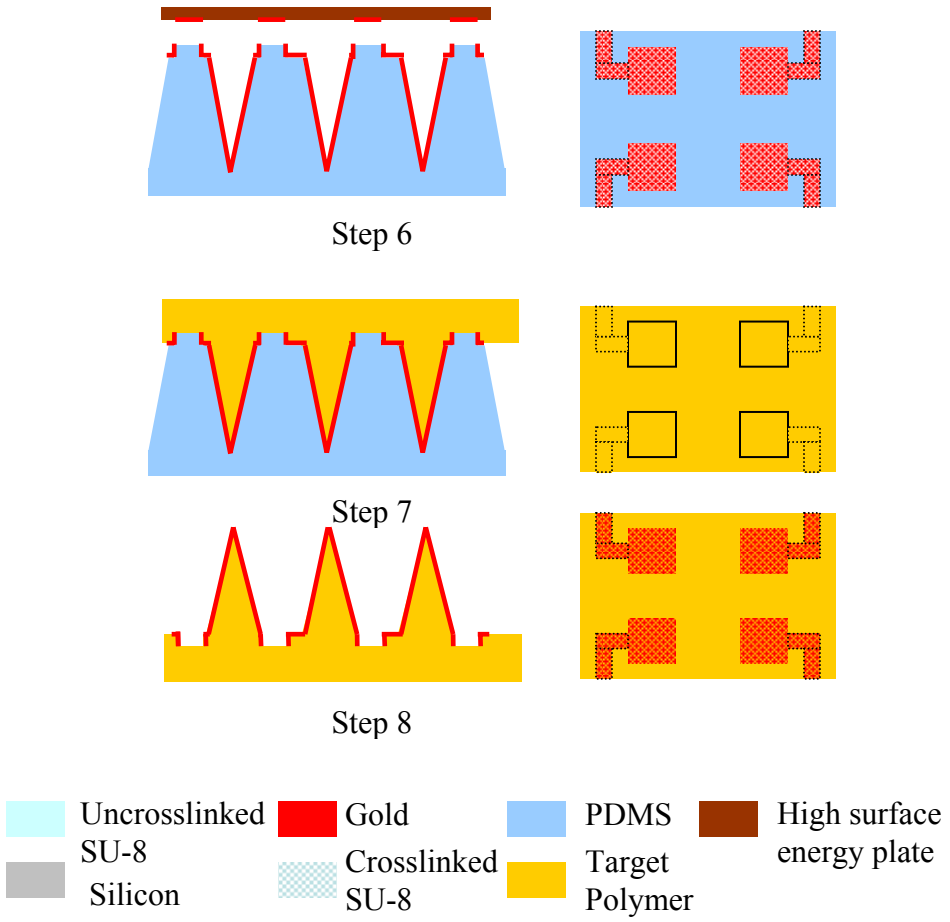

Figure 4.16: Continued.

800µm thick SU-8 2025 (Step 1) using inclined UV lithography as described in Section 4.1.3. A second layer of SU-8 2025 (100µm thick) is spin coated on the mold without developing the first layer. A second mask that has the metal interconnection patterns is aligned with the first layer and then exposed (Step 2) using standard top side exposure. The exposure energy used for this step is 500mJ. Both layers are simultaneously developed in PGMEA after post-exposure baking of 1 hour at 95˚C. This procedure results in a two layer SU-8 rigid mold (Step 3). A master structure is fabricated by pouring and curing a pre-mixed PDMS layer into this rigid mold. Curing procedures are

the same as the ones outlined in section 4.1.3. A sputtered Cr/Au (10nm/150nm) release layer is used to aid the release of the master from the rigid mold. This master structure is metallized (using the same release layer), PDMS is poured and cured to obtain a flexible PDMS mold. This non-planar mold has the same patterns as the original rigid two-layer SU-8 mold (Step 4). To define the electrodes, a Au/Cr layer, (500nm/10nm) is evaporated (Step 5) on the flexible PDMS mold using a filament evaporator or e-beam evaporator (CVC Products, Rochester, NY). Thermal stress resulting in cracking of the PDMS mold is certainly an issue with either tool. This stress can be minimized by utilizing a slower deposition rate (1Å/s) but the cracking is not entirely eliminated. Metal transfer is achieved by bringing a high surface energy plate (such as a silicon wafer or scotch tape) in contact with the metallized PDMS mold (Step 6). Metal is patterned at this step, since the plate comes selectively in contact only with the uppermost metalized surfaces of the non-planar mold; recessed metalized surfaces are unaffected. Patterning is therefore accomplished since the surface energy of PDMS is much lower than the plate that is in contact with the mold resulting in transfer of metal from the uppermost surfaces of the mold to the plate. Once the metal has been patterned, the target polymer can be cast onto and into the patterned PDMS mold (Step 7). Devices using several target polymers including SU-8, PMMA and PU have been fabricated. Exposure (in the case of SU-8) with 5000mJ of I-line UV light and solvent casting (in the case of PMMA and PU) serve as means of release/demolding of the 3-D MEA from the PDMS mold (Step 8). This process yields a patterned 3-D MEA device that has 50 individually addressed 2-D and 3-D electrodes. Figure 4.17 depicts SEM images of two-layer rigid SU-8 molds. Figure 4.18 shows SEM images of the PDMS master fabricated from the SU-8 mold. Figure

4.19 depicts optical micrographs of the top view of SU-8 and PMMA 3-D MEAs respectively. Figure 4.20 portrays optical images of the side views of 3-D MEAs manufactured out of the same materials. Electrodes are embedded in both the base layer and at the tips of the pyramids (300-500µm above the planar surface), offering two levels of electrodes in the z-plane.

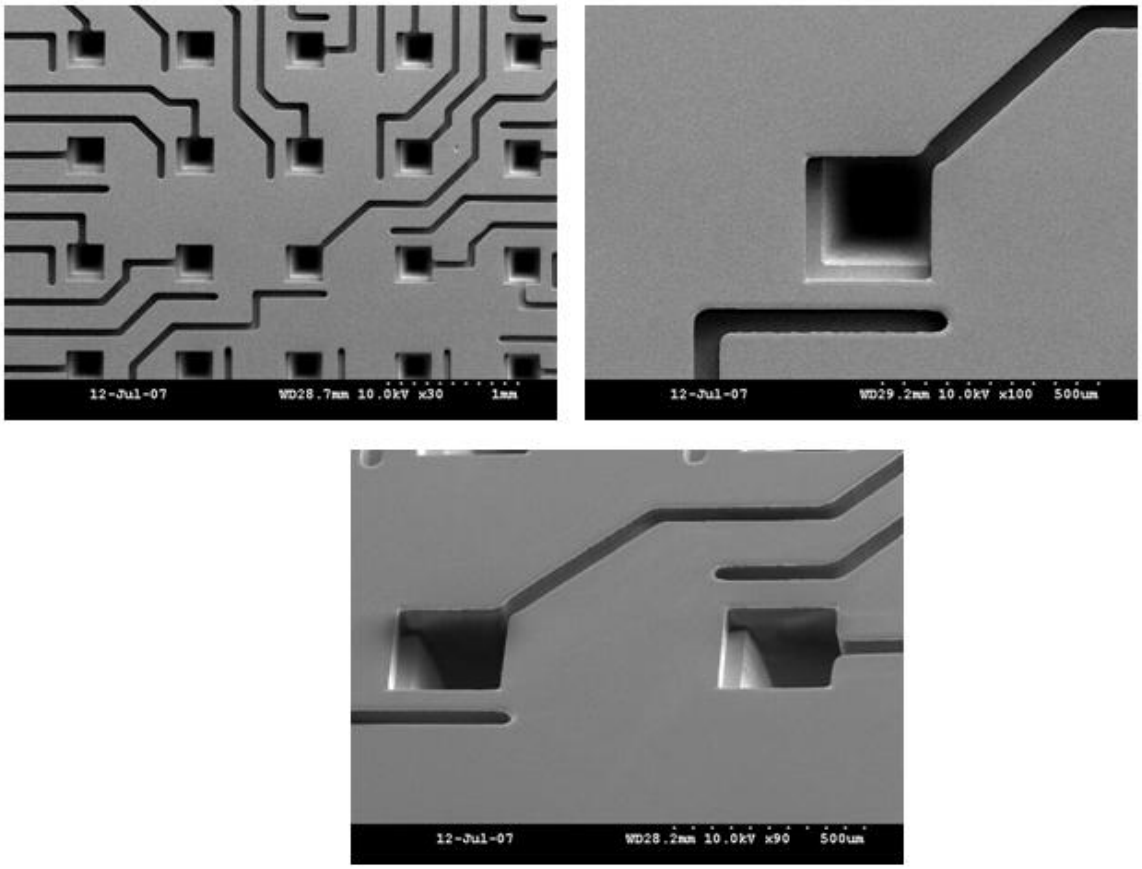

Figure 4.17: SEM images of non-planar SU-8 rigid mold clearly indicating the 3-D trenches, 2-D electrodes and metal traces.

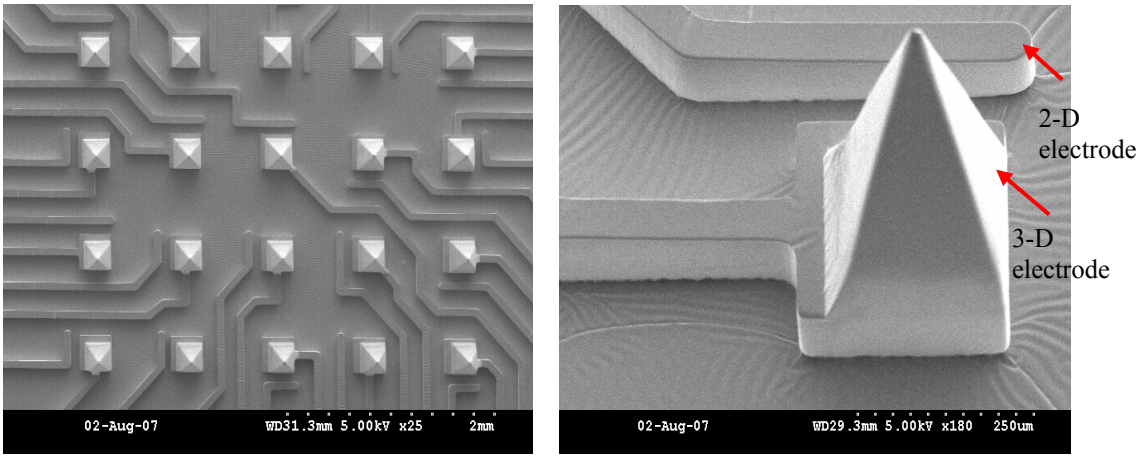

Figure 4.18: SEM images of the top view of a 3-D MEA master (left) fabricated out of PDMS and side view of a close up of a 2-D and 3-D electrode region.

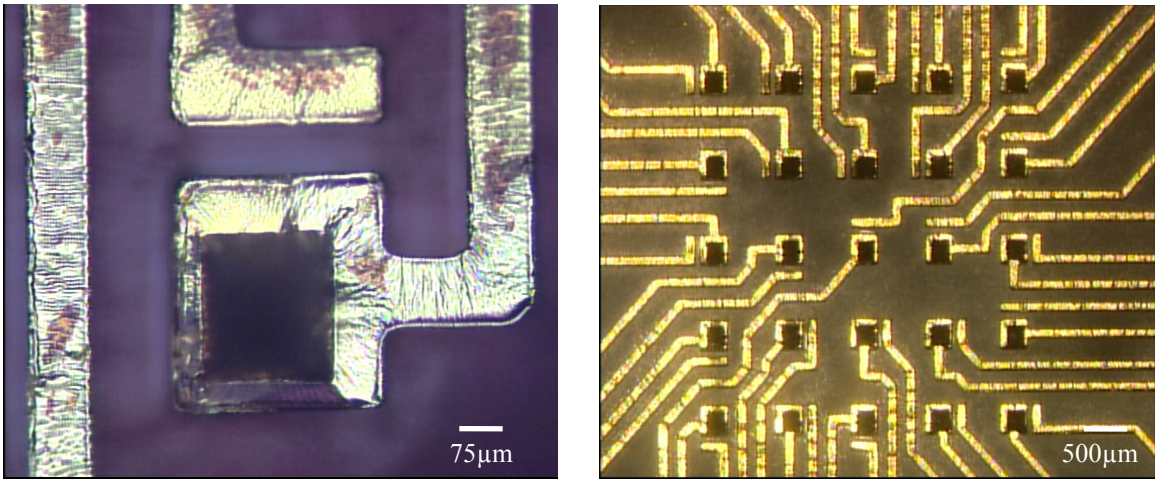

Figure 4.19: Optical micrographs of top views of an SU-8 3-D MEA (left) and PMMA 3-D MEA (right).

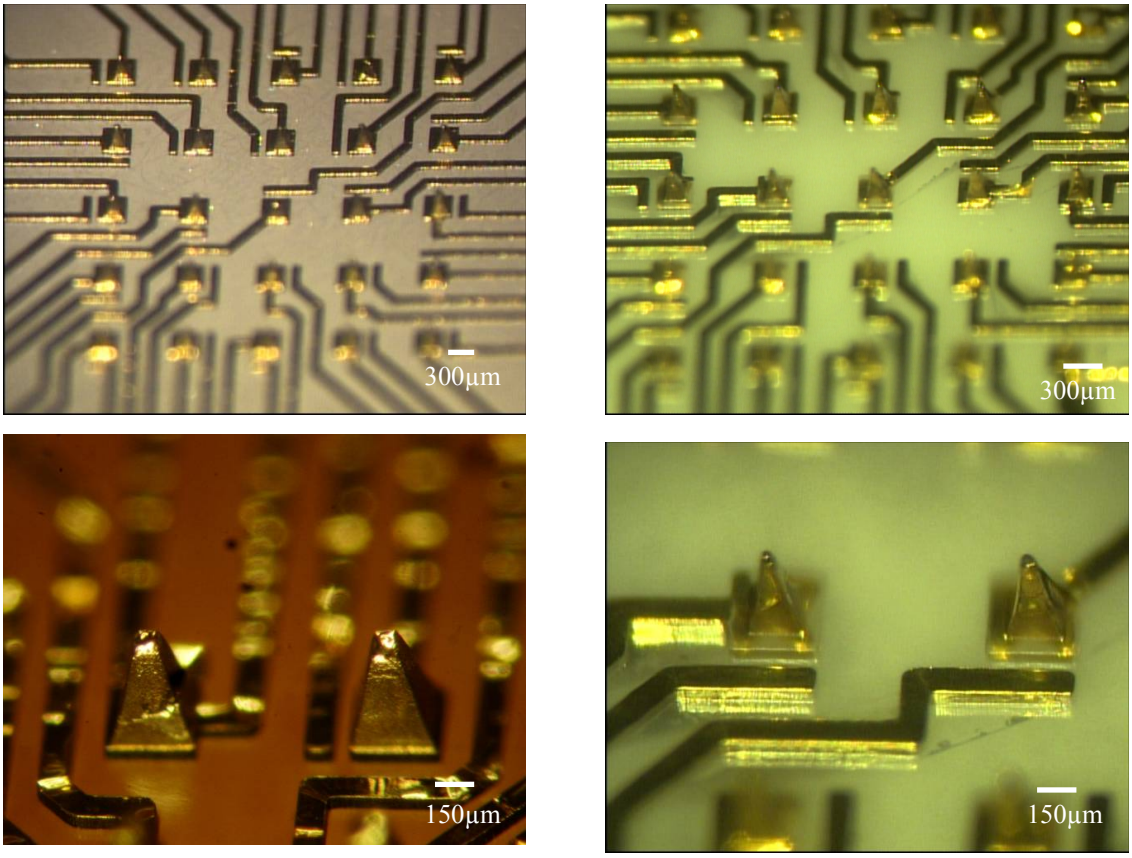

Figure 4.20: Optical micrographs of the side views of PMMA (top left), PU (top and bottom right) and SU-8 (bottom left) 3-D MEAs. Electrodes embedded in 2 planes are clearly visible in these micrographs.

The intentionally formed non-planar mold metallization technique has been used to fabricate the MEAs that have been utilized in the reminder of this chapter. This technique was found to have several advantages over the shadow mask metallization - possibility of multiple usages of the flexible mold and master structures, self-aligned metallization without the use of difficult alignment, elimination of the need for serial processing and hence less processing steps/time. It also has several advantages over other 3-D MEA fabrication technologies (integrated and assembly-based) that have been reported in the literature – simple 2 mask process, elimination of time-consuming assembly processes,

scalability, minimization of cleanroom processing and integration of biocompatible polymers.

4.1.7 Packaging of MTM 3-D MEAs

Packaging is an important consideration in MEMS, semiconductors and biomedical devices. Packaging costs can increase rather rapidly, resulting in increasing the cost of producing a complete product. It has been reported that packaging solutions make up as much as 75% of the cost of the final MEMS, semiconductor or biomedical product [Tummala 2001]. So it is highly desirable to have a packaging technique for 3-D MEAs, which is simple and cost-effective. Printed Circuit Board (PCB) based approaches [Express PCB 2007] could potentially be a solution to this problem; however the MEA chip to PCB bonding could be rather tricky. In this work we report simple techniques to overcome these challenges.

Several techniques to package the MTM 3-D MEAs have been developed. The first technique was similar to the methods used in Chapter 3 to package laser scribed 3-D MEAs but instead of wirebonding to connect the MEA to the bond pads of the packaging chip; conductive epoxy (Master Bond Inc, Hackensack, NJ) was utilized. The packaging chip was fabricated in exactly the same way as described in section 3.1.7 using a standard lift-off process. This is rather a crude method and was executed to perform quick electrical tests on a MTM 3-D MEA. Figure 4.21 depicts an optical image of the packaged MEAs using this technique.

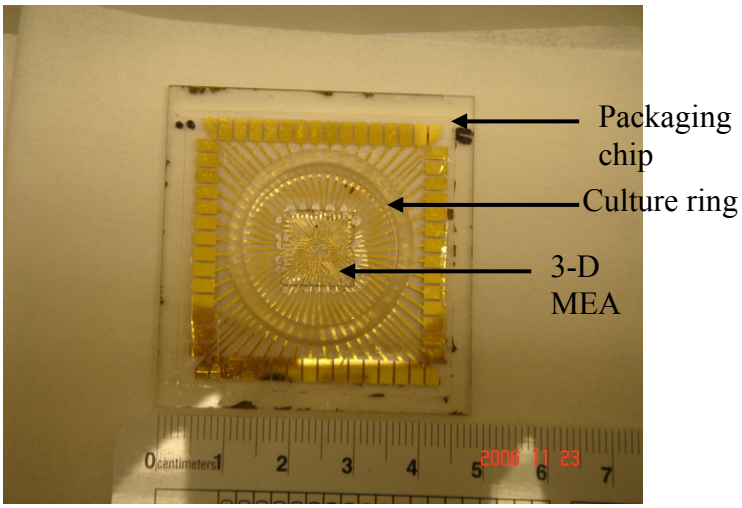

Figure 4.21: Optical photograph of a fabricated, packaged (glass packaging chip) 3-D MEA. A culture ring is attached to the MEA to contain biological culture media.

In order to develop a more manufacturing friendly approach, PCBs were designed and fabricated utilizing commercial PCB vendors. The layout for the PCBs was performed on commercially available software - CAD Soft Eagle (CadSoft Computer Inc, Delray Beach, FL). Figure 4.22 illustrates an exported jpeg image of the PCB layout.

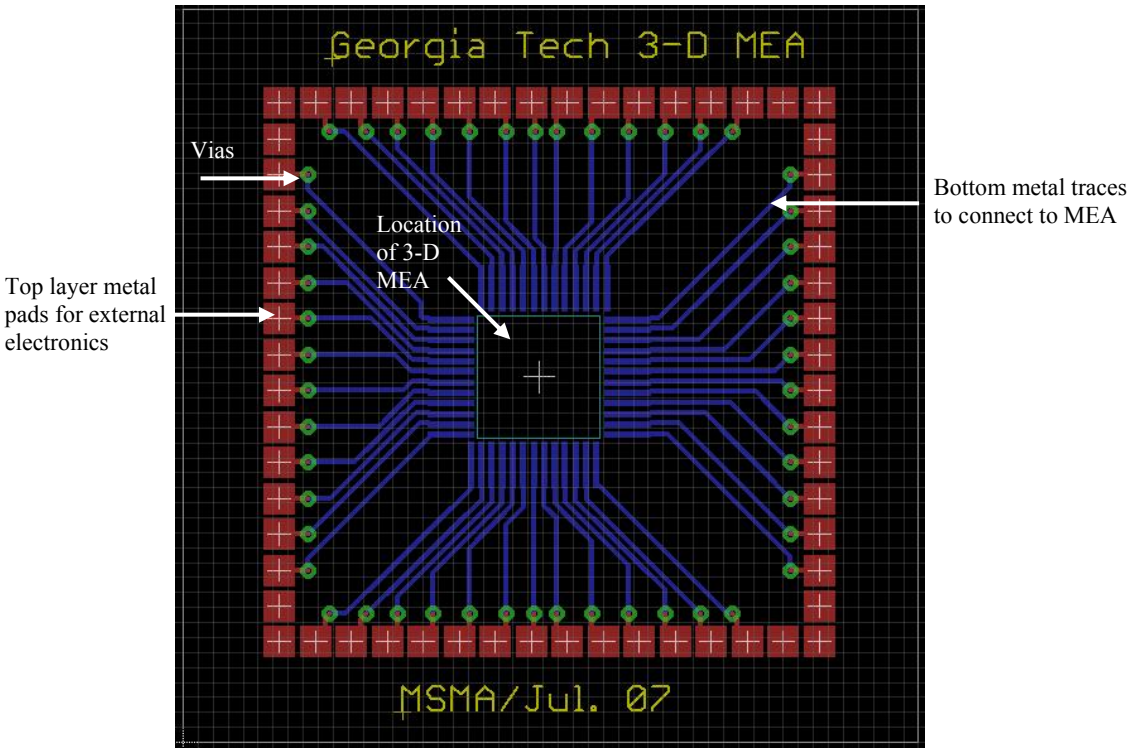

Figure 4.22: Layout for the commercial PCB that was fabricated to package the 3-D MEAs.

The PCB was fabricated at a commercial vendor (Custom PCB, Kuala Lampur, Malaysia). A standard two metal layer (top & bottom, interspersed by one FR4 layer) process was used. A PCB process with 7 mils (177.8µm) minimum feature size was sufficient for this type of boards. The top metal layer was designed to contain metal pads (2mm x 2mm) for interfacing with external electronics. The bottom metal traces (connected to the top metal pads through electroplated vias) were terminated using bond pads (3mm x 360µm) to attach to the 3-D MEA. The overall dimension of the PCB was designed to be 49mm x 49mm to be compatible with Multichannel Systems (MCS, Reutlingen, Germany) pre-amplifier setup which was used for the electrical and

biological measurements (setup and measurements similar to section 3.2). Figure 4.23 is an optical picture of the front and back sides of the PCB.

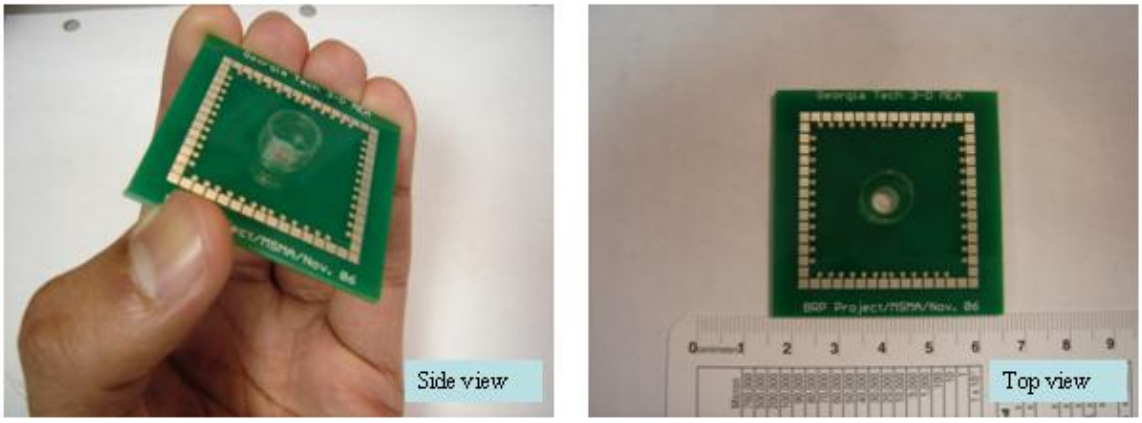

Figure 4.23: Optical images of the side view and top view of the fabricated PCB.

A central port (dimensions: 12mm) was also drilled as part of the PCB fabrication process to serve as an interface between the electrodes and biological culture media (for tissue slices or 3-D cultures). Conductive epoxy was used initially to connect the MEA to the PCB but this technique was found to be unsuitable for: (a) connecting all the electrodes as the pitch (800µm) is too small for manual wiring without shorting adjacent electrodes; (b) this process is not suitable with micro-manufacturing goals of this project; (c) does not allow for scaling; (d) this process is very tedious. Alternative techniques to address this interfacing problem were investigated. After some process development, a technique combining a self-align scheme (custom made silicone gaskets) and force contact using a acrylic spacer (held in place with stainless steel screws) was developed to tackle this complex interconnect problem. The self-align scheme ensures that the attachment of the MEA to the PCB can be performed under a stereoscope. The acrylic spacer holds the MEA and the PCB pads in contact to establish electrical connectivity.

This assembly process is simple and scales well to higher electrode counts. Care was taken to ensure that all the interconnection pieces were biocompatible (FDA approved). A culture ring/well (dimensions: OD: 24mm, ID: 22mm) was fabricated by laser micromachining (CO_2 laser, New Hermes-Gravograph, Duluth, GA) of acrylic sheets (6mm thick) and attached to the PCB using PDMS to complete the packaging. Figures 4.24 and 4.25 represent the front and back sides of an assembled 3-D MEA. Commercial MEAs typically have 5µm insulation (SU-8 or other suitable material) coated on the electrodes. A 25µm thick parylene layer was used in the laser scribed 3-D MEAs to tackle the cytotoxicity issues of the various components involved. In the case of metal transfer micromolded 3-D MEAs, most of the materials used like PMMA, PU, gold, silicone, acrylic and stainless steel are biocompatible (biocompatibility tests were performed on PMMA and PU as described in section 4.4.1).

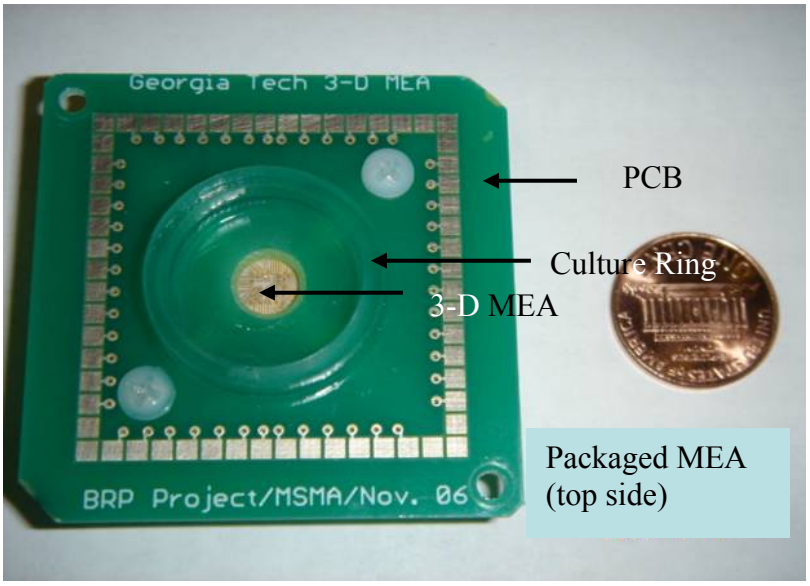

Figure 4.24: Optical image of the top side of a fabricated, completely packaged 3-D MEA. Clearly visible are the PCB with top side metal pads for external electronics, 3-D MEA and a culture ring/well to hold biological culture media.

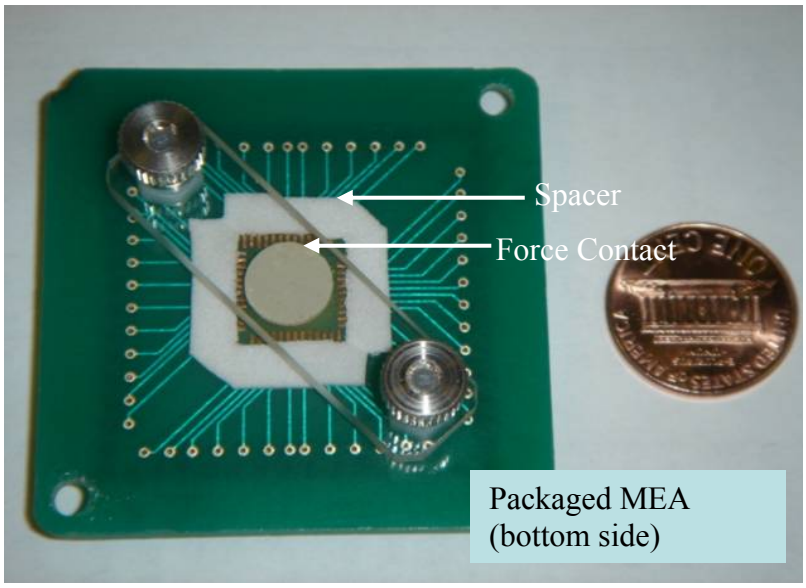

Figure 4.25: Optical image of the bottom side of a packaged 3-D MEA. Clearly visible are the self-align spacer (silicone gasket) and the acrylic force contact mechanism.

The FR-4 composite used in PCB processes however is cytotoxic [Pozzo 1991]. In order to address this potentially problematic issue for long term culture growth, a thin layer of PDMS was coated on the PCB (in the area inside the culture well). Since these devices are potentially less cytotoxic to neural cultures as compared to laser scribed 3-D MEAs, a thinner 5μm parylene layer was coated conformally on the packaged 3-D MEAs. This ensures biocompatibility as well as provides a larger process window for laser micromachining. Recording sites (size 50μm diameter) were defined by a combination of laser micromachining (similar process/protocol to the one described in section 3.1.4) and RIE etching (CHF_3/ O_2 plasma). The RIE etching was carried out in a Plasma Therm tool with a recipe given in Table 4.3 targeted at etching 1μm of parylene.

Table 4.3: Process Parameters for RIE etching of parylene

Parameter	Value
O_2 Flow Rate	45 sccm
CHF_3 Flow Rate	5 sccm
Pressure	200 mTorr
Power	200 Watts
Time	5 mins
Etch Rate	1µm*

* Varies with conditions of machine

Platinum was electrodeposited on recording sites as described in section 3.1.5. Platinum electrodeposited recording sites are shown in Figures 4.26.

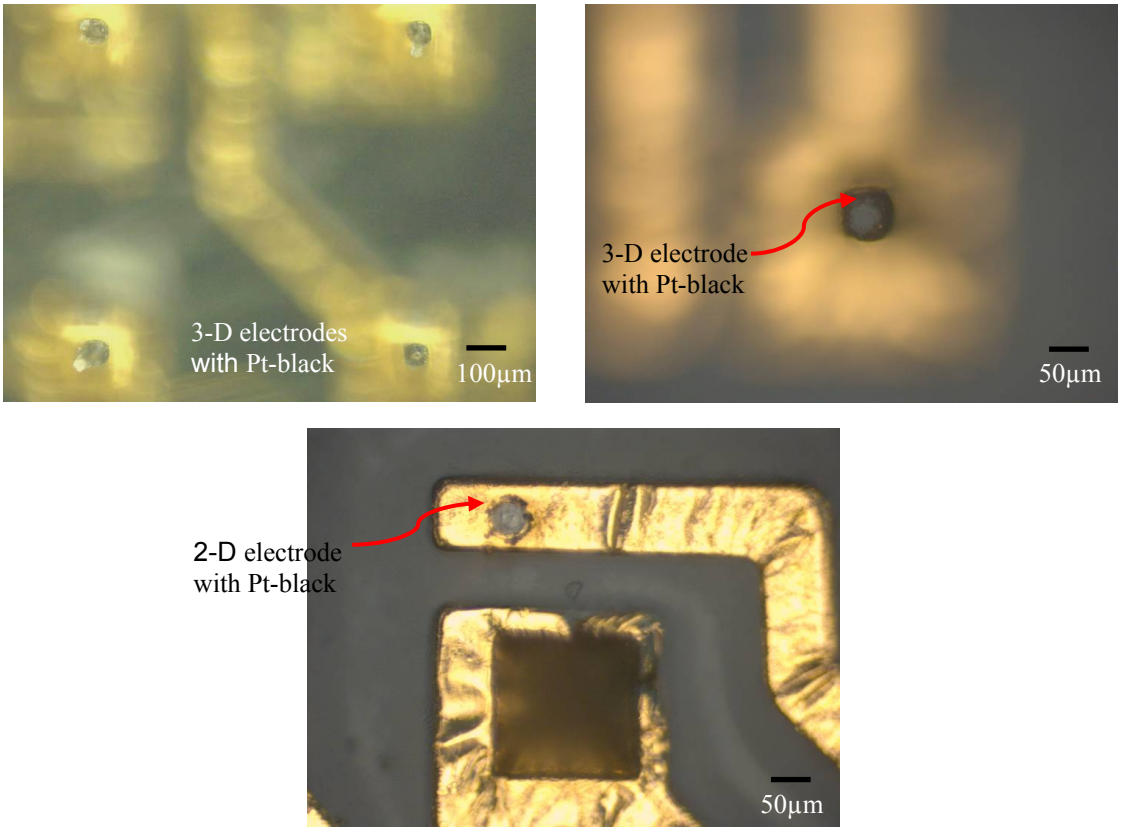

Figure 4.26: Optical micrographs of 3-D (top) and 2-D microelectrodes with platinum-black plating.

Novel microfabrication and packaging technologies to produce 3-D MEAs with relative ease have been developed in this chapter. Electrical characterization of the 3-D MEAs including development of impedance theory, impedance results, comparison between theoretical and experimental results is detailed in section 4.2. Section 4.3 deals with development of processing improvements that could potentially transfer this process from prototyping to manufacturing. Section 4.4 details the biological characterization of these MEAs including biocompatibility and electrophysiology measurements.

4.2 MTM 3-D MEA Characterization: Electrical Results

4.2.1 Impedance Modeling

An impedance model to describe the behavior of the microelectrodes across the frequency spectrum was developed based on the theory described in section 2.2. The lumped equivalent circuit developed in this section for an electrode-electrolyte interface is given in Figure 4.27.

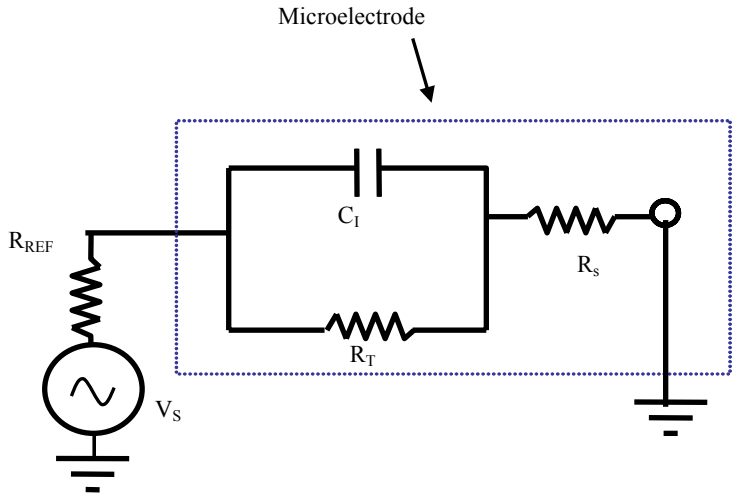

Figure 4.27: Lumped circuit equivalent of an electrode-electrolyte interface.

The equivalent impedance of this circuit is evaluated by a parallel combination of the charge transfer resistance (R_T) and the interfacial capacitance (C_I) in series with the spreading resistance, R_S as given by Equation 4.9.

$$Z = R_S + \frac{\left(R_T\left[\frac{1}{jwC_I}\right]\right)}{\left(R_T + \left[\frac{1}{jwC_I}\right]\right)} \tag{4.9}$$

where w is equal to $2\pi f$ with f being the frequency in Hz. Using simple math Z can be written as a combination of real and imaginary parts as shown in Equation 4.10-4.12.

$$Z = X + jY \tag{4.10}$$

$$X = \frac{\left(R_T + R_S + w^2 C_I^2 R_T^2 R_S\right)}{1 + w^2 C_I^2 R_T^2} \tag{4.11}$$

$$Y = \frac{wC_I R_T^2}{1 + w^2 C_I^2 R_T^2} \tag{4.12}$$

A MATLAB code was generated for this lumped circuit model. The parameters used in the model are outlined (with reference for the source) in Table 4.4. The variation of the magnitude of the impedance (real part) was studied in detail.

Table 4.4: List of parameters for MATLAB code for microelectrode-electrolyte interface

Parameter	Value	Reference
C_I	$0.07 pF/\mu m^2$	Stern 1924
J_0	2×10^{-9} A/cm^2	Najafi 1986
ρ	72 Ω.cm	Physiological saline
V_t	26mV	Borkholder 1998

Impedance was plotted as a function of frequency from 1Hz-100 kHz (which is the primary frequency spectrum of interest for electrophysiology [Borkholder 1998]) for various electrode sizes (circular electrodes with radius r). Impedance was found to drop with increase in electrode size as expected from theory [Borkholder 1998; Franks 2005]. The plot for various electrode sizes from 5µm to 75µm is illustrated in Figure 4.28.

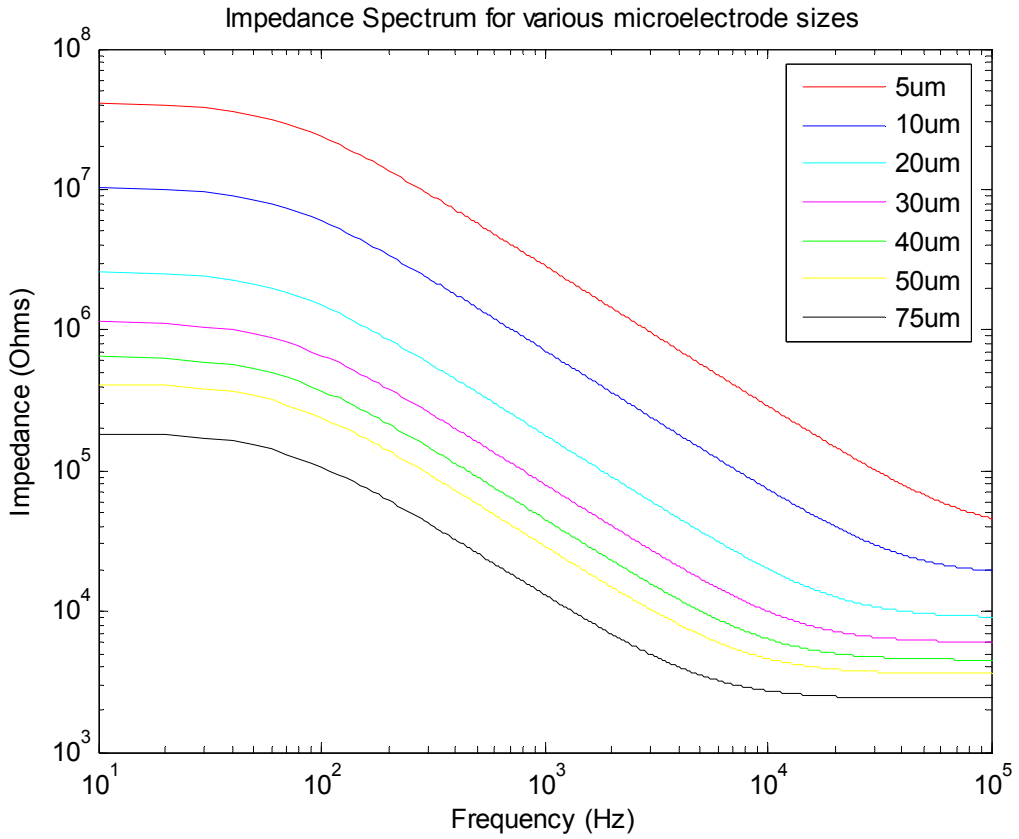

Figure 4.28: Model of the impedance spectrum of various sized microelectrodes.

From the impedance model (based on the microelectrode theory given in section 2.2) it becomes apparent that with systematic design choices and novel processing techniques, it is possible to shape the impedance spectrum of an electrode to suit a given application. For example the interfacial capacitance is a function of the surface area of the electrode

and can be tuned by changing the platinum plating density [Ross 2008]. From Figure 4.28, it is evident that there are three regimes each dominated by one of the elements in the lumped circuit model. The domination of each of these components R_T, C_I and R_S was confirmed by increasing a single component a 100-fold while maintaining the other two a constant in the model. As expected [Ross 2008], the lower frequency regime is dominated by R_T, the mid frequency band by C_I and the high frequency by R_S and this is depicted in Figure 4.29. Each of these components in turn is directly related either to the base area or the surface area of the electrode.

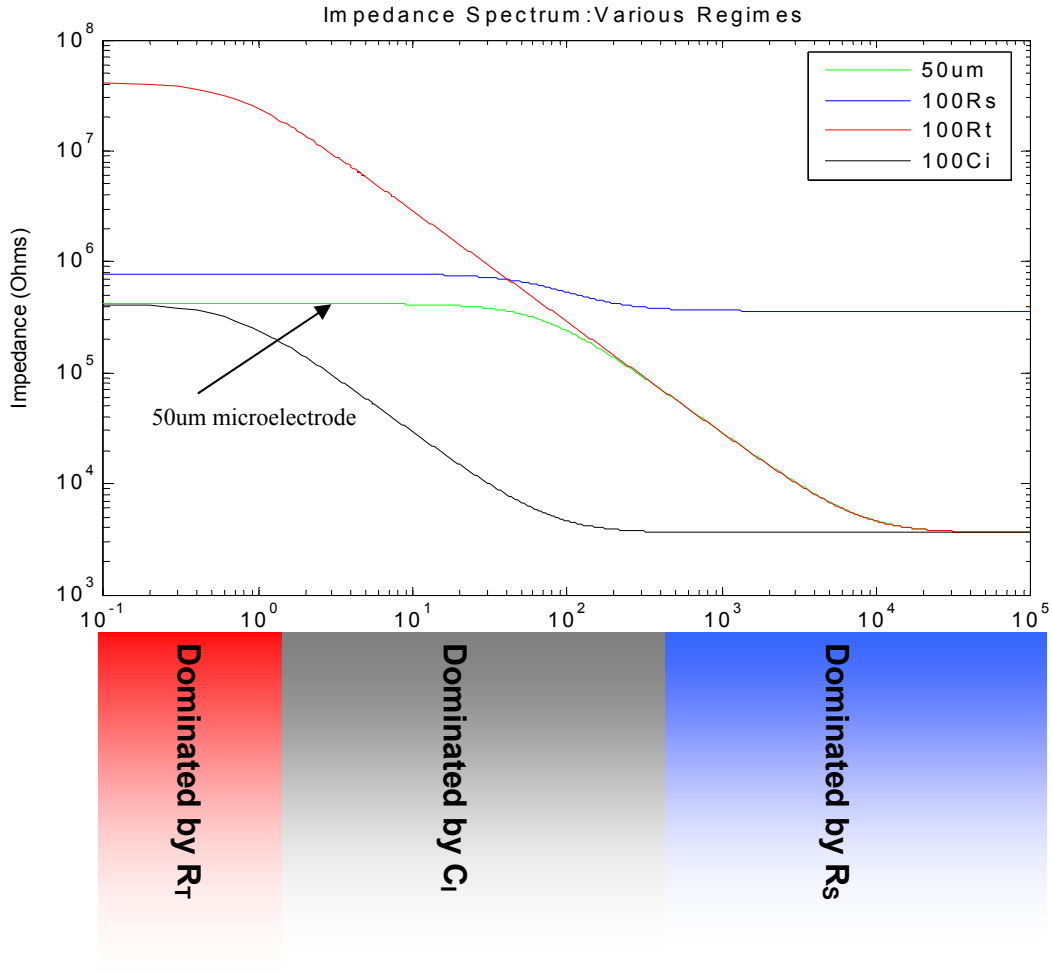

Figure 4.29: Different regimes of the impedance spectrum of a microelectrode.

The high frequency portion of the spectrum is dominated by the spreading resistance R_S and is of particular interest in this work. This circuit element is a function of the base area (or drawn area) of the electrode and can potentially be used as a metric to calculate the quality of the microelectrodes. The spreading resistance is inversely proportional to the radius (r) of a circular microelectrode [Newman 1966] as given by Equation 4.6.

$$R_S = \frac{\rho}{4r} = \frac{\rho\sqrt{\pi}}{4\sqrt{A}} \tag{4.13}$$

Here A is the area of the microelectrode and ρ is the resistivity of the electrolyte in Ω.cm. This can be experimentally verified by measuring the radius of the electrodes and comparing the theoretical and measured impedance. A measure of the quality of the microelectrode and a performance metric to compare this microfabrication approach to others is thus obtained as explained in the next section.

4.2.2 Impedance Results

Impedance was measured at several stages of the microfabrication process using the impedance spectroscopy setup described in detail in Section 3.2.1. The first stage is after the laser micromachining of parylene to define the recording sites. This measurement is expected to produce a low yield of electrodes as the laser process is designed to leave a residue of parylene behind on the recording sites as shown in Figure 4.30. An optical micrograph of the recording site at this stage is also illustrated in the same figure. The impedance of this low-yielding step is given in Figure 4.31.

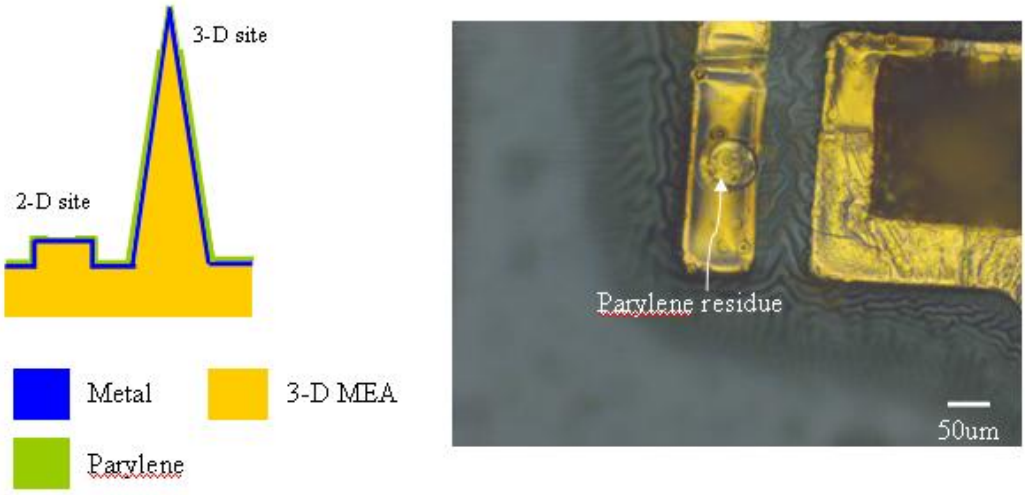

Figure 4.30: Schemtic of parylene residue left behind by the laser micromachining step (left) and an optical micrograph of the result (right).

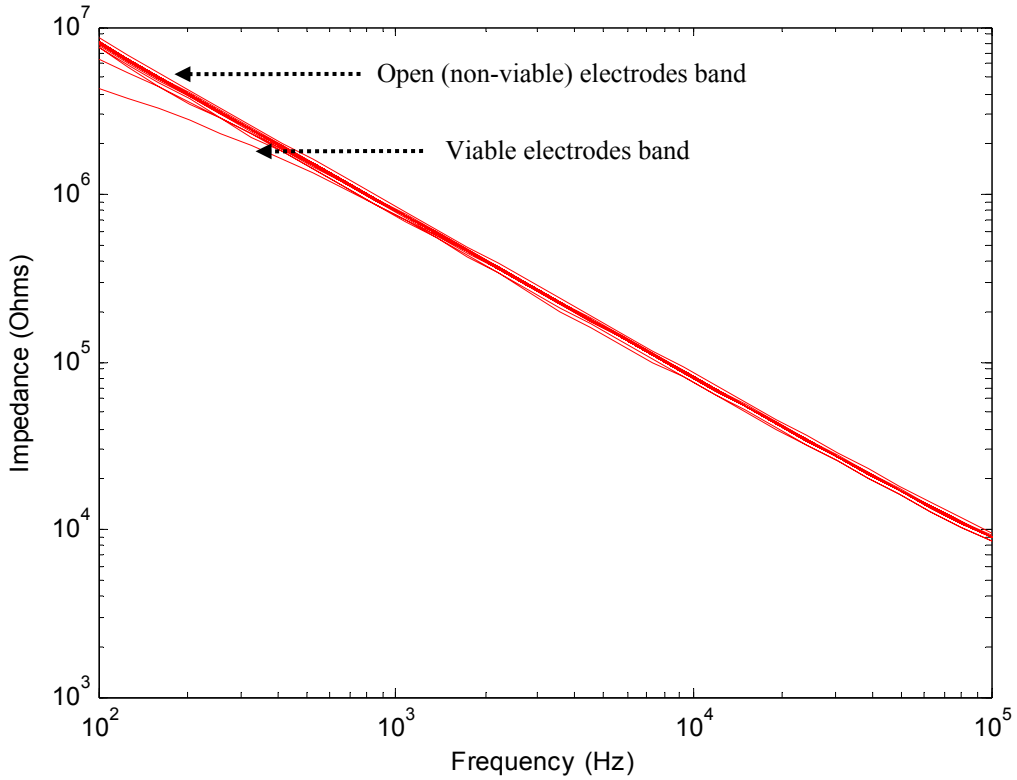

Figure 4.31: Impedance spectrum of a 3-D MEA after laser micromaching of parylene to define the recording sites.

Impedance was also measured after the RIE step that was introduced to remove the parylene residue on the MEA recording sites. As expected this improved the yield of microelectrodes on the 3-D MEAs. A schematic of the expected recording site and the impedance spectrum are shown in Figure 4.32. The "shot-gun" nature of the high frequency spectrum is also indicated in this figure. This impedance should be dominated by the spreading resistance R_S according to theory which means that this can be examined further by optical measurements as suggested in Section 4.2.1. In order to accomplish this, the 3-D MEAs were studied under an optical microscope and the diameters of the recording sites were measured.

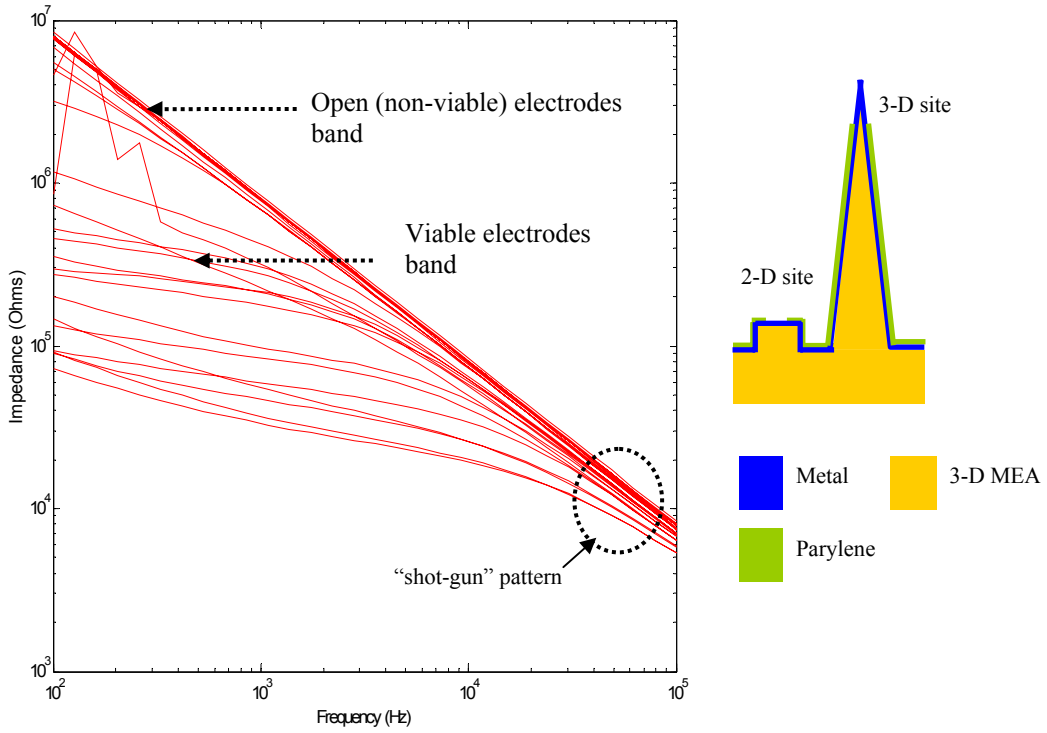

Figure 4.32: Impedance spectrum of a 3-D MEA after the laser micromachining and RIE etching steps (left) and a schematic of the expected result (right). The band clearly indicates a larger yield in the microelectrodes as opposed to the laser micromachining result.

The theoretically predicted (from optically measured radii) and experimentally measured impedances at 10 kHz (extracted from impedance spectrum curves) were plotted in the same graph (Figure 4.33). Though a general trend (inverse variation as predicted) can be observed, there is significant variation in the results. This can be explained by the fact that the geometric estimation of the diameter of electrodes is very approximate. The same problem is also reported in Borkholder [Borkholder 1998] where they see a larger variation between experimental and modeling values as the size of planar 2-D commercial electrodes becomes smaller. Advanced optical programs with pixel estimation of the actual area [Kubinova 2001] might be necessary to evaluate the area of two-dimensional electrodes. For 3-D electrodes it is practically impossible to estimate the geometric area of the electrode as they are shaped more like cones rather than circles exacerbating the problem.

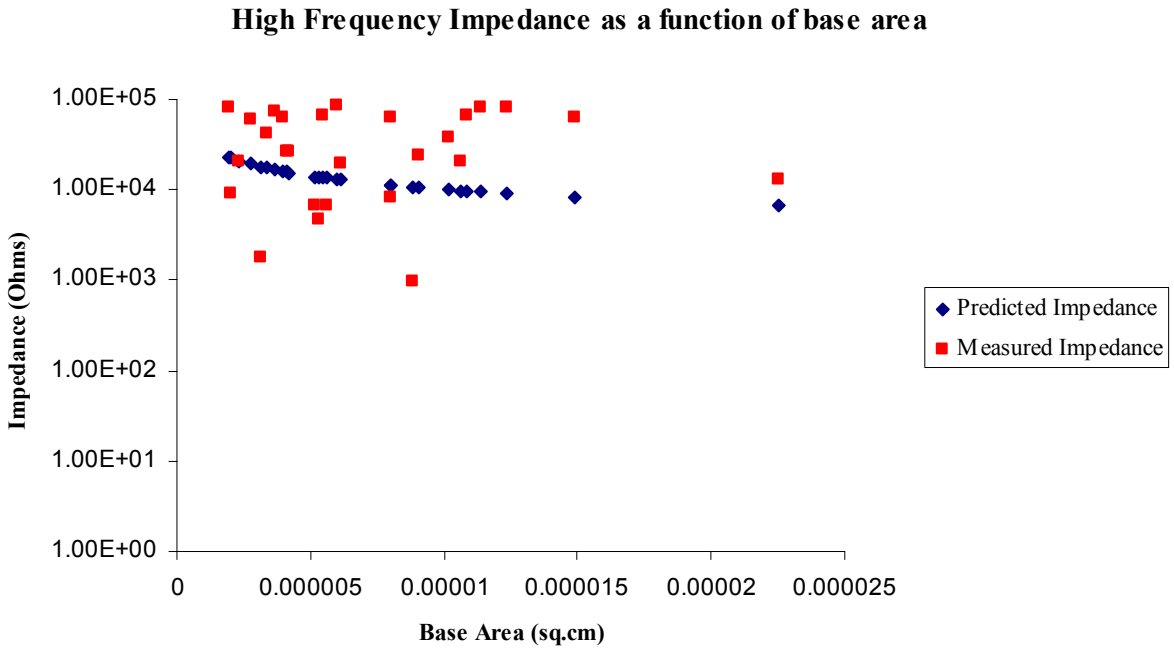

Figure 4.33: Comparison between predicted high frequency impedance (from theory) and measured impedance (from experiments).

Modeling data for an electrode with a radius of 10µm from Section 4.2.1 was plotted along with experimental data for several optically measured 10µm sized (radius) electrodes (Figure 4.34). The correspondence between the two data sets is not excellent at lower frequencies but at higher frequencies, the theoretical data does seem to match the measured data. The geometric estimation errors described above does contribute to some of the data mismatch that is observed. Various parameters were extracted from this measured data and compared to data reported in literature [Stern 1924; Najafi 1986; Borkholder 1998] as shown in Table 4.5. The extracted parameters compare moderately well with what is reported in literature.

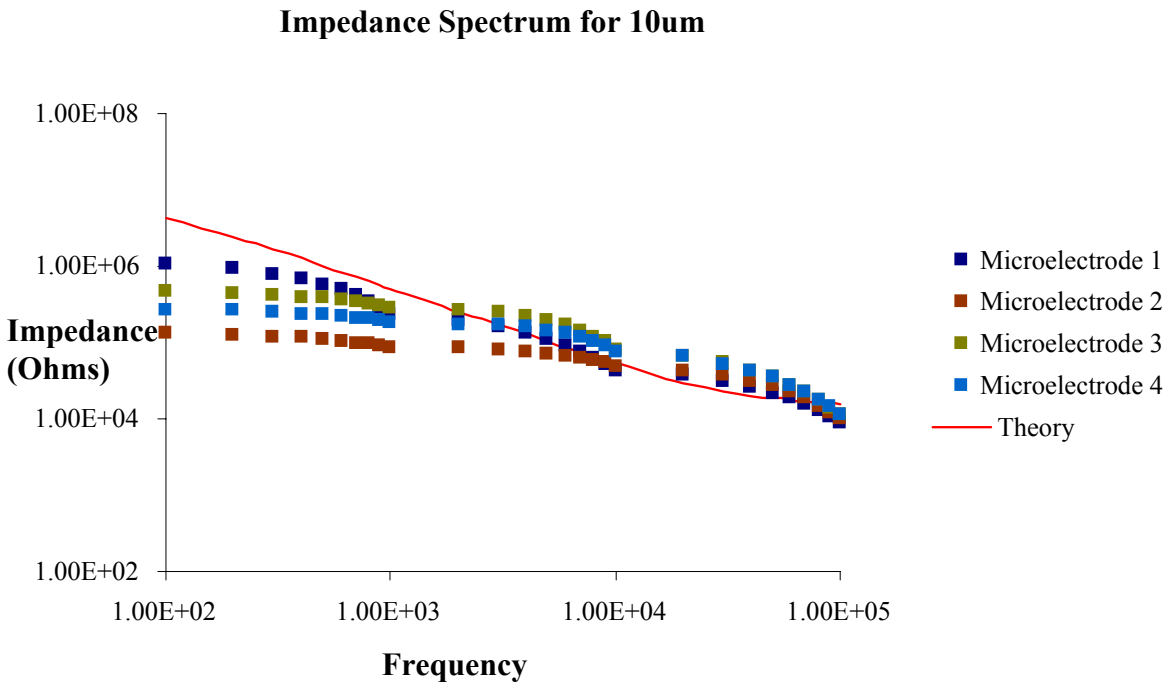

Figure 4.34: Comparison between impedance spectrum of theoretically modeled and experimentally measured 10µm microelectrodes.

Table 4.5: Parameter extraction from measured impedance and comparison to data in literature

Parameter	Average Value (calculated)	Value (reference)	Reference
C_I	0.031pF/μm^2	0.07 pF/μm^2	Stern 1924
J_0	1.23 x 10^{-7} A/cm^2	2 x 10^{-9} A/cm^2	Najafi 1986
ρ	123 Ω.cm	72 Ω.cm	Borkholder 1998

Impedance was also measured after platinum electroplating. Electroplating platinum reduces the impedance of microelectrodes, increases the surface area of the electrodes and makes them more suitable for electrophysiological measurements. Figure 4.35 illustrates the impedance of platinized electrodes at 1 kHz (the most physiologically relevant frequency) for a specific 3-D MEA.

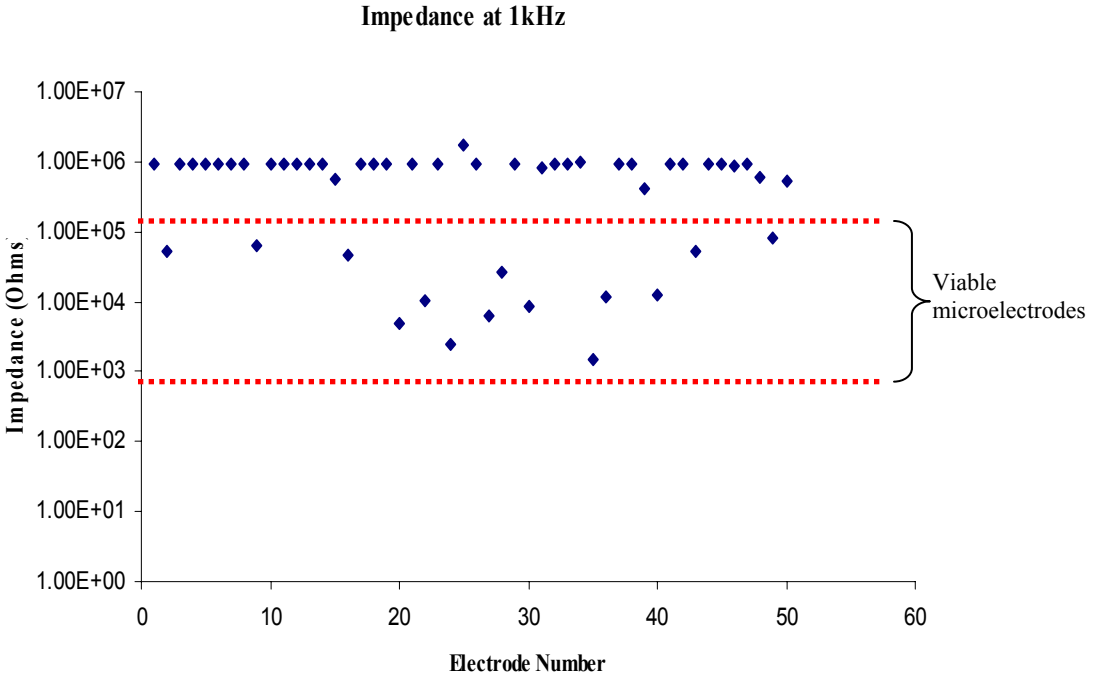

Figure 4.35: Impedance of platinized microelectrodes of a 3-D MEA at 1kHz. The non-viable band also includes unconnected and grounded electrodes.

Figure 4.36 depicts a 2-D map of these electrodes (with the translational map which relates the electrode location on the packaging chip). Viable electrodes are clearly distinguishable from non-viable ones (maroon red in color). The location of electrodes on this map (location indicators are provided in the figure) matches the location on MCS stimulation/recording set-up. These maps help the biologists with determining the exact location of the electrodes (viable and non-viable) during biological recordings/stimulation experiments. This becomes vital when calibrating protocols for experiments and repeat usage of electrodes.

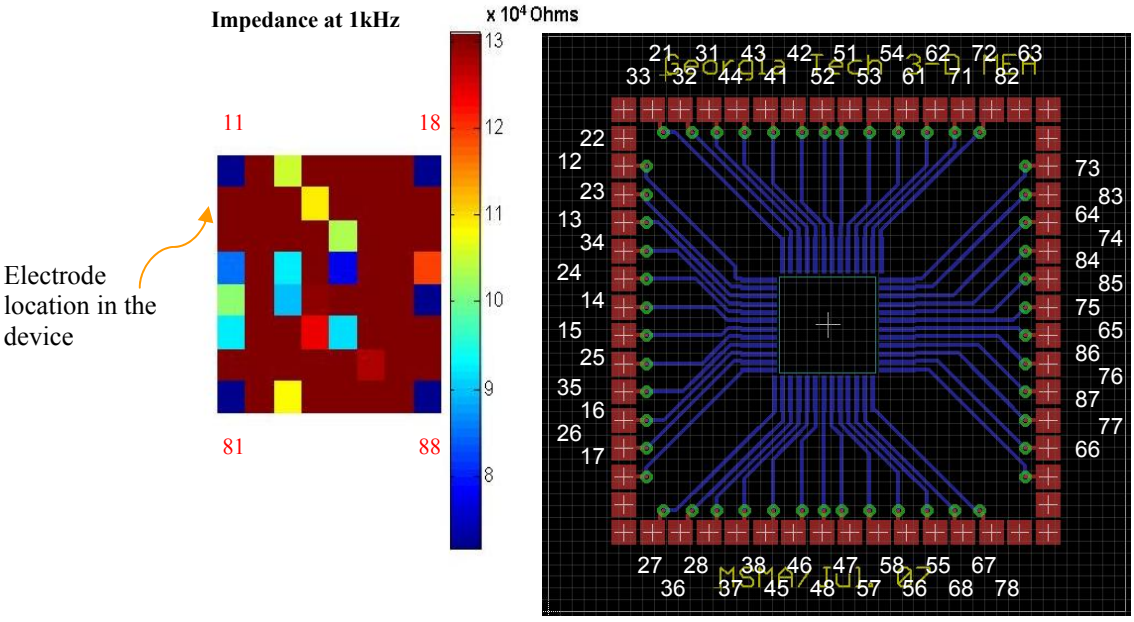

Figure 4.36: 2-D maps of electrode location on an 3-D MEA (left). The four numbers on the corners of the map are the various grounds. The translational map which relates this location to the electrode location on the packaging die is also depicted (right). Viable electrodes can be located using this map resulting in placement/usage of the same electrode in different experiments.

The yield of the electrodes in MTM 3-D MEAs is relatively low (around 30% viable) and needs to be improved for the technique to be considered a micro-manufacturing approach. The thickness of the transferred metal layer and parylene deposition were identified are the two steps that needed to be improved in order to increase the yield of the process. These steps were enhanced with the development of newer techniques. Process improvements are described in Section 4.3 along with the results.

4.2.3 Baseline Noise Modeling and Results

As with most other circuit elements there is intrinsic noise associated with the metal-electrolyte interface. This noise has been shown to be thermal [Gasteland 1959] and can be given by the rms voltage noise of a resistor as shown in equation 4.14.

$$V_{RMS\,Noise} = \sqrt{4kTR_N\Delta f} \tag{4.14}$$

where R_N is the real part of the impedance of a microelectrode, Δf is the frequency bandwidth of interest, k is Boltzmann's constant (1.38×10^{-23} J/K) and T is the temperature in Kelvin. From the real part of the impedance data obtained from the impedance spectrum measurement and with a frequency bandwidth of 10 kHz, the rms noise can be plotted as a function of the impedance using the equation above. This noise is plotted as a function of the magnitude of the impedance measured (Figure 4.37) in section 4.2.3 for a sample of viable electrodes in a device (electrodes 13, 24, 35, 41, 43

from Figure 4.34) and is found to decrease with decreasing impedance which is evident from Equation 4.14.

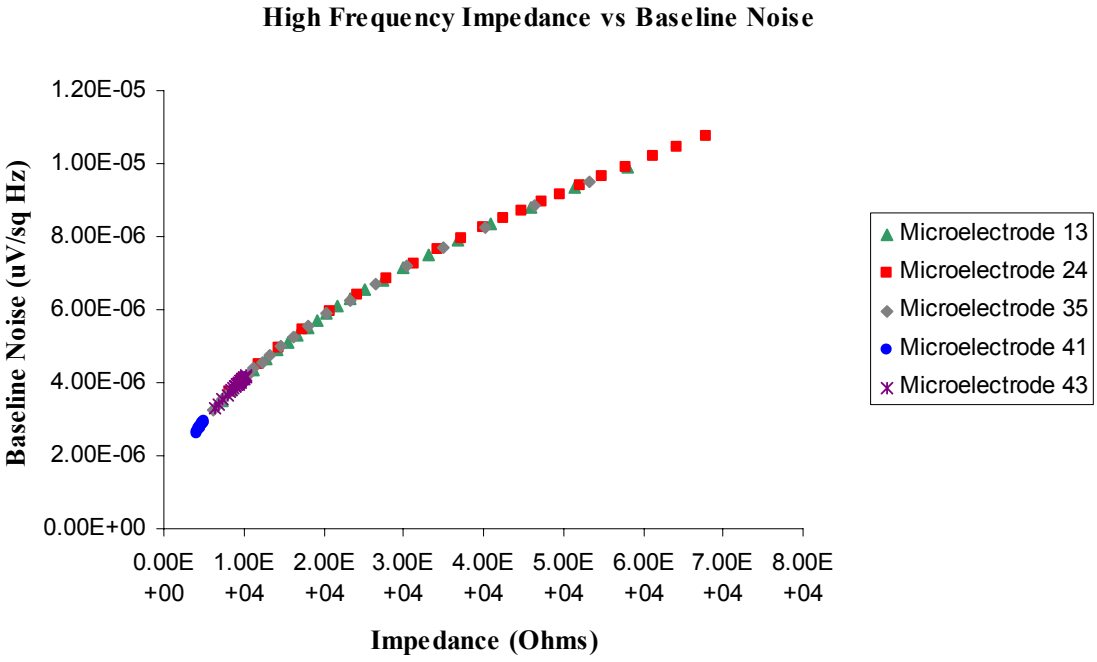

Figure 4.37: Calculation and plot of the variation of baseline noise of microelectrodes on a MEA with respect to impedance of the electrodes.

These electrodes were also in the impedance range $4x10^3$ to $6x10^4$ Ohms at 1 kHz. Measurement of ambient noise of the electrodes is a very important metric for electrophysiological stimulation and recording. The baseline noise of an electrode needs to be low (less than ±40 µV peak-peak or 7 µV RMS [Borkholder 1998]) in order to faithfully record electrophysiological activity from neuronal cultures or tissue slices (with typical signals ≤200µV). This measurement was performed using an MEA-1060 amplifier and MC Rack Software (MCS, Reutlingen, Germany) as described in detail in Section 3.2.2. The packaged MTM 3-D MEA was interfaced with the MCS set-up and

the measurements were made under minimum surrounding noise (no ambient lighting or blowers in hoods) between the microelectrodes, ground and the cellular conducting media (Hank's Balanced Salt Solution). Only viable electrodes which were in the range of 1 kHz impedance described above were electrically connected for the measurement. Non-viable electrodes were grounded during the measurement to minimize noise induced from amplifiers swinging rail-to-rail. Figure 4.38 is a screen shot of the baseline noise of all the electrodes with indications to electrodes in Figure 4.37 that are expected to have low thermal noise figures. A low noise electrode (Microelectrode 41 from Figure 4.37) is also depicted in this figure. This electrode and others like this with noise level lower than ±40μV are suitable for electrophysiological measurements. Some of these are clearly indicated as are grounded electrodes and electrodes with high noise floor.

The noise calculations and experimental comparisons are summarized in Table 4.6. It is to be noted that the experimental data at DC frequency has been estimated from the screen captures. All the modeled electrodes show excellent noise floors suitable for electrophysiological stimulation and recording experiments. This is in good agreement with the theory that has been proposed in the beginning of this section [Gasteland 1959].

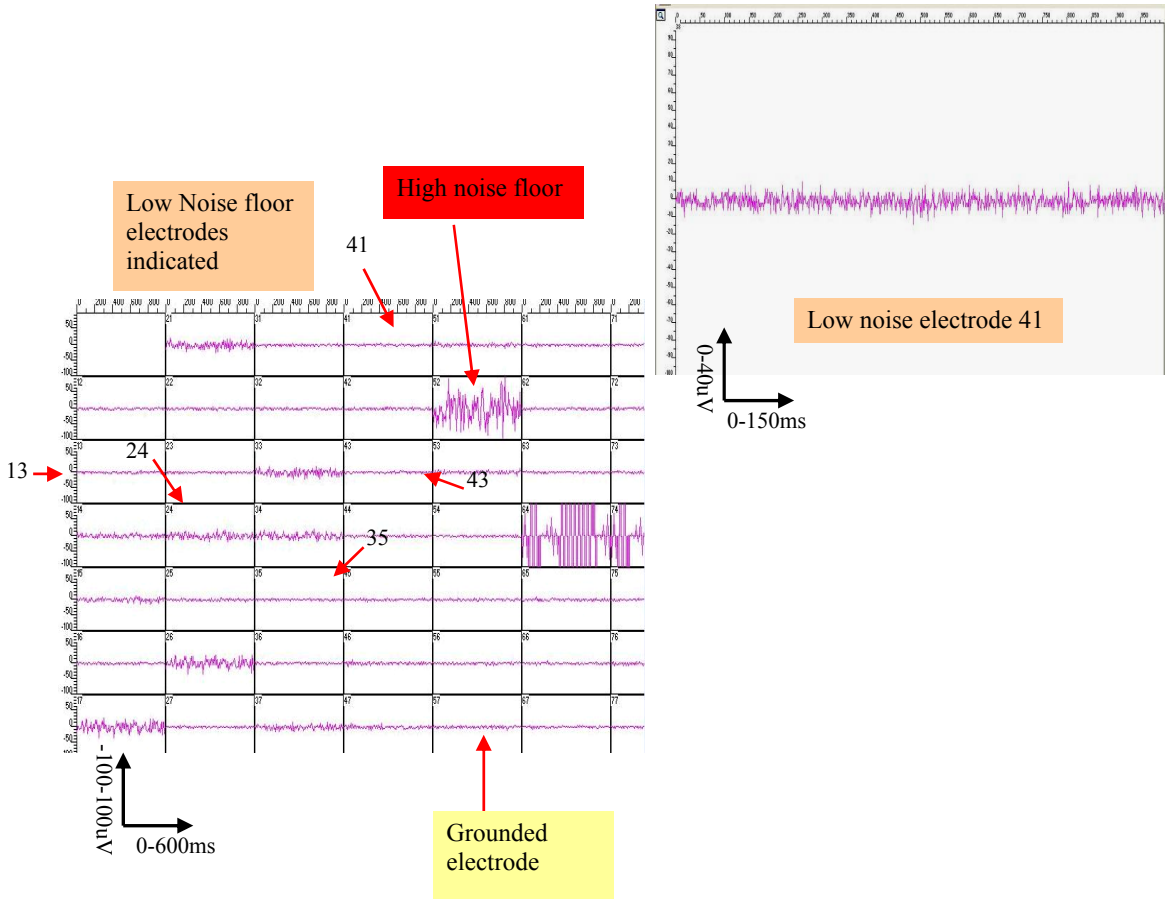

Figure 4.38: Screen capture of baseline noise measurement of various electrodes including low noise, high noise and grounded electrodes. The modeled electrodes are indicated and show acceptable low noise floors.

Table 4.6: Comparison between theoretical and experimental noise predictions

Electrode No.	RMS Theoretical Noise (µV/sq. Hz)	RMS Experimental Noise (µV/sq. Hz)*
13	9.91	~5
24	10.72	~25
35	9.5	<10
41	2.93	<10
43	4.19	<10

* Experimental noise determined by approximation of screen captures.
So a variation of ±10µV/sq. Hz needs to be added to every value

4.3 Metal Transfer Micromolded 3-D MEAs: Process Improvements

The two main areas that contribute to yield loss in the MTM 3-D MEA process were identified as: definition of recording sites and the thickness of metal that is being transferred during the MTM process. Improved microfabrication techniques in these two areas could potentially lead to a greater yield. Electroplating and electroless plating techniques were investigated to address the issue of increasing the metal thickness and a novel technique for parylene deposition with a microfabricated 3-D structure to isolate the recording sites at a micron-scale was investigated to improve the definition of the recording sites. These two techniques are described in the following two sections.

4.3.1 Electroplating and Electroless Plating

One of the factors for low yields of microelectrodes on the 3-D MEAs is the relatively thin metal (less than 0.5μm) that is being transferred during the MTM process. Techniques to strengthen metal layers in microelectronics fall into two categories: electroplating and electroless plating. Unlike traditional MEMS fabrication techniques where a photoresist mold is defined on a seed layer and metal is electrodeposited (thickness: tens to even hundreds of microns) in selected areas using the mold as the barrier for prevention of electroplating in other areas [Allen 1993; Arnold 2004], we already have a well constructed device. The fabrication and packaging processes for the MEA are well defined and characterized. So it was conceived that electroless plating (which can be used to increase the thickness of metal layers post-device construction)

might be a better alternative in the case of MTM 3-D MEAs to strengthen the electrode metal (to at least a couple of microns thick).

Unfortunately selective electroless plating of metals is not easily accomplished as it requires very precise control of the plating bath (composition, temperature and pH) and activation steps (laser induced or catalysts). Even though electroless plating of copper and nickel are common in the PCB industry [Express PCB 2007; Yang 2002; Rohan 2002], they are usually performed on large-scale substrates where metal is plated (as a seed layer) uniformly everywhere [Morris Productions 2008].

Gold was evaluated for selective electroless deposition as it is a biocompatible metal. Technic Inc (www.technic.com) is a premier supplier of electroplating and electroless plating baths, equipment and chemistries. Selective electroless deposition of gold was evaluated with research grade Technic EL gold AT 7000 and 8000 solutions (courtesy: Dr. Kilnam Hwang, Technic Inc). This solution was being developed by Technic engineers for selective plating of gold on polymeric substrates. Table 4.6 lists the parameters that were used for this electroless plating step. The plating was evaluated on test PMMA and SU-8 substrates with metal defined on them (using an MTM process). The objective of these experiments was to ascertain process parameters for electroless plating on 3-D MEAs. The plating rate was evaluated to be around 0.5μm per hour (using a profilometer) at the conditions listed in Table 4.7.

Table 4.7: Parameters for electroless plating of gold on polymeric substrates

Parameter	Value
pH	5.8-6.3
Temperature	58-64 ˚C
Agitation	None
Pre-treatment 1	O_2 Plasma*; 1 min
Pre-treatment 2	Ethanol; 30s
Deposition rate	0.5μm/hour

*O_2 plasma recipe; 200mT pressure, 200W power; O_2 at 40sccm

Figure 4.39 depicts optical micrographs of 3-D MEAs before and after gold electroless plating. The plating time in these experiments ranges from 10 to 45 minutes. Selective plating is definitely evident on the metal traces and electrodes on the micro-towers after the electroless step. Unfortunately when the plating was continued for an hour or more (in order to increase deposit thickness to 0.5μm and beyond), variation in temperature uniformity in the bath and change in pH resulted (both from evaporation of water in plating solution) in non-selective plating as shown in Figure 4.40. Non-selective plating especially on the polymeric substrate implies shorting of adjacent electrodes/metal traces as the figure indicates. This is a detriment to the functionality of the 3-D MEAs.

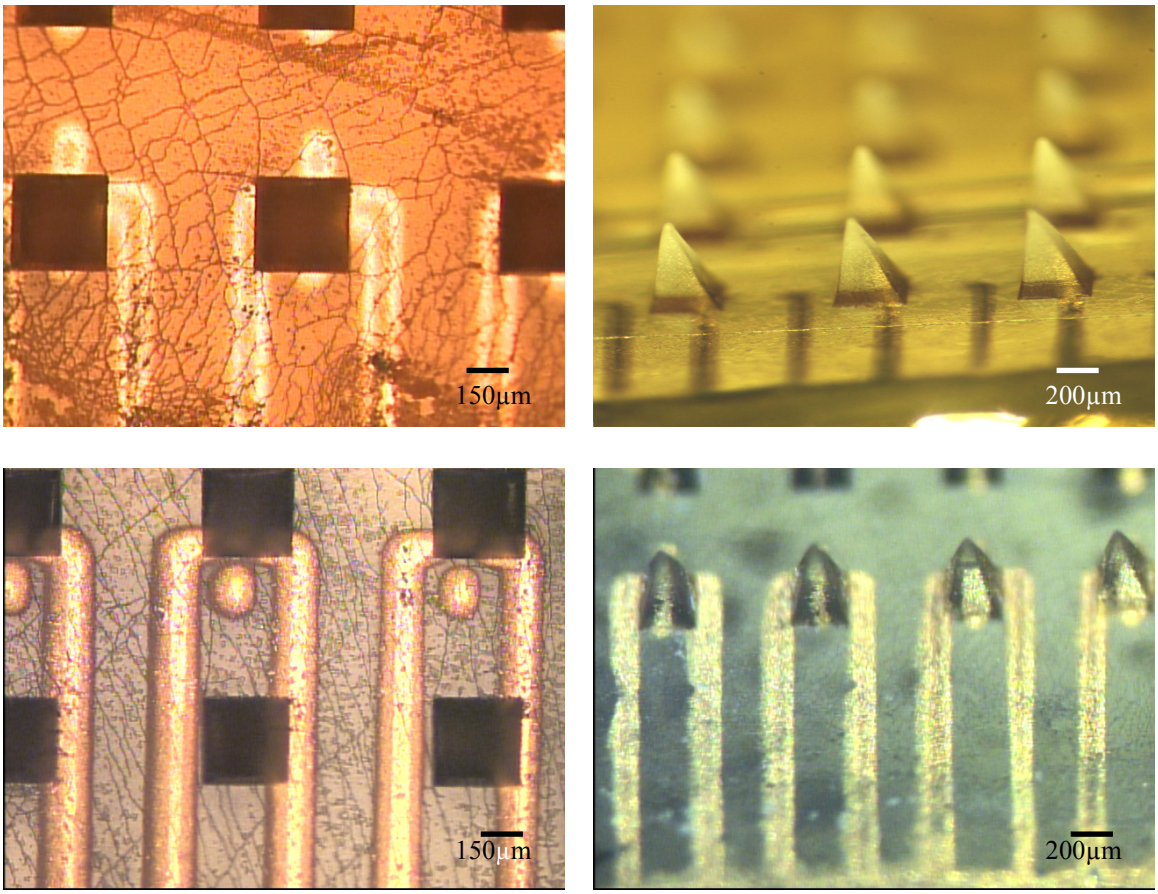

Figure 4.39: Optical micrographs of top (left) and side (right) views of 3-D MEA samples before and after electroless plating. Images on the top are before electroless plating and on the bottom are after electroless plating.

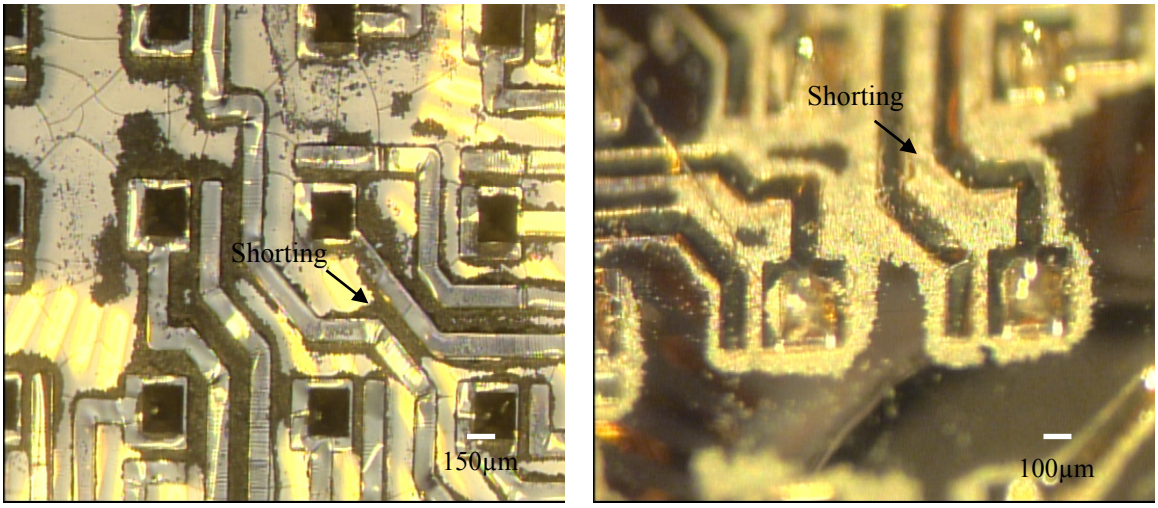

Figure 4.40: Optical micrographs depicting **s**horting of metal traces due to non-selective electroless plating. On the left is a top view and on the right is the side view of a 3-D MEA.

Due to inconsistencies in this electroless plating approach and the fact that the process is slow (deposition rate of 0.5μm/hour) electroplating was evaluated as an option to increase the thickness of the metal traces.

Addition of an electroplating step imposes incorporation of newer features in the mask design. These features are utilized to electrically connect all of the device features, so that potential can be applied during electrodeposition. Further, the features are designed to allow easy isolation of MEA elements post-electroplating. Thus, the mask design depicted in Figure 4.2 was modified to include two new features: "electroplating macro-pads" that will serve as the contact pad for electroplating and traces that connect each individual electrode to the "electroplating macro-pads". Obviously these traces also connect to the rest of the electrode features. This changed design is depicted in Figure 4.41.

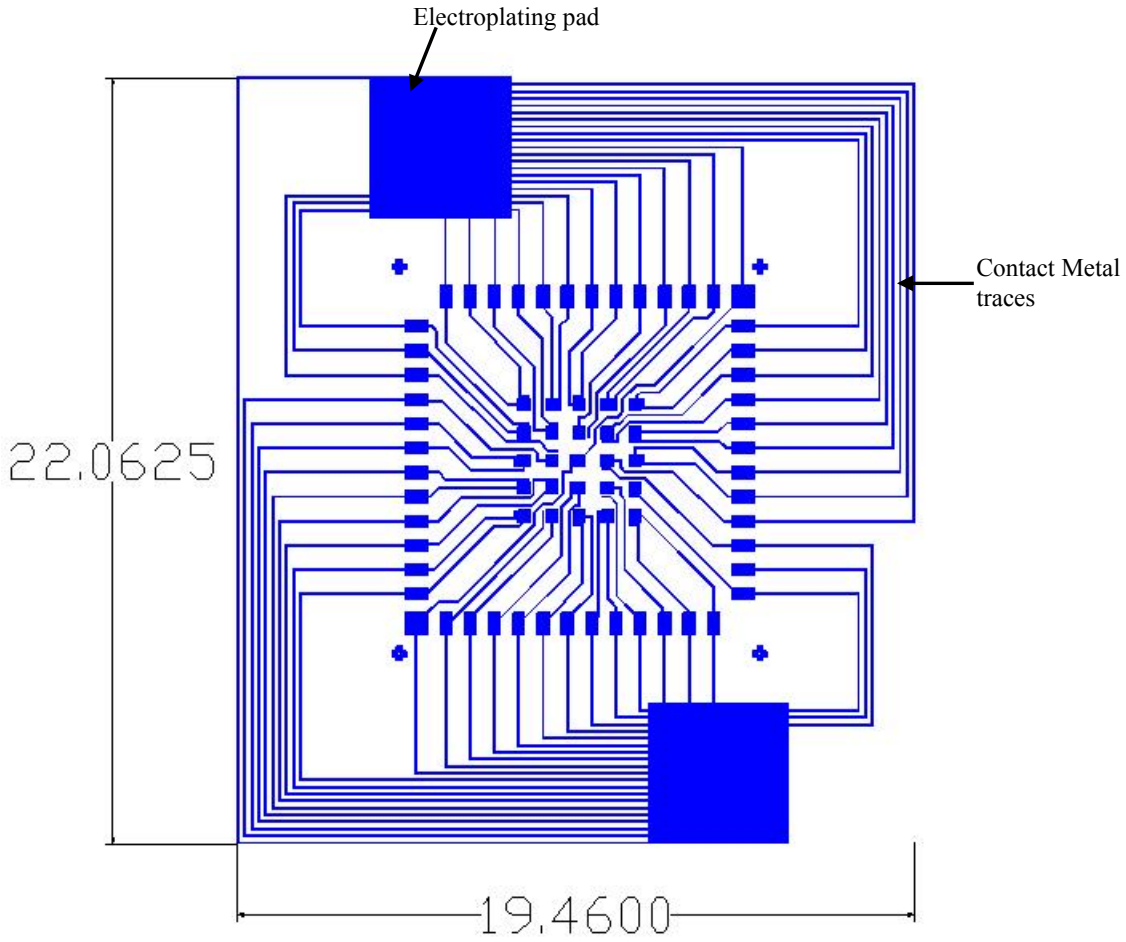

Figure 4.41: Mask design for electroplated 3-D MEAs. Dimensions of the die are in mm.

MTM 3-D MEAs are fabricated using the exact same process as described in Section 4.1.6 but using the mask depicted in Figure 4.41 for the metal traces definition (step 2 in Figure 4.16). The overall substrate size is also increased to 22.06 x 19.46 mm as illustrated in Figure 4.41 to accommodate the increased functionality of the die. Figures 4.42 and 4.43 depict SEM images of the SU-8 rigid master and a flexible PDMS master with these new features.

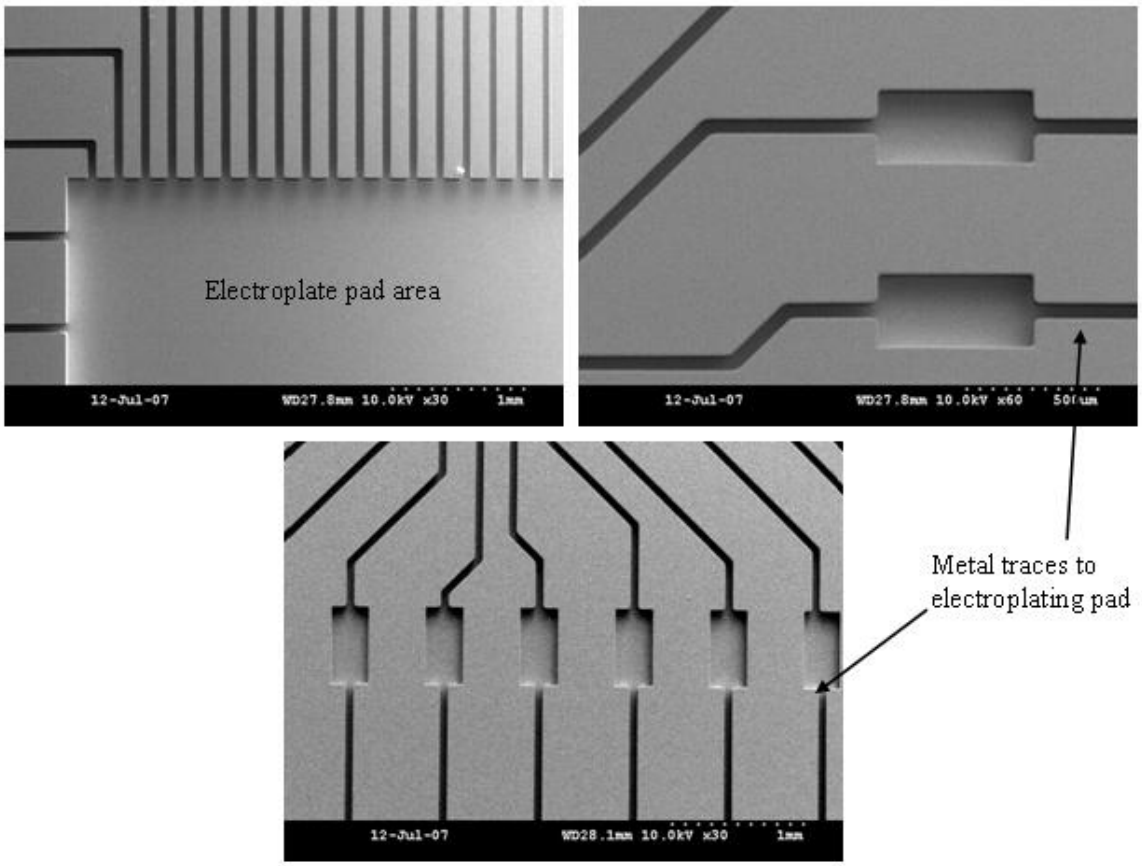

Figure 4.42: SEM images of the double-layer SU-8 master mold that is fabricated to include the newer features for electroplating 3-D MEAs. The new features, the electroplating macro-pad and metal traces for individual electrode plating are clearly indicated.

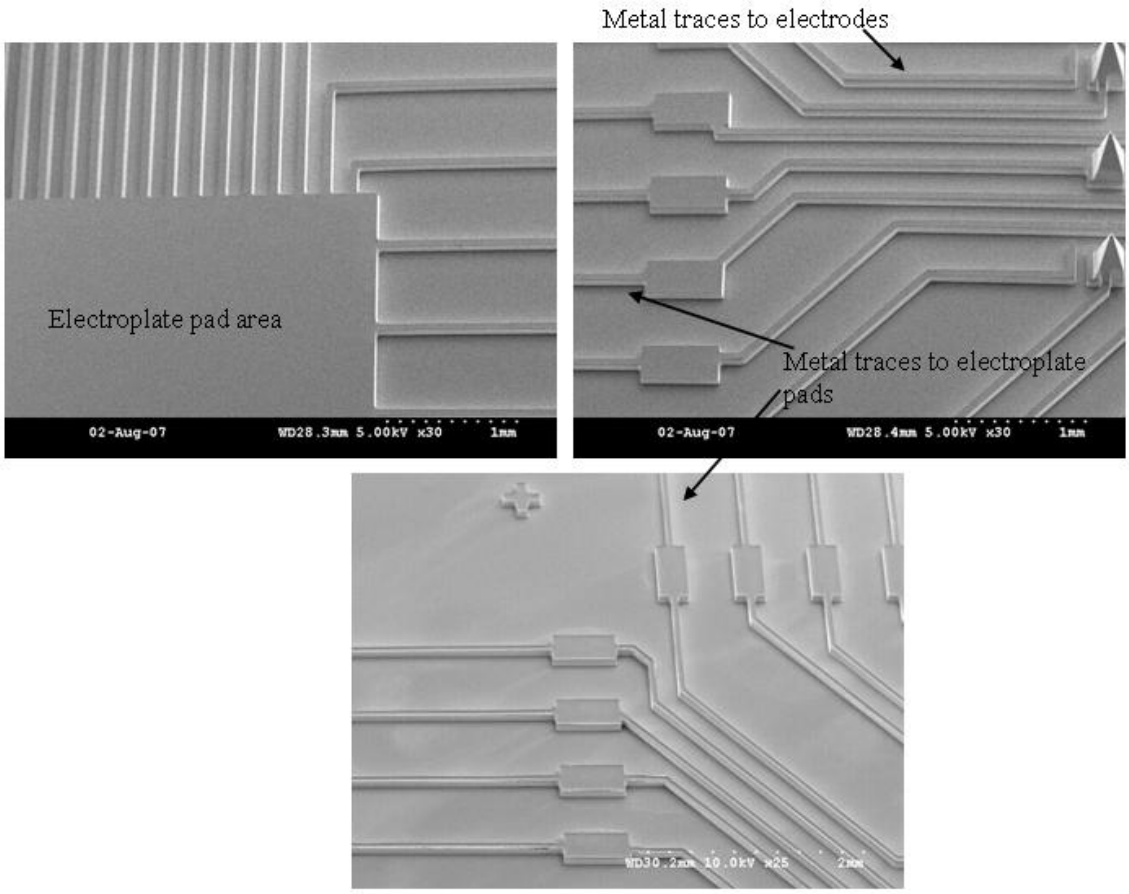

Figure 4.43: SEM images of PDMS master structures fabricated from SU-8 molds for electroplate-3-D MEAs. Clearly visible are the two new added features: electroplate pad and individual metal traces that connect each electrode to the electroplating pad.

Nickel is electrodeposited after the metal transfer micromolding process is completed to fabricate the 3-D MEA in PMMA. The transferred chrome/gold layer is used as the seed layer for the electroplating process. The reasons for electroplating of nickel in spite of its known cytotoxicity [Sunderman 1993] are: familiarity with fabrication parameters as it is used in the laser scribed process, mechanical strength, fast deposition rates and cheaper setup costs compared to gold electroplating (which is the ultimate goal for 3-D MEAs due to biocompatibility of gold). The parameters for nickel plating are given in

Table 4.8. This thickness of the nickel layer was measured to be approximately 6μm using a profilometer.

Table 4.8: Parameters for electroplating nickel for 3-D MEAs

Parameter	Value
Plating Solution	Nickel Sulfamate
Temperature	Room Temperature
Current Density	3mA/cm^2
Area	~14cm^2
Total Current	42mA
Voltage	1.4V at start
Deposition Time	1 hour
Deposition Rate	6μm/hour

Figure 4.44 depicts optical micrographs of the nickel plated 3-D MEAs. On an average 60% of all the metal traces were electroplated which demonstrates an improvement in increased thickness of metal traces thereby providing pathways to improve the overall yield of the microelectrodes. The major problem for this loss in yield is the survival of the continuity of metal traces for several mm during the various molding processes. There is some yield loss at the metal transfer stage as well. The design depicted in Figure 4.41 can be improved to accommodate shorter trace lines and an "electroplating-macro-pad" that is shaped all around the MEA features to alleviate the former problem. Optimized metal transfer with controlled transfer systems can potentially alleviate the latter issue. The electroplated 3-D MEA was then released using the CO_2 laser (New Hermes-Gravograph, Duluth, GA). The size of the final die used for packaging was 11.5mm x 11.5mm.

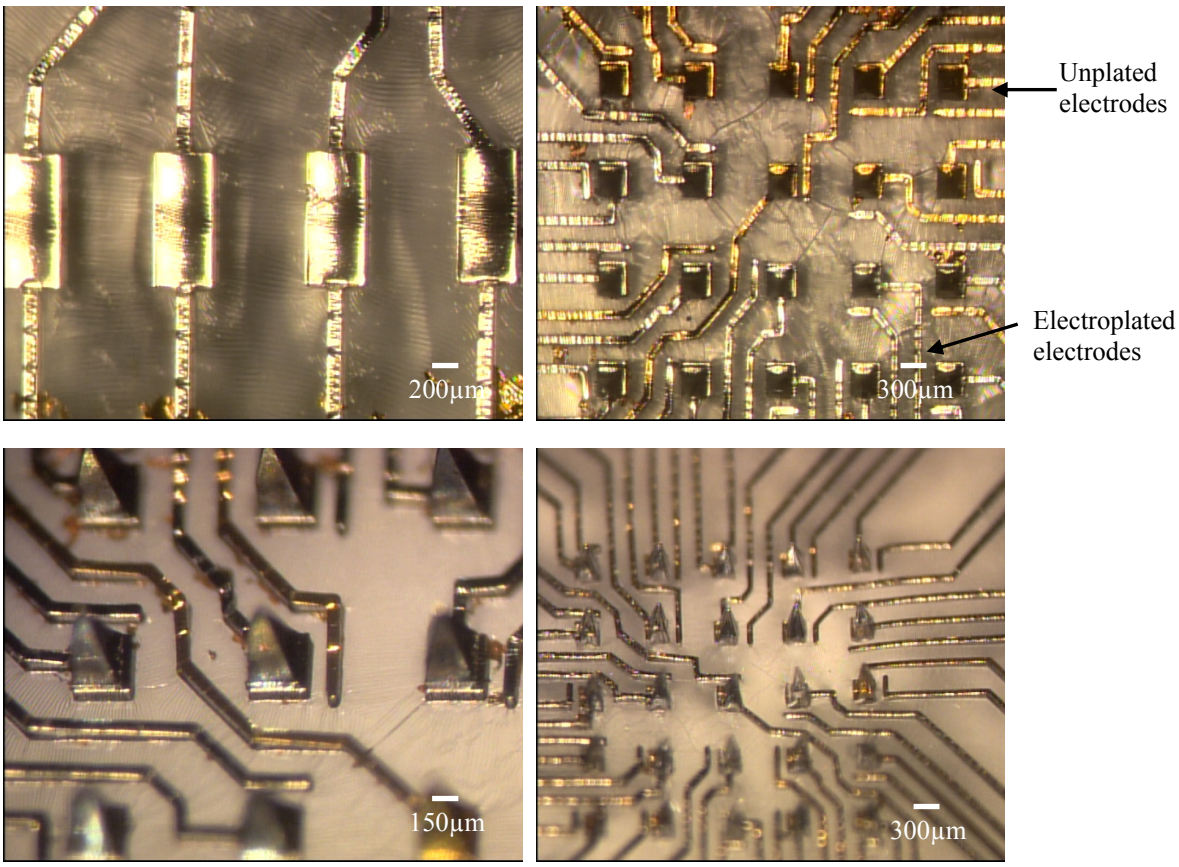

Figure 4.44: Optical micrographs of electroplated 3-D MEAs – top and side views of devices is depicted on the top and bottom side of the figure respectively.

Packaging of the electroplated MEAs was carried out using the same techniques described in Section 4.1.7. The packaging method was PCB-based with a self-alignment and bottom side clamping fixture. Parylene was deposited on these 3-D MEAs utilizing the new "capping" technique described in Section 4.3.2. These MEAs were then evaluated electrically using impedance spectroscopy. A figure of merit for these various developed procedures was developed to demonstrate the yield improvement.

4.3.2 Parylene Deposition: "Capping" Technique

Deposition of parylene on a 3-D MEA, followed by laser micromachining and RIE etching is the technique demonstrated in the MTM process for the final step of defining the microelectrodes or recording sites. An insulator must be deposited after fabrication to isolate the electrical recording sites. Parylene is chosen due to its biocompatibility, as well as its ability to coat surfaces with substantial topography in a uniform manner. This technique has resulted in viable 3-D MEAs but the yield of the microelectrodes is low (around 30%) which is not acceptable for a micro-manufacturing process. One of the reasons for the low yield is the thickness of the transferred metal (less than 0.5μm) and this has been addressed with an electroplating scheme as described in Section 4.3.1. The other reason is the loss of functionality that occurs during laser micromachining where the process window is relatively narrow for excimer laser ablation of thin parylene on thin metal. The predominant reasons for this narrow process window are drift in laser power and focusing errors on 3-D electrodes. Also the laser micromachining technique is too serial for any consideration to a manufacturing extension. This provides the motivations into researching alternative techniques for parylene-based electrode site isolation.

Bhandari et al. [Bhandari 2007] have developed a technique to isolate the tips of 3-D MEAs by "flooding" the entire structure with thick photoresist (AZ 4620) after dielectric deposition on a Utah microprobe array and etching the unprotected dielectric using the RIE. This technique does not result in sufficient yield due to non-uniform coverage of the photoresist coating technique. The removal of the thicker resists after RIE etching also presents a significant challenge. We investigated an arcing method where electric field is

concentrated (by the application of a voltage) at the tips of the MEAs due to their sharp geometry with the intent of producing localized dielectric break down of the parylene at the tips as a result of field concentration. This technique in theory is an elegant way to break down the dielectric only at the tips of the microelectrodes, leaving it intact in all other areas. However, due to high voltages (100s of volts) necessary to break down the dielectric given the high dielectric strength of parylene (6.8 kV/mil [Specialty Coating Systems 2007]), the entire polymeric micro-tower structure was affected.

Exploiting the geometric height difference to isolate the top of the 500µm 3-D electrodes and the rest of the chip is a potential approach to address this issue. Consider for example a "capping" idea as illustrated in Figure 4.45.

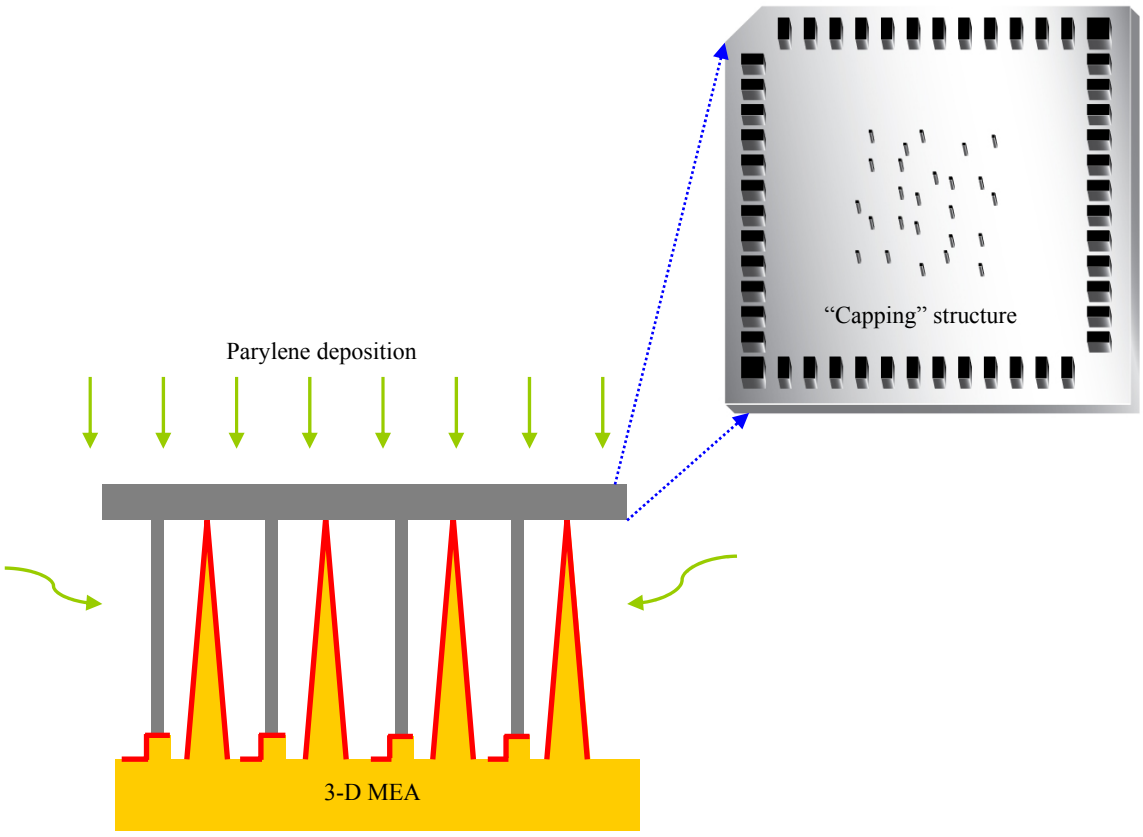

Figure 4.45: Schematic of the proposed "capping" technique for parylene deposition.

Three dimensional “caps” are required to simultaneously isolate the tips of the micro-towers and 2-D recording sites during the parylene deposition as depicted in the schematic in Figure 4.45. This approach eliminates the need for laser micromachining and RIE etching after parylene deposition, thereby reducing process steps and also introducing an elegant way for isolating certain areas in a conformal polymer deposition process. In order to test this approach, 2-D capping structures were initially evaluated to cover the electrode tips. Cured 1mm thick PDMS pieces were diced into 10mm x 10mm substrates (using an exacto knife) to serve as “2-D caps”. These “2-D caps” were placed on a packaged 3-D MEA under a stereoscope to isolate the tips of the 3-D electrodes. Parylene was then conformally deposited. The MEAs were immediately studied using impedance spectroscopy to see the effect of the “2-D cap”. Figure 4.46 outlines the impedance spectrum of a “2-D capped” MEA. The impedance data was exported and the impedance of the electrodes at 1 kHz was plotted separately (Figure 4.47). This figure shows that 14 out of the possible 25 3-D electrodes were viable meaning that their tips were sufficiently exposed post-deposition. The 2-D electrodes were defined after the capping step on this 3-D MEA using the standard process (laser ablation and RIE etching). The impedance spectroscopy of the device was evaluated after this process. It was found that only five of the 2-D electrodes (Figure 4.48 which portrays impedance at 1kHz) were viable. This illustrates that the “capping” technique is a promising approach for defining the electrode recording sites (approximately 60% yield, better than the 30% yield obtained from the laser micromachining/RIE etch process); and also showed that the laser step to define the 2-D recording sites has a relatively low yield.

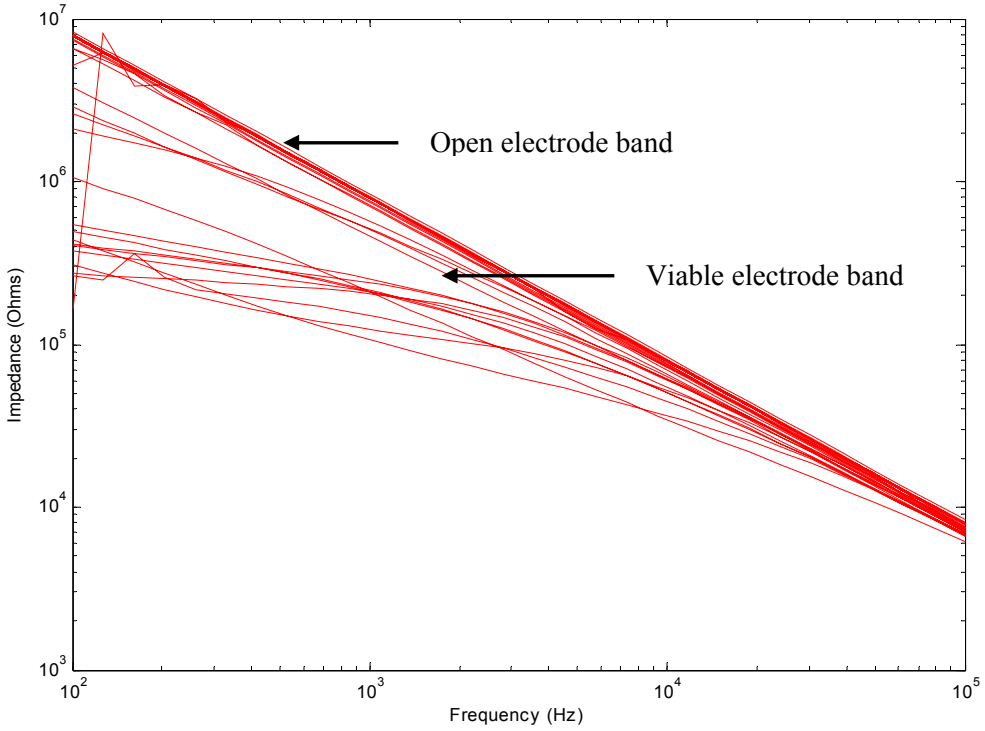

Figure 4.46: Impedance spectroscopy of "2-D capped" MEA structure.

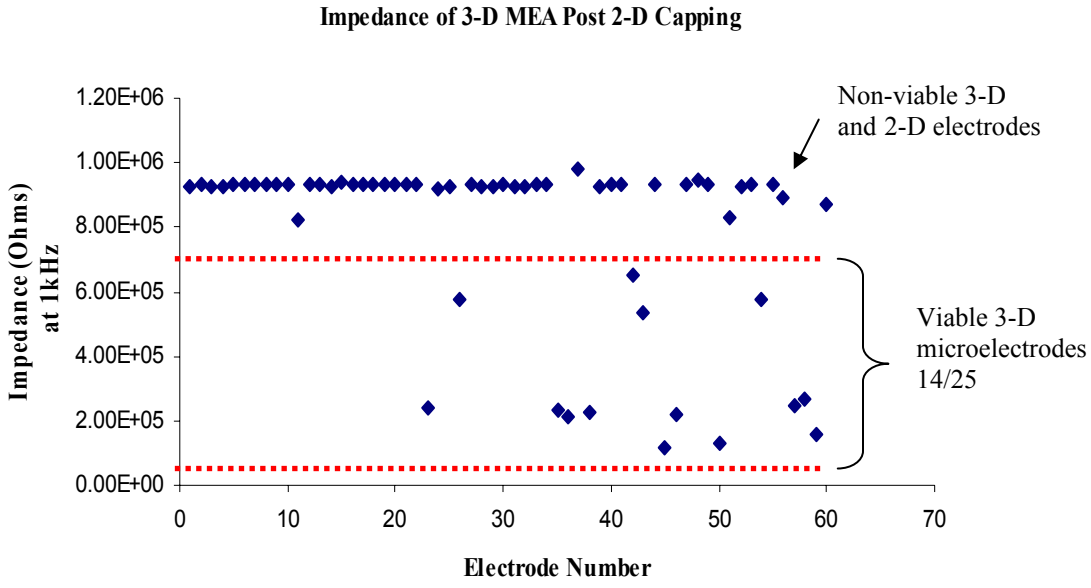

Figure 4.47: Impedance of the "2-D capped" MEA at 1kHz. The non-viable band also includes grounds and unconnected electrodes from the impedance spectroscopy system.

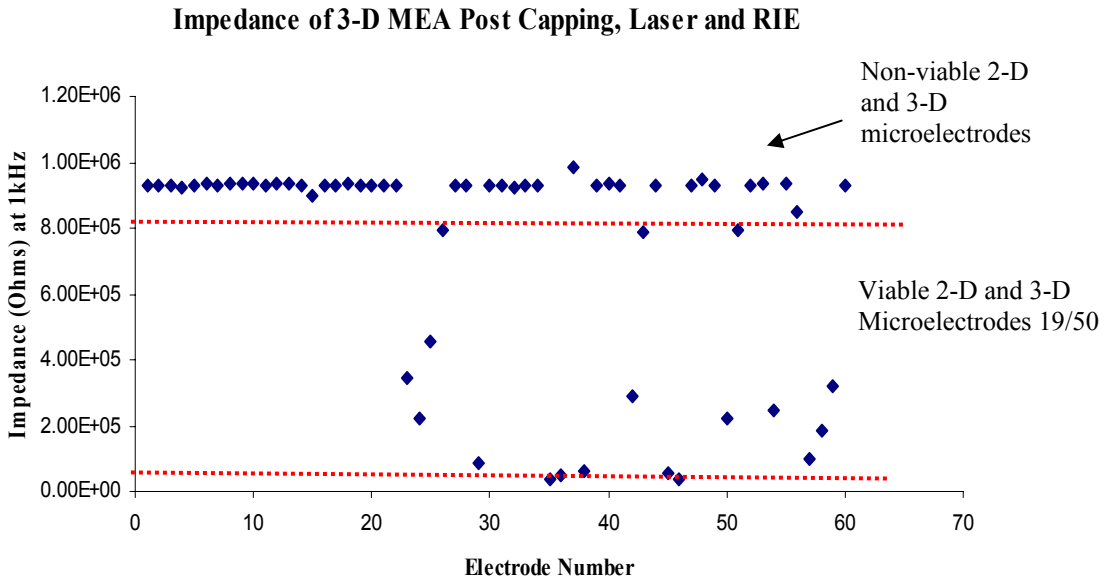

Figure 4.48: Impedance at 1kHz for a 2-D capped MEA with laser micromaching/RIE etching to define 2-D recording sites. The non-viable band also includes grounds and unconnected electrodes from the impedance spectroscopy system.

The results in Figure 4.48 are encouraging for this new proposed approach. However, for full functionality the capping concept must be extended to both MEA tips and bases as shown in the schematic in Figure 4.45. In order to microfabricate these "3-D capping structures", double-side exposure technology of thick SU-8 (described in Chapter 3) was utilized. 2-D structures (to isolate the top of the 3-D MEA) were defined using a 100µm thick layer of SU-8 and a top side exposure step. The 3-D features (bond pads and 2-D recording sites) were fabricated using a bottom-side exposure of thick SU-8 (~400µm thickness to accommodate for the tall MEA structure). Figure 4.49 depicts optical and SEM images of the features of the "capping" structures. Clearly visible are the "micro-pillars" for isolation of the 2-D sites, as well as "micro-cube" structures to isolate the

peripheral bond pads. Isolation of the electrode tips is provided by the base of the capping structure.

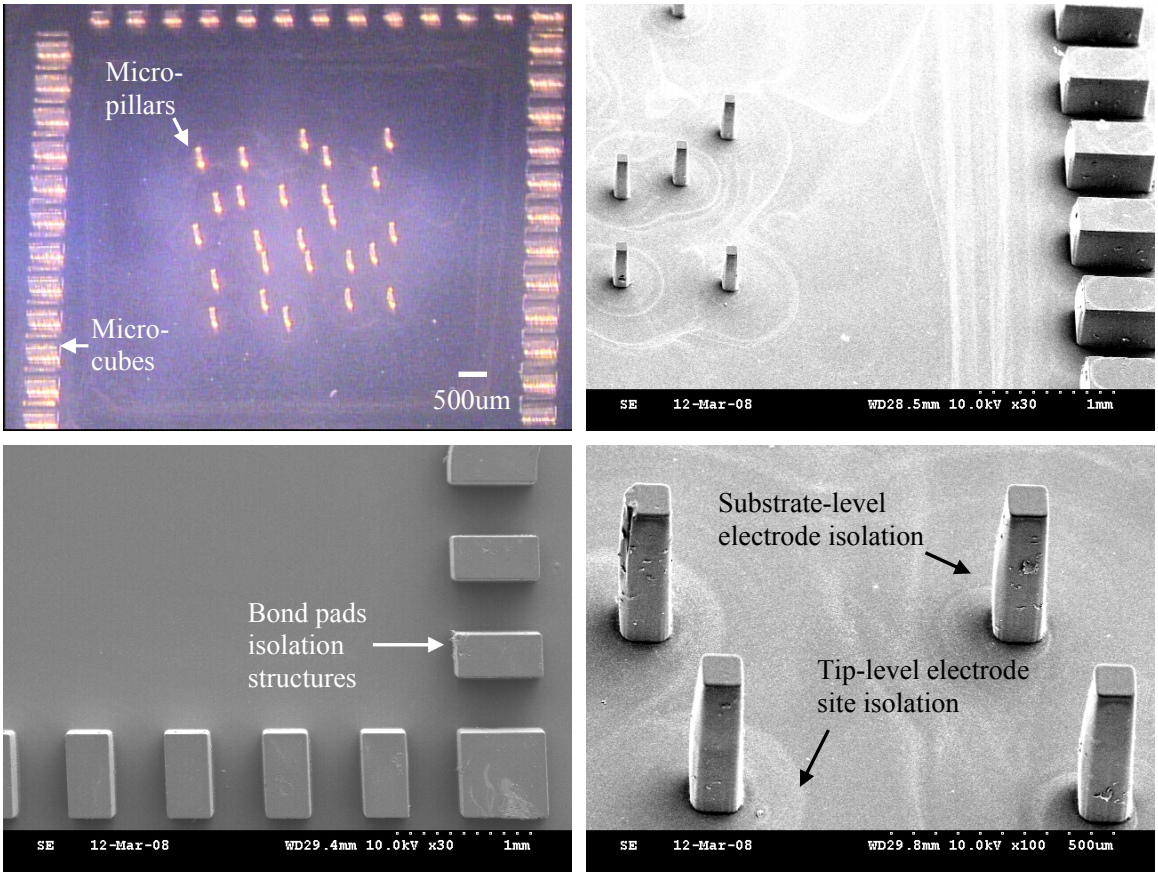

Figure 4.49: Optical and SEM images of the top and side views of 3-D capping structures for geometrical isolation of parylene deposition.

The released "capping" structures were mechanically separated from the 4" glass substrate and aligned with the 3-D MEA under a stereoscope. This structure was immediately transferred to the parylene deposition chamber and 5µm parylene was deposited on the entire assembly. The impedance spectrum of the 3-D MEA was evaluated after removing the "cap" from the MEA and packaging the structure using the techniques described in Section 4.1.4. Figures 4.50 and 4.51 depict the spectrum of the 3-

D MEA and the impedance of the microelectrodes at 1 kHz. Figure 4.52 depicts a 2-D color map of the location of microelectrodes on the MEA.

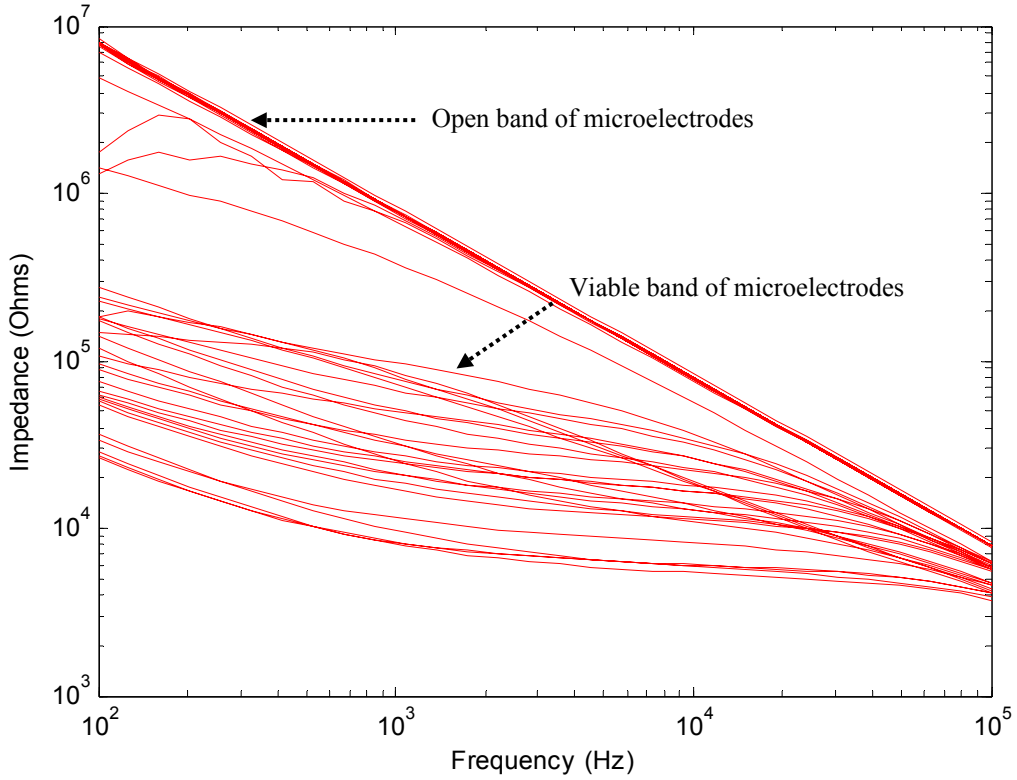

Figure 4.50: Impedance spectrum of a 3-D MEA after "3-D capped" parylene deposition.

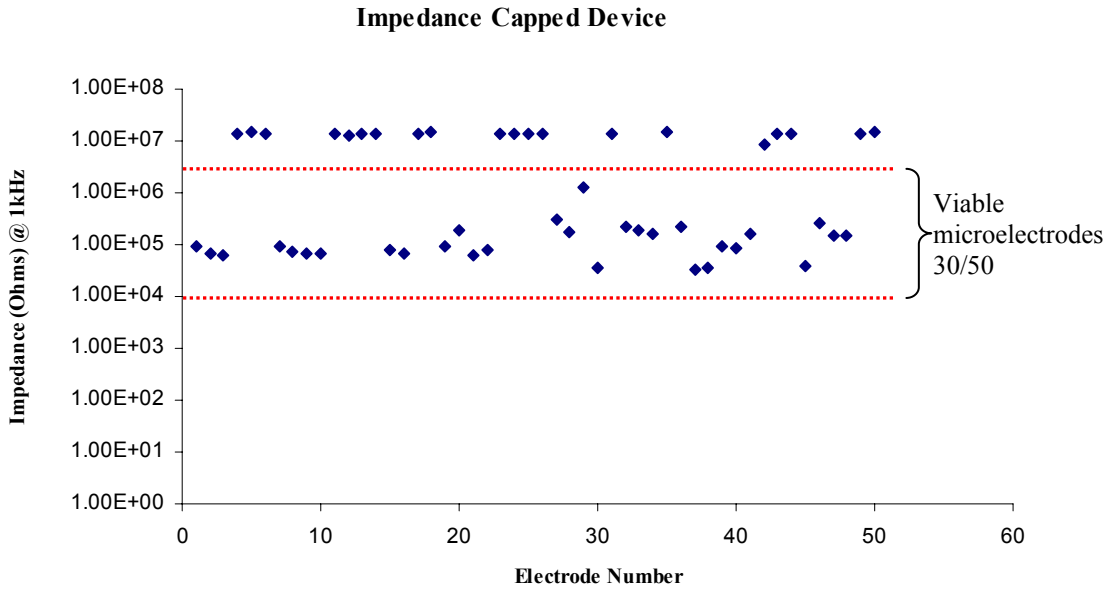

Figure 4.51: Impedance of the microelectrodes at 1kHz depicting a high yield. The non-viable electrode band includes unconnected and ground electrodes.

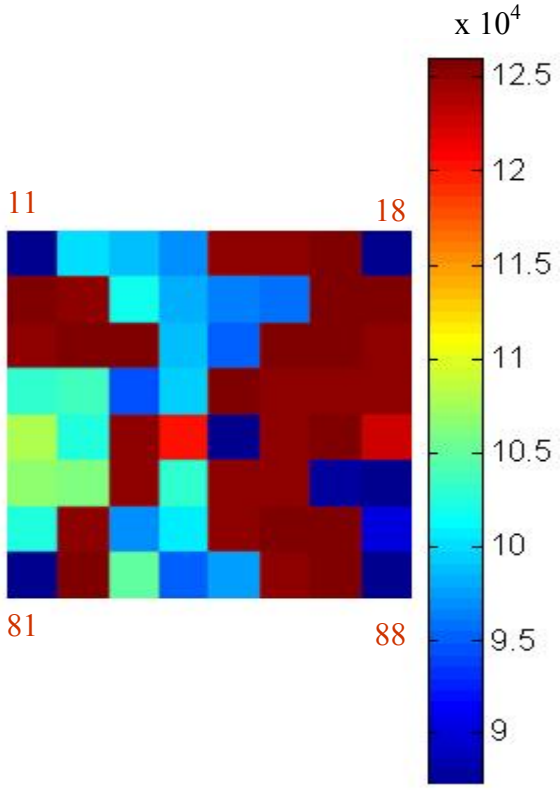

Figure 4.52: Color map of the impedance of the microelectrodes at 1kHz depicting the location of microelectrodes on the array for quantification of biological protocols. For translation map please refer to Figure 4.36.

Although 100% yield was not achieved using the "capping" technique, it is promising. Thirty of the possible fifty electrodes (yield of 60%) were found viable; this is a significant improvement over the laser/RIE method. It also reduces processing time and steps. The alignment inaccuracies of the "cap" to the 3-D MEA is the primary reason for a less than 100% yield and this can be improved by fabricating an alignment structure with raised pillars into which both the MEA and the "cap" can be fitted prior to the deposition of parylene. This is discussed further in the Chapter 6.

4.4 MTM 3-D MEA Characterization: Biological Results

This section summarizes the biological characterization of 3-D MEAs for *in-vitro* applications such as drug screening, testing for toxins, traumatic brain injury and basic neural research. The first section details the biocompatibility experiments that were performed to evaluate the biocompatibility of the new materials used in this fabrication. Section 4.4.2 summarizes the electrophysiological spike recordings from the hippocampal region (which dictates memory) of rat brains.

4.4.1 Biocompatibility Results

Several new materials such as Poly Methyl Methacrylate (PMMA), Poly-urethane (PU) and laser micromachined parylene are being introduced in this work for microelectrode fabrication by the metal transfer micromolding process. Biocompatibility of these materials must be evaluated before these MEAs can be tested for electrophysiological stimulation and recording of dissociated cultures or slices. The

evaluation of biocompatibility was carried out as part of this work utilizing 2-D planar cultures of rat neurons. The procedure for extraction of neurons from pregnant rats is given in section 3.2.3 and was approved by the Georgia Tech's Institutional Animal Care and use Committee (IACUC). These experiments were performed in collaboration with Prof. Michele LaPlaca's group in the department of Biomedical Engineering at Georgia Tech (Ms. Maxine McClain). The following materials made up the sample list for the study:

1. $5mm^2$ piece of PMMA, the polymer used for the construction of MTM 3-D MEAs.
2. $5mm^2$ piece of PU, the other polymer used for the fabrication of 3-D MEAs.
3. A $5mm^2$ piece of PMMA was coated with 10nm/100nm of chrome/gold, followed by 5µm of parylene. Approximately five 100µm wide, 2mm long lines were scribed using the excimer laser. The reason for the preparation of the substrate in this manner was to simulate the recording sites on the MEAs.
4. A $5mm^2$ piece of PU was coated with 10nm/100 nm of chrome/gold followed by 5µm of parylene. Approximately five 100µm wide, 2mm long lines were scribed using the excimer laser. The reason for the preparation of the substrate in this manner was to simulate the recording sites on the MEAs.
5. Control material was a polystyrene well (commercial cell culture plate, from Millipore Inc., Bellerica, MA)

SU-8 was not used in these experiments as the biocompatibility of this material with regard to neuronal cultures has been extensively studied [Vernekar 2008; Berdondini

2006]. A six well culture plate (Sigma Aldrich, St. Louis, MO) was utilized for these experiments. The extracted neuronal cells from dissection of rat brains were plated as a planar culture (2-D) at a cell density of 1250-2500 cells/mm^2 on the materials listed above, each placed in a single well. The remaining two well were used as controls. The cultures were maintained at 37°C and 5% CO_2-95% humidified air in an incubator. The media was changed every 24 hours for 5 days and then imaged using confocal microscopy (Multi-Photon Excitation Confocal Microscope, LSM 510 NLO META, Carl Zeiss Inc, Oberkochen, Germany). Prior to imaging, the samples were fluorescently stained with 1.6 μM Hoechst 33258 and 3 μM propidium iodide (Molecular Probes, Eugene, OR). The details of procedures for live/dead staining are similar to the ones described in section 3.2.3. Figure 4.53 (a)-(e) depicts the fluorescent microscopy images of all five material samples. The viability was evaluated by counting the number of live cells (fluorescing green) and the number of cells with compromised membranes (nuclei fluorescing red). The counting was performed under the confocal microscope by isolating certain regions and capturing images of those regions.

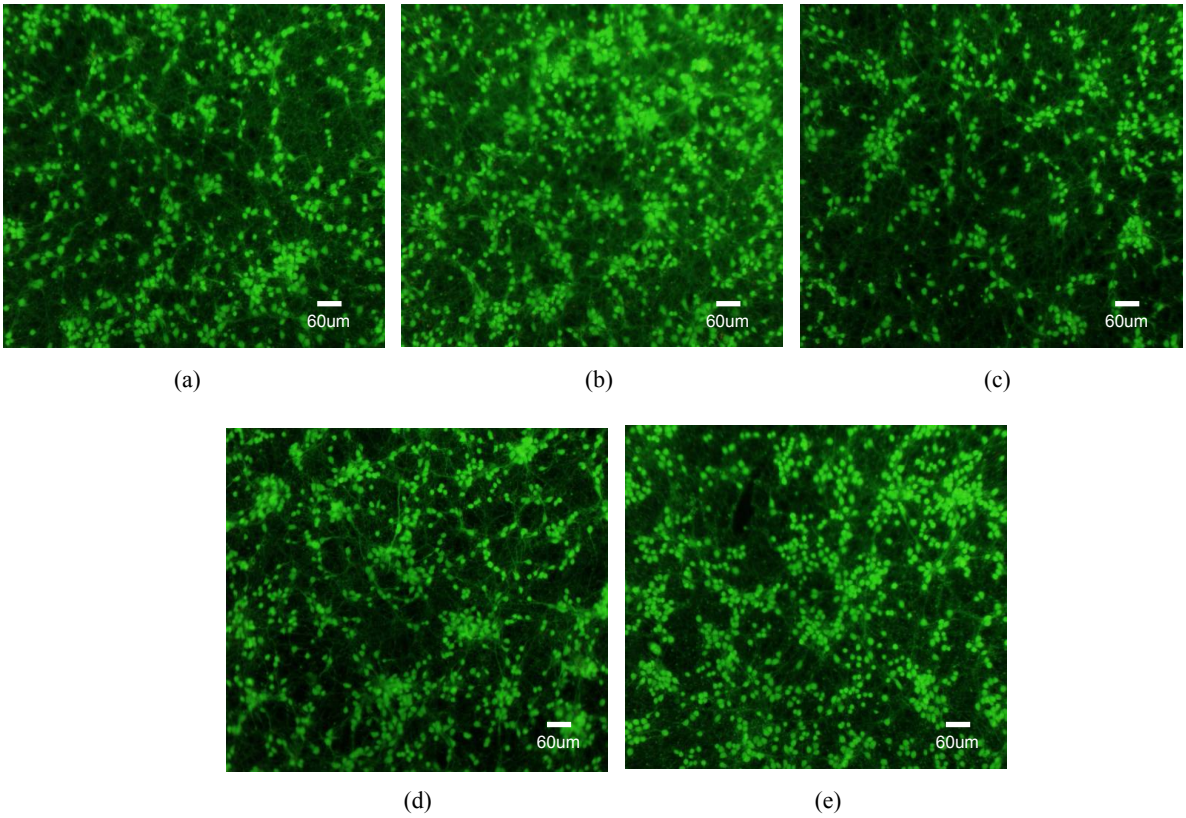

Figure 4.53: The viability of 2-D neuronal cultures on (a) control PS well; (b) PMMA; (c) PU; (d) parylene-coated, laser scribed PMMA; (e) parylene-coated, laser scribed PU.

Viability is expressed as a percentage of the number of live cells divided by the total number of cells plated and given in Equation 4.15.

$$\text{Viability}\,(\%) = \frac{(\text{Total \# cells fluorescing green})}{(\text{Total \# cells fluorescing green \& red})} \tag{4.15}$$

Three to five regions of each culture were imaged and cells counted. The viability of all the materials was very comparable with the control well as represented in Figure 4.54.

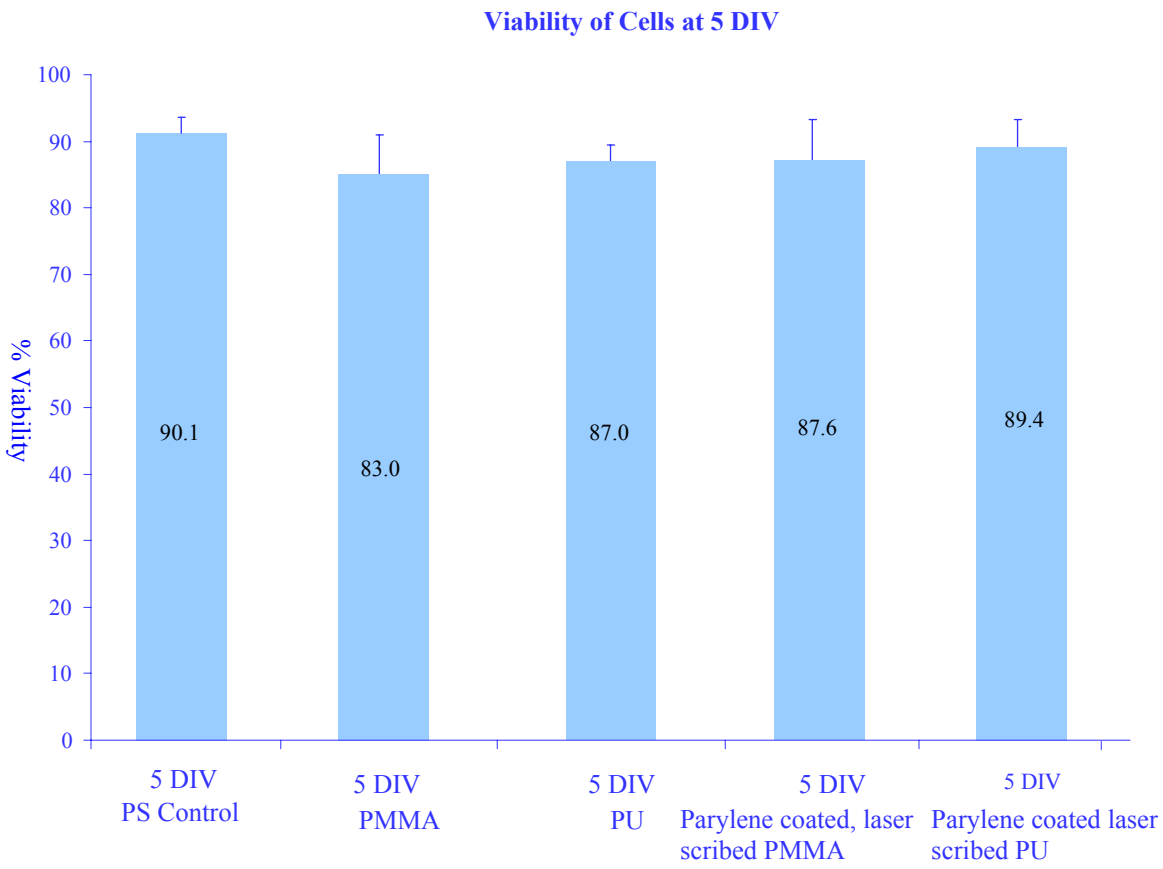

Figure 4.54: Percentage viability of neuronal cells at 5 days in-vitro on the various materials used and control polystyrene wells.

The value of viability for all the materials and the control was within the absolute range: **85% ± 5.1%**. The control demonstrates slightly higher cell viability at 90.1% but the viability of all the various materials is very comparable demonstrating excellent biocompatibility with regard to dissociated neuronal cultures. The excellent viability of parylene-coated, laser scribed PMMA and PU also demonstrates that leachants or toxins potentially emanating from or created by laser micromachining have no discernable effect on the viability and proliferation of neurons on these materials. This study successfully demonstrates the biocompatibility of the materials involved in MTM fabrication. Compared to other electrogenic cellular cultures, neuronal cultures are more

sensitive to material issues (eg. biocompatibility) [Cullen 2005]. Thus, this study is an encouraging sign for similar biocompatibility studies with other electrogenic cells.

4.4.2 Electrophysiological Results

Passive electrophysiological recordings demonstrate the ability of these 3-D MEAs to be used in *in-vitro* applications such as biosensing, pharmacological screening, traumatic injury and basic neural research. Electrophysiological recordings were performed using slices of brain tissue from the hippocampal region of ten day postnatal rat pups. The hippocampal region of the brain is believed to serve important functions such as olfaction, memory and space [Scoville 1957; O'Keefe 1978] and has been extensively studied in rodents. Even though there are obviously significant differences in size and composition of the hippocampal region between a rat and a human, the rat hippocampi serve as an excellent source of information about vertebrate hippocampal regions. *In-vitro* slice culturing was introduced by Gahwiler in 1981 [Gahwiler 1981]. Since then it has been adopted as a highly developed model for studying single neurons and neuronal networks. Since the hippocampal region develops late compared to the neocortex, even though the cells are born in the early post natal period several aspect of cortical development including neurogenesis, axonal pathfinding, neuronal specificity, synapse formation etc. can be studied using cultures from the hippocampi [Forster 2005].

The experiments listed in this section were performed in collaboration with Prof. Michelle LaPlaca's group in the department of Biomedical Engineering at Georgia Tech (Ms. Maxine A. McClain). All the procedures including dissection and maintenance of

rats were approved by Georgia Tech's Institutional Animal Care and use Committee (IACUC). These procedures are briefly discussed below.

A typical dissection kit has scapels, blades, spatula, scissors and forceps. These instruments were autoclaved and kept in a sterile environment before the procedure. In order to isolate the hippocampal region from rat pups, pregnant Sprague Dawley rats were purchased (Charles River, Wilmington, MA) and maintained at Georgia Tech's Animal Care facilities. Rat pups are born at the termination of the pregnancy. At day ten these rat pups were isolated from their mother, anesthetized in 5% isofurane in oxygen and carefully decapitated. After decapitation the skin is removed from the skull using forceps and the skull is opened using a pair of scissors. A spatula is then used to remove the brain and it is placed in ice-cold preparation buffer. This was performed within 10 minutes of the sacrifice in order to maximize tissue viability.

The hippocampal region was removed from the brain carefully using a scalpel in order to induce minimum damage to the integrity of the hippocampi and the neuronal networks. It is sectioned into 500μm thick slices using a McIlwain Tissue Chopper (Mickly Laboratories and Engineering, Surrey, England). The razor blade that is used in this procedure is cleaned with ethanol before the slicing of the tissue. The slices are also placed in ice-cold preparation buffer for the same reason as the brain (in order to maximize tissue viability).

Three slices were separated in Gey's balanced salt solution (Sigma-Aldrich, St. Louis, MO) and arranged on the 3-D MEA and held in place by an organotypic cell culture membrane (Greiner Bio-One, Monroe, NC) and a stainless steel ring. The MEA with the slices arranged on it was moved from the dissection room to the recording facility. Figure

4.55 illustrates a schematic of the entire setup including dissection and recording facilities. A room temperature, oxygenated, extracellular-based, buffered, salt solution bathed the slices during the recording session. To enhance neural firing, the potassium concentration was elevated to higher than normal physiological levels, at 20mM. Recording was done on multiple sets of freshly dissected slices using a MCS recording pre-amplifier (MEA 1060) and MC Rack software. Figure 4.56 represents individual spikes from three different electrodes that are greater than ±50µV.

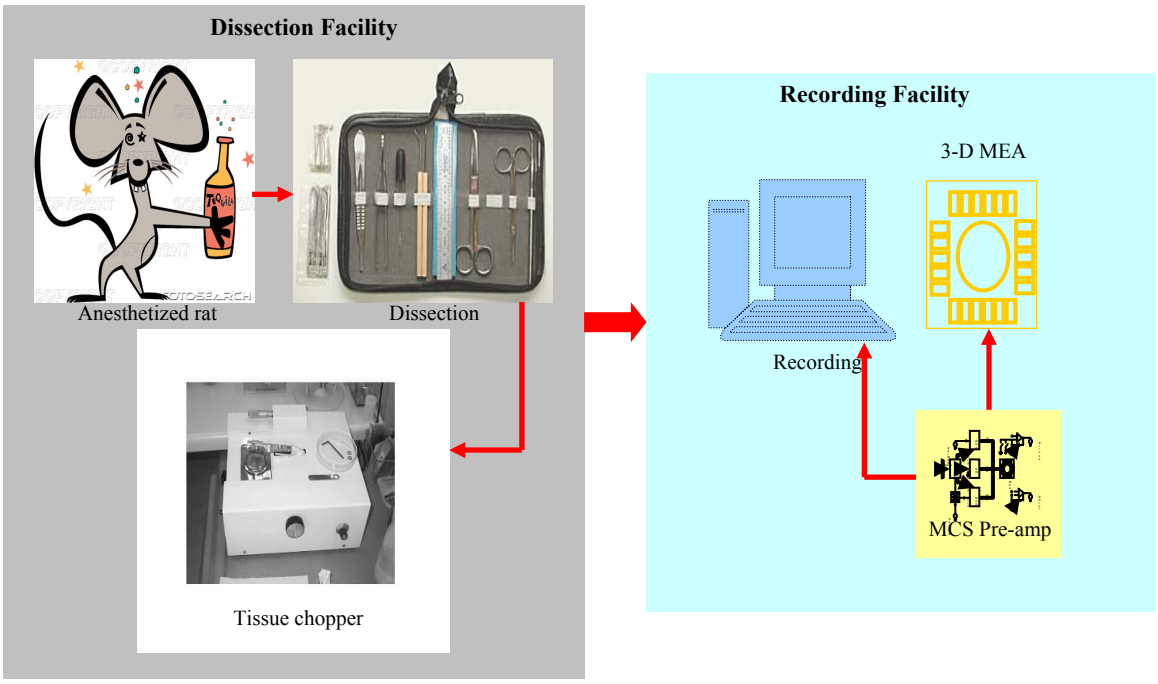

Figure 4.55: Schematic of the chief components of dissection facility (left) and recording facility (right).

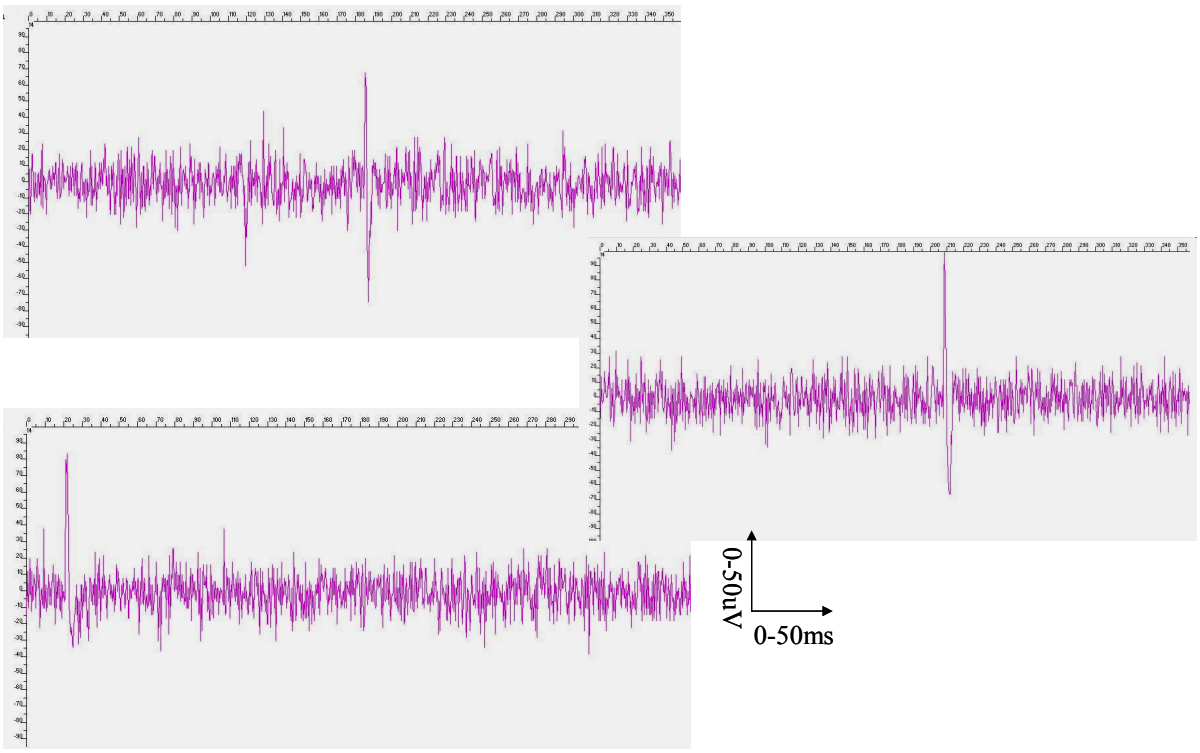

Figure 4.56: Hippocampal tissue slice recordings from three separate electrodes. The spikes are clearly distinguishable from the noise of the system.

Figure 4.57 depicts an optical micrograph of a tissue slices carefully arranged on a 3-D MEA. These experiments were designed to demonstrate the applicability of these MEAs to successfully record electrophysiological spike activity from neuronal aggregates. For acute cultures (like tissue slices), the microelectrodes developed in this dissertation were able to successfully record neuronal activity. Studies on burst patterns and spike recognition algorithms are outside the scope of this dissertation. Pharmacological manipulation can be achieved with a similar setup with the compound of interest being studied by adding it to the medium housing the slices. Other neurological experiments can be performed with protocols developed in this dissertation.

Stimulation is another area of interest in electrophysiology and can likewise be implemented with the procedures described in this section.

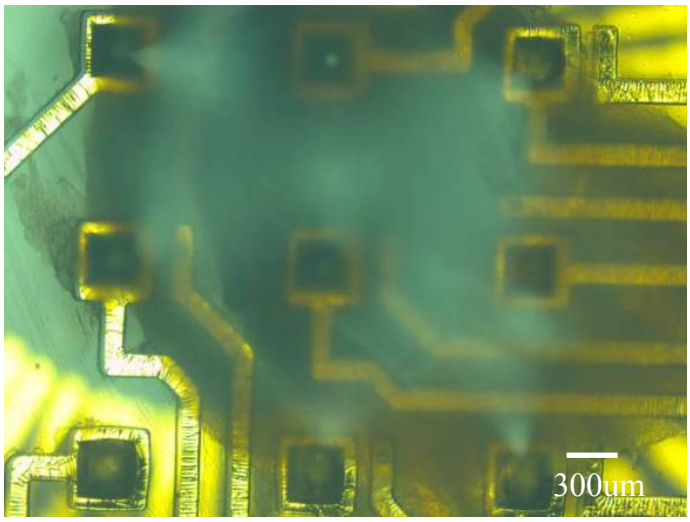

Figure 4.57: Optical micrograph of a hippocampal slice on a 3-D MEA.

4.5 Chapter Discussions Conclusions

This chapter discusses the development of a **new microfabrication technology with multiple applications with enormous promise toward an extension to MEMS manufacturing**. This technology has been named "**Metal Transfer Micromolding**". Advanced micromold fabrication technologies like inclined UV lithography of SU-8 have been combined with functional pattern transfer during soft lithography to usher in the MTM technology that has been demonstrated in this chapter to manufacture 3-D MEAs. Ray tracing algorithm has been utilized to predict the shapes of 3-D MEA mold structures. Two different techniques to define patterned metal in two and three

dimensions have been developed – **shadow masking and intentionally formed non-planar mold**. These MEAs have **been packaged using commercially available PCB technologies** and coated with a parylene insulation layer. Recording sites have been defined utilizing laser micromachining and RIE etching of parylene. Though device functionality is achieved using this final step, the yield of the microelectrodes is low (**approximately 30%**). In order to improve the yield, **electroless and electroplating** have been developed to increase the thickness of the metal traces and electrodes. A **"capping" technology to deposit parylene selectively** on the 3-D MEA has been demonstrated. Incorporation of these techniques doubles the yield of the MTM process to a **reasonable 60%** with scope for further improvement.

Microelectrode impedance theory (from Chapter 2) has been adopted to **develop impedance models for MTM 3-D MEAs**. This analytical model is compared with experimental results resulting in a reasonable match between experiments and theory. Geometric area estimation (during experiments) has been determined as the key reason for the observed variation between theoretical and experimental results. Baseline thermal noise inherent in the 3-D MEAs has been measured and theoretically modeled offering an excellent match between the two values.

In-vitro functionality of the 3-D MEAs is demonstrated first by illustrating biocompatibility measurements for the various materials involved in the MTM process. **85%±5% viability** is established using **2-D cortical cultures of neurons** at 5 days *in-vitro*, demonstrating minimal biocompatibility concerns. **Acute electrophysiological** experiments have been carried out using these MEAs utilizing **passive recordings from**

hippocampal slice cultures of rat brains. This opens the door for a wide variety of *in-vitro* neurological and pharmacological research and development.

CHAPTER 5

MICROMACHINED *IN-VIVO* MEAs: MINIMALLY INVASIVE BIOPOTENTIAL MEASUREMENT

5.1 3-D MEAs for Bipotential Measurement

5.1.1 Introduction

The ability to precisely sense and manipulate the human nervous system without invasively entering the body would enable major advances in neural prosthetics [Wise 2005], therapeutic stimulation [Farina 1986; Scherder 1996], and clinical diagnostics [Disselhorst-Klug 2000]. Classical neural interfaces include surface biopotential electrodes that are used to measure signals for Electromyography (EMG), Electrocardiography (ECG), Nerve Conduction Studies (NCS) [DeLuca 2006] etc. Although surface biopotential electrodes provide a foundation for non-invasive neural interaction, they are limited by three major constraints: (1) signals generated by traditional biopotential electrodes suffer from high noise levels and low spatial resolution; (2) surface stimulation temporarily induces 'blind spots' or artifacts that obscure evoked responses; and (3) anatomical variations between patients or subjects render traditional electrode placement unpredictable. While researchers and physicians are able to partially overcome these shortcomings through training and effort, they quickly encounter fundamental limits to the precision with which they can evaluate and control electroactive tissue. Figure 5.1 summarizes opportunities for biopotential

electrodes in the human body. The inset has the schematic of the proposed electrode system which is described in section 5.2.

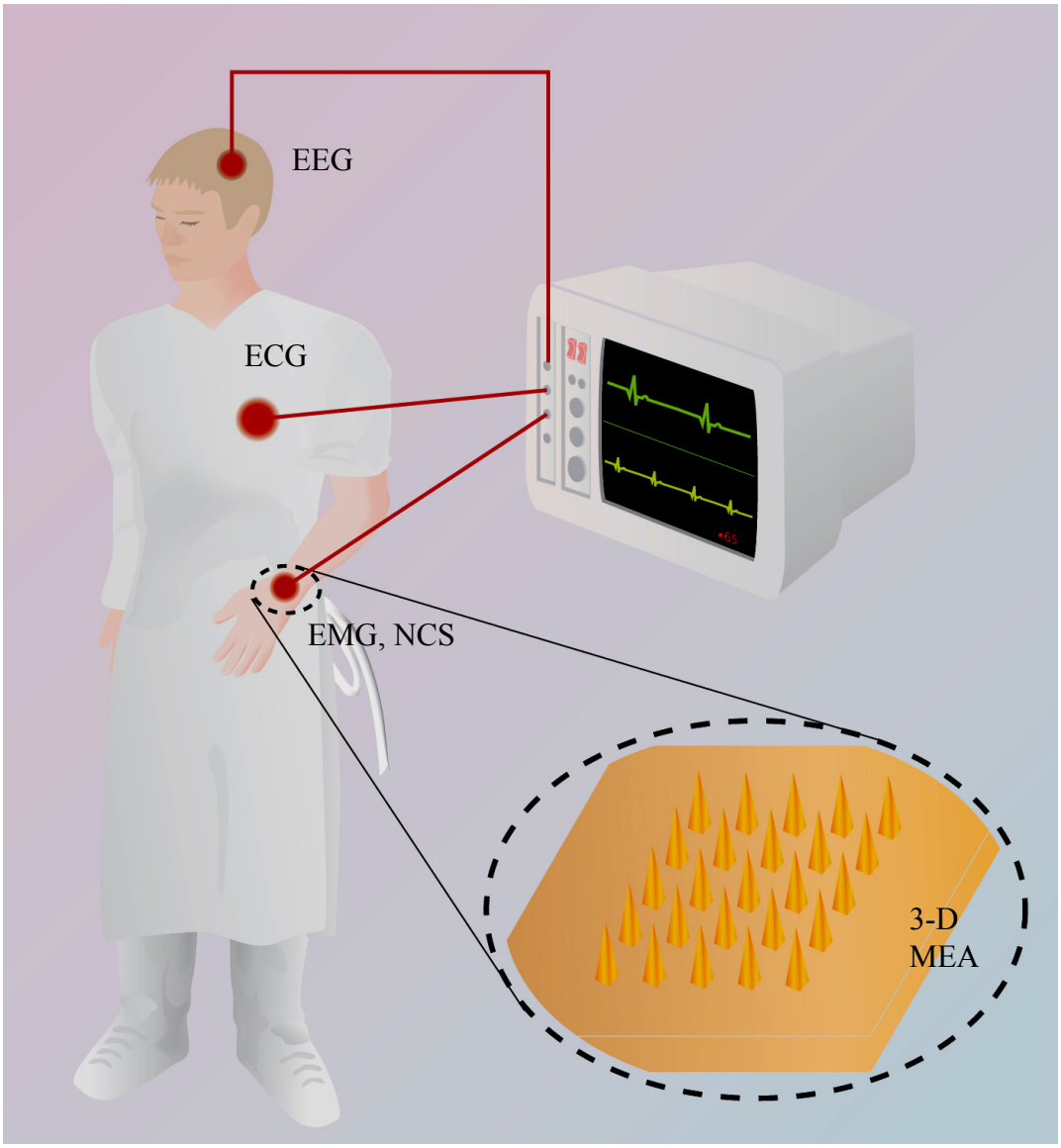

Figure 5.1: Opportunities for bioelectrodes in the human boday. Traditional measurements include ECG, EEG, EMG and NCS with applicability in various areas of study.

As the applications for non-invasive neural devices grow, it has become increasingly evident that bioelectrode technology is struggling to keep pace with the innovative

clinicians and scientists that use it. The non-invasive nature of bioelectrodes, which confers their main advantage, is also directly responsible for its most significant shortcoming—low spatial resolution and poor signal-to-noise ratios (SNR). This complication arises because these non-invasive electrodes sit atop high-impedance skin tissue that impedes the propagation of electrical signals. Specifically, the outermost layer of skin, the *stratum corneum* (SC), is composed of dead skin cells that act as a fluid barrier and possess electrical isolation characteristics [Griss 2001]. Therefore, in order to ensure minimal signal attenuation and noise inference, it is critical to lower the skin interface impedance [Miller 1974; Lin 2008]. This is especially true for stimulation and recording applications, in which high skin impedances not only diminish the amplitude of recording signals, but also imply the requirement of much higher, potentially painful, stimuli.

Today, the most common method for overcoming signal attenuation is to abrasively remove the outer skin layers, apply conducting electrolytic gels (to provide a conductive path through the high impedance area) or a combination of both of these techniques. However, neither of these methods is desirable. The removal of skin can be painful and time consuming to the patient. The use of conductive gels is not only uncomfortable and inconvenient but also is unsuitable for long-term recordings as the gel tends to evaporate [Lin 2008]. Additionally electrolytic gels have also been reported to cause inflammation, swelling and/or infection [Dwyer 1994; Uter 1996; Searle 2000].

Several alternatives for these so-called ***wet electrodes*** have been reported. An ***active electrode strategy*** has been reported by Nishimura et al. and Alizadeh-Taheri et al. [Nishimura 1992; Alizadeh-Taheri 1995]. In this approach a dry electrode (thin metal

strip defined on a silicon substrate) is bonded to a chip with electronics (amplifiers, multiplexers, data processing etc) to amplify and process the signal. Though the idea of having electronics to amplify and process signals in close proximity to bioelectrodes is novel, this approach still ignores the fact that the electrode technology is practically unchanged from standard wet electrodes. Also the integration process used to bond the electrode chip to the electronics chip is rather complex and not repeatable for multiple electrode sets. The importance of disposability of biopotential electrodes has to be emphasized here: the very nature of these measurements makes these electrodes disposable for hygiene reasons.

The other strategy is a class of ***dry spiked electrodes*** has been reported by Griss et al. [Griss 2001; Griss 2002], Lin et al. [Lin 2008] and Sullivan et al. [Sullivan 2008]. The dry spiked electrodes circumvent the skin impedance problem by using microfabricated 3-D silicon electrodes to painlessly pierce the SC, providing direct access to the highly conducting Stratum Granulosum (SG). The comparison between dry spiked and wet electrodes is depicted in Figure 5.2. This strategy poses the additional advantage of significantly reducing the electrode size without increasing the electrode impedance. A reduced electrode area enables much greater specificity, including more targeted and effective stimuli and higher spatial resolution recordings. Despite the benefits reported in these dry spiked electrode strategies, they suffer from two significant drawbacks: (1) expensive, multilayer clean-room processing, and (2) material limitations.

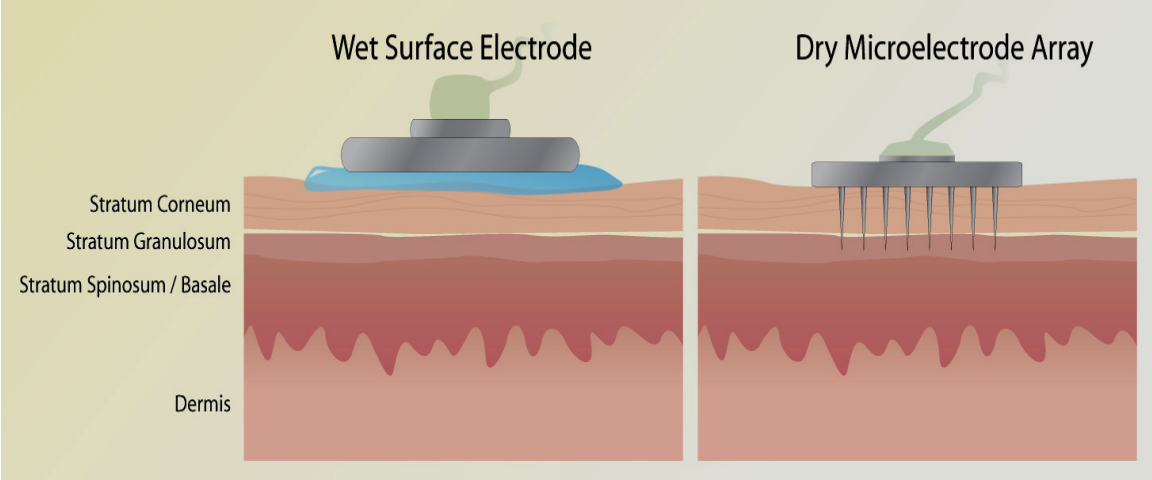

Figure 5.2: Comparison between ***wet surface*** and ***dry spiked*** electrode strategies for biopotential measurement.

The processes reported by Griss et al. [Griss 2001], Lin et al. [Lin 2008] and Sullivan et al. [Sullivan 2008] are very similar. They involve multi-step silicon dry and wet etching to microfabricate the needles (or spikes) followed by single or multiple metal deposition steps to define the electrodes. All these processes are compatible only with silicon micromachining and cannot be adapted to bio-friendly materials such as biocompatible polymers. The expense and material limitations imposed by this technology greatly diminishes its prospects for commercial viability, making it unlikely for researchers and clinicians to ultimately reap its benefits. Therefore, a technology that combines 3-D functionality, scalability and cost-effective mass manufacturing is required to provide pain free, high-fidelity electrodes that overcome the skin impedance problem.

The metal transfer micromolding technology developed in Chapter 4 is an excellent candidate for this rather diverse set of applications in the *in-vivo* arena. Spiked microneedle-type electrodes are the end product of this process and since it is a

micromolding based approach it lends itself to scaling, cost-effective manufacturing and biocompatible materials.

5.1.2 Concept and Design

The design chosen for the 3-D MEA is shown schematically in Figure 5.3. The MEA is a 5x5 array of metallized towers in the center of the chip. The electrodes are accessed from the backside of the array. Thus, it is proposed to have continuous metallization from the front to backside of the chip. The overall chip dimensions are 5mm x 5mm with the base of the towers being 250µm. Micro-towers with various pitch values have been fabricated.

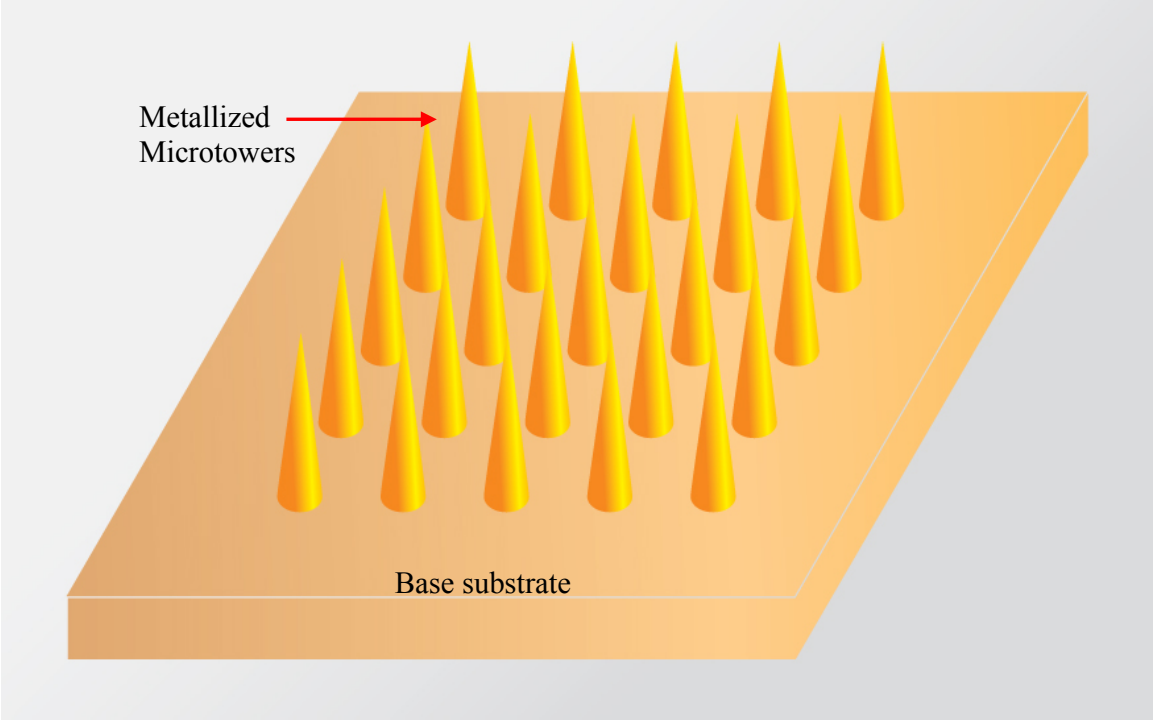

Figure 5.3: Design of the proposed 5x5 3-D MEA for biopotential measurement. Clearly visible are the base substrate and an array of metallized micro-towers fabricated out of the same biocompatible polymer.

The height of the micro-towers has been fixed at 200μm and the reason for that is explained in section 5.1.3. The sharpness of the tip is ideally below 1μm which is rather difficult to accomplish utilizing a micromolding-based approach. However it has been reported in the literature [Choi, 2007] that microneedle arrays fabricated with a sharpness of approximately 15-20μm have successfully penetrated the *stratum corneum* layer. So the target sharpness of these arrays has been fixed at less than 15μm. The fabrication and characterization of these arrays is explained in the next sections.

5.1.3 Skin Impedance Problem

Biopotentials result from the electrical activity of a certain class of cells within the human body called excitable, electrogenic or electrically active cells (which have been discussed in detail in Chapter 2). Detection of biopotentials is closely related to the detection of ionic activity within these cells. This ionic activity is dependent not only on the concentrations of different ions inside and outside the cell but also the characteristics of the semipermeable membrane that encloses a cell. The amplitude of this potential reduces with increasing distance from electrogenic cells. The ionic activity of the cells has to be converted to electronic activity or current for detection by electronic circuitry outside the body and hence a biopotential electrode acts as a transducer that converts ionic current into electronic current [Griss 2001]. Skin anatomy plays a crucial role in electrode function and design. Figure 5.4 depicts a schematic of the cross-section of the skin surface.

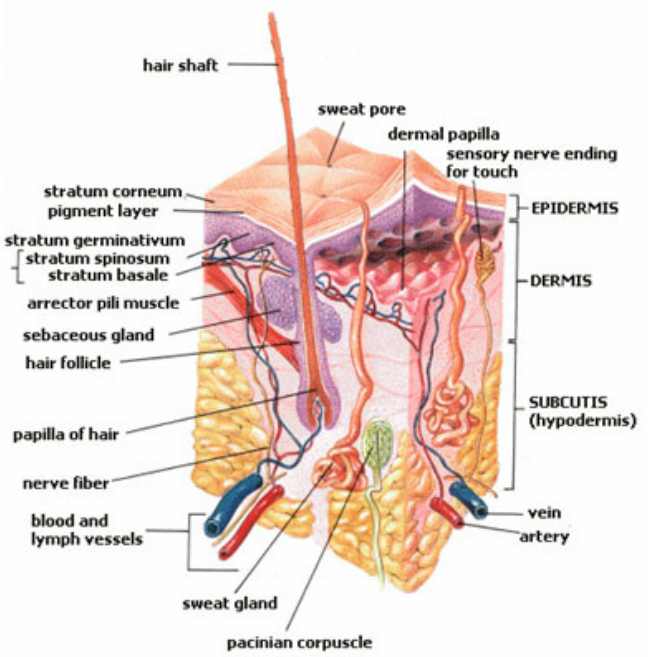

Figure 5.4: A schematic of the cross-section of skin depicting the various layers within skin [Adapted from www.wikipedia.com].

The skin consists of two main layers: the epidermis and the dermis. The epidermis is the outer layer of the skin. It acts as a physical barrier which is responsible for the prevention of desiccation and mechanical agitation. This layer was experimentally measured by Whitton et al. to be approximately 50-400µm thick in various parts of the body [Whitton 1973]. Below the epidermis is the dermis layer that harbors many nerve endings which provide the sensations of touch and heat. The dermis contains hair follicles, sweat glands, blood vessels etc. The dermis acts to supply blood to the epidermis, and mediates thermoregulation and immune surveillance.

The epidermis is composed of *stratum corneum* (SC), *stratum granulosum* (SG) also called *stratum spinosum* and *stratum basale*. The latter two layers combined are referred

to as *stratum germinativum* [Spence 1990]. The SC is the outer-most layer of the skin. It is composed primarily of dead cells and hence acts as both a barrier to fluids and a high impedance resistor to electrical activity. The thickness of the SC layer is 10-50µm. The *stratum germinativum* layer and is composed primarily of living cells that divide and grow. The thickness of this layer is approximately 50-100µm and it can act as an electrolyte for a microelectrode interaction [Spence 1990]. Thus, the height of the biopotential electrodes should be approximately 115µm for it to make contact with the SG layer. As long as the MEAs do not interact with the dermis layer pain-free, minimally invasive electrode-electrolyte interaction can potentially be achieved.

Figure 5.5 depicts the lumped circuit equivalents for this electrode-electrolyte interaction.

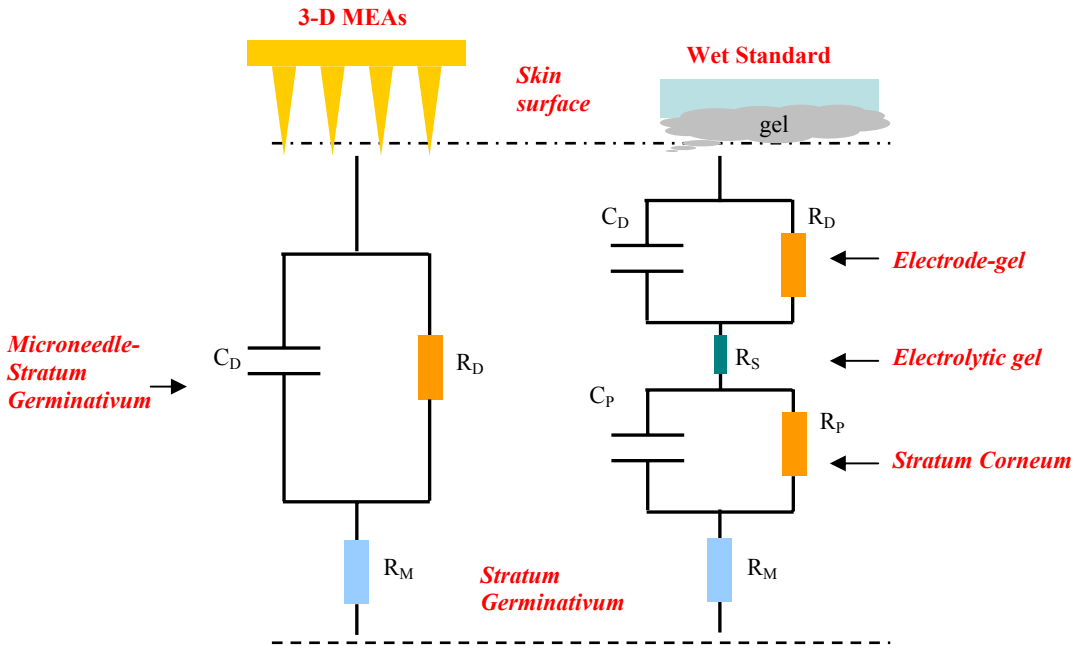

Figure 5.5: Lumped circuit equivalent of electrode-skin interface in the case of 3-D MEA (left) and standard surface electrodes with electrolytic gel (right) [Adapted from Griss 2001].

On the left hand side the circuit representation for direct contact to the SG layer utilizing 3-D MEAs. On the right hand side, the circuit model for conventional electrode interfacing with skin is represented. The circuit representation for the 3-D MEAs is a remarkably simple for such a complex interaction and is composed of a capacitor (C_D) in parallel with a resistor (R_D) that represents the electrode-electrolyte interaction (3-D MEA with SG layer) and a resistor (R_M), the resistance of the SG and underlying tissue which is in series with the parallel pair [Griss 2001]. This type of electrode-electrolyte interaction has been extensively modeled for *in-vitro* applications [Franks 2005; Borkholder 1998] and has been studied as part of this dissertation for *in-vitro* 3-D MEAs in Chapter 4. The lumped circuit for standard 2-D electrodes with electrolytic gel is far more complicated with several elements for the various levels of electrode-electrolyte interface with components for gel, SC and SG layers. First there is the electrochemical electrode-electrolyte interface of the wet electrode and the gel (represented by the components C_D and R_D). The resistance R_S represents the impedance of the electrolytic gel. Secondly the electrolytic gel soaked SC demonstrates distinctive capacitive (C_P) and resistive (R_P) behavior. Finally R_M is the resistance of the SG and underlying tissue. Since R_P is typically very large, high impedance of wet standard electrodes is expected unless the surface area of the standard electrode is made very large [Lin 2008]. Higher impedances lead to poorer signal qualities and spatial resolutions. This is the primary problem that is alleviated by the 3-D MEAs developed in this Chapter.

5.1.4 Microfabrication: Master Structure Fabrication

We have utilized two different fabrication techniques for master structure fabrication. Both these techniques are similar to the fabrication methods that have been developed in Chapters 3 and 4, where they have been discussed in detail. Only a brief overview is provided here.

The first method is similar to the one described in Section 4.1.3. It utilizes inclined rotational UV exposure of thick SU-8 to create an array of trenches that can then be micromolded to create a master structure using PDMS.

The second method is identical to the double-side exposure of SU-8 developed in Chapter 3 to fabricate micro-tower arrays (solid and hollow micro-tower structures) and in Chapter 4 to create "capping" structures for parylene deposition. There are several critical differences:

1. The backside exposure in this case was controlled to achieve "taper" shaped micro-towers as depicted in Figure 5.6. This was accomplished by lowering the backside exposure energy from 5000mJ to 3000mJ.

2. The device substrate SU-8 layer was defined to be 200μm thick instead of 100μm. This was accomplished by changing the parameters for spin coating of SU-8 and also with increased bake and topside exposure energies. Both these changes to the process were incorporated to fabricate micro-towers that can be sharpened using the RIE to achieve a tip sharpness that can be controlled to suit the EMG application.

Both these master structures need to be sharpened using the RIE for use in the EMG application. Sharpening processes were developed for both the polymers: SU-8 and PDMS. Since PDMS is a silicon-based polymer, the required etch chemistry is different

from other polymers which are carbon and hydrogen based. These polymers (including SU-8) can be etched with oxygen plasma but the siloxane bonds (silicon-oxygen-silicon) that make up the backbone of polymer chains in PDMS are not easily broken by oxygen plasma. Alternative etching schemes need to be developed for PDMS. Garra et al. [Garra 2002] report both wet and dry etching techniques for PDMS. They report some success in wet etching of PDMS in a 3:1 solution of tetrabutylammonium fluoride and n-methyl-2-pyrrolidinone and dry etching with a 3:1 mixture of CF_4 and O_2 in an RIE system. CF_4 is reported to etch PDMS in the same way it etches silicon dioxide by the formation of volatile SiF_x by-products.

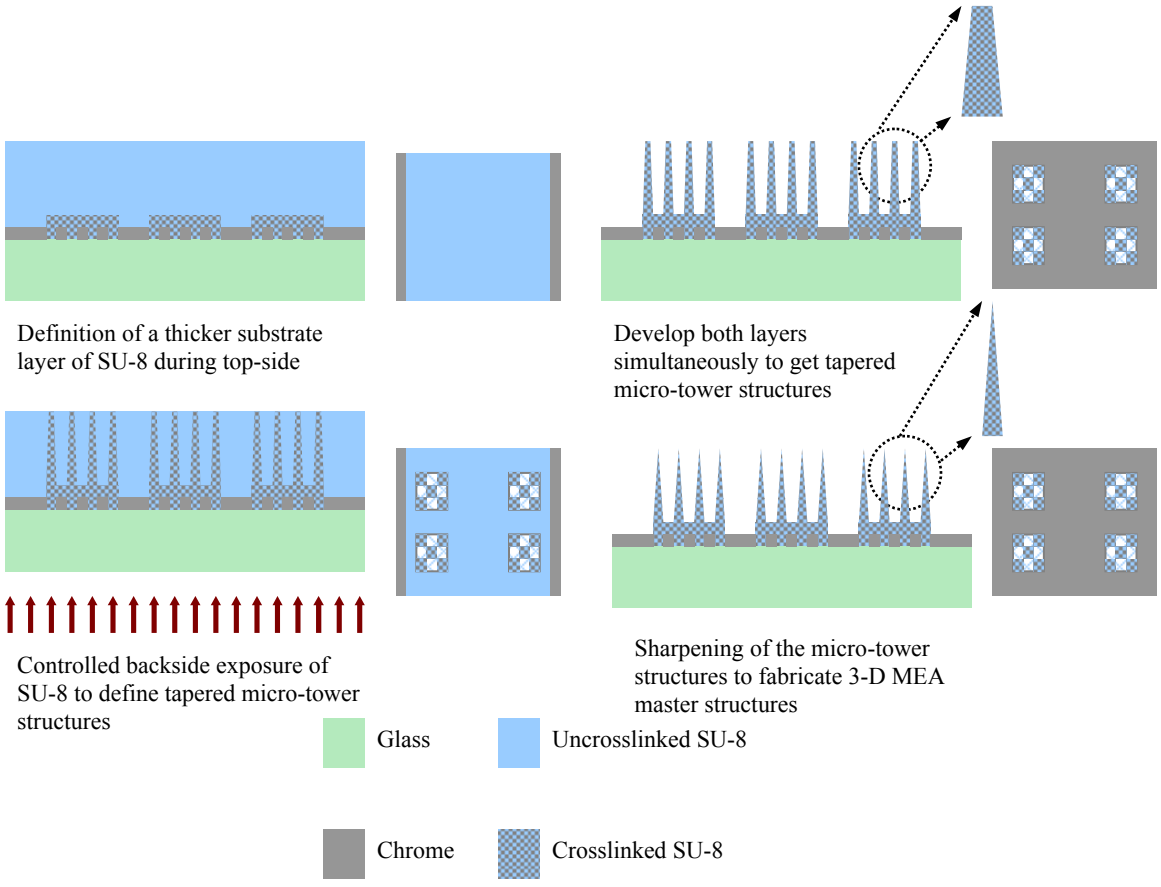

Figure 5.6: Abbreviated process flow for microfabrication of tapered shaped micro-tower structures with an SU-8 substrate obtained by double-side exposure of SU-8. The sharpening of the micro-tower structures is also depicted. Side view of the main steps is illustrated on the left with top views on the right hand side of each step.

The PDMS master structure was etched using two different chemistries: CHF_3/ O_2 and SF_6/O_2. The gas ratios and pressures were varied to achieve sharpening of the tips while minimizing etching of the substrate on which the towers are constructed. Table 5.1 summarizes the various etch conditions with results. Figures 5.7 to 5.9 depict SEM images of the tips etched using various recipes listed in Table 5.1.

Table 5.1: Design of experiments for PDMS sharpening using RIE and Results

Pressure (mTorr)	**Power (Watts)**	**Time (mins)**	**Gas Pressure (O_2)**	**Gas Pressure (CHF_3)**	**Gas Pressure (SF_6)**	**Comments**
200	200	10	15 sccm	45 sccm	0	Practically no effect
200	200	10	15 sccm	75 sccm	0	Some sharpening
200	200	10	7.5 sccm	75 sccm	0	Best sharpening
200	200	10	0	0	50	Flattening the PDMS tip

Even though some success in sharpening the tips of the master structures is achieved using the 10:1 ratio of CHF_3 and O_2, surface roughness, poor repeatability and variation across the die are potential problems for this technique.

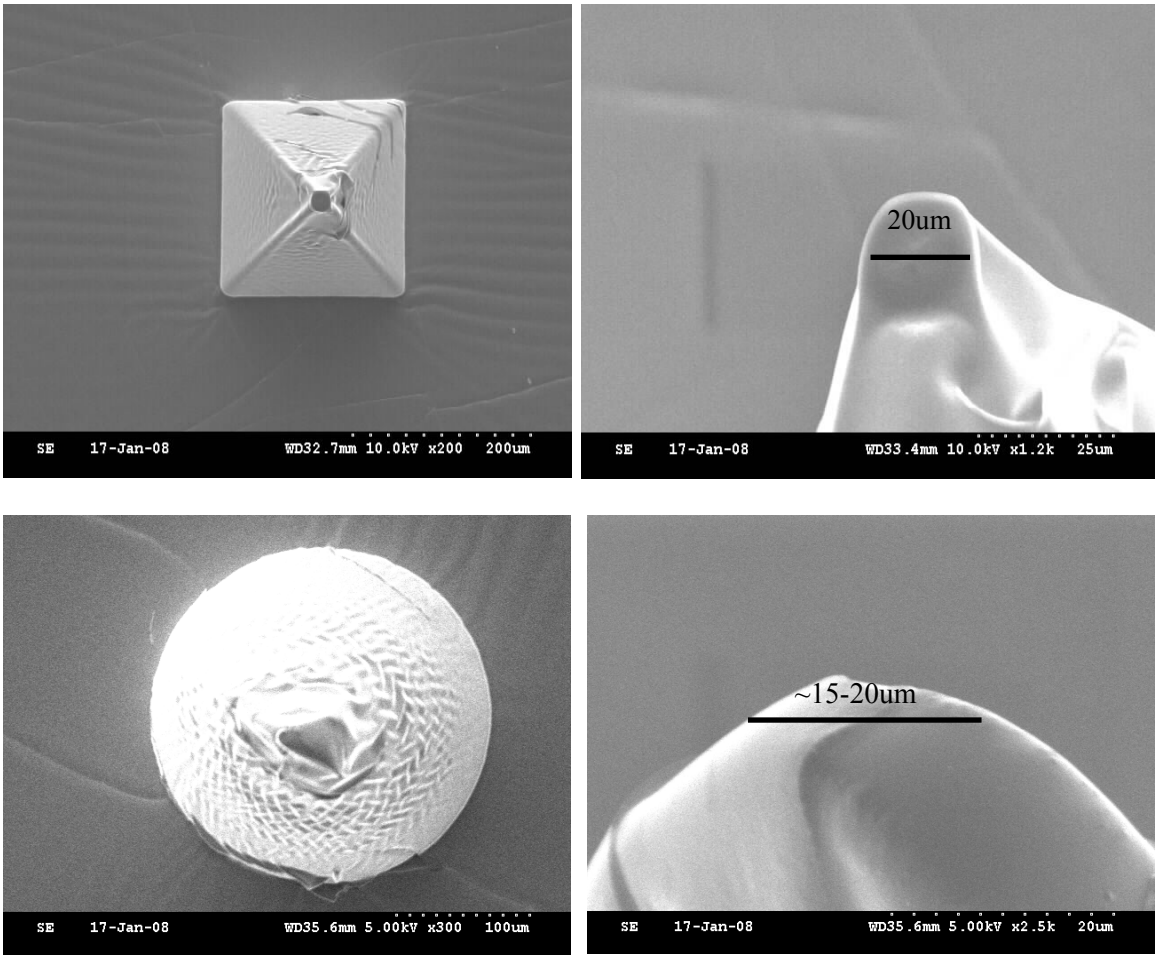

Figure 5.7: SEM images of the top view and side view (top) of a PDMS master sample etched in 1:3 ratio of O_2 and CHF_3 showing practically no etching from the beginning point of 20-22μm sharpness. Etching with 1:5 ratio of O_2 and CHF_3 (bottom) depicting some amount of etching from the beginning point of 20-22μm.

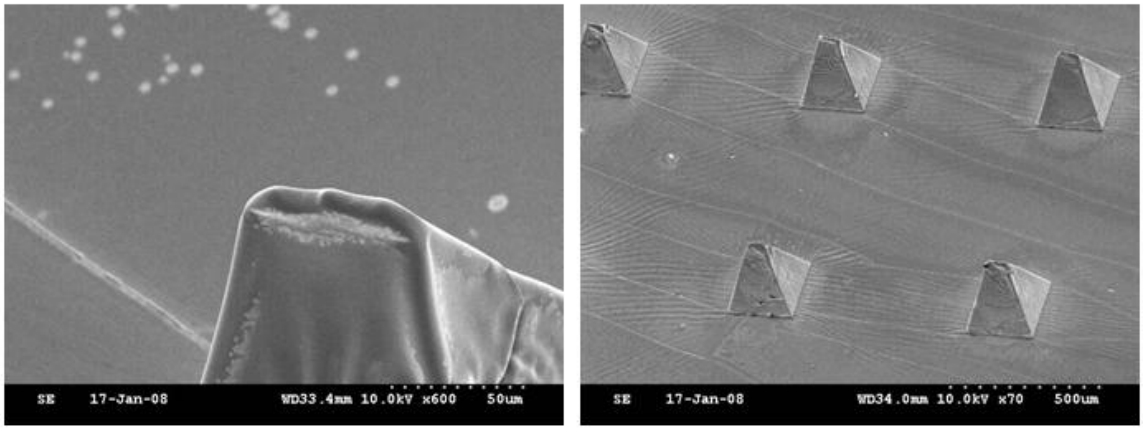

Figure 5.8: PDMS master structure etching with SF_6 for 10mins showing flattening of the tip, which is not useful for the 3-D MEA application.

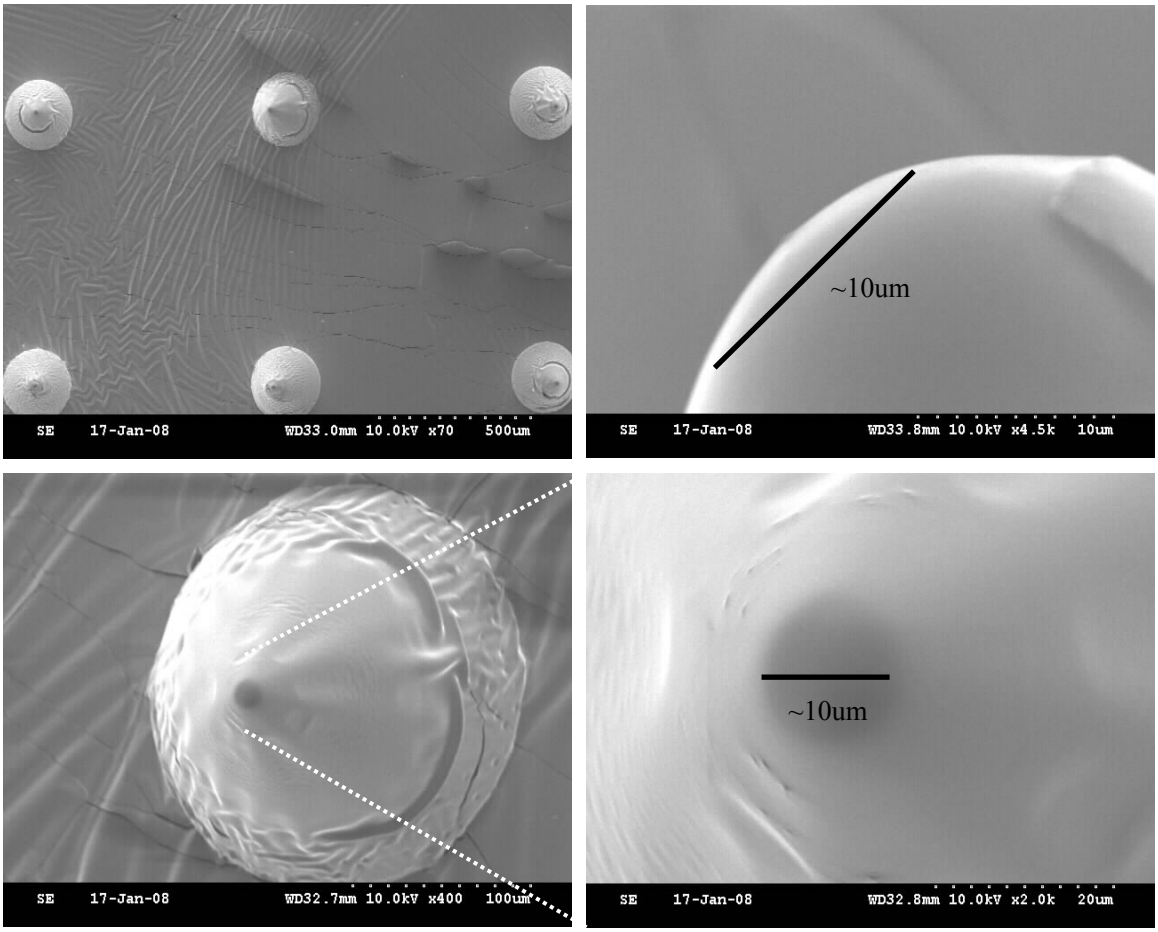

Figure 5.9: PDMS master structure etching with 1:10 ratio of O_2 and CHF_3 for 10mins showing much better etching results to a tip sharpness of 10µm from the beginning point of 20-22µm sharpness obtained from the MTM process.

RIE etching of the SU-8 master structure can be a potential solution for sharpening. The chemical structure of SU-8 is given in Figure 5.10.

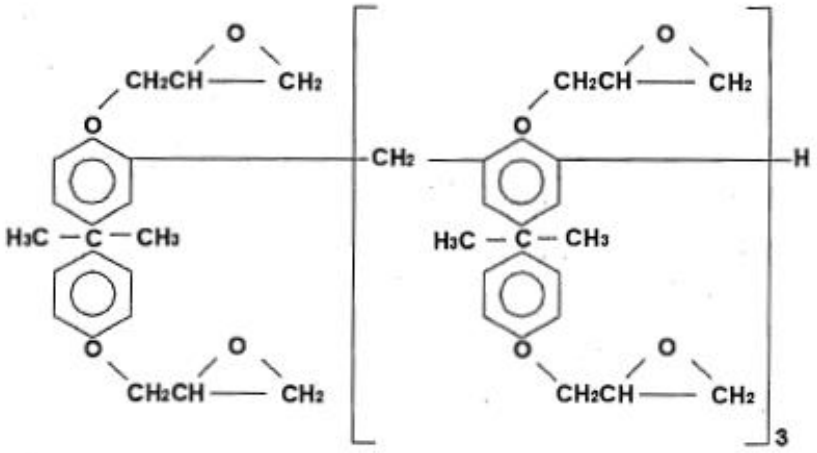

Figure 5.10: Chemical structure of SU-8 which is an epoxy derivative of Bis-phenol A Novalak. SU-8 is a better candidate for etching using oxygen plasma being predominenetly made up of hydrogen and carbon unlike PDMS.

Oxygen-rich plasma should be able to break the bonds to etch SU-8. We have utilized an O_2/CHF_3 plasma to etch the SU-8 master structure. An isotropic etch on the tapered surfaces at the tips of the microneedles leads to sharpening of the structure. The process parameters for this etch process are summarized in Table 5.2.

Table 5.2: Etching Parameters for RIE etching of SU-8

Parameter	Value
O_2 Flow Rate	100 sccm
CHF_3 Flow Rate	10 sccm
Pressure	1000 mTorr
Power	100 W
Time	varies
Etch Rate	measured optically

The 4” substrate with arrays of tower structures was introduced into a Plasma Therm RIE and etched using this recipe. In order to achieve a measure of the tip sharpness, the sample was divided into four quadrants and the amount of SU-8 removed was measured in separate micro-tower arrays optically every 30 minutes of etching. This not only measures the variation of the material removed across the 4” substrate but also is helpful in observing the change in geometry of the tip. The amount of SU-8 removed is shown graphically for the top diameter in Figure 5.11 (a). This monitors the change in tip sharpness. The amount of SU-8 removed is depicted graphically for the bottom diameter in Figure 5.11 (b). The SU-8 removed at the base of the micro-tower arrays is shown in Figure 5.11 (c).

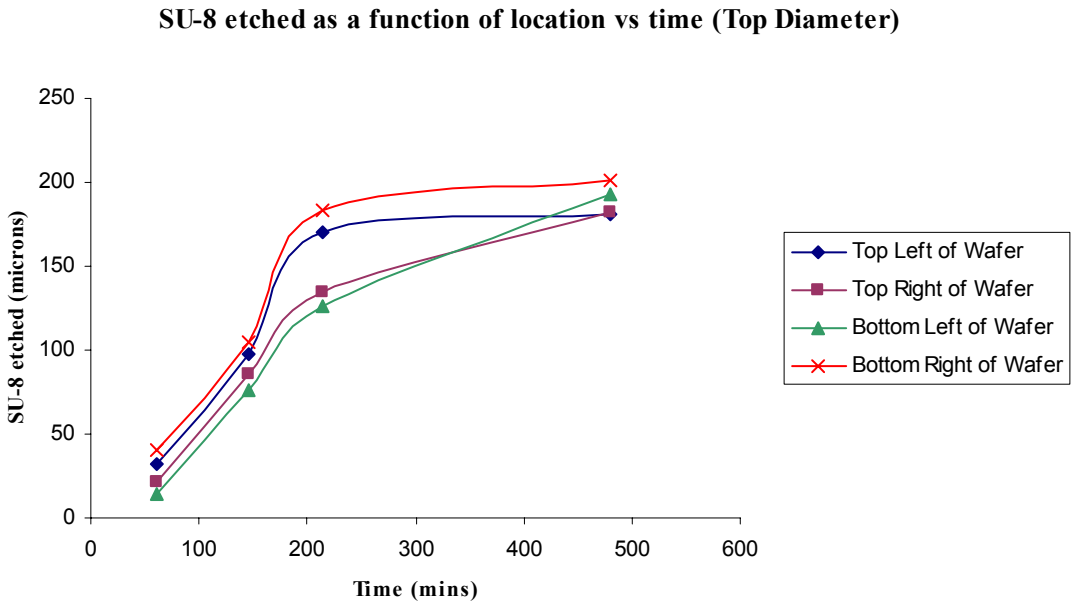

(a)

Figure 5.11: Measurement of amount to SU-8 etched to monitor tip sharpness (a), anisotropicity (b) and height of the substrate (c).

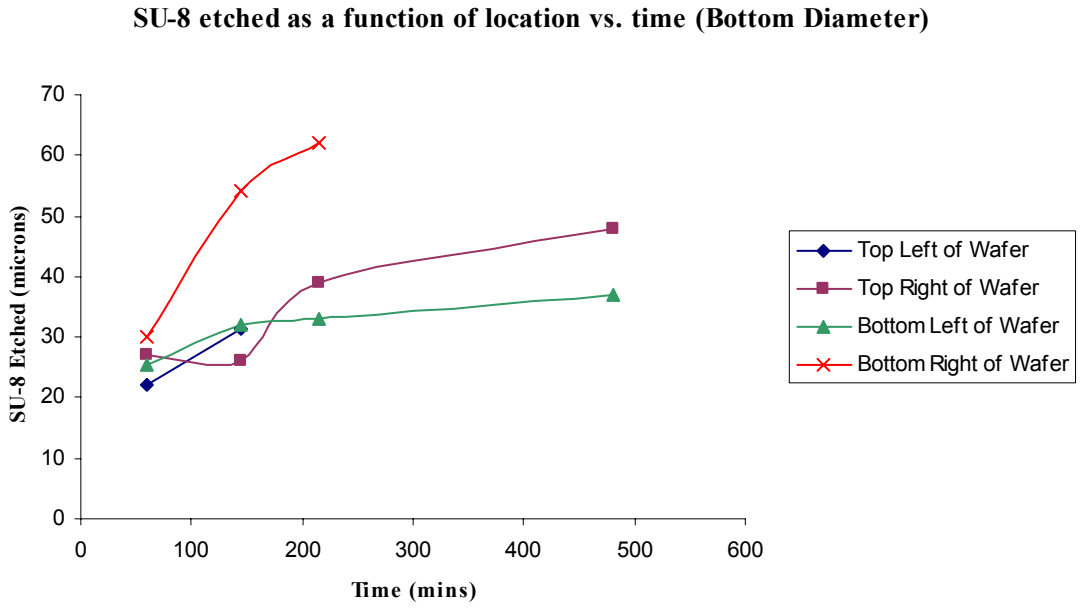

(b)

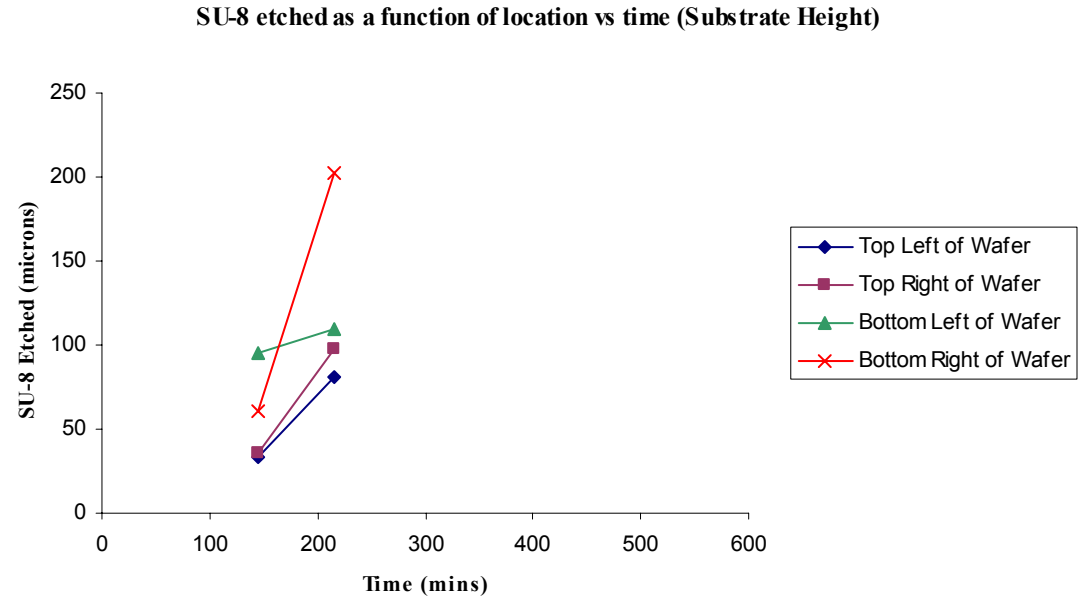

(c)

Figure 5.11: Continued.

This serves as a measure of substrate height (to monitor top-down etch rate). The isotropic nature of the etch in combination with the tapered structure leads to more than twice the etch rate observed at the tips as compared to the substrate SU-8 leading to sharp tips. The variation of the amount of SU-8 etched as a function of micro-tower location is perplexing. The lack of control of materials used in the RIE tool is a likely reason for this variation. With the exception of one data point that shows almost all of the 200μm of the substrate etched, minimum amount of substrate material is etched using this process. Figure 5.12(a)-(d) depict optical micrographs of 3x3, 5x5 and 9x9 arrays of master structures fabricated using this process.

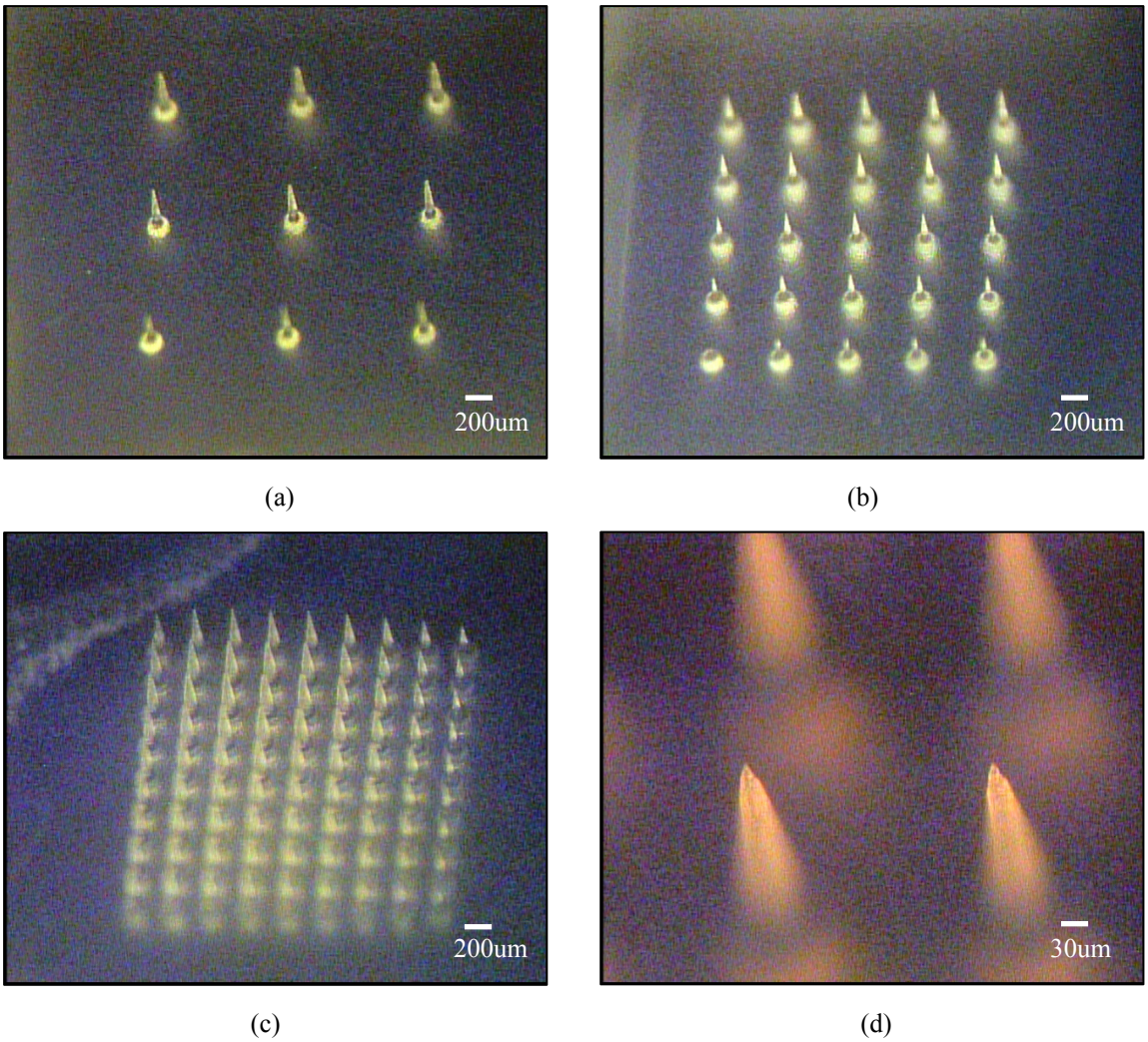

Figure 5.12: Optical micrographs of various sharpened SU-8 master structures – (a) 3x3 array of micro-towers; (b) 5x5 array of micro-towers; (c) 9x9 array of micro-towers; (d) Close-up view of the 5x5 array depicting the <10μm sharpness of the tips.

5.1.5 Microfabrication: Metal Transfer Micromolding

The fabrication of the final 3-D MEAs from the master structure involves two molding steps:

1. The first micromolding step to construct a flexible mold that has the negative structure of the 3-D MEA.

2. The second molding step to fabricate the MEAs from this flexible mold.

It should be noted here that once the master structure has been fabricated using either of the two techniques that are described in section 5.1.4, it can be used multiple times to fabricate 3-D MEAs using these two simple steps. This two step molding process is depicted in Figure 5.13 and is very similar to the MTM process developed in Chapter 4. It begins with coating of a release layer, Cr/Au (10nm/150nm) on the SU-8 or PDMS master (Step 1). PDMS is mixed and poured on to this structure (Step 2). Once the PDMS is cured (24 hours at 50˚C) the flexible mold is carefully demolded from the rigid master (Step 3). A functional metal layer is embedded in the final 3-D MEAs by coating a layer of Au/Cr (300nm/15nm) using a sputter coater (Step 4) on the flexible mold and transferring it to the final structure (made out of PMMA) during the molding process (Step 5). This is accomplished due to the surface energy differences between PDMS and PMMA as explained in chapter 4. A process of solvent casting is used in this final molding process. The 3-D MEAs with functional metal layers are demolded from the PDMS mold (Step 6). Figure 5.14 depicts SEM images of the 3-D MEAs for biopotential measurement. Figure 5.15 depicts optical micrographs of the 3-D MEAs.

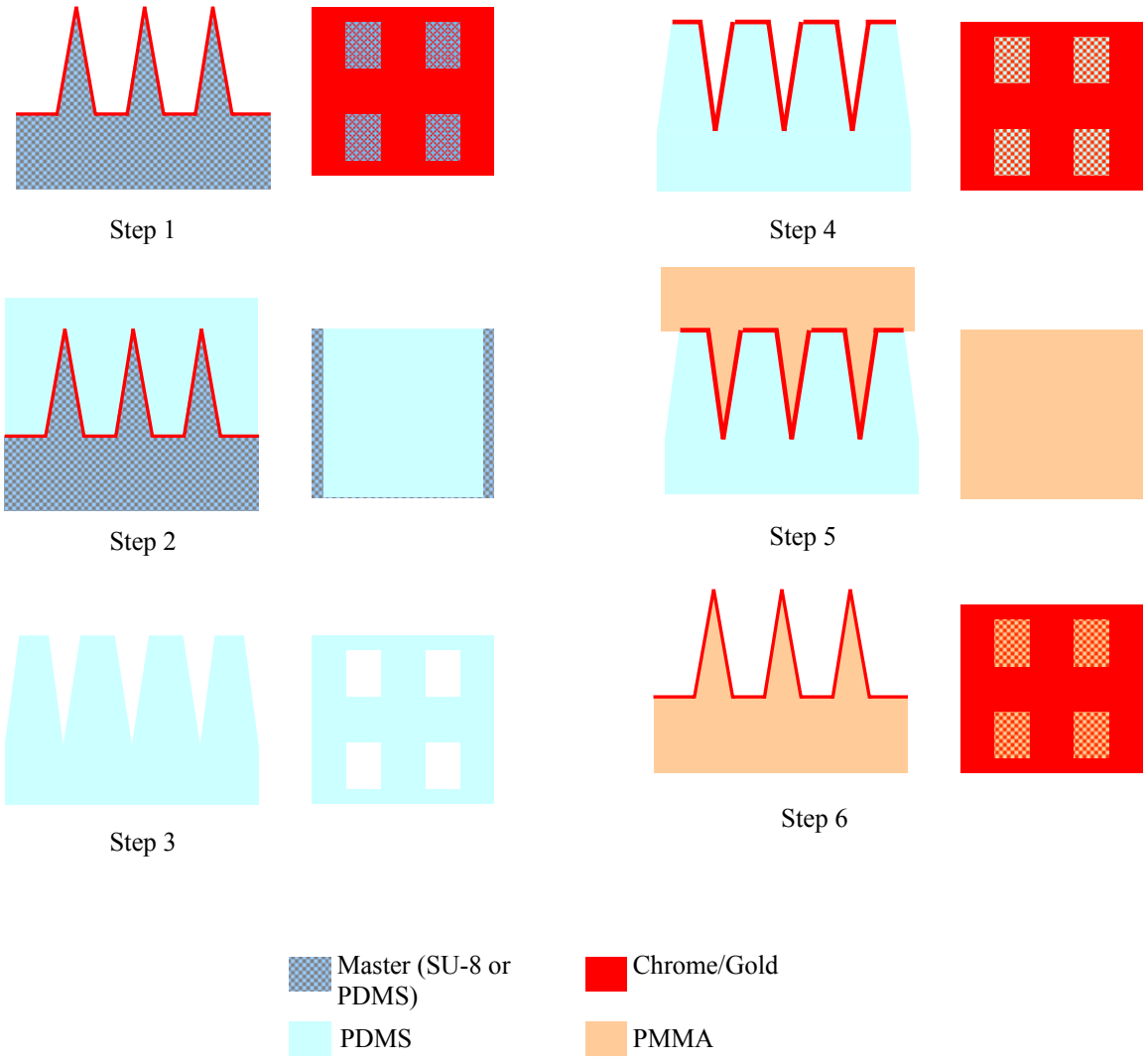

Figure 5.13: Fabrication process flow for construction of 3-D MEAs from master structures (SU-8 or PDMS).

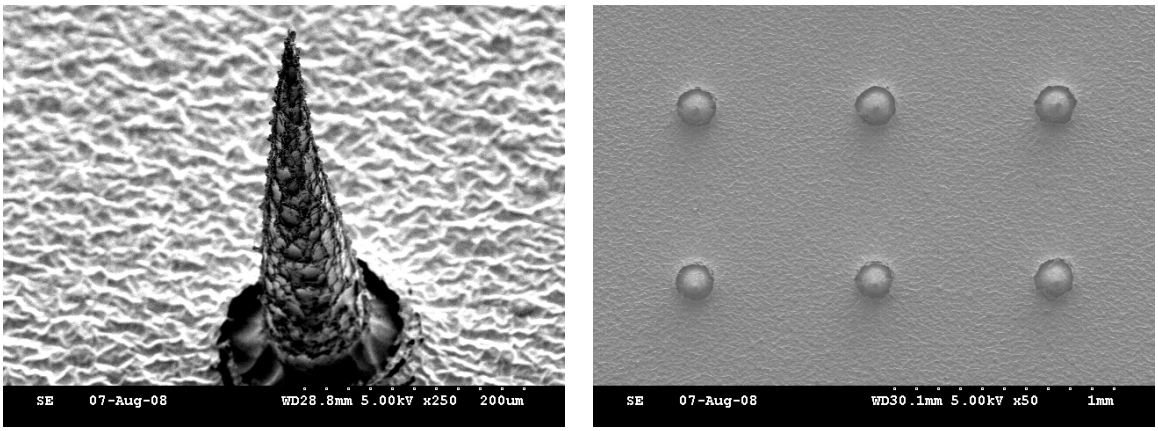

Figure 5.14 SEM images of the final 3-D MEA – side view of a single needle (left); top view of an array (right).

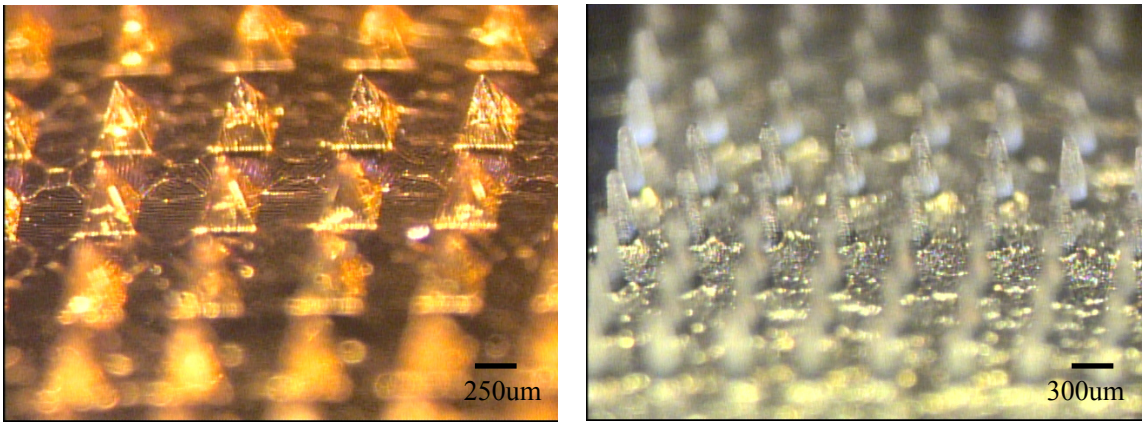

Figure 5.15: Optical images of the final 3-D MEA fabricated out of PMMA – side view of a pyramidal MEA (left) and conical MEA (right).

The device in Figure 5.15 (left) is made from a master structure fabricated using the inclined UV lithography technique (discussed briefly in Section 5.1.4 and in detail in Chapter 4). The devices depicted in Figures 5.14 and 5.15 (right) and are fabricated from a master structure produced using RIE etching of a mold master that is fabricated utilizing doubleside exposure of thick SU-8 (discussed briefly in Section 5.1.4 and in detail in Chapter 3).

5.1.6 Packaging of 3-D MEAs for Biopotential Measurement

The requirements for the packaging process for the biopotential 3-D MEAs are simplicity and cost-effectiveness. The primary reason behind these requirements is the need for disposable usage. This is similar to hypodermic needles or microneedle patches which are discarded after a single use due to hygiene reasons. The MEAs are designed to be accessed from the backside for electronics interfacing. The frontside (microelectrode side) of the MEAs is designed for the *in-vivo* biopotential measurement. So front to back

electrical continuity is necessary. This was accomplished by protecting the frontside of the MEA and metalizing the backside. The MEA was placed with the microelectrode side down on a 10mm x 10mm x 1mm PDMS die. The backside of the 3-D MEAs was metalized protecting the frontside to achieve front to back electrical continuity as shown in Figure 5.16.

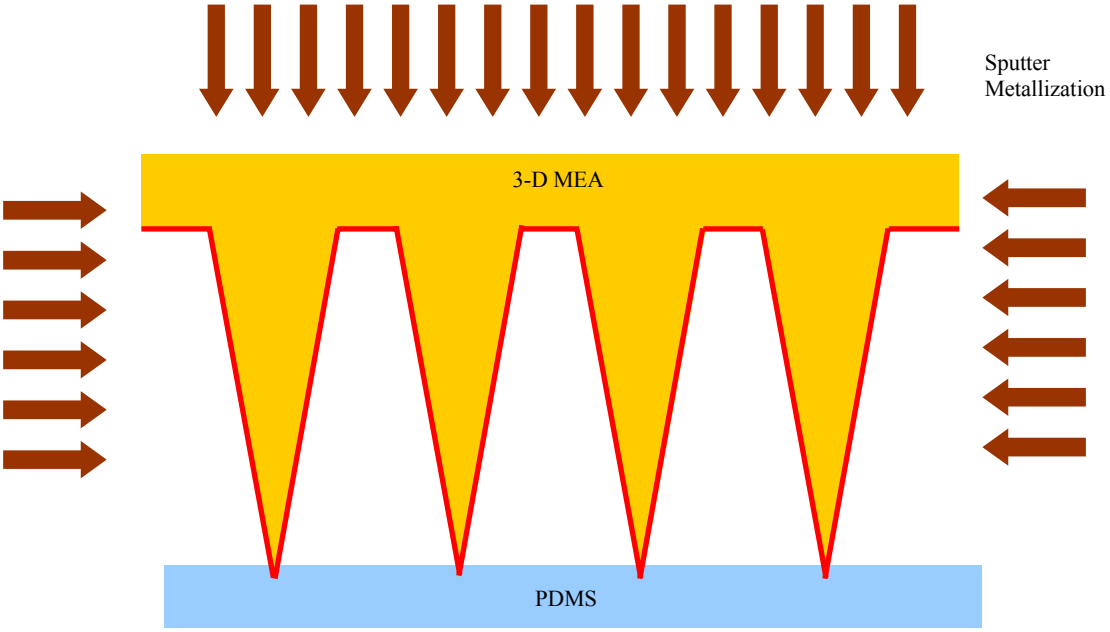

Figure 5.16: Establishment of front-back electrical continuity through sputter metallization.

This was performed on a sputter coater (Unifilm Sputterer) with a 15nm/200nm layer of chromium/gold. The deposition was performed with low deposition rates so as to minimize the thermal stress on the released 3-D MEA. The MEA was then packaged for various characterization experiments. For the packaging substrate, a thin Kapton sheet (125-150µm thick) was machined into 16mm diameter circular substrates with a 3mm central port using a CO_2 laser (LS-500 New Hermes-Gravograph, Duluth, GA). The 3-D

MEA was attached to this substrate utilizing a layer of two-part epoxy (3M Products, St. Paul, MN). For backside interconnection a wire was attached to the MEA using conductive epoxy (Master Bond, Hackensack, NJ) encapsulated with two-part epoxy to add mechanical strength to the conductive epoxy connection. The front-back electrical connectivity was confirmed using multimeter probes. Figures 5.17(a) and (b) depict optical images of the front and back sides of the packaged 3-D MEAs.

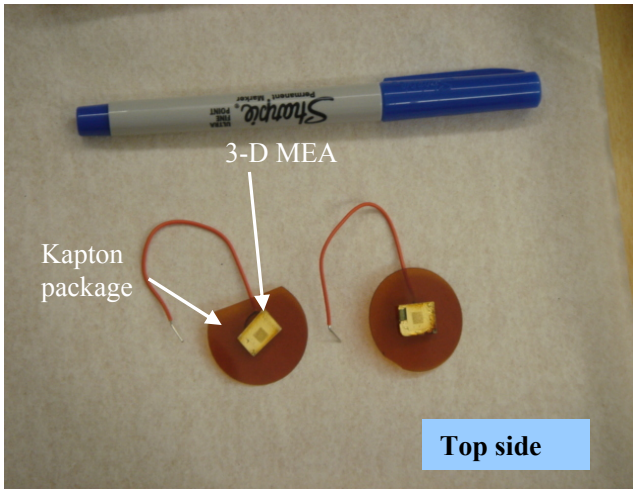

(a)

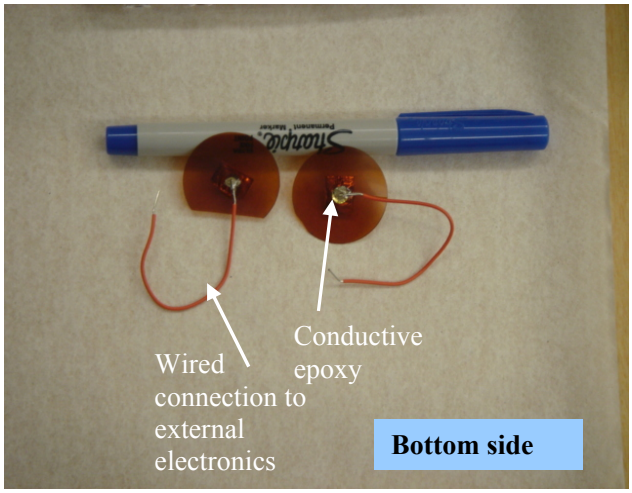

(b)

Figure 5.17: Fabricated, assembled and packaged 3-D MEAs – (a) optical image of the top side of the MEA; (b) optical image of the bottom side depicting the conductive epoxy and wire connection for external electronics.

These techniques ensure that the MEAs can be packaged rapidly and in a cost-effective fashion.

5.2 3-D MEAs for Biopotential Measurement: Characterization

The microfabricated and packaged MEAs should be characterized utilizing minimally-invasive *in-vivo* biopotential measurements. A nerve conduction demonstration was selected as the appropriate vehicle for *in-vivo* MEA testing, since for a given electrode area, improvements in nerve conduction measurements over those achievable using conventional electrodes that do not pierce the stratum corneum would demonstrate the reduced impedance principle of the 3-D MEAs. Nerve conduction work was performed in collaboration with the Department of Neurology, Emory University (Dr. J. Alex Bragg) with the approval of its Institutional Review Board (IRB).

In nerve conduction experiments, an electrical stimulation signal is applied to the proximal portion of a nerve and the response signal at the distal nerve/muscle junction is measured. If stimulation is provided by the brain, the resultant experiment is classified as electromyography (EMG); if stimulation is provided by a second electrode, the experiment is classified as traditional nerve conduction (NCS). Each of these is described below.

5.2.1 Electromyography (EMG) Measurements

Electromyography (EMG) is the study of muscle function through the measurement of the electrical signals that emanate from muscles. The signal itself is an electrical

manifestation of the neuromuscular activity associated with a contracting muscle [Basmajian 1985]. It is a complicated signal that depends on several factors including the properties of the muscle that is contracting, the control scheme of the peripheral nervous system and the instrumentation that is being used to measure it. Needle electrodes, wire electrodes and surface electrodes are the common tools to measure EMG. The former two tools are invasive and painful causing major discomfort to the patient compared to the latter. Two schemes are historically popular for surface EMG [DeLuca 2006]: monopolar and bipolar. The former uses one detection surface electrode on the skin and a reference electrode to record EMG data. The problem with this setup is the detection electrode records all the electrical signals in the vicinity of the detection surface. This includes EMG data from muscles that are not being investigated.

The bipolar scheme on the other hand uses two detecting surface electrodes and a reference electrode (which is placed further away from the detecting electrodes, so as to have no influence on the muscular signal of interest) as shown in Figure 5.18. These two electrodes detect two potentials in the muscle of interest (in our case forearm). These two signals are then fed to a differential amplifier which amplifies the difference of the two signals, thus eliminating any common mode components in the two signals. The differential amplifier used in this measurement is a Brownlee 440 amplifier setup (Tektronix Inc, Richardson, TX). The gain used is 2K with a bandwidth of 75-500Hz.

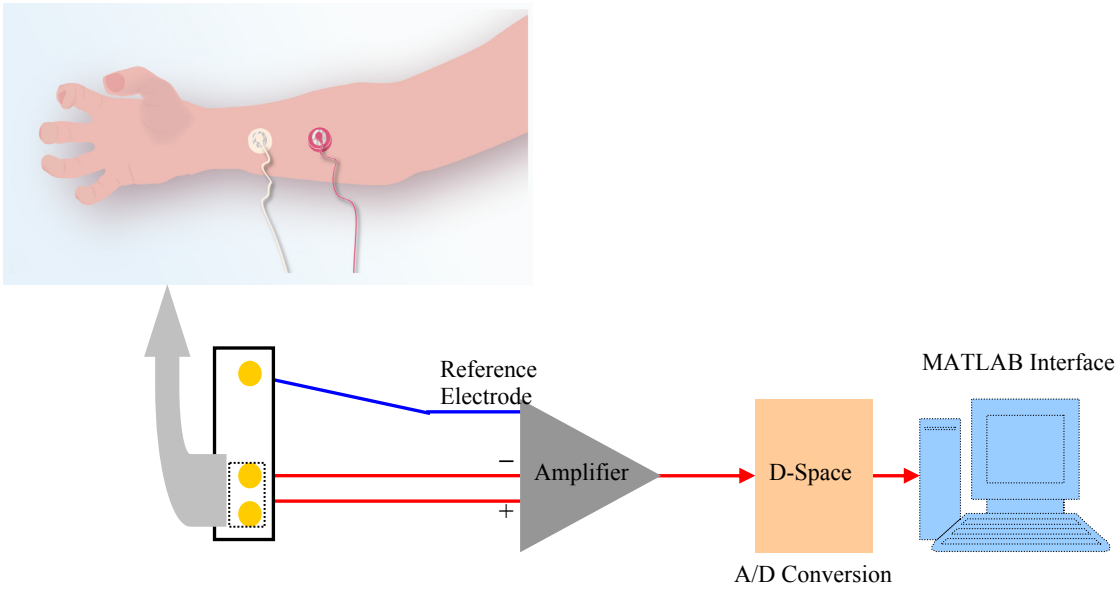

Figure 5.18: Bipolar EMG measurement setup used in the EMG experiments depicting the placement of electrodes on the test subject, with signal amplification, A/D conversion and MATLAB read-out.

The raw analog signal is then converted into a digital signal by a D-Space A/D converter (dSPACE Gmbh, Paderborn, Germany) and subsequently read out by an oscilloscope or a computer (for MATLAB interface). Figure 5.19 depicts raw EMG data collected from standard wet electrodes and from 3-D MEAs on a test human subject (muscles of the forearm) during one of the multiple experiments that were conducted. Figure 5.20 provides an analysis of the results with error bars depicting the variation in results during multiple experiments on both hands of the subject. This graph demonstrates a **100% improvement in signal power** for the 3-D MEA as compared to the conventional approach.

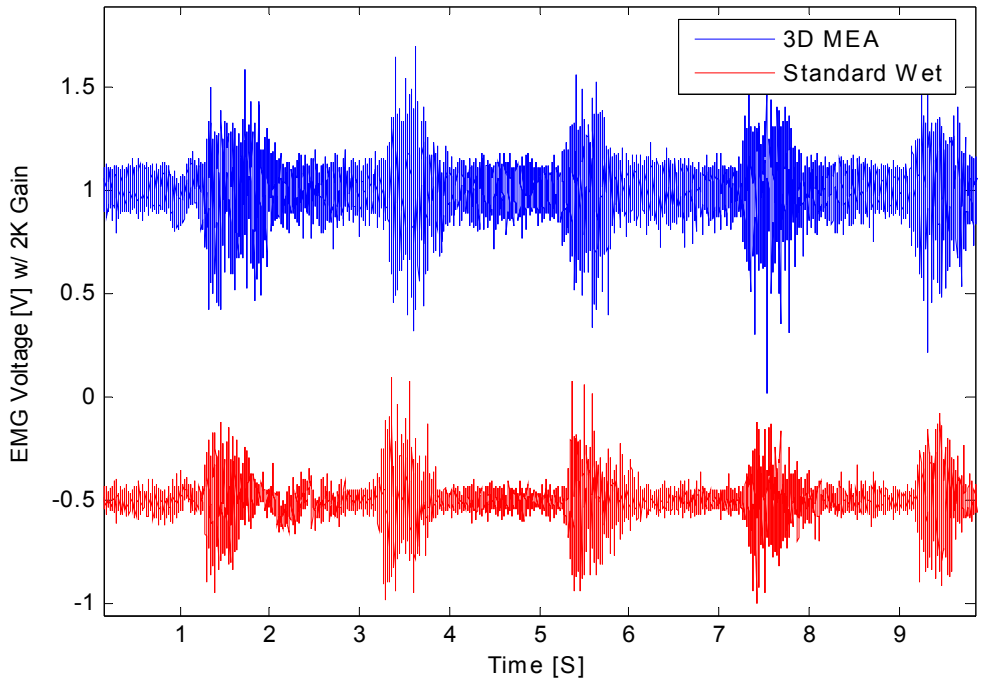

Figure 5.19: Raw EMG sample from a test human subject depicting the muscular activity of the forearm.

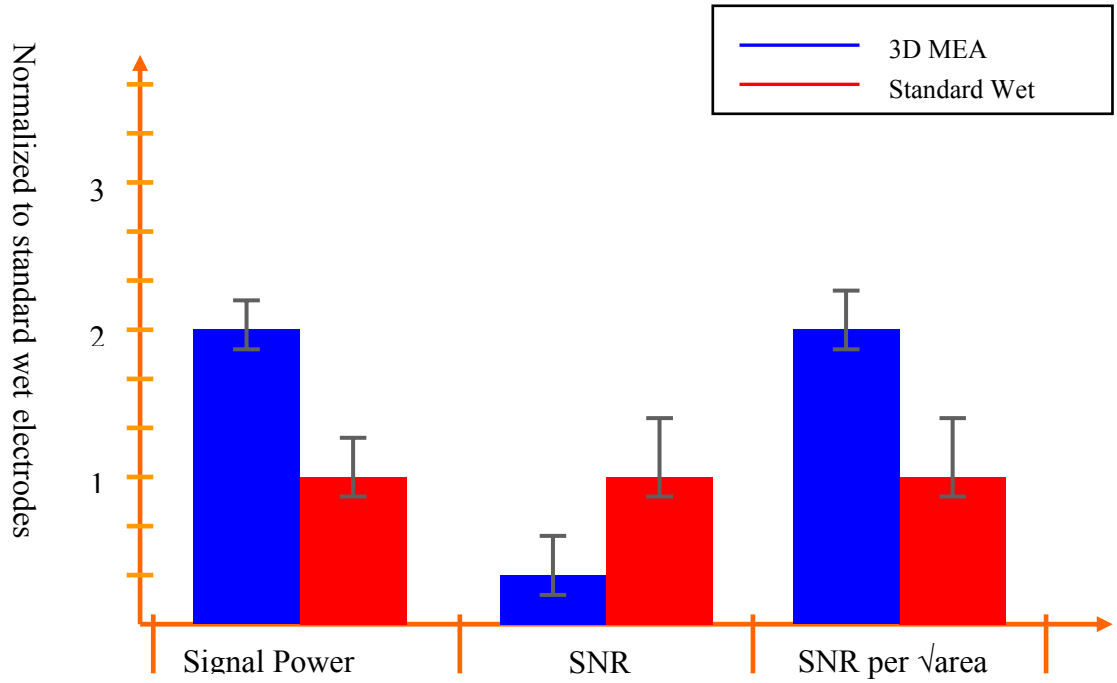

Figure 5.20: Analysis of the EMG result for multiple experiments on a test human subject for a comparison between 3-D MEAs and standard bioelectrodes.

The noise signal is higher for the 3-D MEAs. This can be explained by the size difference between the 3-D MEAs and traditional bioelectrodes. The ratio of the electrode area between the wet and dry electrodes is 12.56:1. The noise in EMG measurement is expected to scale with 1/√area of the electrodes [Huigen 2002]. Thus, the lower the area, the higher the noise floor and hence the expected increment in the noise level if the 3-D MEA is 3.54 times that of the conventional electrode. The average experimental noise increment is found to be around 4.4 times for the 3-D MEA which matches well with theoretical predictions. Thus, measurement of EMG using 3-D MEAs developed in this work demonstrates the reduced impedance advantages of these types of MEAs. The measurement of the EMG signal has several applications in a clinical diagnostic setting. Some of these are mentioned below:

1. Sensing fatigue in muscle during strengthening and conditioning [Cramer 2000].
2. Facial EMG measurements to study early indications of stroke and paralysis [Huang 2004].
3. Carpal tunnel syndrome has been studied in clinical setting by White et al. [White 1988] by harnessing EMG procedures.

5.2.2 Nerve Conduction Measurements

Bioelectrode technology demonstrates its greatest potential when it can be reliably used for *automated* diagnostic, prosthetic, and therapeutic applications. Unfortunately, person-to-person anatomic variability coupled with bioelectrode signal loss (i.e., the skin impedance problem) and signal distortion greatly hinders automation. As a result, many

biopotential applications require the manual attention of highly skilled operators. This is especially true in the context of traditional nerve conduction studies (NCS), which are used to diagnose disorders of peripheral nerve and muscle ranging from carpal tunnel syndrome [Tsaiweichao-Shozawa 2008], Guillain-Barre syndrome [Miller 1987], amyotrophic lateral sclerosis (ALS) or commonly known as Lou Gehrig's disease [Cornblath 1992] to locations of abnormal sensations of pain, numbness at any location in the body. Nerve conduction studies are usually performed along with electromyography for the diagnosis of the conditions listed above. These studies usually stimulate a particular nerve and measure the ability of that nerve to send a signal to a corresponding muscle. It is helpful in determining blockages in the nerve pathways.

Traditional nerve conduction studies are performed by placing a pair of electrodes on the skin overlying a nerve for recording and another electrode for stimulation. Current pulses are provided to the stimulating electrodes, leading to the depolarization of underlying nerves, which is recorded and analyzed.

Figure 5.21 depicts a typical placement of stimulation and recording electrodes in the right hand of a test human subject.

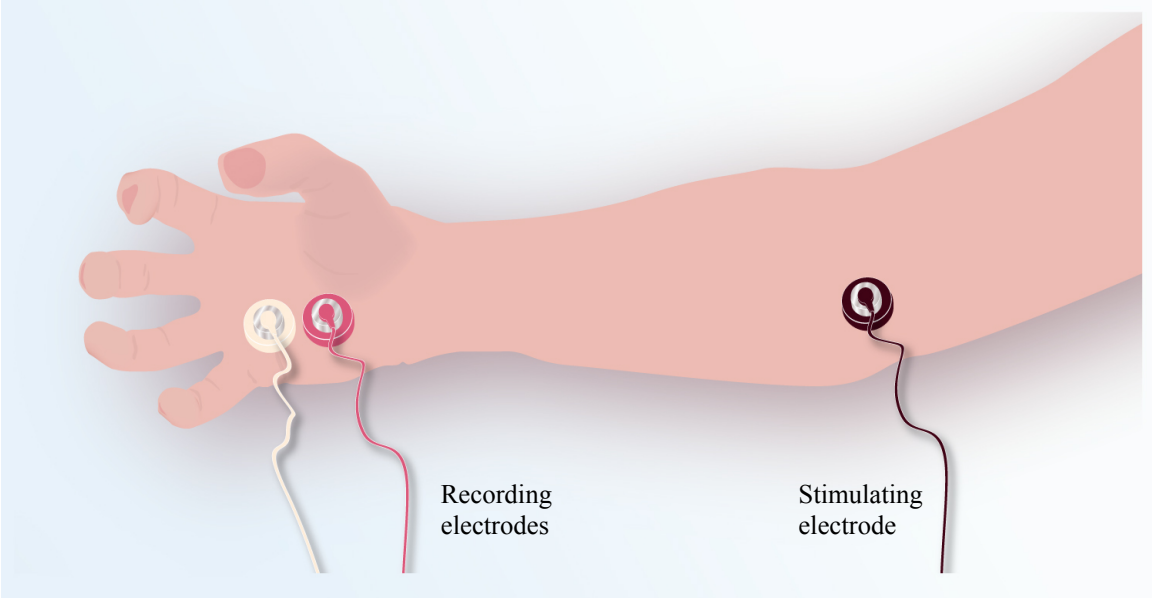

Figure 5.21: Schematic depicting the location of bioelectrodes for typical NCS measurements.

All stimulation and recording was performed using an FDA-approved Nicolet Viking IV EMG unit (Nicolet Biomedical, Madison, WI). Recording electrodes were placed over the abductor pollicis brevis muscle of the hand − with the active electrode over the belly of the muscle, a reference electrode over the proximal knuckle and a ground electrode over the dorsum of the hand. Voltage stimuli (duration 100msec) were applied over the median nerve at the wrist or further away on the forearm − the stimulus intensity was started at 50V and gradually increased until supramaximal response amplitude was obtained. In all the clinical trials, the supramaximal response amplitude was achieved at voltages less than the maximum stimulus voltage of 400V. Response amplitude was measured as the maximum negative deviation of the recorded waveform from baseline. Distal latency was measured as the delay between the delivery of the stimulus and the initial deviation of the response from the baseline.

Figure 5.22 shows the results of this motor nerve conduction studies performed on the median nerve of a test human subject. This figure compares the evoked compound motor action potential recorded by conventional wet electrodes (trace 1) and 3-D MEA electrodes (trace 2). The response recorded by the 3-D MEA showed **larger amplitude** and a **faster rise time**, suggesting lower electrode impedance. Recordings using conventional electrodes post-MEA measurements (trace 3) show improved characteristics, suggesting piercing of the epithelial layer by the spiked MEAs.

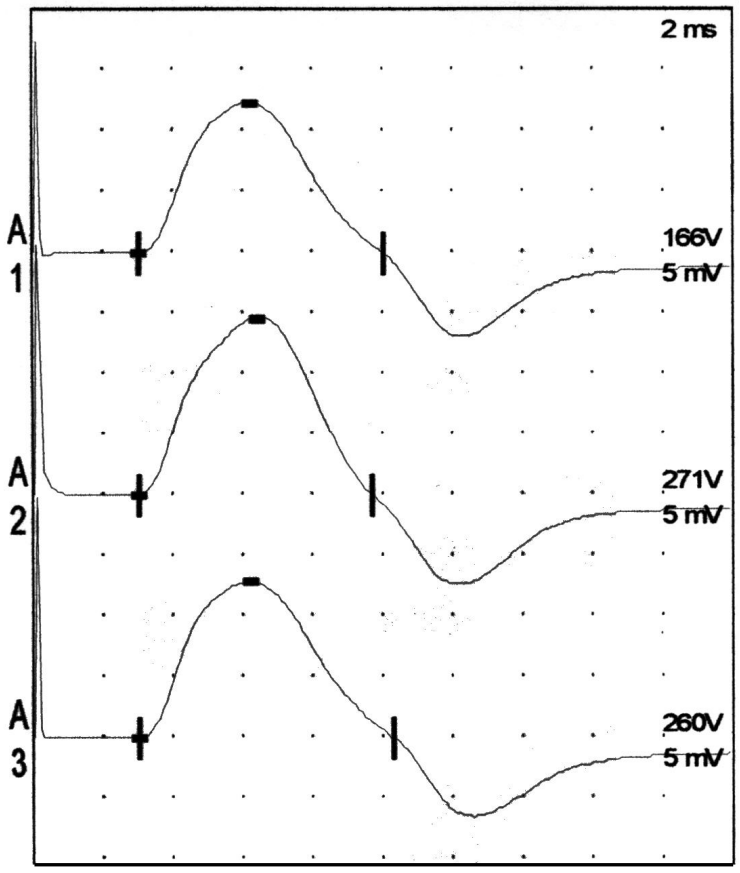

Figure 5.22: Nerve conduction studies performed on test human subject with – A1: standard wet electrodes; A2: 3-D MEAs clearly showing higher signal voltages and faster response times; A3: standard electrodes after the usage of the 3-D MEAs.

5.2.3 Application to Nerve Tracking for Disease Diagnosis and Monitoring

The technology developed in this Chapter can be utilized for several clinical diagnostic applications. The extension of this work will feature patches of 3-D MEAs in conjunction with electronic circuits that suppress stimulation artifact [Brown 2008] utilized in automatic nerve tracking for disease diagnostics. In conventional nerve conduction studies, nerves are localized by placing stimulation and recording electrodes over anatomically typical locations, and then moving them in a trial-and-error process in order to maximize the amplitude of the recorded evoked response elicited by a given response intensity. This is a time-consuming process requiring multiple painful shocks (severe discomfort to the patient), as different locations of the stimulating and recording electrodes are repeatedly tested in order to find a pair of locations that both directly overlie the nerve. With the 3-D MEA patch (a proposed schematic is depicted in Figure 5.23) the ability to record from multiple electrode locations at the same time makes it possible to detect the electrodes closest to the nerve with many fewer trials. Lowered impedance further enhances the spatial resolution of this approach. Stimulation can be provided either by the brain (EMG) or a second electrode (NCS).

Artifact elimination circuitry will also improve the recorded signal quality from those electrodes immediately adjacent to the stimulating electrodes, further accelerating the process of nerve registration. This diagnostic technique will be invaluable in the diagnosis and monitoring of a wide range of the diseases listed in Table 5.3. The initial localization process will consist of individual bipolar stimulation pulses being generated at the electrodes along the periphery of the patch array, followed immediately by

recording of any evoked responses in all patch electrodes (including the stimulating electrode).

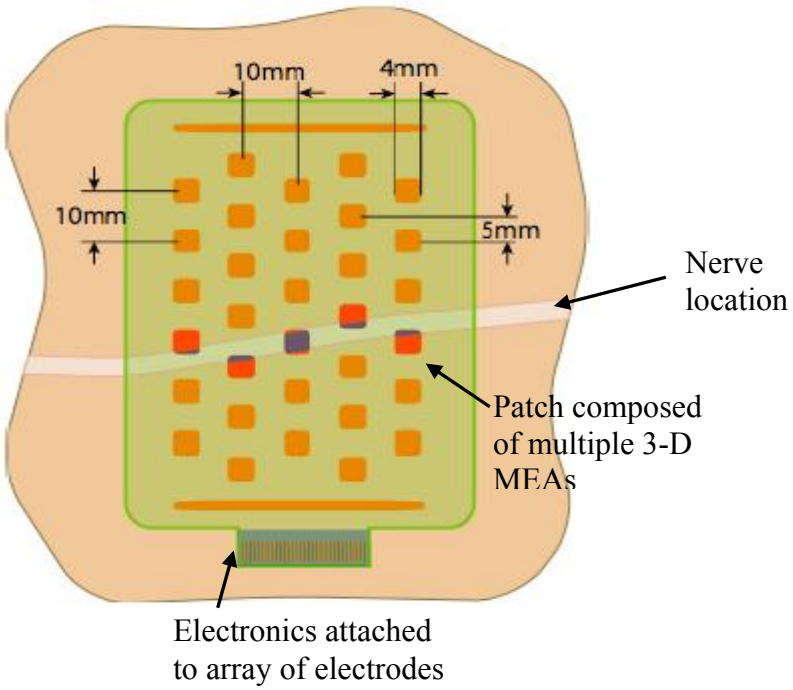

Figure 5.23: Schematic of a proposed 3-D MEA patch along with circuitry to diagnose several neuro-muscular disorders.

Table 5.3: Diseases that could potentially benefit from an automated NCS systems

List of Diseases/Syndromes	
Neurotrauma	Radiculopathies
Lymphedema	Plexopathies
Carpal Tunnel Symdrome	Neuropathies
Motor Neuron Diseases	Nerve Compression Syndromes
Myopathies	Neuromuscular junction disorders

Electrodes at which a maximal response is recorded indicate locations under which a nerve is located. While this process is analogous to the manual mapping of subcutaneous nerves described in [Park 2003], the use of multiple simultaneous recording electrodes will dramatically reduce both the time and the number of shocks required to map out the nerve course. Once the nerve is mapped, this proposed system can quickly and accurately determine the nerve's maximum response amplitude and conduction velocity. We believe that this technology can be adapted rather rapidly for such an application.

5.3 Chapter Discussions and Conclusions

In this Chapter we have demonstrated an ***in-vivo*** **application for the 3-D MEA** technology developed in Chapter 4. The metal transfer micromolding technology has been utilized to **micro-manufacture biopotential microelectrodes**. Design changes to accommodate this application have been performed. **Two different master structure fabrication techniques have been demonstrated: inclined UV lithography-micromolding-RIE sharpening and double-side exposure of SU-8-RIE sharpening**. Master structure sharpening techniques (for both a PDMS master and a SU-8 master) to achieve sharp (<10μm) microneedle tips have been developed using the RIE. This master structure, once developed can be used multiple times through micromolding to fabricate 3-D MEA mold structures. The 3-D MEAs themselves can be fabricated with a functional metal layer transferred during micromolding using metal transfer micromolding process.

EMG measurements and nerve conduction measurements have been used in a clinical setting. Such measurements are typically used to diagnose several neurological

disorders including carpal tunnel syndrome and Lou Gehrig's disease. These measurements have been demonstrated using the 3-D MEAs developed in this chapter. The MEA technology shows **improved signal quality**, **less preparation time, no wet electrolytic gels and less pain/discomfort to the patient** for both these measurements as compared to standard electrodes.

This work has the potential to improve a commercial technology that has been stagnant for several decades. The 3-D MEAs developed in this chapter can not only be produced in a cost-effective way but also show promise for no-prep improved bioelectrode performance for several applications such as EMG, NCS, EEG and EKG.

CHAPTER 6

CONCLUSIONS

6.1 Summary of this Research

In this dissertation, we presented micromachining techniques for three-dimensional microelectrode arrays (3-D MEAs) for both *in-vivo* and *in-vitro* environments. The goal of this work was the development of integrated microfabrication technologies for micro-manufacturing 3-D MEAs from polymeric substrates. Associated goals included the development of manufacturing-friendly packaging and assembly techniques for a complete MEA and evaluation of the MEAs in both *in-vitro* and *in-vivo* settings. In this Chapter the key contributions of this dissertation to the fields of micromachining and medical science are summarized. Additionally future directions in this area of research – additional functionalities of the MEA and future applications utilizing this technology platform are discussed.

Chapter 1 outlined the goals of this dissertation and makes the case for microelectrode arrays (MEAs). The Chapter concluded with an overview of this dissertation.

Chapter 2 provided the background work that has been reported prior to this work in the field of MEAs. First, an overview of the various planar or 2-D MEA technologies is provided with highlights indicating major accomplishments in this area. Secondly, 3-D MEA technologies developed by various researchers around the world are described. An interesting note is that the number of 3-D MEAs developed world-wide is rather limited

due to the complex nature of microfabrication and/or assembly techniques that are required. Conventional electrode-electrolyte theory for *in-vivo* and *in-vitro* microelectrodes is described in this Chapter. The historical development of this theory is traced culminating in the description of the lumped equivalent circuit that describes the electrode-electrolyte interaction – RC parallel pair in series with a resistor. The biological cellular networks, neural and neuro-muscular are also described with key characteristics of the cell structures and function. The microelectrode theory described in this Chapter is utilized to develop an analytical model in Chapter 4.

Chapter 3 presented the first 3-D MEA that was developed in this dissertation – laser scribed 3-D MEAs. The design of this 3-D MEA included a 24 channel microelectrode array with hollow channels for microfluidic perfusion and a 26 channel array with no microfluidics. Three separate microfabrication technologies were developed in this chapter – a double-side exposure technique of thick SU-8 (~600μm tall) to define batch fabricated micro-tower arrays; characterization of thin parylene (1μm thick) on thin film metal (<1μm thick) and fabrication of 3-D MEAs by laser scribing a parylene mold on micro-tower arrays and electroplating the microelectrodes using the mold. A theoretical calculation (that agreed with experimental results) was performed to estimate the energy required for parylene dissociation. The MEA is packaged with parylene insulation and recording sites defined using laser micromachining. Platinum is electrodeposited to reduce the impedance using a custom-designed setup which is described. The characterization test setups for electrical impedance spectroscopy and baseline noise were described along with the results (low yield of electrodes due to serial laser micromachining issues and low noise characteristics). Protocols for *in-vitro* 3-D co-

cultures of neurons and astrocytes were described. These cultures were grown successfully on the MEAs for 21 days *in-vitro*, at which point the evaluated cell viability compared well with control polystyrene culture wells and commercial 2-D MEAs.

Chapter 4 described the second developed 3-D MEA technology – metal transfer micromolding, whose primary motivations were improvement of microelectrode yield and establishing a manufacturing-friendly process. The design of this MEA was fixed as a 50 channel microelectrode array with no microfluidics. Large area, low cost micromolding techniques were incorporated to address the manufacturing goals of this project. Inclined UV lithography was introduced as an advanced mold fabrication technique to fabricate the complex shape of the 3-D MEA with a target height of 300-500μm. Ray tracing algorithms were used to predict the shapes (in 3-D) of square footprints (in 2-D). Two separate techniques – an intentionally formed non-planar mold and a shadow mask were developed to selectively metallize a low surface energy flexible PDMS mold. Metal was transferred (from this mold) due to surface energy differences to various polymers (SU-8, PMMA and PU) during the final molding step for the 3-D MEAs. The MEAs were packaged using commercial PCB substrates and insulated using parylene deposition. Two techniques – laser micromachining/RIE etch and "capping" were developed to isolate the recording sites. The "capping" technique along with an electroplating step to strengthen the transferred metal provided an improvement in the microelectrode yield (60% from 12.5%). Electrical characterization of the MEAs – impedance spectroscopy and baseline noise measurements were carried out. An analytical model for the impedance was developed and provided a moderate match to the experimentally observed data. A model evaluating the rms noise of the electrodes was

developed and matched well with experimentally observed noise. Protocols for *in-vitro* 2-D cortical cultures of neurons were described along with biocompatibility experiments performed to evaluate the compatibility of all the materials introduced in this process. These materials (PU, PMMA, laser scribed parylene-coated PU and PMMA) demonstrated excellent neuronal viability (85±5%) in these *in-vitro* experiments. Electrophysiological spike recordings, utilizing hippocampal slices from brains of 10-day post natal rat pups was also successfully carried out. Protocols for dissection and extraction of these slices were also described. These results can be extended into a biosensing or pharmacological screening application.

Chapter 5 introduced an *in-vivo* application of the 3-D MEA technology. Metal transfer micromolded 3-D MEAs were utilized in a clinical setting to a nerve tracking application. The 3-D MEA design was fixed at a 25 microneedle (shorted together to form one electrode) format though other designs (9 and 81 microneedles in the same form factor) were fabricated. The microfabrication technologies developed during the course of this dissertation were leveraged to fabricate these bioelectrodes. A master structure was created using two separate techniques – inclined UV lithography followed by micromolding and double-side SU-8 exposure. The master structures were then sharpened to address a critical need of this application – <10μm tip sharpness for the microneedle arrays. RIE sharpening techniques for both the master structures (PDMS from micromolding; SU-8 from double-side exposure) were developed. Metal transfer micromolding and simple packaging solutions were used to construct the final device. The device was then characterized in a clinical setting demonstrating their utility. The MEAs developed in this Chapter, performed better than commercial surface electrodes in

all these measurements. They demonstrated improved signal quality and higher amplitude signals attributable to the reduced electrode-skin impedance enabled by the 3-D MEAs. Their smaller size makes then ideally suited to be utilized in an array format along with interfacing electronics and software algorithms in a nerve tracking application. This will allow clinical nerve conduction studies to be performed in a fraction of the time without the usage of cumbersome gels and using many fewer painful stimuli than using conventional techniques.

6.2 Contributions of this Dissertation

The contributions of this dissertation fall under the following four categories:

(1) Development of Microfabrication Technologies: Multiple 3-D MEMS technologies have been developed in this dissertation – (a) A double-side exposure of thick SU-8 to fabricate high aspect ratio micro-towers (both solid and hollow) has been developed. These micro-towers have been used to create 3-D MEAs, coupled microfluidic MEAs, microneedle master structures and "capping" devices for selective parylene deposition in 3-D microstructures. (b) Laser micromachining of thin polymer on thin film metal has been characterized extensively. (c) Metal transfer micromolding technology for microfabrication of *in-vitro* and *in-vivo* 3-D MEAs. Two schemes for selective metal deposition on the MEAs – shadow masking and an intentionally formed non-planar mold have been developed.

(2) Development of ancillary processes for MEAs: Packaging technologies have been developed and yield evaluation has been carried out as part of this dissertation – (a)

Glass-based, PCB-based and Kapton®-based packages have been developed for the 3-D MEAs in this work. These packages have been created in a form factor compatible with commercial testing equipment. Platinum electrodeposition on the gold microelectrodes has been demonstrated for lowering the impedance of the electrodes. (b) Yield improvement techniques have been demonstrated for microelectrodes. Critical processes that caused a lower yield have been identified and improvements have been implemented.

(3) Development of 3-D MEA Applications: Applications of 3-D MEAs have been demonstrated as part of this dissertation – (a) *In-vitro* growth and survival of 3-D co-cultures of neurons and astrocytes has been demonstrated. (b) *In-vitro* hippocampal brain tissues from post-natal rat pups have been dissected and passive electrophysiological recordings performed. (c) *In-vivo* biopotential measurements (stimulation and recording) demonstrating superior performance compared to commercial bioelectrodes for EMG and nerve tracking measurements has been shown.

(4) Development of analytical models: Analytical models for microelectrodes have been developed and theoretical impedance has been compared to experimentally evaluated impedance. Mismatch between the impedances have been explained and a tool for potentially developing tailored impedances explored. A simple model estimating the baseline noise of the electrodes has been implemented. Ray tracing has been adopted to develop 3-D shape prediction algorithms for micro-molds developed in this dissertation. A theoretical calculation for energy required for parylene dissociation has been performed.

6.3 Recommendations for Future Research

The work presented in this dissertation focuses on the development of 3-D microelectrode arrays (MEAs) and applications of this technology in both *in-vitro* and *in-vivo* arenas.

Future directions of this research could take many forms. Firstly integration of microfluidics though demonstrated in Chapter 3 for the laser scribed 3-D MEAs has not been characterized. Fluidics is critical in long-term culture/slice studies in order to prolong cellular life and prevent necrosis at the center of the cultures due to lack of aeration, waste removal and nutrient perfusion. Metal transfer micromolded MEAs with microfludics could provide a manufacturing platform for such research. Parallel laser micromachining (to fabricate multiple fluidic sites at the same time) or innovative photolithographic techniques that integrate fluidics along with the mold/master fabrication could serve as means to incorporate fluidics into this platform. Appendix A explores some techniques to create these microfluidic ports. These techniques need to be characterized and improved further.

Secondly the selective parylene deposition process can be explored further, and utilized as a platform for post-processing of MEMS devices, where complex 3-D structures need to be encapsulated utilizing a dielectric as the last step of the process. Further, modularity in this processing scheme can be introduced to eliminate alignment requirements.

Finally, the applications portfolio of the MTM technology can be expanded. Potential applications could include biosensing, *in-vivo* deep brain stimulators, screening of compounds for pharmacological applications, cardiac pacing, epilepsy research and *in-*

vitro acute power harvesting. The power harvesting application is particularly intriguing with potential implementation using electric eel cell/tissue cultures. These interesting invertebrates have biological circuits in their bodies that convert ATP into electrical energy. 3-D MEAs could be utilized along with accompanying circuitry to capture and store this energy thereby creating the micro-bio-electric power converters.

APPENDIX A

INCORPORATION OF MICROFLUDICS IN 3-D MICROELECTRODE ARRAYS

The representation of *in-vivo* behavior of electrogenic cellular networks in an *in-vitro* setting is motivated by the fact that thick preparations or engineered 3-D constructs better represent network behavior than monolayer cultures [Cullen 2007; Fawcett 1995]. However, the thicker the culture the more difficult it becomes to satisfy the metabolic demands of the cells removed from the planar surface. Thicker preparations rapidly decay due to insufficient cellular oxygenation and lack of nutrient perfusion in the 3-D construct. Hence, it is desirable to fabricate 3-D scaffolds with controlled dimensions and carefully engineered microfluidic perfusion ports in both 2-D and 3-D to support the fluidic circulation of nutrients and removal of depleted media. This prevents the necrosis deep in the tissue as demonstrated by a 700μm thick neuronal-astrocytic constructs with greater than 90% viability, two days *in-vitro* [Cullen 2007]. This section details some of the techniques that have been developed as part of this dissertation to integrate microfluidic ports in both Laser Micromachined 3-D MEAs (Chapter 3) and Metal Transfer Micromolded 3-D MEAs (Chapter 4).

A1. Integration of 3-D and 2-D Microfluidics in Laser Scribed 3-D MEAs

Three-dimensional microfluidic ports are defined on the 3-D MEA as explained in Section 3.1.3. This is performed lithographically. However, for the construction of 2-D ports which are on the substrate SU-8 layer in the process depicted in Figure 3.3, it

becomes difficult to perform fabrication on a perforated substrate. Laser micromachining of SU-8 was explored as an option to micromachine these ports after microtower arrays have been fabricated. An excimer laser operating at 248nm wavelength has been successfully used to micromachine SU-8 [Ghantasala 2001]. This laser was used in Section 3.1.4 to ablate thin parylene on thin-film metal to microfabricate a mold for metal electroplating. Extensive characterization of the parylene process was performed due to the sensitive nature of the process. In the case of SU-8 microfluidic ports, the laser micromachining serves as a tool to ablate material completely in certain areas making the process less sensitive compared to the parylene process. Table A1 lists the typical ablation parameters of such a process.

Table A1: Typical ablation parameters for SU-8

Parameter	**Nominal Value**	**Comments**
Energy	200mJ	Constant
Pulses	100	Varies
Power Delivered	75%	Constant for maximum power delivery
Ablation Depth	52μm	
Frequency	90Hz	Constant

It can clearly been inferred from the Table that SU-8 ablates rather rapidly at moderate energy levels. In order to ablate the ~100μm thick SU-8 substrate, the process described above is repeated twice. We further evaluated the size of the 2-D perfusion port for various perfusion rates (1:1, 2:1 etc). The size of this microfluidic port depends on the substrate thickness, height, perfusion level and diameter of the 3-D microfluidic port [Vukasinovic 2006]. Using these variables we can calculate the diameter of the 2-D microfluidic ports using Equation A.1.

$$\frac{D(2D)}{D(3D)} = \left(\frac{At}{t+h}\right)^{1/4} \qquad (A.1)$$

where A is the perfusion ratio (1:1, 2:1 etc), t is the thickness of the substrate, h is the height of the microtower above the substrate and D(2D) and D(3D) are the microfluidic port diameters in two and three dimensions respectively. Utilizing this equation and calculating the diameter of the 2-D port for certain perfusion and 3-D port diameters, we can tailor the SU-8 laser micromaching process to achieve specific port sizes. The microtower arrays were mounted on a perfusion chamber [Vukasinovic 2006] using PDMS before the ablation process. Figure A.1 depicts a schematic of the perfusion chamber, optical photograph of the perfusion chamber, and laser micromachined 2-D microfluidic ports. Figure A.2 illustrates SEM images of the fabricated devices.

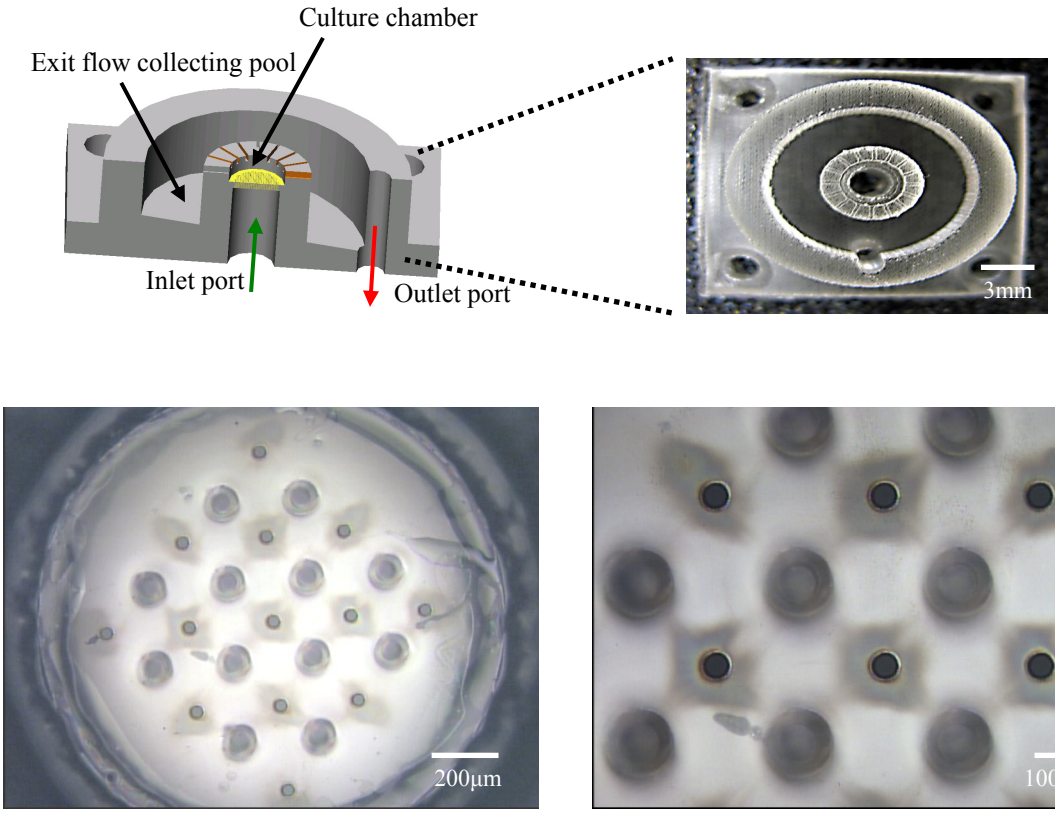

Figure A.1: Schematic (top left) of perfusion chamber and optical images of the perfusion chamber and 2-D & 3-D microfluidic ports.

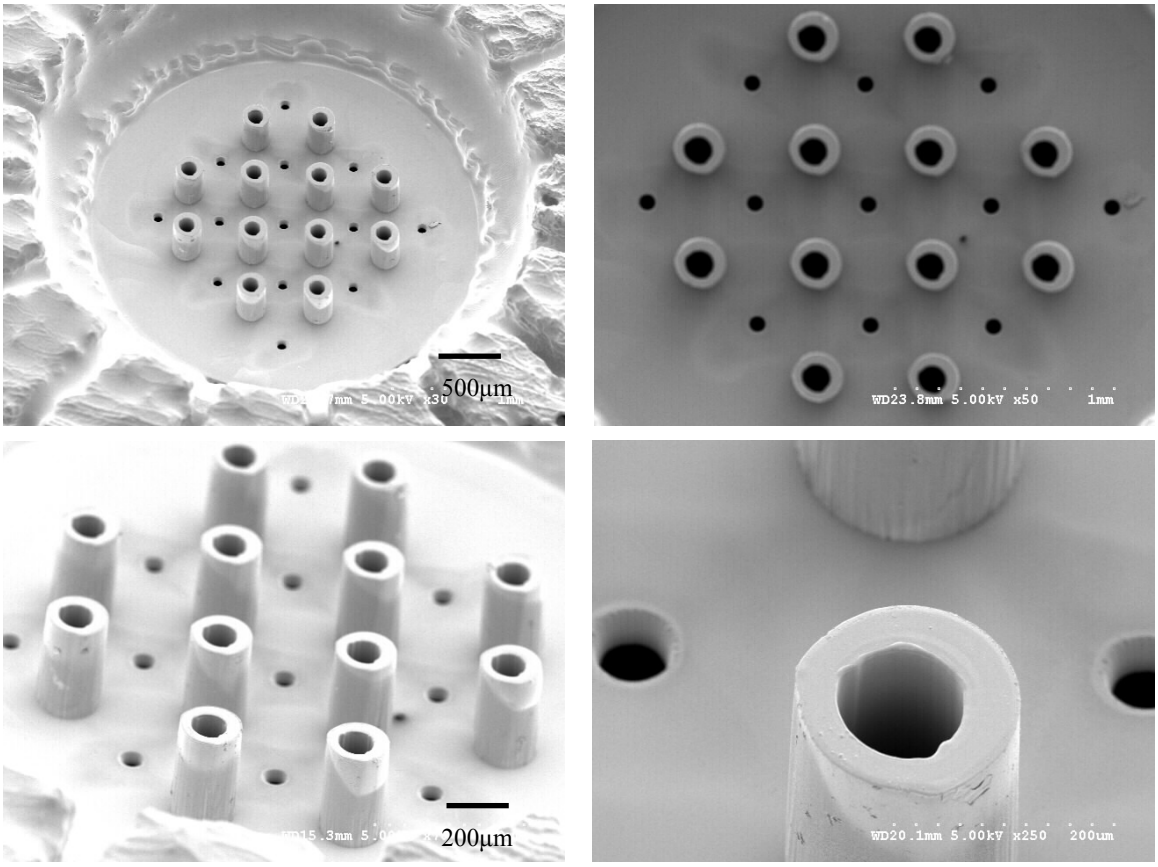

Figure A.2: SEM images of 2-D and 3-D microfluidic ports fabricated on SU-8 microtower arrays. Top views of the microfluidic ports are depicted above and side views below.

Microfluidic perfusion experiments with these devices were not carried out as part of this dissertation as the focus of this work is in the microelectrode functionality of 3-D MEAs. However, this technique motivates the need for fluidics and demonstrates potential pathways to achieve integrated microelectrode, microfluidic devices. These can be utilized for 3-D cultures of electrogenic cells that could be perfused and hence demonstrate viability that far exceeds what is currently state of the art. This will potentially facilitate micro-instrumentation for long term *in-vitro* research.

A2. Integration of 3-D and 2-D Microfluidics in Metal Transfer Micromolded 3-D MEAs

Metal Transfer Micromolded MEAs were developed using techniques described in Chapter 4. The techniques described in this chapter enable microelectrode functionality but microfluidic functionality was not incorporated in this technique. A laser micromachining approach was developed for addressing this issue. Lithographic approaches to address the same problem are currently being developed by the MSMA group.

Laser micromachining approaches were developed for poly-methyl-methacrylate (PMMA) and poly-urethane (PU) in addition the techniques described for SU-8 in section A1. An excimer laser operating at 248nm is ideally suited to accurately machine both PMMA and PU as these polymers absorb UV radiation at 248nm [Wochnowiski 2000; Buruiana 2005]. We have used techniques similar to the ones described in Chapter 3 for parylene ablation and Section A1 for SU-8 ablation. Similar to the SU-8 ablation, the function of this step was to create microfluidic ports all the way through the substrate, so detailed characterization of the ablation process was not performed. Table A2 depicts processing parameters for PU ablation. Ablation was performed in 2-D sites to create 2-D ports.

Table A2: Ablation parameters for PU laser micromachining

Parameter	**Nominal Value**	**Comments**
Energy	250mJ	Constant
Pulses	1500	Varies
Power Delivered	60%	Constant for maximum ablation
Ablation Depth	~1mm	
Frequency	90Hz	Constant

It can be observed from this data that relatively thick (~1mm) PU ablates rather rapidly at a moderate energy level even though the number of bursts required is high. Figure A.3 illustrates optical images of 70μm diameter two-dimensional microfluidic ports laser micromachined in a 3-D MEA. Backside illumination has been utilized to confirm the ablation all the way through the substrate as evidenced by green light from the backside illuminating the ports. These ports are smaller (~50μm) on the bottom of the PU substrate due to the tapered profiling obtained with excimer laser micromachining.

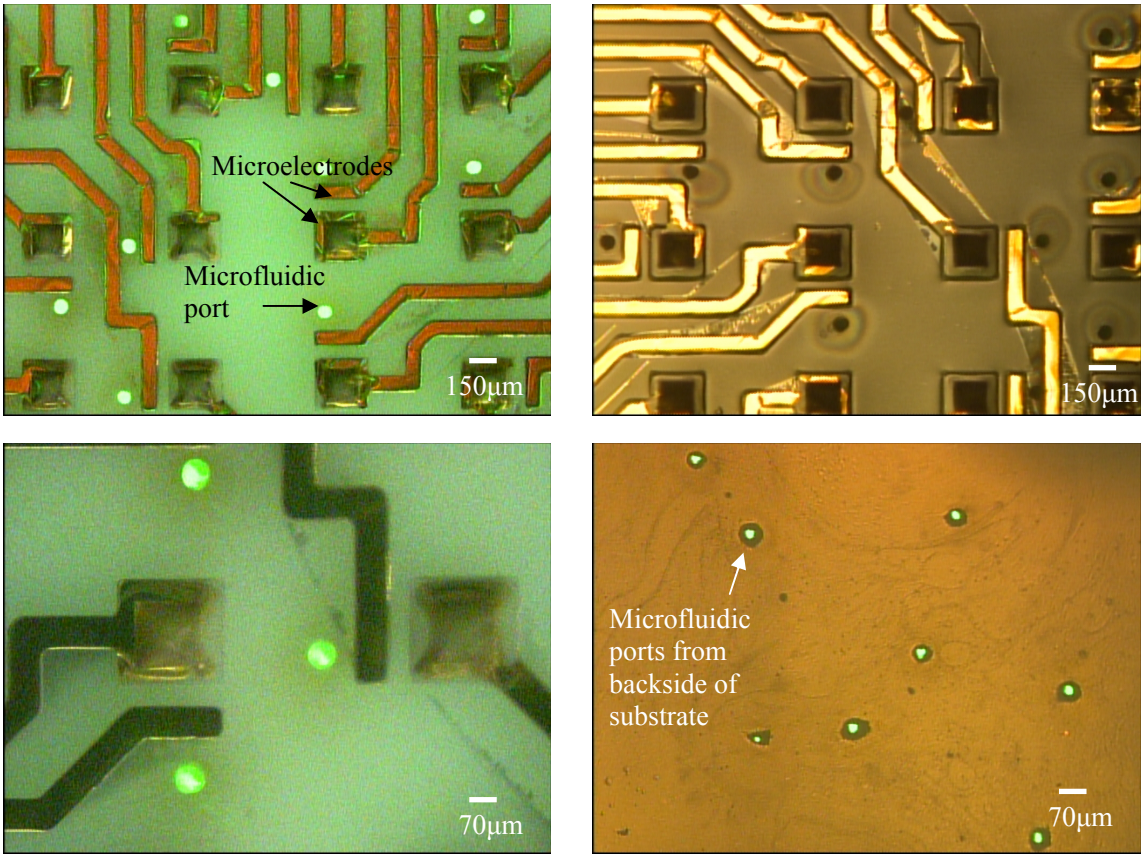

Figure A.3: Optical images with top-side and bottom-side illumination of the microfluidic ports. The microelectrodes (2-D and 3-D) are clearly visible along with the microfluidic ports with backside illumination (green). The image in the bottom left corner depicts the 2-D ports from the backside of the substrate.

PMMA 3-D MEAs were micromachined for both 2-D and 3-D microfluidic ports. Table A3 illustrates typical ablation parameters for PMMA.

Table A3: Ablation parameters for PMMA laser micromachining

Parameter	**Nominal Value**	**Comments**
Energy	300mJ	Constant
Pulses	2500	Varies
Power Delivered	75%	Constant for maximum ablation
Ablation Depth	~1mm	
Frequency	90Hz	Constant

From Table A3 it is evident that ablation of PMMA requires higher power level and increased number of pulses as opposed to both PU and SU-8. 2-D microfluidic ports were ablated using laser micromachining from the top-side while 3-D ports were machined with the device flipped 180° (bottom side). Figure A.4 portrays optical and SEM images of both 2-D and 3-D microfluidic ports that have been fabricated on a PMMA 3-D MEA.

Laser micromachining is not an ideal technique for micromachining ports in metal transfer micromolded 3-D MEAs due to the following reasons:

- The process is very serial. So ports have to be machined one at a time
- The process is time consuming.
- Variation of laser ablation parameters from port to port leads to variation in microfluidic port sizes.
- For 3-D ports backside laser micromachining is not very accurate.

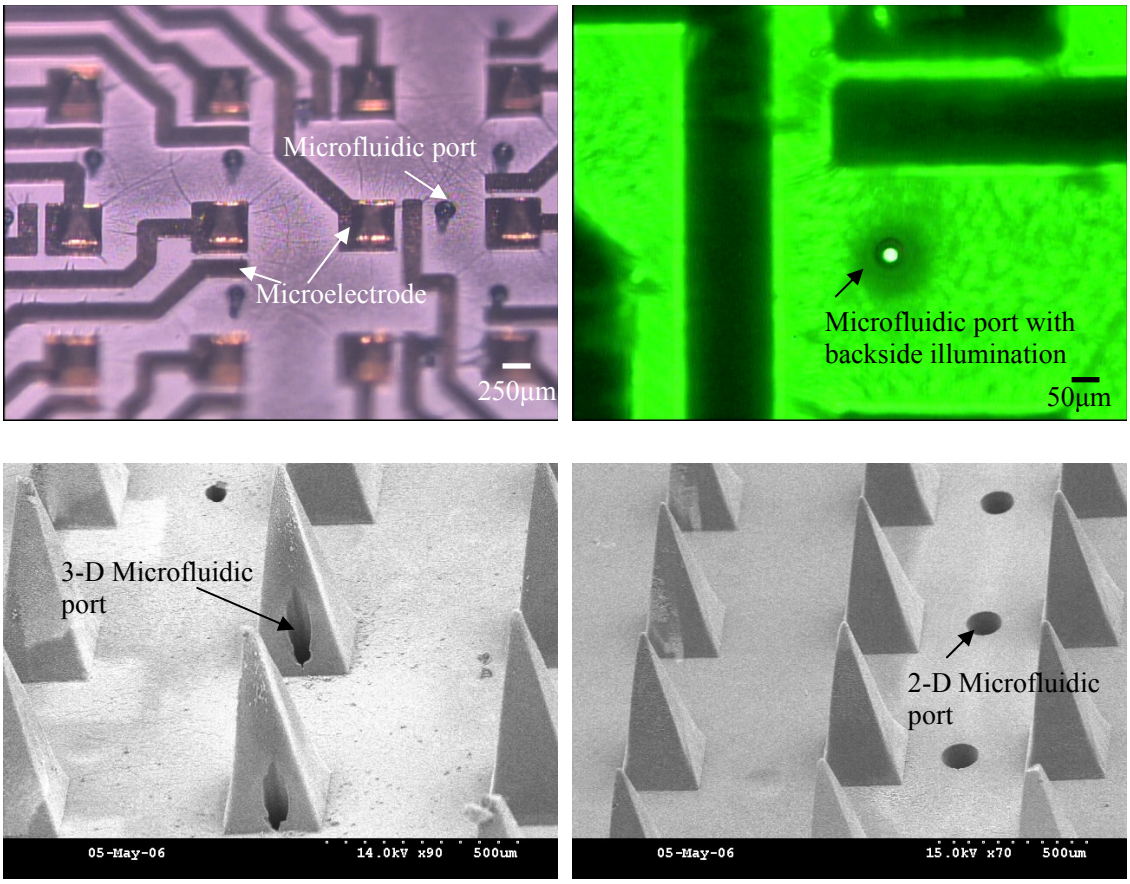

Figure A.4: Optical images (top) of microfluidic ports with both topside (left) and bottom-side (right) illumination. The microelectrodes (2-D and 3-D) are clearly visible along with the microfluidic ports with backside illumination (green). SEM images of 3-D (left) and 2-D (right) microfluidic ports on a PMMA MEA.

Due to some of the reasons listed above only "proof of concept" device fabrication was performed and the devices were not tested. Lithographic based approaches are currently under investigation to accomplish microfluidic functionality in 3-D MEAs.

REFERENCES

B. Alizadeh-Taheri, R.L. Smith, and R.T. Knight, "An Active, Microfabricated, Scalp Electrode-array For EEG Recording," *Solid-State Sensors and Actuators, 1995 and Eurosensors IX..Transducers '95. The 8th International Conference on*, 1995, pp. 67-70.

M.G. Allen, "Polyimide-based Processes for the Fabrication of Thick Electroplated Microstructures," *Proc. of the 7th Intr. Conf. on Solid State Sensors and Actuators (IEEE Transducers 93)*, 1993, pp. 60-65.

D.P. Arnold, S. Das, F. Cros, I. Zana, J.H. Lang, and M.G. Allen, "Magnetic induction machines embedded in fusion-bonded silicon," *Solid-State Sensor, Actuator, and Microsystems Workshop*, Transducers Research Foundation, 2004, pp. 129-132.

S. Balslev, A.M. Jorgensen, B. Bilenberg, K.B. Mogensen, D. Snakenborg, O. Geschke, J.P. Kutter, and A. Kristensen, "Lab-on-a-chip with integrated optical transducers," *Lab on a Chip*, vol. 6, no. 2, 2006, pp. 213-217.

J.V. Basmajian, and C.J. DeLuca eds., Muscles Alive, Williams and Wilkins, 1985.

G.P. Behrmann, and M.T. Duignan, "Excimer laser micromachining for rapid fabrication of diffractive optical elements," *Applied Optics*, vol. 36, 1997, pp. 4666-4676.

T.E. Bell, and K.D. Wise, "A dissolved wafer process using a porous silicon sacrificial layer and a lightly-doped bulk silicon etch-stop," *Micro Electro Mechanical Systems, 1998. MEMS 98. Proceedings., The Eleventh Annual International Workshop on*, 1998, pp. 251-256.

T.E. Bell, K.D. Wise, and D.J. Anderson, "A flexible micromachined electrode array for a cochlear prosthesis," *Solid State Sensors and Actuators, 1997. TRANSDUCERS '97 Chicago., 1997 International Conference on*, 1997, pp. 1315-1318.

L. Berdondini, M. Chippalone, P.D. van der Wal, K. Imfeld, N.F. de Rooij, M. Koudelka-Hep, M. Tedesco, S. Martinoia, J. van Pelt, G. Le Masson, and A. Garenne, "A microelectrode array (MEA) integrated with clustering structures for investigating in vitro neurodynamics in confined interconnected sub-populations of neurons," *Sensors and Actuators B-Chemical*, vol. 114, no. 1, 2006, pp. 530-541.

L. Berdondini, T. Overstolz, N.F. de Rooij, M. Koudelka-Hep, S. Martinoia, P. Seitz, M. Wany, and N. Blanc, "High Resolution Electrophysiological Activity Imaging of in-vitro Neuronal Networks," *IEEE-EMBS Spec. Topics on Microtechnologies in Medicine and Biology*, IEEE, 2002.

R. Bhandari, S. Negi, L. Rieth, R.A. Normann, and F. Solzbacher, "A Novel Method of

Fabricating Convoluted Shaped Electrode Arrays for Neural and Retinal Prosthesis," *Transducers 2007: The 14th International Conference on Solid-State Sensors, Actuators and Microsystems*, IEEE, 2007, pp. 1231-1234.

Biosystems, Ayanda "http://www.ayanda-biosys.com/," 2007 (Date Accessed – June 2007).

Biosystems, Axion "http://www.axionbiosystems.com/," 2008 (Date Accessed – November 2008).

B. Bohl, R. Steger, R. Zengerle, and P. Koltay, "Multi-layer SU-8 lift-off technology for microfluidic devices," *Journal of Micromechanics and Microengineering*, vol. 15, 2005, pp. 1125-1130.

S.A. Boppart, B.C. Wheeler, and C.S. Wallace, "A Flexible Perforated Microelectrode Array for Extended Neural Recordings," *IEEE Transactions on Biomedical Engineering*, vol. 39, no. 1, 1992, pp. 37-42.

D.A. Borkholder, "Cell Based Biosensors using Microelectrodes," Department of Electrical Engineering, Stanford University, Palo Alto, CA, 1998.

D.A. Borkholder, J. Bao, N.I. Maluf, E.R. Perl, and G.T.A. Kovacs, "Microelectrode arrays for stimulation of neural slice preparations," *Journal of Neuroscience Methods*, vol. 77, no. 1, 1997, pp. 61-66.

S. Brittain, K. Paul, X.M. Zhao, and G. Whitesides, "Soft lithography and microfabrication," *Physics World*, vol. 11, no. 5, 1998, pp. 31-36.

I. Brodie, H.R. Gurnick, C.E. Holland, and H.A. Moessner, Method for Providing Polyimide Spacers in a Field Emission Panel Display, USPTO, 1990.

E.A. Brown, J.D. Ross, R.A. Blum, N. Yoonkey, B.C. Wheeler, and S.P. DeWeerth, "Stimulus-Artifact Elimination in a Multi-Electrode System," *Biomedical Circuits and Systems, IEEE Transactions on*, vol. 2, no. 1, 2008, pp. 10-21.

E.C. Buruiana, V. Melinte, T. Buruiana, T. Lippert, H. Yoshikawa and M. Mashuhara, "Synthesis and characterisation of new hard polyurethanes with triazene pendants" *Journal of Photochemistry and Photobiology A: Chemistry*, vol. 171, 2005, pp. 261-267.

P.K. Campbell, K.E. Jones, R.J. Huber, K.W. Horch, and R.A. Normann, "A Silicon-based, 3-Dimensional Neural Interface - Manufacturing Processes for an Intracortical Electrode Array," *IEEE Transactions on Biomedical Engineering*, vol. 38, no. 8, 1991, pp. 758-768.

D.L. Chapman *Phil. Mag.*, vol. 25, no. 6, 1913, pp. 475.

S.-O. Choi, "An Electrically Active Microneedle Electroporation Array for Intracellular Delivery of Biomolecules," School of Electrical and Computer Engineering, Georgia Institute of Technology, Atlanta, GA, 2007.

S.-O. Choi, S. Rajaraman, Y.K. Yoon, X. Wu, and M.G. Allen, "3-D Metal Patterned Microstructure using Inclined UV Exposure and Metal Transfer Micromolding Technology," *Proc. of Solid State Sensors, Actuators and Microsystems Workshop*, 2006.

Y. Choi, "A three-dimensional coupled microelectrode and microfluidic array for neuronal interfacing," School of Electrical and Computer Engineering, Georgia Institute of Technology, Atlanta, GA, 2005.

Y. Choi, K. Kim, and M.G. Allen, "Continuously-varying, three-dimensional SU-8 structures: fabrication of inclined magnetic actuators," *IEEE MEMS Conf.*, 2002, pp. 176-179.

H.-Y. Chu, T.-Y. Kuo, B. Chang, S.-W. Lu, C.-C. Chiao, and W. Fang, "Development of the Three Demensional Multi-Electrode Array for Neural Interfacing," *Solid-State Sensors, Actuators and Microsystems, 2005. Digest of Technical Papers. TRANSDUCERS '05. The 13th International Conference on*, IEEE, 2005, pp. 1804-1807.

P. Churchland, and T. Sejnowski eds., The Computational Brain, The MIT Press, 1992.

D.R. Cornblath, R.W. Kuncl, E.D. Mellits, S.A. Quaskey, L. Clawson, A. Pestronk, and D.B. Drachman, "Nerve-Conduction Studies in Amyotrophic-Lateral-Sclerosis," *Muscle & Nerve*, vol. 15, no. 10, 1992, pp. 1111-1115.

J.T. Cramer, T.J. Housh, G.O. Johnson, K.T. Ebersole, S.R. Perry, and A.J. Bull, "Mechanomyographic and electromyographic responses of the superficial muscles of the quadriceps femoris during maximal, concentric isokinetic muscle actions," *Isokinet. Exerc. Sci.*, vol. 8, 2000, pp. 109-117.

F. Cros, and M.G. Allen, "High Aspect Ratio Structures Achieved by Sacrificial Conformal Coating," *Proc. Solid State Sensors and Actuators Workshop*, 1998, pp. 261-264.

F. Cros, K. Kim, and M.G. Allen, "A Single-Mask Process for Micromachined Magnetic Devices," *Proceedings Solid State Sensor and Actuator Conference*, Tranducers Research Foundation, 2000, pp. 138-141.

D.K. Cullen, "Traumatically-induced degeneration and reactive astrogliosis in three-dimensional neural co-cultures: Factors influencing neural stem cell survival and integration," Wallace H. Coulter Department of Biomedical Engineering, Georgia Tech/Emory University, Atlanta, GA, 2005.

D.K. Cullen, J. Vukasinovic, A. Glezer, and M.C. LaPlaca, "Microfluidic engineered high cell density three-dimensional neural cultures," *Journal of Neural Engineering*, vol. 4, no. 2, 2007, pp. 159-172.

S.P. Davis, M.R. Prausnitz, and M.G. Allen, "Fabrication and characterization of laser micromachined hollow microneedles," *IEEE Transducers Solid-State Sensors, Actuators and Microsystems, 12th International Conference on,* 2003, pp. 1435-1438.

B.D. DeBusschere, and G.T.A. Kovacs, "Portable cell-based biosensor system using integrated CMOS cell-cartridges," *Biosensors and Bioelectronics*, vol. 16, 2001, pp. 543-556.

C.J. DeLuca, "Encyclopedia of Medical Devices and Instrumentation," Series Encyclopedia of Medical Devices and Instrumentation, 2006.

Department of Chemistry, Michigan State University, "http://www.cem.msu.edu/," 2009 (Date Accessed – Jan. 2009).

C. Disselhorst-Klug, J. Bahm, V. Ramaekers, A. Trachterna, and G. Rau, "Non-invasive approach of motor unit recording during muscle contractions in humans," *European Journal of Applied Physiology*, vol. 83, no. 2-3, 2000, pp. 144-150.

M.H. Droge, G.W. Gross, M.H. Hightower, and L.E. Czisny, "Multielectrode Analysis of Coordinated, Multisite, Rhythmic Bursting in Cultured CNS Monolayer Networks," *Journal of Neuroscience*, vol. 6, no. 6, 1986, pp. 1583-1592.

C.M. Dwyer, R.S. Chapman, and A. Forsyth, "Allergic Contact-Dermatitis From Tens Gel," *Contact Dermatitis*, vol. 30, no. 5, 1994, pp. 305-305.

J.P. Eckmann, O. Feinerman, L. Gruendlinger, E. Moses, J. Soriano and T. Tiusty, "The Physics of Living Nueral Networks", *Physics Reports-Review Section of Physics Letters*, vol. 44, no. 1-3, 2007, pp. 54-76.

W. Ehrfeld, F. Gotz, D. Munchmeyer, W. Schelb, and D. Schmidt, "LIGA process: sensor construction techniques via X-ray lithography," *Solid-State Sensor and Actuator Workshop*, Transducers Research Foundation, 1988, pp. 1-4.

B. Eversmann, M. Jenkner, F. Hofmann, C. Paulus, R. Brederlow, B. Holzapfl, P. Fromherz, M. Merz, M. Brenner, M. Schreiter, R. Gabl, K. Plehnert, M. Steinhauser, G. Eckstein, D. Schmitt-Landsiedel, and R. Thewes, "A 128 /spl times/ 128 CMOS biosensor array for extracellular recording of neural activity," *Solid-State Circuits, IEEE Journal of*, vol. 38, no. 12, 2003, pp. 2306-2317.

T. Fan-Gang, and H. Heng-Tsang, "A novel micro optical system employing inclined polymer mirrors and Fresnel lens for monolithic integration of optical disk pickup

heads," *TRANSDUCERS, Solid-State Sensors, Actuators and Microsystems, 12th International Conference on,* 2003, pp. 599-602.

S. Farina, F. Granella, G. Malferrari, and G.C. Manzoni, "Headache and Cervical Spine Disorders: Classification and Treatment with Transcutaneous Electrical Nerve Stimulation," *Headache*, vol. 26, no. 8, 1986, pp. 431-433.

J.W. Fawcett, R.A. Barker, and S.B. Dunnett, "Dopaminergic neuronal survival and the effects of bFGF in explant, three dimensional and monolayer cultures of embryonic rat ventral mesencephalon" *Experimental Brain Research*, vol. 106, 1995, pp. 275-282.

T.A. Fofonoff, S.M. Martel, N.G. Hatsopoulos, J.P. Donoghue, and I.W. Hunter, "Microelectrode array fabrication by electrical discharge machining and chemical etching," *IEEE Transactions on Biomedical Engineering*, vol. 51, no. 6, 2004, pp. 890-895.

E. Forster, M. Bartos, and S. Zhao eds., Hippocampal Slice Cultures, New Methods for Culturing Cells from Nervous Tissues., 2005.

K. Frank, and M.C. Becker eds., Microelectrodes for recording and stimulation, Physical Techniques in Biological Research, Academic Press, 1964.

W. Franks, F. Heer, I. McKay, S. Taschini, R. Sunier, C. Hagleitner, A. Hierlemann, and H. Baltes, "CMOS monolithic microelectrode array for stimulation and recording of natural neural networks," *TRANSDUCERS, Solid-State Sensors, Actuators and Microsystems, 12th International Conference on,* 2003, pp. 963-966.

W. Franks, I. Schenker, P. Schmutz, and A. Hierlemann, "Impedance characterization and modeling of electrodes for biomedical applications," *Biomedical Engineering, IEEE Transactions on*, vol. 52, no. 7, 2005, pp. 1295-1302.

A.B. Frazier, D.P. O'Brien, and M.G. Allen, "Two dimensional metallic microelectrode arrays for extracellular stimulation and recording of neurons," *Micro Electro Mechanical Systems, 1993, MEMS '93, IEEE*, 1993, pp. 195-200.

J.L. Fritz, and M.J. Owen, "Hydrophobic recovery of plasma-treated polydimethylsiloxane," *Journal of Adhesion*, vol. 54, no. 1-2, 1995, pp. 33-45.

B.H. Gahwiler, "Organotypic monolayer cultures of nervous tissue," *Journal of Neuroscience Methods*, vol. 4, 1981, pp. 329-342.

L. Galvani, "De Viribus Electricitatis in Motu Musculari Commentarius," 1791.

J. Garra, T. Long, J. Currie, S. T., R. White, and M. Paranjape, "Dry etching of polydimethylsiloxane for microfluidic systems," *J. Vac. Sci. Technol. A*, vol. 20, no.

3, 2002, pp. 975-982.

R.C. Gesteland, B. Howland, J.Y. Lettvin, and W.H. Pitts, "Comments on Microelectrodes," *Proc. of the IRE*, 1959, pp. 1856-1862.

M.K. Ghantasala, J.P. Hayes, E.C. Harvey, and D.K. Sood, "Patterning, electroplating and removal of SU-8 moulds by excimer laser micromachining," *Journal of Micromechanics and Microengineering*, vol. 11, no. 2, 2001, pp. 133-139.

G. Gholmieh, S. Courellis, S. Fakheri, E. Cheung, V. Marmarelis, M. Baudry, and T. Berger, "Detection and classification of neurotoxins using a novel short-term plasticity quantification method," *Biosensors & Bioelectronics*, vol. 18, no. 12, 2003, pp. 1467-1478.

M. Ghovanloo, and K. Najafi, "A Three-Dimensional Microassembly Structure for Micromachined Planar Microelectrode Arrays," *Proc. IEEE EMBS Conf.*, 2005, pp. 112-115.

R.W. Gill, and J.D. Meindl, "Low power integrated circuits for an implantable pulsed Doppler ultrasonic blood flowmeter," *Solid-State Circuits, IEEE Journal of*, vol. 10, no. 6, 1975, pp. 464-471.

M. Gouy, "Sur la constitution de la charge electrique a la surface d'un electrolyte," *Journal of Physics*, vol. 9, 1910, pp. 457-468.

F. Grinnell, "Fibroblast biology in three-dimensional collagen matrices," *Trends in Cell Biology*, vol. 13, 2003, pp. 264-269.

P. Griss, P. Enoksson, H.K. Tolvanen-Laakso, P. Merilainen, S. Ollmar, and G. Stemme, "Micromachined Electrodes for Biopotential Measurements," *IEEE Journal of Microelectromechanical Systems*, vol. 10, no. 1, 2001, pp. 10-16.

P. Griss, H.K. Tolvanen-Laakso, P. Merilainen, and G. Stemme, "Characterization of micromachined spiked biopotential electrodes," *IEEE Transactions on Biomedical Engineering*, vol. 49, no. 6, 2002, pp. 597-604.

G.W. Gross, "Simultaneous single unit recording in vitro with a photoetched laser deinsulated gold multimicroelectrode array," *IEEE Trans. Biomed. Eng.*, vol. BME-26, no. 5, 1979, pp. 273-279.

G.W. Gross, E. Rieske, G.W. Kreutzberg, and A. Meyer, "A new fixed-array multi-microelectrode system designed for long-term monitoring of extracellular single unit neuronal activity in vitro," *Neuroscience Letters*, vol. 6, no. 2-3, 1977, pp. 101-105.

F. Heer, S. Hafizovic, W. Franks, A. Blau, C. Ziegler, and A. Hierlemann, "CMOS

microelectrode array for bidirectional interaction with neuronal networks," *IEEE Journal of Solid-State Circuits*, vol. 41, no. 7, 2006, pp. 1620-1629.

H.L. Helmholtz, "Studien uber electrische grenzschichten," *Ann. Phys. Chem.*, vol. 7, 1879, pp. 377-382.

M.O. Heuschkel, M. Fejtl, M. Raggenbass, D. Bertrand, and P. Renaud, "A three-dimensional multi-electrode array for multi-site stimulation and recording in acute brain slices," *Journal of Neuroscience Methods*, vol. 114, no. 2, 2002, pp. 135-148.

H. Hillborg, and U.W. Gedde, "Hydrophobicity recovery of polydimethylsiloxane after exposure to corona discharges," *Polymer*, vol. 39, no. 10, 1998, pp. 1991-1998.

A. Hodgkin, and A. Huxley, "A quantitative description of membrane current and its application to conduction and excitation in nerve," *J. Physiol.*, vol. 117, 1952, pp. 500-544.

A.S. Holmes, S.M. Saidam, and R.A. Lawes, "Low cost LIGA processes," *Microengineering Technologies and How to Exploit Them (Digest No: 1997/076), IEE Colloquium on*, 1997, pp. 2/1-2/4.

C.-N. Huang, C.-H. Chen, and H.-Y. Chung, "The Review of Applications and Measurements in Facial Electromyography," *Journal of Medical and Biological Engineering*, vol. 25, no. 1, 2004, pp. 15-20.

E. Huigen, A. Peper, and C.A. Grimbergen, "Investigation into the origin of the noise of surface electrodes " *Medical and Biological Engineering and Computing*, vol. 40, no. 3, 2002, pp. 332-338.

B. Hultberg, A. Andersson, and A. Isaksson, "Copper ions differ from other thiol reactive metal ions in their effects on the concentration and redox status of thiols in HeLa cell cultures," *Toxicology*, vol. 117, no. 2-3, 1997, pp. 89-97.

S.-H. Hur, D.-Y. Khang, C. Kocabas, and J.A. Rogers, "Nanotransfer printing by use of noncovalent surface forces: Applications to thin-film transistors that use single-walled carbon nanotube networks and semiconducting polymers," *Applied Physics Letters*, vol. 85, no. 23, 2004, pp. 5730-5732.

M. Ikeuchi, and K. Ikuta, "Artificial Capillary Network Chip for In-vitro 3-D Tissue Culture," *Transducers 2007: The 14th International Conference on Solid-State Sensors, Actuators and Microsystems*, 2007.

Incorporated, DuPont "http://www.dupont.com," 2008 (Date Accessed – June 2008).

Incorporated, MicroChem "http://www.microchem.com," 2008 (Date Accessed – July

2008).

Incorporated, Resonetics "http://www.resonetics.com/," 2007 (Date Accessed – Jan 2007).

Industry, NeuroTech "http://www.neurotechindustry.org/," 2008 (Date Accessed – July 2008).

R.J. Jackman, S.T. Brittain, A. Adams, M.G. Prentiss, and G.M. Whitesides, "Design and fabrication of topologically complex, three-dimensional microstructures," *Science*, vol. 280, no. 5372, 1998, pp. 2089-2091.

M. Janders, U. Egert, M. Stelzle, and W. Nisch, "Novel thin film titanium nitride micro-electrodes with excellent charge transfer capability for cell stimulation and sensing applications," *Engineering in Medicine and Biology Society, 1996. Bridging Disciplines for Biomedicine. Proceedings of the 18th Annual International Conference of the IEEE*, 1996, pp. 245-247.

C.H. Ji, F. Herrault, and M.G. Allen, "A metallic buried interconnect process for through-wafer interconnection," *Journal of Micromechanics and Microengineering*, vol. 18, no. 8, 2008.

D. Johnston, and S. Wu eds., Foundations of Cellular Neurophysiology, The MIT Press, 1995.

K.E. Jones, P.K. Campbell, and R.A. Normann, "A Glass Silicon Composite Introcortical Electrode Array," *Annals of Biomedical Engineering*, vol. 20, no. 4, 1992, pp. 423-437.

I.K. Jun, Y.H. Koh, S.H. Lee, and H.E. Kim, "Novel fabrication of a polymer scaffold with a dense bioactive ceramic coating layer," *Journal of Materials Science-Materials in Medicine*, vol. 18, no. 8, 2007, pp. 1537-1542.

D. Juncker, H. Schmid, A. Bernard, I. Caelen, B. Michel, N. de Rooij, and E. Delamarche, "Soft and rigid two-level microfluidic networks for patterning surfaces," *Journal of Micromechanics and Microengineering*, vol. 11, 2001, pp. 532-541.

E.W. Keefer, A. Gramowski, D.A. Stenger, J.J. Pancrazio, and G.W. Gross, "Characterization of acute neurotoxic effects of trimethylolpropane phosphate via neuronal network biosensors," *Biosensors & Bioelectronics*, vol. 16, no. 7-8, 2001, pp. 513-525.

D.T. Kewley, M.D. Hills, D.A. Borkholder, I.E. Opris, N.I. Maluf, C.W. Storment, J.M. Bower, and G.T.A. Kovacs, "Plasma-etched neural probes," *Sensors and Actuators A - Physical*, vol. 58, no. 1, 1997, pp. 27-35.

J. Kim, and X. Xu, "Excimer Laser Fabrication of Polymer Microfluidic Devices," *Journal*

of Laser Applications, vol. 15, no. 4, 2003, pp. 255-260.

S. Kisban, S. Herwik, K. Seidl, B. Rubehn, O. Paul, P. Ruther, T. Stieglitz, and A. Jezzini, "Microprobe Array with Low Impedance Electrodes and Highly Flexible Polyimide Cables for Acute Neural Recording," *Engineering in Medicine and Biology Society, EMBS 2007. 29th Annual International Conference of the IEEE*, 2007 pp. 175-178.

S.H. Ko, I. Park, H. Pan, C.P. Grigoropoulos, A.P. Pisano, C.K. Luscombe, and J.M.J. Frechet, "Direct nanoimprinting of metal nanoparticles for nanoscale electronics fabrication," *Nano Letters*, vol. 7, no. 7, 2007, pp. 1869-1877.

H. Kobsa, "Micromachining with Lasers," *Industrial Physicist*, 1996, pp. 32-33.

P. Koltay, R. Steger, B. Bohl, and R. Zengerle, "The dispensing well plate: a novel nanodispenser for the multiparallel delivery of liquids (DWP Part I)," *Sensors and Actuators a-Physical*, vol. 116, no. 3, 2004, pp. 483-491.

K.I. Koo, H. Chung, Y. Yu, J. Seo, J. Park, J.M. Lim, S.J. Paik, S. Park, H.M. Choi, M.J. Jeong, G.S. Kim, and D.I.D. Cho, "Fabrication of pyramid shaped three-dimensional 8 x 8 electrodes for artificial retina," *Sensors and Actuators A - Physical*, vol. 130, 2006, pp. 609-615.

C. Koppl, and O. Gleich, "Evoked cochlear potentials in the barn owl," *Journal of Comparative Physiology a-Neuroethology Sensory Neural and Behavioral Physiology*, vol. 193, no. 6, 2007, pp. 601-612.

G.T.A. Kovacs ed., Microelectrode models for neural interfaces, Enabling technologies for cultured neural networks, Academic Press, 1994.

G.T.A. Kovacs, "Electronic sensors with living cellular components," *Proceedings of the IEEE*, vol. 91, no. 6, 2003, pp. 915-929.

L. Kubinova, and J. Janacek, "Confocal microscopy and stereology: Estimating volume, number, surface area and length by virtual test probes applied to three-dimensional images," *Microscopy Research and Technique*, vol. 53, no. 6, 2001, pp. 425-435.

H. Kuo-Yung, H. Heng-Tsang, and T. Fan-Gang, "A novel fabrication technology for smooth 3D inclined polymer microstructures with adjustable angles," *IEEE Transducers, Solid-State Sensors, Actuators and Microsystems, 12th International Conference on, 2003*, pp. 821-824.

N.C. LaBianca, J.D. Gelorme, E. Cooper, E. O'Sullivan, and J. Shaw, "High Aspect Ratio Optical Resist Chemistry for MEMS Application," *188th Meeting JECS*, Electrochemical Society, 1995, pp. 500-501.

S.P. Lacour, C. Tsay, S. Wagner, Y. Zhe, and B. Morrison, III, "Stretchable micro-electrode

arrays for dynamic neuronal recording of in vitro mechanically injured brain," *Sensors, 2005 IEEE*, 2005.

F. Lehmann-Horn, and K. Jurkat-Rott, "Voltage-Gated Ion Channels and Hereditary Disease," *Physiological Reviews*, vol. 79, no. 4, 1999, pp. 1317-1372.

C.T. Lin, L.W. Ko, J.C. Chiou, J.R. Duann, R.S. Huang, S.F. Liang, T.W. Chiu, and T.P. Jung, "Noninvasive neural prostheses using mobile and wireless EEG," *Proceedings of the IEEE*, vol. 96, no. 7, 2008, pp. 1167-1183.

S. Linder, H. Baltes, F. Gneadinger, and E. Doering, "Photolithography in Anisotropically Etched Grooves," *Proc. IEEE MicroElectroMechanicalSystems Conf.*, 1996, pp. 38-43.

Y.-L. Loo, R.L. Willett, K.W. Baldwin, and J.A. Rogers, "Additive, Nanoscale Patterning of Metal Films with a Stamp and a Surface Chemistry Mediated Transfer Process: Application in Plastic Electronics," *Applied Physics Letters*, vol. 81, no. 3, 2002, pp. 562-564.

H. Lorenz, M. Despont, N. Fahrni, J. Brugger, P. Vettiger, and P. Renaud, "High-aspect-ratio, ultrathick, negative-tone near-UV photoresist and its applications for MEMS," *Sensors and Actuators A*, vol. 64, no. 1, 1998, pp. 33-39.

H. Lorenz, M. Despont, N. Fahrni, N. LaBianca, P. Renaud, and P. Vettiger, "SU-8: a low-cost negative resist for MEMS," *Journal of Micromechanics and Microengineering*, vol. 7, no. 3, 1997, pp. 121-124.

H. Lorenz, M. Despont, P. Vettiger, and P. Renaud, "Fabrication of photoplastic high-aspect ratio microparts and micromolds using SU-8 UV resist," *Microsystem Technologies*, vol. 4, 1998, pp. 143-146.

J.K. Lumpp, L. Hua, and S. Al-Banna, "Excimer laser assisted deposition of metal films on aluminum nitride," *Advanced Applications of Lasers in Materials Processing/Broadband Optical Networks/Smart Pixels/Optical MEMs and Their Applications. IEEE/LEOS 1996 Summer Topical Meetings,* 1996*,* pp. 61-62.

M.P. Maher, J. Pine, J. Wright, and Y.C. Tai, "The neurochip: a new multielectrode device for stimulating and recording from cultured neurons," *Journal of Neuroscience Methods*, vol. 87, no. 1, 1999, pp. 45-56.

A. Mata, A.J. Fleischman, and S. Roy, "Fabrication of multi-layer SU-8 microstructures," *Journal of Micromechanics and Microengineering*, vol. 16, no. 2, 2006, pp. 276-284.

G.A. May, S.A. Shamma, and R.L. White, "A tantalum-on-sapphire microelectrode array," *Electron Devices, IEEE Transactions on*, vol. 26, no. 12, 1979, pp. 1932-1939.

M.A. McClain, M.C. LaPlaca, and M.G. Allen, "An Integrated Elastomer Mesh and Microelectrode Array for Neurophysiology," *Georgia Life Sciences Summit*, 2008.

Med Sciences, Alpha "http://www.med64.com/," 2007 (Date Accessed – Feb. 2007).

J. Meindl, J. Plummer, P. Salsbury, and J. Brugler, "Integrated electronics for a reading aid for the blind," *Solid-State Circuits Conference. Digest of Technical Papers. 1969 IEEE International*, 1969, pp. 50-51.

S. Metz, M.O. Heuschkel, B. Valencia Avila, R. Holzer, D. Bertrand, and P. Renaud, "Microelectrodes with Three-Dimensional Structures for Improved Neural Interfacing," *Proc. of 23rd Annual EMBS Intr. Conf.*, IEEE, 2001, pp. 765-768.

T. Meyer, K.H. Boven, E. Gunther, and M. Fejtl, "Micro-electrode arrays in cardiac safety pharmacology - A novel tool to study QT interval prolongation," *Drug Safety*, vol. 27, no. 11, 2004, pp. 763-772.

Micro Tec, Suss "http://www.suss.com/," 2007 (Date Accessed – April 2007).

H.A. Miller, and D.C. Harrison eds., Biomedical Electrode Technology: Theory and Practice, Academic Press, 1974.

R.G. Miller, C. Peterson, and N.L. Rosenberg, "Electrophysiological Evidence of Severe Distal Nerve Segment Pathology in the Guillain-Barre- Syndrome" *Muscle & Nerve*, vol. 10, no. 6, 1987, pp. 524-529.

J. Mohr, "Free space optical components and systems based on LIGA technology," *Optical MEMS, 2000 IEEE/LEOS International Conference on*, 2000, pp. 147-148.

V.B. Mountcastle, "The columnar organization of the neocortex," *Brain*, vol. 120, 1997, pp. 701-722.

K. Najafi, and K.D. Wise, "An implantable multielectrode array with on-chip signal processing," *IEEE Journal of Solid State Circuits*, vol. 21, no. 6, 1986, pp. 1035-1044.

K. Najafi, K.D. Wise, and T. Mochizuki, "A High Yield IC-Compatible Multichannel Recording Array," *IEEE Transactions on Electron Devices*, vol. 32, no. 7, 1985, pp. 1206-1211.

Neurotechnology Systems, Cyberkinetics "http://www.cyberkineticsinc.com/," 2007 (Date Accessed – August 2007).

J. Newman, "Resistance for flow of current to a disk," *J. Electrochemical Society*, vol. 113, no. 5, 1966, pp. 501-502.

P. Nga Phuong, E. Boellaard, J.N. Burghartz, and P.M. Sarro, "Photoresist coating methods for the integration of novel 3-D RF microstructures," *Microelectromechanical Systems, Journal of*, vol. 13, no. 3, 2004, pp. 491-499.

W. Nisch, J. Bock, U. Egert, H. Haemmerle, and A. Mohr, "A thin film microelectrode array for monitoring extracellular neuronal activity in vitro," *Biosensors and Bioelectronics*, vol. 9, 1994, pp. 737-741.

S. Nishimura, Y. Tomita, and T. Horiuchi, "Clinical application of an active electrode using an operational amplifier," *Biomedical Engineering, IEEE Transactions on*, vol. 39, no. 10, 1992, pp. 1096-1099.

R.A. Normann, "Technology Insight: future neuroprosthetic therapies for disorders of the nervous system," *Nature Clinical Practice Neurology*, vol. 3, no. 8, 2007, pp. 444-452.

J.L. Novak, and B.C. Wheeler, "Recording from the Aplysia Abdominal-Ganglion with a Planar Microelectrode Array," *IEEE Transactions on Biomedical Engineering*, vol. 33, no. 2, 1986, pp. 196-202.

D.P. O'Brien, T.R. Nichols, and M.G. Allen, "Flexible microelectrode arrays with integrated insertion devices," *Micro Electro Mechanical Systems, 2001. MEMS 2001. The 14th IEEE International Conference on*, 2001, pp. 216-219.

J. O'Keefe, and L. Nadel eds., The Hippocampus as a Cognitive Map, Oxford University Press, 1978.

M. Ota, H. Okano, and M. Yoshida, "Manipulation of micro solid particles and induced flows in water by laser irradiation," *Journal of Thermal Science*, vol. 16, no. 2, 2007, pp. 176-180.

B. Pan, Y.K. Yoon, J. Papapolymerou, M. Tentzeris, and M.G. Allen, "Design and Fabrication of Substrate-Independent Integrated Antennas Utilizing Surface Micromachining," *Asia-Pacific Microwave Conference (APMC)*, 2005.

D. Papageorgiou, S.C. Bledsoe, M. Gulari, J.F. Hetke, D.J. Anderson, and K.D. Wise, "A shuttered probe with in-line flowmeters for chronic in-vivo drug delivery," *Proc. of IEEE MEMS Conference*, 2001, pp. 212-215.

J.H. Park, S.O. Choi, R. Kamath, Y.K. Yoon, M.G. Allen, and M.R. Prausnitz, "Polymer particle-based micromolding to fabricate novel microstructures," *Biomedical Microdevices*, vol. 9, no. 2, 2007, pp. 223-234.

J.I. Park, "Preoperative Percutaneous Cranial Nerve Mapping in Head and Neck Surgery," *Arch Facial Plast Surg.*, vol. 5, 2003, pp. 86-91.

PCB, Express, "http://www.expresspcb.com/," 2007 (Date Accessed – July 2007).

N.P. Pham, J.N. Burghartz, and P.M. Sarro, "A model for film thickness using direct spray coating," *Electronics Packaging Technology, 2003 5th Conference (EPTC 2003)*, 2003 pp. 773-776.

J. Pine, "Recording Action Potentials from Cultured Neurons with Extracellular Microcircuit Electrodes," *Journal of Neuroscience Methods*, vol. 2, 1980, pp. 19-31.

K.I. Pokhodnya, M. Bonner and J.S. Miller, "Parylene Protection Coatngs for Thin Film V[TCNE]x Room Temperature", Chem. Mater., vol. 16, 2004, pp. 5114-5119.

S.M. Potter, D.A. Wagenaar, and T.B. DeMarse eds., Closing the Loop: Stimulation Feedback Systems for Embodied MEA Cultures, Advances in Network Electrophysiology using Multi-Electrode Arrays, Springer, 2005.

R.L. Pozzo, A.S. Malicsi, and I. Iwasaki, "Removal of Lead from Printed Circuit Board Scrap by an Electrodissolution Delamination Method," *Resources Conservation and Recycling*, vol. 5, no. 1, 1991, pp. 21-34.

Morris Productions, "http://www.morris.com.au," 2008 (Date Accessed – May 2008).

B. Qing, K.D. Wise, and D.J. Anderson, "A high-yield microassembly structure for three-dimensional microelectrode arrays," *Biomedical Engineering, IEEE Transactions on*, vol. 47, no. 3, 2000, pp. 281-289.

S. Rajaraman, S.O. Choi, R.H. Shafer, J.D. Ross, J. Vukasinovic, Y. Choi, S.P. DeWeerth, A. Glezer, and M.G. Allen, "Microfabrication technologies for a coupled three-dimensional microelectrode, microfluidic array," *Journal of Micromechanics and Microengineering*, vol. 17, no. 1, 2007, pp. 163-171.

S. Rajaraman, H. Noh, P.J. Hesketh, and D.S. Gottfried, "Rapid, low cost microfabrication technologies toward realization of devices for dielectrophoretic manipulation of particles and nanowires," *Sensors and Actuators B-Chemical*, vol. 114, no. 1, 2006, pp. 392-401.

S. Rajaraman, Y. Zhao, X. Wu, S.-H. Kim, and M.G. Allen, "Metal transfer micromolding (MTM) process for high-aspect-ratio 3-D structures with functional metal surfaces," *International Symposium on Flexible Automation (ISFA 2008)*, ASME, 2008.

D.C. Rodger, A.J. Fong, W. Li, H. Ameri, I. Lavrov, H. Zhong, S. Saati, P. Menon, E. Meng, J.W. Burdick, R.R. Roy, V.R. Edgerton, J.D. Weiland, M.S. Humayun, and Y.C. Tai, "High-Density Flexible Parylene-Based Multielectrode Arrays for Retinal and Spinal Cord Stimulation," *Solid-State Sensors, Actuators and Microsystems Conference, 2007. TRANSDUCERS 2007. International*, 2007, pp. 1385-1388.

J.R. Rohan, G. O'Riordan, and J. Boardman, "Selective electroless nickel deposition on copper as a final barrier/bonding layer material for microelectronics applications," *Applied Surface Science*, vol. 185, no. 3-4, 2002, pp. 289-297.

J.D. Ross, "Microstimulation and Multicellular Analysis: A Neural Interfacing System for Spatiotemporal Stimulation," Department of Bioengineering, Georgia Institute of Technology, Atlanta, GA, 2008.

P.J. Rousche, and R.A. Normann, "Chronic recording capability of the Utah Intracortical Electrode Array in cat sensory cortex," *Journal of Neuroscience Methods*, vol. 82, no. 1, 1998, pp. 1-15.

L. Rowe, M. Almasri, N. Fogleman, A.B. Frazier, and G.J. Brewer, "An active microscaffold for culturing 3-D neuronal networks," *Solid-State Sensors, Actuators and Microsystems, 2005. Digest of Technical Papers. TRANSDUCERS '05. The 13th International Conference on*, 2005 pp. 948-951.

L. Rowe, M. Almasri, K. Lee, N. Fogleman, G.J. Brewer, Y. Nam, B.C. Wheeler, J. Vukasinovic, A. Glezer, and A.B. Frazier, "Active 3-D microscaffold system with fluid perfusion for culturing in vitro neuronal networks," *Lab on a Chip*, vol. 7, no. 4, 2007, pp. 475-482.

B.V. Safronov, V. Pinto, and V.A. Derkach, "High-resolution single-cell imaging for functional studies in the whole brain and spinal cord and thick tissue blocks using light-emitting diode illumination," *Journal of Neuroscience Methods*, vol. 164, no. 2, 2007, pp. 292-298.

H. Sato, J. Kakinuma, S. Go, and S. Shoji, "A Novel Fabricatioin of In-channel 3-D Micromesh Structure Using Maskless Multi-Angle Exposure and Its Microfilter Application," *IEEE MEMS Conf*, IEEE, 2003, pp. 223-226.

E. Scherder, A. Bouma, and A. Steen, "Effects of a follow-up treatment of short-term transcutaneous electrical nerve stimulation on memory and affective behaviour in a patient with probable Alzheimer's disease," *Behavioural Neurology*, vol. 9, no. 1, 1996, pp. 33-35.

W.B. Scoville, and B. Millner, "Loss of Recent Memory after Bilateral Hippocampal Lesions," *Journal of Neurol. Neurosurg. Psych.*, vol. 20, 1957, pp. 11-21.

A. Searle, and L. Kirkup, "A direct comparison of wet, dry and insulating bioelectric recording electrodes," *Physiological Measurement*, vol. 21, no. 2, 2000, pp. 271-283.

S. Sia, and G.M. Whitesides, "Microfluidic Devices Fabricated in Poly(dimethylsiloxane) for Biological Studies," *Electrophoresis*, vol. 24, 2003, pp. 3563-3576.

Silicones, Dow Corning "http://www.dowcorning.com/," 2008 (Date Accessed – August 2008).

A.P. Spence ed., Basic Human Anatomy, The Benjamin Cumming Publishing Co, 1990.

O. Stern, "Zur theorie der elektrolytischen doppelschicht," *Z. Elektrochem.*, vol. 30, 1924, pp. 508-516.

A. Stett, U. Egert, E. Guenther, F. Hofmann, T. Meyer, W. Nisch, and H. Haemmerle, "Biological application of microelectrode arrays in drug discovery and basic research," *Analytical and Bioanalytical Chemistry*, vol. 377, no. 3, 2003, pp. 486-495.

T. Stieglitz, M. Schuettler, and K.P. Koch, "Implantable Biomedical Microsystems for Neural Prostheses," *IEEE Engineering in Medicine and Biology Magazine*, vol. 24, no. 5, 2005, pp. 58-65.

T.J. Sullivan, S.R. Deiss, J. Tzyy-Ping, and G. Cauwenberghs, "A brain-machine interface using dry-contact, low-noise EEG sensors," *Circuits and Systems, 2008. ISCAS 2008. IEEE International Symposium on*, 2008, pp. 1986-1989.

F.W. Sunderman, "Search for Molecular Mechanisms in the Genotoxicity of Nickel," *Scandinavian Journal of Work Environment & Health*, vol. 19, 1993, pp. 75-80.

Systems, MultiChannel "http://www.multichannelsystems.com/," 2007 (Date Accessed – December 2007).

Systems, Specialty Coating "http://www.scscoatings.com/," 2007 (Date Accessed – May 2007).

K. Takei, T. Kawashima, H. Takao, K. Sawada, and M. Ishida, "Si Micro Probe and SiO2 Micro Tube Array with NMOSFETs," *Transducers 2007: The 14th International Conference on Solid-State Sensors, Actuators and Microsystems* IEEE, 2007, pp. 1381-1384.

S. Tatic-Lucic, Y.-C. Tai, J.A. Wright, and J. Pine, "Silicon-Micromachined Cultured Neuron Probes for In Vivo Studies of Neural Networks," *Proc. of ASME winter Annual Meeting*, ASME, 1994.

P. Thiebaud, C. Beuret, M. Koudelka-Hep, M. Bove, S. Martinoia, M. Grattarola, H. Jahnsen, R. Rebaudo, M. Balestrino, J. Zimmer, and Y. Dupont, "An array of Pt-tip microelectrodes for extracellular monitoring of activity of brain slices," *Biosensors & Bioelectronics*, vol. 14, no. 1, 1999, pp. 61-65.

P. Thiebaud, N.F. deRooij, M. KoudelkaHep, and L. Stoppini, "Microelectrode arrays for electrophysiological monitoring of hippocampal organotypic slice cultures," *IEEE*

Transactions on Biomedical Engineering, vol. 44, no. 11, 1997, pp. 1159-1163.

C.A. Thomas, P.A. Springer, G.E. Loeb, Y. Berwald-Netter, and L.M. Okun, "A Miniature Microelectrode Array to Monitor the Bioelectric Activity of Cultured Cells," *Exp. Cell Res.*, vol. 74, no. 1, 1972, pp. 61-66.

Y. Tsaiweichao-Shozawa, M. Sonoo, and T. Shimizu, "Patterns of Nerve Conduction Abnormalities in Severe Carpal Tunnel Syndrome," *Journal of Clinical Neurophysiology*, vol. 25, no. 5, 2008, pp. 281-286.

A.W. Tucker, and M. Birnbaum, "Laser chemical etching of vias in GaAs," *Electron Device Letters, IEEE*, vol. 4, no. 2, 1983, pp. 39-41.

R.R. Tummala ed., Fundamentals of Microsystems Packaging, McGraw-Hill, 2001.

W. Uter, and H.J. Schwanitz, "Contact dermatitis from propylene glycol in ECG electrode gel," *Contact Dermatitis*, vol. 34, no. 3, 1996, pp. 230-231.

V. Vernekar, D.K. Cullen, N. Fogleman, Y. Choi, A.J. Garcia, M.G. Allen, G.J. Brewer, and M.C. LaPlaca, "SU-8 2000 Rendered Cytocompatible for Neuronal BioMEMS Applications," *Journal of Biomedical Materials Research A*, vol. Published Online, 2008.

M. von Allmen, and A. Blatter, Laser-Beam Interactions with Materials: Physical Principles and Applications, Springer-Verlag, 1995.

J. Vukasinovic and A. Glezer, "Centimeter-scale diagnostics incubator with integrated perfusion", Proc. 10th Int. Conf. on Miniaturized Systems for Chemistry and Life Sciences (MicroTAS), 2006, Tokyo, Japan.

D.A. Wagenaar, J. Pine, and S.M. Potter, "Effective parameters for stimulation of dissociated cultures using multi-electrode arrays," *Journal of Neuroscience Methods*, vol. 138, no. 1-2, 2004, pp. 27-37.

J.C. White, S.R. Hansen, and R.K. Johnson, "A comparison of EMG procedures in the carpal tunnel syndrome with clinical-EMG correlations," *Muscle Nerve*, vol. 11, no. 11, 1988, pp. 1177-1182.

J.T. Whitton, and J.D. Everall, "The thickness of the epidermis," *British Journal of Dermatology*, vol. 89, 1973, pp. 467-476.

K.D. Wise, "Silicon microsystems for neuroscience and neural prostheses," *Engineering in Medicine and Biology Magazine, IEEE*, vol. 24, no. 5, 2005, pp. 22-29.

K.D. Wise, D.J. Anderson, J.F. Hetke, D.R. Kipke, and K. Najafi, "Wireless implantable microsystems: high-density electronic interfaces to the nervous system,"

Proceedings of the IEEE, vol. 92, no. 1, 2004, pp. 76-97.

K.D. Wise, and J.B. Angell, "A Low-Capacitance Multielectrode Probe for Use in Extracellular Neurophysiology," *Biomedical Engineering, IEEE Transactions on*, vol. BME-22, no. 3, 1975, pp. 212-219.

K.D. Wise, J.B. Angell, and A. Starr, "An Integrated Circuit Approach to Extracellular Microelectrodes," *Proc. of Intrl Conf. on Med and Bio Engr.*, 1969, pp. 14-15.

X. Wu, Y. Zhao, Y.-K. Yoon, S.-O. Choi, J.-H. Park, and M.G. Allen, "Wafer-scale Micromolding of Unitary Polymeric Microstructures with Simultaneously Formed Functional Metal Surface," *Proc. of Intr. Conf. on MicroTotal Analysis Systems*, 2005, pp. 205-207.

H. Yang, and C.T. Pan, "Excimer laser-induced formation of metallic microstructures by electroless copper plating," *Journal of Micromechanics and Microengineering*, vol. 12, no. 2, 2002, pp. 157-161.

Y.K. Yoon, J.H. Park, and M.G. Allen, "Multidirectional UV Lithography for Complex 3-D MEMS Structures," *Microelectromechanical Systems, Journal of*, vol. 15, no. 5, 2006, pp. 1121-1130.

Y.K. Yoon, J.W. Park, and M.G. Allen, "Polymer-core conductor approaches for RF MEMS," *Journal of Microelectromechanical Systems*, vol. 14, no. 5, 2005, pp. 886-894.

Y. Zhao, X. Wu, Y.-K. Yoon, J.-H. Park, S.J. Kennedy, Z. Schwartz, B.D. Boyan, and M.G. Allen, "Fabrication of Micromachined Mold Masters for 3-D, High-aspect-ratio Cell Culturing Substrates," *Proc. of ASME IMECE Conf.*, 2005, pp. 1-7.

VITA

SWAMINATHAN RAJARAMAN

Swaminathan Rajaraman was born in New Delhi, India in 1977. He grew up in the city of Madras (now called Chennai), India where he finished his high school in 1994. He got his B.S (in Electronics Engineering) from Bharathidasan University (Trichy, India) in 1998. He then moved to the US to pursue a masters' degree at the University of Cincinnati (Cincinnati, OH). He received a M.S (in Electrical Engineering) from the same university in 2001. His master's thesis was on the fabrication and development of silicon-MEMS based microneedles.

He then went to work in the MEMS industry mainly with Analog Devices (Cambridge, MA) for the next 2 years.

In Jan. 2003, he came to the Georgia Institute of Technology in pursuit of a PhD in the area of Microsystems/Biotechnology. During his tenure at Georgia Tech, Mr. Rajaraman has worked in the areas of MicroTAS, microneedles, microtweezers and microelectrode arrays (MEAs).

From 2004-2005, Mr. Rajaraman worked for CardioMEMS (Atlanta, GA) as a Technical Staff member on the development of MEMS-based implantable pressure sensors for heart pressure monitoring.

His PhD thesis work is on the development of 3-D MEAs for *in-vitro* and *in-vivo* applications. Aside from his thesis work he is also involved since 2007, in two start-up companies on campus as Principal Technical Staff – Axion Biosystems and Teneo Microinstruments.